Statistical analysis of the vertical human walking forces and human structural interaction effects

Angus Ewan Peters

Department of Engineering

University of Cambridge

This dissertation is submitted for the degree of

Doctor of Philosophy

Wolfson College 2023

I want to dedicate this thesis to my wife, Ilijana, and parents, Ewan, Caroline and Matthew.

Declaration

I hereby declare that except where specific reference is made to the work of others, the contents of this dissertation are original and have not been submitted in whole or in part for consideration for any other degree or qualification in this, or any other University. This dissertation is the result of my own work and includes nothing which is the outcome of work done in collaboration, except where specifically indicated in the text. This dissertation contains less than 65,000 words including appendices, bibliography, footnotes, tables and equations and has less than 150 figures.

Angus Ewan Peters

2023

Acknowledgements

First and foremost, I would like to acknowledge Professor John Orr, who has provided me with guidance and freedom to create and form my PhD. Whilst, in hindsight, there were many periods where I was lost with my direction and work, John provided me with enough guidance and freedom to steer me back on course. I would also like to acknowledge the many skills John has taught me, such as creating my academic network and engaging with other researchers. This proved invaluable throughout my PhD when my topic changed.

Next, I acknowledge the many collaborators I worked with throughout my PhD. However, none more so than Dr Vitomir Racic and Dr Stana Zivanovic. Both have been instrumental in my PhD and provided me with hours of meetings and guidance throughout the years. I would not have been able to produce any of the work without their direction and data, so I am eternally grateful for their charity and thank them for replying to a random email from me to collaborate.

I want to acknowledge the help of various past and present friends at Cambridge, mainly Wolfson College, Wolfson College Bar staff and the CURUFC. Whilst they did not directly aid with my PhD, they provided an outlet for frustration and keepers of good times. Namely An, Margot, Bodhi and Danny.

Finally, I would like to thank my marvellous wife, Ilijana Parojcic. She has been with me through the depths and highs of the PhD and life events, from being unable to walk for a year and my father's death to getting married (TWICE). She has provided me with unconditional support and love throughout. She now probably knows just as much about my PhD as me, having proofread my papers and thesis several times. So, I would like to acknowledge and thank her.

Abstract

The increased ambition of architects, advancements in structural materials, and the rapidly growing pressure on the civil engineering sector to reduce embodied carbon has resulted in more slender pedestrian structures. Such structures are susceptible to excessive vibrations due to human activities, for example, walking, which is the most frequent human activity. Due to the slender design, modern structures provide a greater likelihood to have low natural frequencies. Low natural frequencies can result in resonant walking paces matching a vertical mode of the structure. Therefore, the structures are prone to resonant and often excessive vibrations that may compromise the serviceability limit state. Current industry guidance is used ubiquitously to provide all information on the vibration serviceability assessment due to walking, with academic research outcomes often overlooked. Recent research concludes that industry load models incorporate inherent bias through the limited intra-subject variation and poor correlation with actual walking loads.

Current guidance pertaining to the vibration serviceability assessment does not disclose or encourage human structure interaction effects, even though a significant body of research demonstrates the benefits of its inclusion. Current estimations of structural responses do not align with the physical measurements of structures. The resultant acceleration estimations from the guidance are often overestimated compared to the actual structural response. Therefore, many structures may have been overdesigned due to the exclusion of human structural interaction effects and inaccurate load models within current guidance.

For the stated reasons, demand for further investigation into the correct representation of vertical walking forces and the human structure interaction is required. This thesis seeks to deepen understanding of both topics' appropriate and accurate representation through an experimental campaign and analysis, to reduce the error between predicted and monitored results.

An innovative method of extracting walking load parameters encompasses all information within the close frequency range of the walking frequency. A representative interpolation of the vertical walking is formed through the successive sampling of individual footsteps based on both the inter- and intra-subject variation. The proposed model is demonstrated to

minimise the error between the resultant acceleration output of the structure compared to the acceleration of real walking loads, than any current guidance. Furthermore, it is statistically shown that walking parameters and characteristics depend on the participants' sex.

Current industry guidance and research load models are then investigated in their ability to model the acceleration response of structures compared to their real load counterparts. It is demonstrated that current research models in the low and high-frequency ranges outperform current industry load models, with respect to minimising the difference between the synthetic force and real force acceleration output. Several current industry guidance models oversimplify the vertical walking load, causing an overestimation of acceleration results compared to real walking forces. Such models are shown to overestimate the acceleration response by double that of real walking loads. One of the two models, that produced the smallest errors with respect to real walking, has been published for over 12 years. However, there needs to be more uptake within the engineering community for the models' use. A disconnect between industry and academia is noted, resulting in poor dissemination of knowledge and current best practices.

Current representations of the human structure interaction effects of the moving pedestrian, modelled through a single degree of freedom (SDOF) spring, mass, and damper (SMD), are compared to physical measurements of a flexible fibre-reinforced polymer bridge. These estimations of the human structure interaction are used to provide a numerical approximation of the vertical acceleration of the structure, by comparing the responses to the actual measurement of 56 volunteers. It is shown that all numerical simulations of SDOF SMD parameters from research, bar one paper, provide consistent responses with those monitored on the structure. Yet the specific parameters demonstrate a wide range of acceptable values. Many current parameter estimations are viewed monolithically through a single deterministic value; however, an entire spectrum of parameter values is evidenced. Finally, an inverse analysis of the measured accelerations is used to produce updated human structure interaction parameter estimates of the SDOF SMD human model. The resultant mean estimations of the parameters produce values both consistent and inconsistent with previously published results; however, the consequent acceleration response is within the physical range of the volunteer acceleration time histories. A limitation of the study and previous studies is highlighted. As the exact walking force is unknown, the parameters' estimations diverge depending on the input walking force.

Contents

List of Figures

List of Tables

ABBREVIATIONS

AISC DG11	American Institute of steel construction design guide 11
ASD	Auto Spectral Density
BS	British standard
CCIP	Cement and Concrete industry publication
CDF	Cumulative density function
COM	Centre of mass
CoV	Coefficient of variation
DFT	Direct Fourier transformation
DLF	Dynamic Load Factor
FEA	Finite Element Analysis
FFT	Fast Fourier transformation
FRF	Frequency response function
GFR	Ground force reaction
GFRP	Glass fibre reinforced polymer
GP	Gaussian Process
HSI	Human Structure interaction
IMU	Inertial Mass Unit
ISO	International Organisation for standards

LTE	Local truncated error
MAP	Maximum a posterior
MDOF	Multiple degree of freedom
MLE	Maximum Likelihood estimate
NN	Neural Network
ODE	Ordinary differential equation
OLS	Ordinary least squares
PDE	Partial differential equation
PDF	Probability density function
PSD	Power Spectral Density
RK	Runge-Kutta
RMS	Root Mean Squared
RMSE	Root mean squared error
S.D	Standard deviation
SCI	Steel Construction Institute
SDOF	Single degree of freedom
SLS	Serviceability limit state
SMD	Spring mass damper
VSA	Vibration serviceability assessment

LIST OF VARIABLES

A	Fitting Constant
$arg \max_{\emptyset} P(\quad \mid \quad)$	What is the set of parameters that maximise the probability of the conditional probability
c	Damping constant matrix of
d	Pedestrian density
d_{jam}	Jamming density
DLF_n	Dynamic load factor of nth harmonic
$\overline{DLF_n}(f_n)$	N^{th} DLF as a function of normalised walking frequency
$F(t)$	Force function
Δf	Frequency resolution
$\mathcal{F}\{\}$	Fourier transformation of
f_n	Natural Frequency of structure
f_{norm}	Normalised walking frequency
f_p	Walking Frequency
g_{peak}	Peak factor to determine mean acceleration
$H(\omega)$	Frequency response function of system

i	Imaginary unit
I_{eff}	Effective impulse
k	Stiffness matrix of
l	Step length
m	Modal mass of
N (,)	Normal distribution with mean and standard deviation
N_p	Number of people crossing the structure
$p_\omega(\omega)$	Probability density function of walking frequency
$P(\quad \mid \quad)$	Probability of first variable given second variable
$P( )$	Probability of event happening
$\ddot{q}_n$	Modal acceleration of Nth mode
$\dot{q}_n$	Modal velocity of Nth mode
q_n	Modal displacement of Nth mode
$S_F(\omega)$	PSD of force function
$S_{out}(\omega)$	PSD of output
$sup\| \quad \|$	Supremum
t	Time
v	Walking velocity
$\bar{v}$	Average free velocity

W	Weight of pedestrian (N)
$X(\omega)$	Input signal in frequency domain
$\ddot{x}$	Acceleration of
$\dot{x}$	Velocity of
x	Displacement of
$Y(\omega)$	Frequency response of output
z_{max}	Mean maximum acceleration
θ_n	Phase angle of nth
α_G	Correction factor for geographical location
α_T	Correction factor for travel purpose
γ	Fitting constant for velocity
σ^2	Variance of
ξ	Modal damping ratio of
σ	Standard deviation of
$\theta_n(f_{norm})$	N^{th} phase angle as a function of normalised walking frequency
ϕ	Mode shape of
μ_p	Ratio of pedestrian to structural mass
$\overline{\mu}$	Sample mean of
$\overline{\sigma}$	Sample standard deviation

$\rho_{[\ ,\ ]}$	Correlation of vector one and two
α	Significances level
ω	Angular frequency

Chapter 1 Introduction

1.1 Problem statement and motivation

Architectural trends and innovations in structural materials have led to the ever-increasing slenderness and longer spans of civil engineering structures [1]. Further trends in lightweight construction methodologies result in the stiffness-to-mass ratio decreasing. Thus, the desire for more slender structures has ultimately reduced the natural frequency of structures to a range excitable by human activities [2–4]. Such processes can result in a resonant and often excessive vibrations response [1,5].

Over the last 25 years, several high-profile vibration serviceability issues have come to light and questioned the understanding of civil engineering structures' vibration serviceability assessment (VSA) [6–8]. The design of civil engineering structures, such as footbridges, floors and grandstands [9–12] has increasingly become governed by the Vibration Serviceability Assessment (VSA) [9–11,13], with human-induced vibrations producing the majority of serviceability complaints [5,14,15].

A survey by the Institution of Structural Engineers from 2015 sheds light on the current situation within the structural engineering industry regarding vibration serviceability [9]. The survey indicates the following critical limiting factors:

- Low level of competence of structural engineers when dealing with vibration serviceability,
- Poor and lacking codes and design guidance,
- Poor dissemination of knowledge from academia to industry.

The poor state of the current vibration serviceability can be partially attributed to the lack of implementation of research into the industry, with no vibration serviceability guidance added

in recent years, barring that of the AISC DG11 in 2016 [16]. The vibration analysis of human activities is not a common topic taught within engineering curricula at the degree level. As a result, engineers rely on the relevant knowledge from industry guidance.

There are multiple loads on a structure, but the human dynamic force has resulted in several problematic scenarios [9–11,13] and avid media scrutiny [6–8]. The failures are predominantly attributed to human walking activities. Whilst walking is not the most energetic of human activities [3], it can be sustained for extended periods. This dangerous circumstance allows the resonant build-up of vibrations and subjects the structure to excessive vibrations.

A modern concern has also arisen from industries requiring high-precision processes, such as computer hardware and scientific laboratory manufacturing. These activities require environments subject to strict low-level vibration environments. This new ultra-stringent requirement to produce such facilities has further amplified the uncertainty of the VSA and provided complex issues other than the typical resonant response [17,18].

Current design philosophies dictate that the design of a structure is governed by the worst-case scenario [16,19–22]. However, little consideration is given to the probability of such a load occurring [23]. Current guidance [16,19–22] regarding human walking, suggests that the response should be determined from the average person, or persons, crossing the structure at a walking frequency that matches that of the structure [17,20,21,23,24], even though the likelihood of perfect synchronisation is low and not represented in design methodologies. Structural design philosophies and approaches are often provided by oversimplifications that can lead to ill-poised design decisions [24–27]. Current VSA dictates the use of deterministic processes [16,19,28]. However, human locomotion is stochastic [29,30]. Current guidelines neglect the inherent variability of humans and human locomotion, resulting in the actual response of a structure deviating from that of the idealised model [27].

If guidance is oversimplified or incomplete, then the issue will propagate. An update in guidance and current state-of-the-art knowledge must be addressed to understand the critical issues better. The varied model inputs and assumptions of the excitation force further amplify the problems in the current VSA. Such information is often dictated by guidance, resulting in

unnatural and unrealistic vibration assessments [23–25,31]. The accurate prediction of the vibration response is a necessary component of design that, if not done correctly in the design phase, can pose a financial burden and cost time to retrofit after construction [6,7,13]. For example, the lateral sway retrofit of the London Millennium Bridge increased the bridge's cost by 30% [6,7,13].

The results of unreliable VSA can further lead to poor design scenarios where extra material is added to increase the stiffness or mass of a structure, despite all strength and static deformation limits being met. In the current context of the climate emergency and the need to urgently reduce whole-life carbon emissions, adding excess material could be considered wasteful [1,32,33].

Several researchers have attempted to review current guidance regarding vertical walking loads [9,23,24,27,34]. All agree that the proposed load models are limited, outdated, and do not accurately replicate the structure response compared to the real structural response [9,23,24,27,34]. A limitation of most studies is the need for more monitored structures [9,23,24,27,34]. Additionally, there is a lack of data historically used to form the vertical walking load models [19], [20] coupled with the lack of integration of human structure interaction effects distorting acceleration responses [35,36].

The current state of the VSA highlights several important limitations that persist throughout all guidance. Therefore, this thesis seeks to address and unify the current knowledge of the VSA, allowing for the reliable assessment of structures due to vertical walking forces.

The remaining sections of this chapter provide the objectives of the thesis along with the original research contributions (Section 1.2) and the organisation of the thesis (Section 1.3).

1.2 Objectives and main contributions of research

The overarching focus of the thesis is to reduce the error between numerical approximation and monitored outcomes of the vibration serviceability assessment for walking activities on structures. This focus is discussed by the constituting parts of reducing the error of the walking force time history model and the average moving human modal properties with

respect to physical measurements on real structures. The research's main scientific objectives and original contribution are summarised as follows.

- **Production of an updated Fourier series vertical walking load model borne from continuous measurements of walking**. A new Fourier series model accounts for the intra- and inter-subject variation of walking. The model is provided as an update to existing Fourier models, utilising continuous walking force measurements compared to previous single footfall measurements.
- **Evaluate current high and low-frequency load models in industry and research compared to real footfall measurements**. Therefore, producing a recommendation of the most accurate vertical load model or models in the low and high-frequency range, with respect to minimising the error between actual and predicted structural acceleration response.
- **Evaluate the suitability of moving human structure interaction parameters on an independent, flexible structure**. The evaluation compares the acceleration time history of various participants to their numerical analysis counterparts and recommends the most suitable model parameters. Finally, the investigation provides an inverse analysis to predict a new set of moving human parameters.

1.3 Organisation of text

The thesis is divided into six chapters, with a summative outline below for each chapter.

Chapter 1 of the thesis outlines the motivation and problem statement of the thesis. It provides an overview of the current state of the vibration serviceability assessment of structures and its limitations.

Chapter 2 reviews current literature regarding the human walking load and the multiple parametric forms it has taken. The review covers the time and frequency-based load models, including models that pertain to high and low-frequency structures. The study further investigates integrating human structure interaction effects into the serviceability assessment.

Chapter 3 investigates the current largest dataset of continuous walking force time histories, to the author's knowledge. The chapter's objective is to devise a generalised walking load that can be used for both high and low-frequency structures. The load model is constructed considering the inter and intra-subject variation of various parameters that describe the walking force. Finally, the chapter explores the variation in walking forces produced due to the sex of the walking participant.

Chapter 4 compares numerous current industry and academic walking load models, including the work of Chapter 3, in their ability to accurately approximate the vertical acceleration of structures. Multiple synthetic walking force models are compared to their real walking force time history counterparts. A robust assessment methodology is provided to cover an array of structural situations. Finally, recommendations for the most appropriate load models are given for various scenarios.

Chapter 5 presents an investigation to determine the average moving human structure interaction parameters through an inverse analysis of a flexible glass fibre-reinforced polymer bridge. 56 participants were recruited to walk over the bridge at four prescribed walking frequencies, with one of the walking frequencies being a resonant natural frequency of the first vertical mode. The inverse problem is solved through numerical simulations and presents a set of optimal design variables. Current parameters of the human structure interaction are then compared concerning measured acceleration responses.

Chapter 6 summarises the most relevant conclusions of the research and provides recommendations for future research concerning each chapter.

Chapter 2 Literature review

The present chapter provides an overview of the current research within the VSA. The investigation focuses on the vertical human walking load model, its various interpolations, and the representation and effects of the human structure interaction.

The magnitude and shape of the walking vertical force time history can vary from person to person [4,15,17,37]. The dynamic force generated by a single person is best described as a narrow-band process [29,30,38–42]. Therefore, the force and temporal parameters can vary from the characteristic M-shape of a single footfall in Figure 2.1.

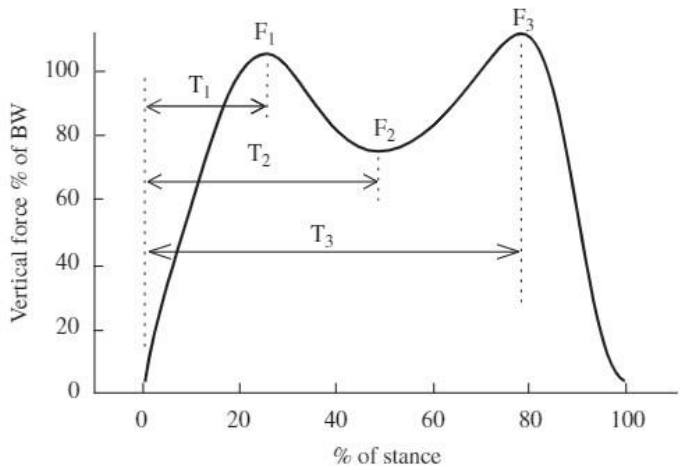

Figure 2.1 Vertical ground force reaction indicating a single footstep's key points and timing points. F1-F3 are the first peak, valley load and second peak, respectively, after [31]

Traditionally the vertical force is described via the Fourier series with limited integer terms truncated at the 4th integer [16,28,43–46]. Early studies considered the variability between successive footfalls (intra-subject) irrelevant for predicting vibration response

[44,45]. Historically within the context of Civil Engineering, ground force reaction (GFR) measurements were obtained from singular force plates that only consider a single step in the walking process [45]. This results in earlier models exhibiting no intra-subject variation [19,20,45]. Parameters of the Fourier series were based on temporally replicating the single footfall [45,47], limited by the equipment available in studies, thus inducing bias. Single footsteps do not adequately contain the necessary representation of the intra-subject variation. The frequency-domain expression of singular or double footfall temporally shifted differs from continuous walking measurements (Figure 2.2& Figure 2.3).

Biomechanics researchers have used continuous treadmill data of human gait since 1982 [48–50]. Using the instrumented treadmill allowed an unlimited number of successive steps to be recorded. However, civil engineers only recently recognised the need to include intra-subject variability [51].

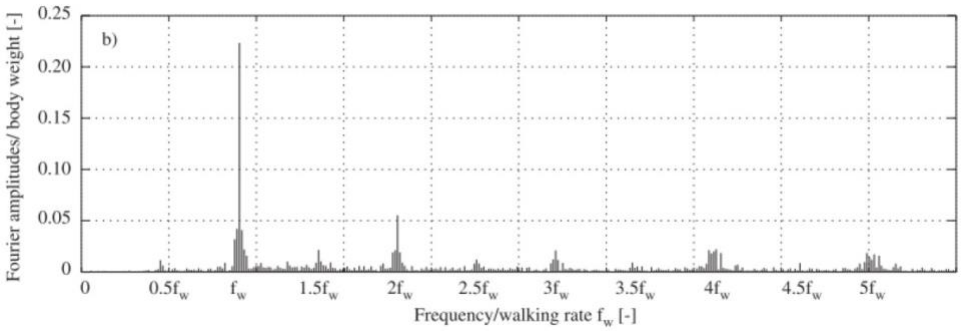

Figure 2.2 Frequency domain representation of discrete sampled walking load, showing energy leakage around harmonic values demonstrating intrasubject variation, after [52]

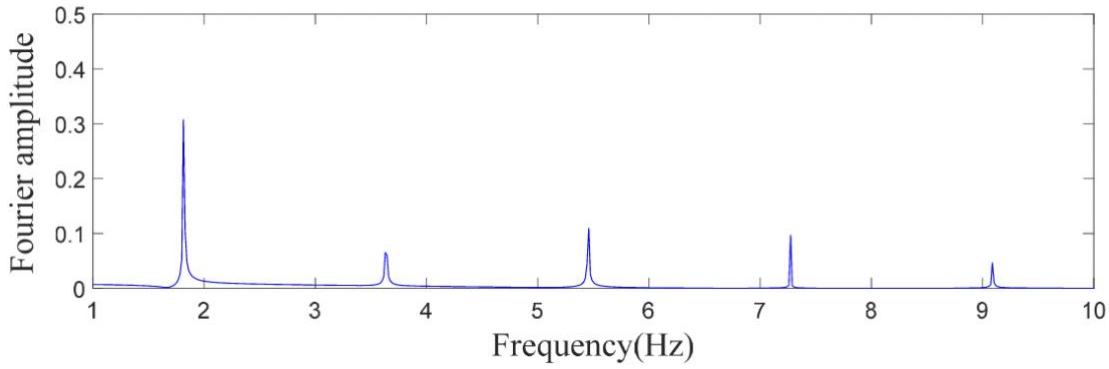

Figure 2.3 Frequency domain representation of double footfall temporally replicated walking signal. Sampled from a discrete signal but visualised as a continuous signal incorrectly after [53]

The proceeding chapter is divided into three key sections. Section 2.1 Time-domain models, Section 2.2 Frequency domain models and Section 2.3 Human Structure Interaction (HSI).

2.1 Time-domain models

Various methodologies exist to model the vertical force of walking in the time domain, from Fourier series [4,43–46,54] to polynomials [18,55] to modelling the auto spectral density of variance of the signal [52]. Such models are described in either a deterministic or probabilistic fashion. The proceeding subsections describe various time domain models and the statistical and deterministic parameters they pose. Section 2.1.1 demonstrates the division of load models based on a structure's natural frequency. Section 2.1.2 explains

Fourier series-based approximation of vertical loads. Section 2.1.3 presents probabilistic-based time domain models. Section 2.1.4 offers alternative time domain models. Finally, Section 2.1.5 presents high-frequency load models.

2.1.1 Low- Vs High-frequency structures

Historically, structures have been categorised into two broad groups of low or high-frequency structures for VSA [56]. The assignment to either group is based on the structure's characteristic vibration response and the structure's natural frequency. With each separate grouping being assigned a different load model. Low-frequency structures exhibit steady-state responses to walking forces, while transient responses characterise high-frequency structures. Previous and current guidance set hard limits on the boundary between high and low frequency [16,19–22,28,56] (Table 2.1). Zivanovic et al. [34] conversely demonstrated that the methodology produces erroneous results. When structures teeter on the borderline, neither force model represents the acceleration response for the high or low frequency correctly. The model that provided the closest prediction to the real response was that of the combined modelling of both high- and low-frequency models.

While most footfall models are based on a Fourier series approximation [16,19,20,28,55], they only contain force information to a limited number of discrete harmonics in the frequency domain. This is due to the nature of the measurement techniques when only single or double steps measurements are taken [45,53]. Therefore, the historical use of older force reconstructions has forced a false sense of belief in load models fundamentally changing on higher or lower natural frequency structures. The inability to reconstruct the full frequency content of walking has caused the deviation.

In high-frequency models, an impulse is used to model each footstep as energy content. In lower frequencies, it is deemed unnecessary as the structure's response is said to exhibit a transient response of each footstep[15,17,18]. Figure 2.4 demonstrates that this assumption is incorrect. Clear peaks around harmonic integers can be seen well into the 12th harmonic, so a resonant-like response is plausible. Therefore, a gap in research exists to form a generalised model that presents the entire frequency content of a vertical walking signal.

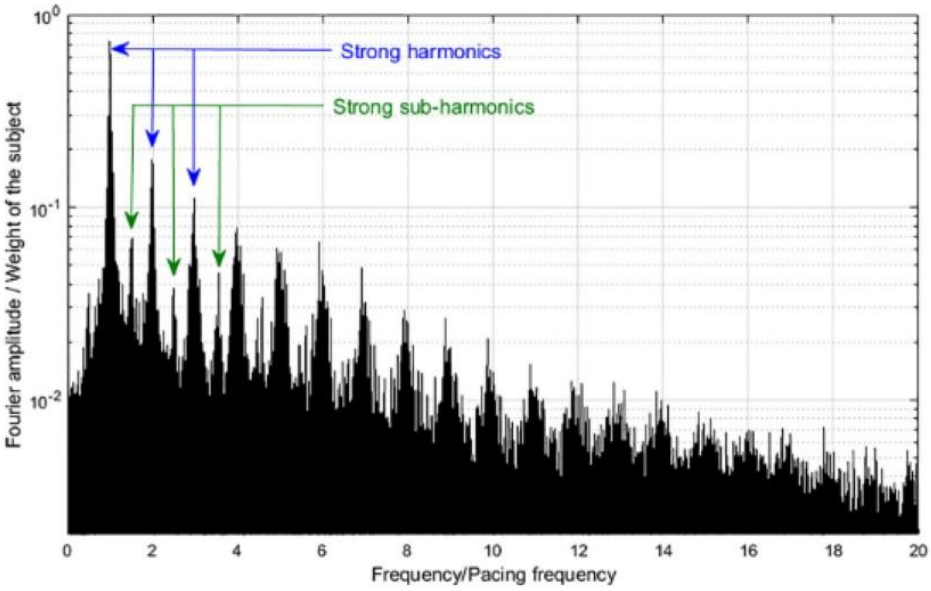

Figure 2.4 Frequency domain representation of typical walking signal showing the presence of harmonics of walking beyond the fifth harmonic, sub harmonics and the lowering magnitude of successive harmonics after [17]

Brownjohn and Ellis [15,57] indicate that the typical cut-off frequency between high and low-frequency structures (Table 2.1) is overly conservative. A resonant response can occur with fundamental frequencies above 15 Hz. Substantial research efforts have been focused on low-frequency structures due to the larger proportion of constructed structures exhibiting lower-frequency natural modes [5,58]. Such historical bias has caused researchers to have oversight of the real issue of producing a universal model that can model the entire frequency domain. Only limited studies provide adequate models simultaneously describing the high and low-frequency content of walking signals [51,52].

Most current low-frequency vertical load models are curtailed at the fourth [16,19–21,28] or fifth [43,59] harmonic of walking. No information is seen after 12.5 Hz. However, Figure 2.4 contradicts this statement and shows similar Fourier amplitude values for higher integer harmonics after this limit. The exclusion of higher energy content is not critical to low-frequency structures. However, it is required when designing a structure to the stricter and smaller range of vibration limits for high-frequency structures or structures with multimodal responses.

Table 2.1 Cut-off frequency of low to high-frequency structures.

Author	Cut-off frequency (Hz)
Ohlsson [60]	8
Wyatt et al. [61]	7
Mohammed et al. [17]	14
AISC Design Guide 11 [16]	8.8
ISO 10137 [21]	8-10
Technical report 43 appendix G [28]	11.2
CCIP Mean value [20]	11.2
CCIP design value [20]	11.2
SCI P35[19]	8.8
SETRA [55]	7.2
Zivanovic et al. [62]	12.5
García-Diéguez et al.[63]	13
Varela et al. [64]	7.8

2.1.2 Fourier series

Traditionally time-domain models are presented as a deterministic process [54–57] through a Fourier series of harmonic integers of walking frequencies:

$$F(t) = W\left(1 + \sum_{n=1}^{N} DLF_n \sin\left(n\, 2\pi\, f_p t + \theta_n\right)\right) \quad \text{Eq 1}$$

Where W is the pedestrian weight, DLF is the dynamic load factor (Fourier amplitude), n is the integer harmonic of walking, f_p is the walking frequency θ_n is the phase angle of the integer harmonic of walking.

The parameters of the Fourier approximation vary throughout the literature and do not produce a consensus [Section 2.1.2.1 - 2.1.2.4]. The variation can be due to data acquisition techniques, sample population size and ethnicity, all contributing to statistically different results of force time history parameters. It is demonstrated that such a deterministic approach to modelling individual pedestrian loading needs to be revised under the industry's recommended guidance [9,20,28,44,69]. The following subsection presents the deterministic and statistical ranges for all inputs into the Fourier model, Eq 1.

2.1.2.1 Walking Frequency

A comprehensive collection of the mean and standard deviation of walking frequencies can be found in Table 2.2. The inter-subject variation of the walking frequency is typically represented through a normal distribution [35,41,58–65]. Matsumoto [58], Zivanovic [43] and Pachi [59] all demonstrate lower walking frequencies on footbridges. This is hypothesised to result from the human tendency not to excite resonant modes causing excessive vibrations and avoiding "lock-in" mechanisms [77].

Variations in walking frequencies can be seen country-by-country, directly resulting from countries' cultural norms or average temperatures affecting the speed and, coincidently, the walking pace [78]. Zivanovic [34] states that step length and walking frequency are independent normal distributions. However, there exists a physically defined relationship between both parameters. This fact should be remembered in vibration assessments. This oversight may increase the variance in the evaluation, resulting in the unnatural injection of variation from sampling extreme results. Additional work must be conducted to provide the conditional probability of walking frequency, step length and speed concerning each other.

Table 2.2: Mean and standard deviation of walking frequencies from various studies

Author	Mean Walking Frequency (Hz)	The standard deviation of walking frequency (Hz)	Country	Population size
Matsumoto et al. [58]	1.99	0.173	Japan	505
Zivanovic [43]	1.87	0.186	Montenegro	1976
Pachi [59] Footbridge	1.80	0.11	United Kingdom	400
Shopping centre	2.0	0.13	United Kingdom	
Male Footbridge	1.80	-	United Kingdom	
Female Footbridge	1.86	-	United Kingdom	
Male Shopping	2.00	-	United Kingdom	
Female Shopping	2.03	-	United Kingdom	
Varela et al. [60]	1.71-1.77	-	Brazil	6
Schulze et al. [61]	2.00	0.13	Germany	N/a

Kramer et al. [62]	2.2	0.2	Germany	N/a
Chen et al. [37]	1.937	0.296	China	2204
Zhang et al. [63] Force plate	1.7958	0.1347	China	9101
Zhang et al. [63] Video	1.87	0.1713	China	11387

An unbiased comparison of studies is difficult to achieve with various population sizes, ethnicity, location, and measurement techniques. Comparing Zhang et al. [63] 's two methods of data acquisition (i.e., force plates in a cafeteria compared to video analysis of a hallway), there is a difference in the mean and standard deviation. Such a study indicates that assuming overlapping populations, the analysis methods are inconsistent, or the measurement location affects walking characteristics, a research area presently unfounded. Other studies have used rudimentary approaches, leaving the results open to questionable validity. Pachi et al. [59] used a stopwatch to count the number of steps over a given distance. No recording was conducted, nor was there any indication of any other person to cement the result of the single-person counting and timing.

Variations in male and female participants are seen through the studies of [53,71,79] and indicate differences in walking characteristics. It is shown that women walk at higher walking frequencies but at slower speeds and shorter step lengths. Whittle et al.[79] (Table 2.3) demonstrates that the onset of age results in a natural decrease in walking frequency, stride length, and velocity for both males and females. The results show that the decline in each value is more pronounced in males. Females show a reduction in walking frequency but more considerable stride length and speed reductions at older ages than males. Such age-related variations are not currently seen in practice.

Table 2.3 Age dependant variations in walking frequency, stride length and velocity, after [79]

Age (Years) /Gender	Walking Frequency (Hz)	Stride length (m)	Velocity (m/s)
18-49/Female	1.63-2.30	1.06-1.58	0.94-1.66
18-49/Male	1.51-2.25	1.25-1.85	1.10-1.82
50-64/Female	1.62-2.28	1.04-1.56	0.91-1.63
50-64/Male	1.36-2.10	1.22-1.82	0.96-1.68
65-80/Female	1.60-2.26	0.94-1.46	0.80-1.52
65-80/Male	1.35-2.08	1.11-1.71	0.81-1.61

Intra-subject variations of the walking frequency are rarely monitored. This intra-subject variation leads to the natural narrow-band and energy leakage around harmonics. Researchers have means to directly quantify this process by empirically modelling the energy leakage around harmonics in the frequency domain [34,38–41,52,80] or by sampling each step individually in the time domain [46,51,52,59,81]. Brownjohn et al. [29] and Chen et al. [4] indicate that the coefficient of variation (CoV) of intra-subject variation of walking frequency is 3% - 3.25%. García-Diéguez et al. [59] similarly defines the intra-subject variation of walking frequency through the successive time intervals between steps. García-Diéguez et al. [59] describes the time intervals through several interdependent empirical factors.

Besides sampling the walking frequency from the various independent probability distributions, authors define the walking frequency through alternative relationships. Walking frequency, step length, and speed are all interconnected. Thus, knowing two values of the relationships, the third can be inferred:

$$f_p = \frac{v}{l} \qquad \text{Eq 2}$$

Where l is the step length (Section 2.1.2.6) and v the walking velocity (Section 2.1.2.5). Other proposed relationships are seen, such as Butz [82] linear model of the walking frequency concerning walking velocity:

$$f_p = 0.7886 + 0.7868v \quad \text{Eq 3}$$

whilst Riccardelli et al. [83] proposes lower walking frequencies for the given velocity

$$f_p = 0.024 + 0.754v \quad \text{Eq 4}$$

Venuti et al. [84] propose a cubic function by fitting the data of [50]:

$$f_p = 2.93\,v - 1.59v^2 + 0.35v^3 \quad \text{Eq 5}$$

Most velocity equations, barring that of Venuti et al. [84], do not hold physical mean at velocities out of the range of the experiment whence they were derived. The equations show a residual walking frequency at zero velocities for linear mapping. Therefore, whilst the models fit the data analytically, it does not hold for all physical ranges.

The use of narrow-band vertical walking forces in industry is non-existent, mainly due to the complexity of most narrow-banded models that need to be better-suited to the intended user: industry engineers [43,52,63]. A common reoccurrence within the review is the need for more clarity between current research and current best practice in industry [9]. Furthermore, consideration for the likelihood of a walking frequency matching a natural vibration mode and causing resonance needs to be addressed in the guidance [16,19,20,28]. Current guidance assesses a structure based on a worst-case scenario, even when the probability of the outcome is near negligible.

2.1.2.2 Weight

Table 2.4 and WHO [85] reveal that the mass or weight characterisation varies with geographic location and sex. Consideration of the weight distributions in Eq 1 has never been addressed in the context of VSA of structures. Current international guidance reduces this parameter to a singular deterministic value of 750 N [16,19,21,28]. However, multiple weights should be sampled to provide a comprehensive structural assessment. The assessment of a structure should determine the likely range of all outcomes, not an idealisation and simplification of the expected acceleration output.

Table 2.4 Variation of the weight of pedestrian from various studies.

Author	Mean Weight (N)	CoV
International Guidance [16,19,21,28]	750	-
Walpole et al. [86] - Global Average	608	-
Walpole et al. [86] - USA	804	-
Walpole et al. [86] - UK	736	-
Walpole et al. [86] - China	598	-
Pedersen et al. [87] - Denmark	-	0.18
Chen et al. [37]- China	641	0.15
Portier et al. [88] - USA	784	0.25

2.1.2.3 Dynamic Load Factor (DLF)

DLF values are the Fourier amplitudes of the approximated pseudo-periodic load. In this manner, the Fourier series replicates discrete integer values of the frequency domain in lieu of modelling the entire frequency domain. The DLF values are not correlated to pedestrian weight [52]. Therefore, DLF and weight variables can be uncoupled.

Extraction methods of the DLF are often naïve. Peak picking of the Fourier amplitudes in the frequency domain is often a result of the data quality. When singular or a limited number of steps are temporally replicated, unnatural distributions of energy leakage around harmonic integers are seen [20,28,45,53].

In recent years more advanced methods of data measurement have been used, such as treadmills [51,59], insole pressure sensors [26,46,80,81], Computer Vision [92,93], and Inertial measurement units (IMU) [94–97]. Ahmadi et al. [90] demonstrated (Figure 2.5) that all the data measurement methods produce some consensus. As there is no baseline of walking force signals, it is merely speculation about which method reproduces vertical walking forces correctly. Racic et al. [31] provides an in-depth comparison of methods, along with detailed merits and flaws of each technology and their suitability.

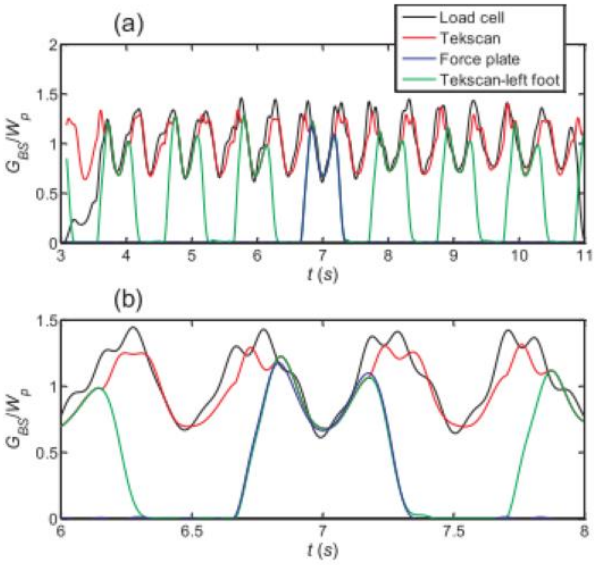

Figure 2.5 Comparison of various data measurement techniques of the vertical walking force, load cell, insole pressure, force plate, after [90]

Table 2.5 Historic DLF values from DLF_1 to DLF_4 obtained from various industry and research sources

Label	Author	Year	1st Harmonic	2nd Harmonic	3rd Harmonic	4th Harmonic
M1	Blanchard [65]	1977	0.257	-	-	-
M2	Bachmann[66]	1987	0.37	0.1	0.12	0.04
M3	Allen et al. [67]	1993	0.5	0.2	0.1	0.05
M4	Petersen [98]	1996	0.073 0.408 0.518	0.138 0.079 0.058	0.018 (1.5Hz) 0.018 (2Hz) 0.041 (2.5Hz)	-
M5	Kerr [45] Mean	1999	$-0.265f_p^3+1.321f_p^2-1.760f_p+0.761$	0.07	0.05	-
M6	Kerr [45] 5%	1999	$-0.1801f_p^3+0.898f_p^2-1.1966f_p+0.5177$	-	-	-

M7	Kerr [45] 95%	1999	$-0.3497f_p^3+1.7432f_p^2-2.3228f_p+1.0049$	-	-	-
M8	BS 5400[99]	1999	0.24 (180 N)	-	-	-
M9	Ellis [100]	2000	-	-	0.07	0.07
M10	Allen et al. [56]	2001	$290\ e^{-0.35fp}$ floors $410\ e^{-0.35fp}$ footbridges	-	-	-
M11	Japanese load code [101]	2004	0.4	0.2	0.06	-
M12	Brownjohn et al. [29]	2004	$0.37\ f_p - 0.42$	0.053	0.042	0.041
M13	SETRA[55]	2006	0.4	0.1	0.1	-
M14	Willford et al. [102] 75%	2006	$0.41(f_p - 0.95)$	$0.069+0.0056x2\ f_p$	$0.033+0.0064x3\ f_p$	$0.013+0.0065x4\ f_p$
M15	Willford et al. [102] mean	2006	$0.37(f_p -0.95)$	$0.054+0.0044*2\ f_p$	$0.026+0.005x3\ f_p$	$0.010+0.0051x4\ f_p$
M16	Zivanovic [43,62]	2006	$-0.2649f_p^3+1.3206f_p^2-1.7597f_p+0.7613$ Std. 0.16	0.07 s.d. 0.03	0.05 s.d. 0.02	0.05 s.d. 0.02
M17	ISO 10137 [21]	2007	$0.37(f_p - 1)$	0.1	0.06	0.06
M18	Smith [19]	2007	$0.436\ (f_p- 0.95)$	$0.006(2\ f_p+12.3)$	$0.007(3\ f_p+5.2)$	$0.007(4\ f_p+2)$
M19	Nguyen[46] 90%	2013	$0.313\ f_p - 0.226$	$0.113\ f_p - 0.078$	$0.037\ f_p + 0.008$	$0.036\ f_p - 0.002$
M20	Nguyen[46] 95%	2013	$0.406\ f_p - 0.355$	$0.126\ f_p - 0.084$	$0.031\ f_p + 0.027$	$0.047\ f_p - 0.014$

M21	Chen et al. [37]	2014	$0.2358f_p - 0.2010$	0.0949	0.0523	0.0461
M22	Toso et al [54]	2016	$0.22f_p^2-0.45f_p+0.35$	$0.0243+6.87*10^{-5}c-2.46*10^{-6}$	$-0.0638+0.0024M-1.09*10^{-6}K+1*10^{-8}MK-1.38*10^{-5}M^2$	-
M23	AISC design guide 11 [16]	2016	0.5	0.2	0.1	0.05
M24	Zhang et al[53]	2017	Mean 0.4058 Std. 0.1663	-	-	-
M25	Chen et al. [4]	2019	$0.301f_p - 0.323$	$0.0301f_p+0.053$	$-0.054f_p+0.264$	$-0.1121f_p+0.053$
M26	Varela [64]	2020	$0.1556\ f_p^2-0.1816*f_p+0.0356$	0.065 if $f_p < 2$ $0.1958\ f_p-0.3266$ if $f_p > 2$	-	-

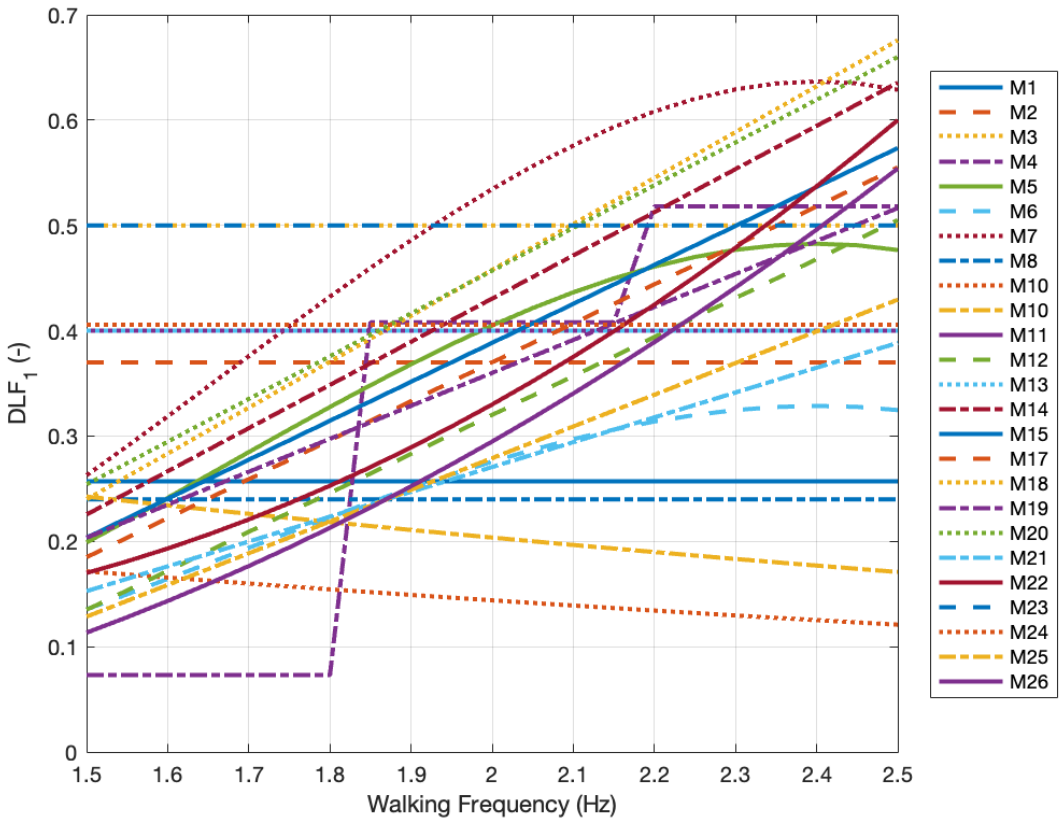

Figure 2.6 Comparison of DLF_1 models from the models of Table 2.5

Figure 2.6 and Table 2.5 illustrate the wide variation in the DLF_1 values (First integer DLF). There is no clear trend in data, with some values increasing and others decreasing with walking frequency. Such variation is likely attributed to differing extraction and measurement techniques. The outcomes of [19,20,28,45,53,65,68,103] are the results of single or double footfall analysis, and the data is misrepresentative of real walking forces that naturally vary spatially and temporally. Including such limited data biased the DLF models; the models are based on a limited number of footfalls. Kerr's [45] dataset contains only 1000 individual steps, compared to Racic et al. [52] dataset of continuous treadmill vertical force time histories encompassing over 1.7 million steps. Thus, including data from poor-quality sources produced a falsehood surrounding the reliability of industrial DLF load models [16,19–21,28].

Table 2.5 illustrates that the DLF is often described through a walking frequency or a deterministic value. This reflects the extraction method of DLF, with most favouring Fourier Transformation (FT) of the data into the frequency domain and then extracting the peak value. Other authors [54,104–106] have tried to estimate DLFs based on different parameters such as velocity, mass, stiffness and damping of the participant. However, the latter studies of [53,95–97] are subject to low participation numbers in their experiments, compared to other published studies, leading to statistically unreliable results. As such, the results are overfitted to the relatively smaller populations, and do not generalise.

Both Kerr [45] and Varela et al. [64] indicate a robust positive correlation between the first and second DLF values and participants' heights, the latter producing a stronger correlation of results concerning the first DLF, compared to excluding the height of participants in the DLF calculation. Varela et al. [64] attributes the change in DLF pertaining to height as the result of taller people more likely having bigger feet, and therefore, resulting in larger potential energy transferred from the foot. However, this rationale needs to be founded with citation or justification and is currently only hypothesised by Varela et al. [64].

The deterministic nature of the DLF models suggests that there is an "absolutely correct" value of DLF for a given walking frequency (Table 2.5). Zhang et al. [53] and Zivanovic et al. [34] made a rare attempt to represent the DLFs variation through a Gaussian or log-normal distribution. However, the suggested distributions occasionally produce a negative DLF value, which is physically counteractive to the true nature of walking, and demonstrates where the physical limitations of empirical models exist. A more complete data set, such as [52] must perform an in-depth statistical regression analysis defining the likelihood of possible DLFs.

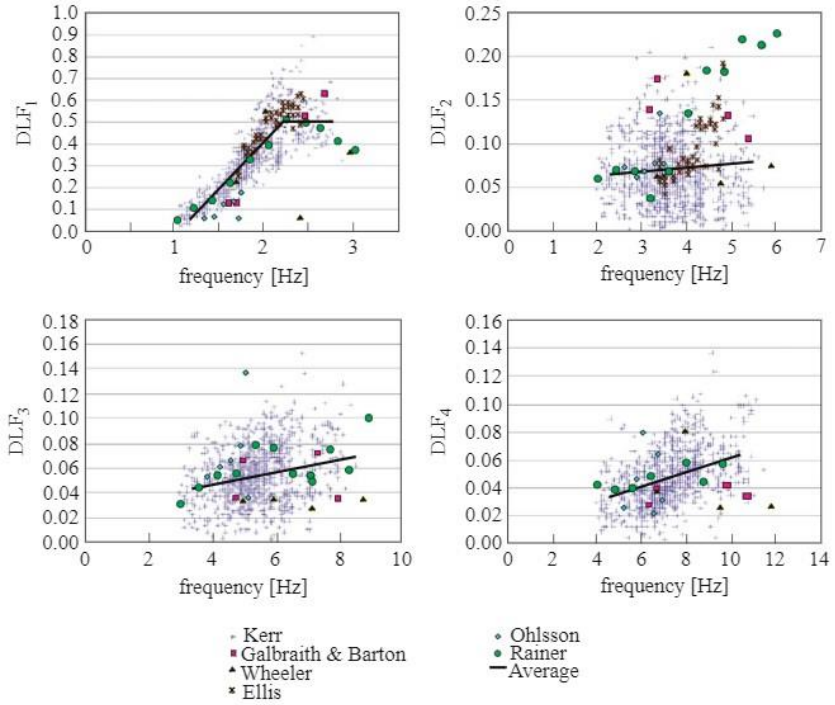

Figure 2.7 Data points of DLF 1 - 4 from [45,47,100,107,108]

Studies have tried to estimate "error" bounds on DLFs [20,45,46]. Misguidance has resulted in authors producing the *likelihood* of the parameters describing the DLFs. This is evident because any error inference should be independent of model parameters [109,110]. Therefore, any estimation provided, such as 95% of the DLF, makes the frequentist statistic statement, "*for similarly drawn samples, the true value of the parameter occurs within the interval 95% of the time*". This statement, therefore, does not show the variation in DLF but an estimate that the true value of the parameter describing the DLF is within a specific interval a proportion of the time. This misunderstanding has likely arisen due to a need for more knowledge. However, using Willford's Arup model [20] is the most common practice. The claim of adding a 75% probability of exceedance is misguided. Such practices artificially increase each DLF and neglect most of the population.

Further to Table 2.5, limitations arise for each model. Whilst Section 2.1.2.1 provides the statistical range of the walking frequency, various models have limited their capacity to cover all possible ranges of walking frequencies.

Table 2.6 Limits on walking frequency ranges for each Fourier series model identified.

Model	Walking frequency limits (Hz)
AISC Design Guide 11 [16]	1.6-2.2
ISO 10137 [21]	1.2-2.4
Technical report 43 appendix G [28]	1-2.8
CCIP Mean value [20]	1-2.8
CCIP design value [20]	1-2.8
SCI P35[19]	1.6-2.2
SETRA [55]	1.6-2.4
Peters et al.	1.5-2.5
Zivanovic et al. [62]	1.5-2.5
García-Diéguez et al.[63]	1.5-2.6
Racic et al. [52]	1.5-2.5
Muhammad et al.[51]	1.5-2.5
Varela et al. [64]	1.4-2.6
Chen et al. [4]	1.4-2.6
Zhang et al[53]	1-3
Toso et al [54]	1.35-2.12

Researchers have shown that walking occurs through a normal distribution centred at 1.8-2Hz and can exceed walking frequencies of 1 – 3Hz [53,70,71]. Therefore, limiting the walking

frequency of a model devalues structures with natural frequencies just out of the range. The limitation of international guidance on walking frequency further causes misinformation about vertical walking forces by perceiving walking frequencies out of the ranges as unimportant. This may result in higher-order harmonics of a lesser walking frequency being used to match a resonant mode instead of a higher-frequency first-order mode. Furthermore, the curtailment of walking frequency is concerning since the data used to model the DLFs of the limited model is primarily from Kerr[45], where walking frequencies from 1-3Hz are monitored and measured.

The direct comparison of all the DLF models is difficult due to varying population sizes, ethnicity, extraction techniques, and genders. No study exists that investigates evidence of differing DLF or walking characteristics based on ethnicity or location of the population. There exist several varying approximations of DLF values (Figure 2.6). However, more guidance is needed on the suitability of the models to model the vertical walking force accurately compared to real measurements. Present industry models such as [16,19,20,28] use data that does not adhere to more appropriate extraction methods. Therefore, a gap in research on the accuracy of each current load model compared to real measurements is identified.

2.1.2.4 Phase Angle

More research is needed on the various phase angles of the Fourier model of single-person excitation. This is partly due to the limited data and information on the Fourier transform of single temporally shifted data. Furthermore, single-person excitation and the corresponding relative phase angles of harmonics provide little additional information on the vibration response when a structure is dominated by one vibration mode. Phase angles become essential only when multiple persons and/or multimodal responses occur. Historically, likened to DLFs, phase angles are given as a deterministic value [16,19,20,28]. However, Zivanovic et al. [62] and Racic et al. [52] demonstrate that phase angles are more aptly described as a uniform random distribution across all frequency ranges bounded by $-\pi$ and π. Varela et al. [64] determine the second and third harmonic phase angles through their statistical representation mean 85.6, 89.4 and standard deviation: 38.3 and 23.7 degrees.

Varela et al. [64] data does not follow any known distribution. Using the deterministic nature of phase angle seems implausible as it assumes that there is an absolute way to walk for a given walking frequency. However, it has been previously demonstrated that walking is a stochastic process ideally structured through random or quasi-periodic (narrow-banded) processes.

2.1.2.5 Average walking velocity

The average walking velocity is an overlooked parameter of the human walking model [2,52,111]. Whilst the velocity does not traditionally feature in the Fourier force equation, it is required to know the position and time to cross the structure and thus is crucial to the modal force. The key parameters that dictate the velocity of human locomotion are step length and walking frequency. Both parameters have been shown to have varying experimental relationships with one another (Section 2.1.2.1 and 2.1.2.6). Studies [112–115] establish a linear relationship between walking velocity and step length. When determining these variables experimentally, controlling one parameter leads to varying relationships between walking frequency and speed [116].

Table 2.7 provides estimations of the mean and standard deviation of walking speed from various studies. Whilst some authors chose a probabilistic range [117,118], others determined an expected value based on mean free walking speed [119,120]. Venuti et al.[84] proposes that when spatially unrestricted, walking yields a free flow of pedestrians dependent on geographical area and the travel purpose. The model distinguishes between leisure, commuting or rush hour and geographic location.

$$v = \bar{v}\alpha_G\alpha_T \qquad \text{Eq 6}$$

Were $\bar{v}$ is the average free speed (1.34 m/s) [119], and α_G and α_T are related to geographic and travel purposes, respectively. In cases where pedestrian density is greater than $0.7 person/m^2$, pedestrians' free movement is restricted, and the influence of other humans must be considered. Therefore, the velocity reduction is seen as a function of pedestrian density. The velocity v is formulated by [120] and then generalised by [84]:

$$v = \bar{v}\left(1 - e^{-\gamma\left(\frac{1}{d} - \frac{1}{d_{Jam}}\right)}\right) \quad \text{Eq 7}$$

Where $\bar{v}$ is the average free walking speed, γ is the fitting constant, and d_{jam} is the maximum pedestrian density before a zero speed is reached. Venuti et al. [84] give the jamming density between 5-6 *persons/m*^{2} and states that the variability dependent on geographical area and travel purpose. Similarly, Weidmann [120] provides the jamming density as 5.4 *persons/m*^{2}.

Table 2.7 Mean and standard deviations of walking velocity from various studies

Author	Mean speed (m/s)	Standard deviation (m/s)	Location
Fruin et al. [121]	1.40	0.15	USA
Hankin et al.[122]	1.60	n.a.	UK
Koushki et al.[123]	1.08	n.a.	UAE
Lam et al.[124]	1.19	0.26	Hong Kong
Pauls et al.[125]	1.25	n.a.	USA
Ricciardelli et al.[126]	1.41	0.224	Italy
Sahnaci et al.[118]	1.37	0.15	n.a.
Butz et al.[127]	1.23	n.a.	Germany
Virkler et al. [128]	1.22	n.a.	USA
Weidmann [120]	1.34	n.a.	Germany
Sahnaci et al. [117]	1.54	0.18	Germany

Buchmueller et al. [119]	1.34	n.a.	Germany

Daamen [129] provides a survey of all walking speeds. Daamen [129] indicates that walking speeds are appropriately modelled through a Gaussian distribution. Table 2.7 results also indicate a variation in velocity depending on the country of origin. Koushki [123] showed that Saudi Arabian people have a mean walking speed of 1.08 m/s, whilst the counterparts of Hankin et al. [122] in the United Kingdom have an average free walking speed of 1.6 m/s. Hankin et al. [122] results are the fastest in Table 2.7. However, the estimates are based on the walking speeds of schoolboys. The results were also taken from two manual stopwatches in less-than-ideal experimental conditions, so the findings are only partially justifiable due to the skew in population and methodology. Koushki [123] hypothesises that the regional effect of walking speed is due to the greater distances on average people surveyed were walking along with the extreme temperatures resulting in all together slower speeds.

Pedersen et al. [130] found that the walking velocity is independent of the response and hypothesised that if a realistic value is chosen, there is no need to consider it a random variable. Keller et al. [131] and Masani et al. [132] demonstrate the relationship between a person's velocity increases and the maximum vertical force normalised by weight in male and female participants. The study concluded that the maximum force exerted was linearly correlated up to a velocity of 3.5 m/s, where the maximum force appeared to then plateau.

Figure 2.8 presents the variation in the walking frequency with walking speed. The possible range of walking frequency is vast (1-3Hz), and as such, deterministic relationships of velocity mapping to walking frequency need to be better-posed and can result in prominent misconceptions of relationships. Other stochastic processes are required in the VSA to account for the variation of walking velocity to walking frequency. More fundamental research on the complexity of velocities involvement within the VSA is needed.

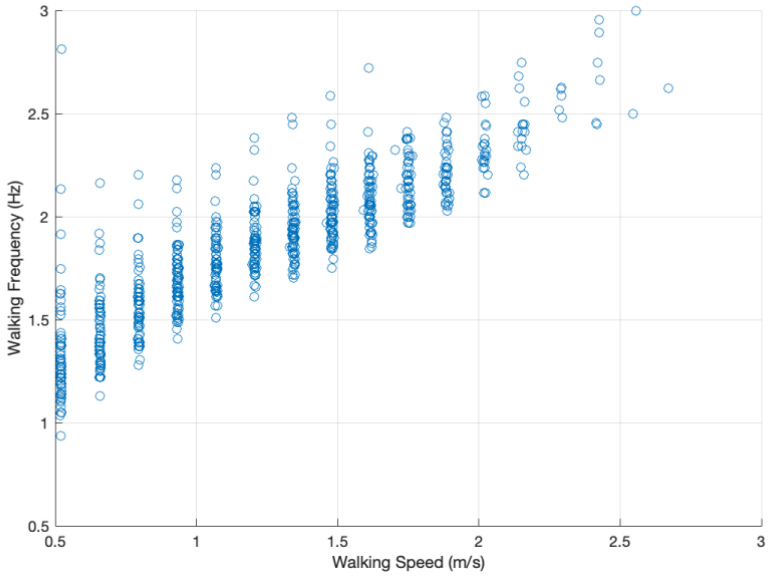

Figure 2.8 Walking velocity vs walking frequency showing the linearity of the data, from the dataset of Racic [52]

2.1.2.6 Step length

Step length is typically defined through the normal distribution N(0.71,0.005) [m] [71,83,118,126]. No study has yet to establish any co-dependent experiment evidence of step length due to the difficult task of controlling step length. Therefore, the variable is randomly assigned or inferred, given knowledge of the walking frequency and velocity.

2.1.3 Probabilistic walking force models in the time domain

As seen in Section 2.1.2.3, the DLF magnitude varies across all walking frequencies. However, such a variation is not seen in models. These deterministic models are hypothesised to result from a binary pass or fail of VSA. Such assessment results in a worst-case design scenario even if the probability of such an outcome is low.

Mohammad et al. [51] used the experimental data set of [52] to produce a probabilistic framework as a function of the walking speed for individual steps. The key parameters are the walking speed, step contact time, double-stance period of walking, first peak time and load,

valley time and load, and second peak load and time (Figure 2.9). Each parameter's successive steps are sampled considering the inter and intra-subject variation. The inter-subject variation of the parameters is independent of each other. This lack of correlation with each parameter may lead to overestimating the variance of the loads due to sampling extreme results. The model does not address all the co-dependent relationships of the distribution. As noted in Garcia-Dieguez et al. [59], the main problem with most probabilistic models is that spatial and temporal factors are considered independent, thus inducing a higher level of variance in the structural response.

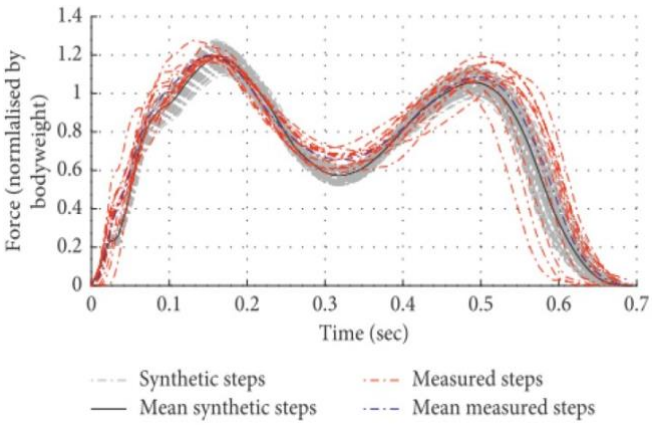

Figure 2.9 Reconstruction of footsteps for the same average walking frequency via the method of Muhammad et al. [51]

Chen et al. [4] proposed using intra and inter-subject variation factors that describe each DLF and walking frequency for successive steps. Chen et al. [4] demonstrates that the intra-subject variation of DLF is walking frequency independent and can be expressed through a standard distribution independently. Garcia-Dieguez et al. [104] present a step-by-step stochastic walking model based on variable time periods and DLF values. Both parameters are computed for each footstep via sampling various relationships describing mean values and their variation over time, along with an auto-regressive component and error term distribution. The model produces DLF values lower in magnitude than Kerr's [45]. The model is computationally more complex and less likely to be used in industrial settings due to the

amount of empirically fitted data and/or the time-consuming nature of getting force histories. The model is validated against the experimental results of Racic et al. [51], and produces a close consensus with the treadmill force time signals. The likeness in data indicates that both datasets come to similar conclusions. The model is a natural progression of Chen [4], providing interconnect relationships of parameters and demonstrating that the parameters are auto-regressive to some degree and not completely random.

2.1.4 Alternative time-domain models

Attempts have been made to transition away from the Fourier modelling approach [18,51,133]. Middleton [18] and Muhammad et al. [51] fitted the single footfall trace to several critical points on the force curve (1st peak, valley load, and second peak in Figure 2.9) and several other intermediate points. The force at the intermediate points is then linearly fitted to the three key points to produce the entire spline curve from 17 and 34 different interpolation points, respectively. Similarly, the time to each point was fitted using nonlinear regression to present the full walking load. Muhammad et al. [51] model considers inter and intra-subject variations of the three key points and overall step time to provide a model that represents the natural narrow-band nature of walking.

Feldmann et al. [133] developed a force model using an eighth-order polynomial function to model the individual footsteps. Each fitting parameter is found empirically based on a fitting process dependent on the walking frequency f_p. Muhammad et al. [24] demonstrate that the Feldmann et al. [133] model produces force magnitudes and acceleration responses far greater than that of its likened guidance [16,19,20,28] and overestimates the actual vibration response of real walking.

Racic et al.[52] proposed a stochastic process that models both the inter-and intra-subject variability of the vertical walking load. The inter-subject variation is modelled through the force-time history of 842 different instances of continuous walking. The shape of the footfall is described using multiple Gaussian functions. The variable footfall timings are generated from an Auto Spectral Density (ASD) of their variation. Two signals with zero mean and the same standard deviation have the same ASD. Moreover, they have statistically the same

pattern of variation for successive footfalls. Using random phases, variations can be artificially generated. Because of random phases, the two signals are never the same but have the same standard deviation.

No comparative study or analysis has been performed to determine the most accurate vertical load model with respect to any metric of analysis. As demonstrated, many load models are in circulation, yet more research needs to be focused on selecting the most accurate or applicable load model that represents universally models vertical walking forces.

2.1.5 High Frequency structures

Contemporary load models do not contain information in higher frequencies, and a high-frequency force function is required. This issue results from singular walking force records with limited information at higher frequencies. It is estimated that this area of research will soon be phased out when more general load models are developed, such as that of Racic et al. [52]. Nevertheless, some researchers have built improvements on the historical models. The most used model is Arup's effective impulse model [20]. The effective impulse is derived from Kerr's [45] temporally shifted data and, therefore, already exhibits inherent bias in the data. Each force was simulated on a SDOF system with a mass of 1Kg and varying natural frequency from 10- 40 Hz. Next, the resulting velocity of the system is taken. The peak velocity is numerically equivalent to the integral of the force-time history over one step. Such an impulse is defined as the effective impulse. The effective impulse is defined as :

$$I_{eff} = A\frac{f_p^{1.43}}{f_n^{1.3}} \qquad \text{Eq 8}$$

F_p is the walking frequency, f_n is the structure's natural frequency, A is the fitting constant taken as a mean of 42, and the effective impulse has a standard deviation of 0.4. Wilford et al. [20] suggest using A equal to 54 to give a 25% chance of not exceeding. The use of arbitrary statistical limits results in unnatural increases in structural response. SCI guidance [19] suggests A to be 64 due to the requirements of BS EN 1990 [134]. Pavic et al. [135] compared the model of Arup and found that whilst in 2003 it was the most ubiquitous used in

2003, it still overestimated the response of actual structures. The models indicate that a non-resonant reaction occurs from 10Hz due to the limits set in Table 2.6. However, this statement is countered by the increase in the high to low-frequency range cut-off shifting higher, as seen in Section 2.1.1. Furthermore, with the advancement of vertical walking measurement techniques, researchers have tended toward multiple footfall measurements [38,52,63]. Such representations indicate peaks in the frequency domain exist well beyond the 4th harmonic of walking frequency, showing a resonant response is likely to occur if a vibration mode lies at the resonant natural frequency.

Mohammod et al. [17] proposes a new high-frequency model based on data from treadmills provided by [52]. The model also includes damping "amplification effects" due to near harmonic integer of walking at higher harmonics, causing a resonant-like response. The amplification factor is based on an imperial function of the natural frequency of the structure (from 14Hz- 40Hz) and the walking frequency. Mohammod et al. [17] damping "amplification effects" are introduced to account for near resonant harmonics of a walking frequency with a resonant mode of the structure, above 14Hz and damping ratios different to 3%. Mohammod et al. [17] model gives a closer approximation to the actual response of the simulated structure. However, a thorough investigation of the current model has yet to be performed, so it is unclear if the model is universally better.

Models like those mentioned above are used widely because they appear in current industry guidance as best practices. Still, current models exist in academia that represent the entire frequency domain [43,51,52,59]. Presenting separate models depending on limits attributed to the quality of data acquisition at the time, such as in Table 2.1, seems redundant. Therefore, a shift in perspective of modelling walking is suggested, enabling one to model the entire frequency domain and not just discrete pockets.

2.2 Frequency domain models

The discrete integer Fourier series modelling approach needs to address the narrow-band nature of walking. As such, the frequency content around the harmonics of walking frequencies is not considered. A time signal can be defined through the infinite Fourier series

but is often truncated for reasons described in Section 2.1.1. Due to the duality of the time and frequency domain, vertical walking forces can be expressed through a narrow-band process in the frequency domain. The resultant output in the frequency domain can be calculated as follows:

$$Y(\omega) = H(\omega)X(\omega) \qquad \text{Eq 9}$$

Where $Y(\omega)$ and $X(\omega)$ are the output and input frequency response, whilst $H(\omega)$ is the frequency response function (FRF). A signal's complete frequency domain representation is not required, as portions of the FRF can be zero magnitude and only provide nonzero values around resonant modes.

If walking is considered a stationary narrow banded random process (i.e. statistical properties do not vary as a function of time) formed from a stochastic process, classical random vibration theory can be used to interoperate the resultant output of physical system subject to a random process [136] . As demonstrated in [136] the power spectral density (PSD) of a physical systems output, be it displacement, velocity, or acceleration, is defined by Eq 10 and provides the central result of the random vibration theory. The power spectral density of the output ($S_{out}(\omega)$), is found through the PSD of the random stationary input signal ($S_F(\omega)$) and the modulus squared of the FRF.

$$S_{out}(\omega) = |H_s(\omega)|^2 S_F(\omega) \qquad \text{Eq 10}$$

The variance of the output (acceleration, velocity or displacement) can be obtain for a random process [136] and is to be defined by integrating all possible frequencies of the spectral response. Given that the PSD is an even, real function of the angular frequency ω, it is convenient to only consider the positive frequencies and double the value of the integral to yield the same area under the PSD curve. Thus, the variance of the out of the system is defined as:

$$\sigma_{out}^2 = 2\int_0^\infty S_{out}(\omega)d\omega \qquad \text{Eq 11}$$

If the response of a linear system is assumed to be dominated by a singular resonant mode subjected to light modal damping. The variance of the maximum acceleration can be calculated as [137]:

$$\sigma_{out}^2 = \frac{\pi\omega}{2\xi m^2} S_F(\omega) \qquad \text{Eq 12}$$

Where $\xi$and m are the modal damping ratio and modal mass, respectively. Considering the output signal representing the acceleration, the maximum response of the acceleration is seen through:

$$z_{max} = g_{peak}\sigma_{Out} \qquad \text{Eq 13}$$

z_{max} and σ_{Out} are the mean and standard deviation of the maximum acceleration of the mode, whilst g_{peak} is the peak factor. The standard deviation of the maximum acceleration (σ_{Out}) response is found through the variance (σ_{out}^2) of the maximum acceleration, which can be defined through the PSD of the acceleration [136]. The peak factor (g_{peak}) is given initially through Davenport [138]. However, the assumptions of the peak factor can often lead to inaccurate results [30,80]. The resulting peak factor is given below, assuming a non-zero mean process:

$$g_{peak} = \left(\sqrt{2\ln f_e T} + \frac{0.5772}{\sqrt{2\ln f_e T}}\right) \qquad \text{Eq 14}$$

The definitions of each parameter are examined in Bassoli [80]. The PSD model of the input force has numerous input parameters, Section 2.1.2. However, the variability of each parameter could be better represented in the frequency domain.

The variability in the frequency domain arises from the PSD of the vertical walking signal $S_F(\omega)$ as the FRF is known to have a high level of accuracy, due to the known structure modal properties. Brownjohn et al.[29] was one of the first researchers to consider the frequency domain representation of the vertical walking force-time history. The Fourier

amplitudes around the harmonics are modelled through Gaussian functions fitted using data from continuous force measurements. One major drawback of Brownjohn et al.[29] is the entire frequency domain is not represented, only discrete pockets at harmonic values. As shown by Chen et al. [139], sub-harmonics can account for 8.5% of the energy of a signal, with the remaining energy above the fourth harmonic accounting for 6-17% energy content of the signal. The fitting parameters of the Gaussian functions could be overfitted due to only three individuals participating. Thus, the result may not generalise to entire populations.

Zivanovic [43] improved the model of Brownjohn et al.[29] by using a similar analysis on nine people over various walking velocities Eq 15 - Eq 17, Figure 2.10. In total, 95 force-time histories are created. A Fourier series model is proposed that accounts for sub-harmonics and the energy leakage of a signal by defining the Fourier amplitude of DLFs at incremental values around the first five harmonic and sub-harmonic. Chen [37] and Bachmann [103] show sub-harmonics presence due to the imperfections and asymmetry of walking. Racic [52] findings conversely did not present sub-harmonics of such magnitude. Such variations are likely due to the variations in the populations. The complete force-time history is defined by summating the sub-harmonics and harmonics. $\overline{DLF_n}(f_n)$ is the DLF function based on the normalised walking frequency f_n. $\theta_n(f_n)$ is the phase angle dependant on the normalised walking frequency. Superscript s denotes the sub-harmonic.

$$F_n(t) = W.DLF_n \sum_{n-0.25}^{n+0.25} \overline{DLF_n}(f_n) cos\left[2\pi f_n f_p t + \theta_n(f_n)\right] \quad \text{Eq 15}$$

$$F_n^s(t) = W.DLF_n^s \sum_{n-0.25}^{n+0.25} \overline{DLF_n^s}\,(f_n^s) cos\left[2\pi f_n^s f_p t + \theta_n(f_n^s)\right] \qquad \text{Eq 16}$$

$$F(t) = F_n(t) + F_n^s(t) \qquad \text{Eq 17}$$

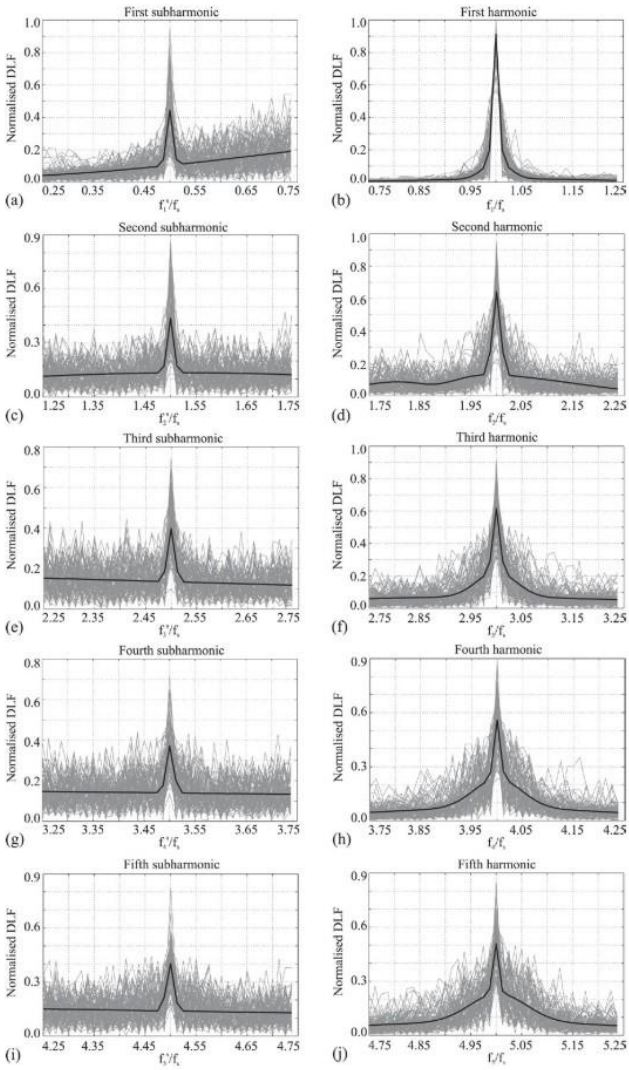

Figure 2.10 Normalised sub-harmonic and harmonic of the first five harmonics of walking frequency, after [43]

The sub-harmonic for each pedestrian is based on the first DLF [43]. The assumption of asymmetric walking based on a peak in the first harmonic is provided with no justification. Frier et al. [140] compared the model of Zivanovic [43] with its counterpart of no energy

leakage. The integer value model produced higher accelerations. On occasion, the resultant acceleration was 35% different from the integer model. Sahanci [118] illustrates the effect of limb dominance on participants. Such development is presented through sub-harmonics between the bands of primary harmonics of walking in the auto spectral plot. Therefore, the assumption of perfect synchronisation between left and right legs is incorrect [141], and modelling legs as separate step characteristics should be addressed in future models. Sahanci [118] cites that excluding sub-harmonics can lead to a 50 percent error in acceleration response when they are not considered.

The entire frequency domain representation of the Zivanovic [43] signal is not complete. Small bandwidth still exists with no information at the boundaries of sub-harmonics and harmonics. Whilst these portions only account for minor energy content in a signal, they are required to provide a full representation of the entire signal in the frequency domain. Caprani [42] addresses such an issue with a pseudo-excitation method building on the work of Zivanovic [43] and Brownjohn et al. [29]. A Lagrange polynomial interpolation approximates the low-lying amplitude in the regions of no information.

Chen et al. [139] improved on the PSD model of [42] and [29] by addressing the primary downfall of the models: the lack of data. Chen et al. [139] underwent an experimental program of 56 people producing 1528 time histories. The original time histories only lasted 20-35 seconds, giving a low-frequency resolution of 0.05 Hz. Chen et al. [139] artificially increased the total time by stacking the same histories. This model will be biased towards the values of that walking time and, therefore, not representative of the total intra-subject variation.

In some cases, the force-time history was increased by nearly 100 times. Chen et al. [139] define the PSD in the integer and half-integer range [$0.95nF_p$ $1.05nF_p$] to the fourth harmonic. Considering only the range stated, 83-94% of the entire energy content of a walking signal up to 50 Hz is considered. The increase in energy content increases with walking frequency. However, the sub-harmonics only account for 2.5-8.5% of the entire energy content of the signal. Chen et al. [139] define the PSD load model through two Gaussian fit functions for each integer and half-integer range. To account for the other 6-17

percent of the energy, a cubic function is fitted empirically to connect the integer and half-integer ranges, similar to that of Caprani [42]. The PSD of the input force is then found through the summation of the harmonics, sub-harmonics and other constituent parts normalised by the person's location and the pedestrian point divided by the number of people on the structure.

Butz et al. [127] proposes a model that considers the various pedestrian densities of a structure, from unrestricted flow to crowding. Again, the PSD is modelled using exponential functions with different fitting parameters, similar to [29,43]. Butz et al.[127] presents a model with the mean walking frequency of the stream of people. Further empirical factors are added to consider the number of people, non-synchronisation of walking frequency, and the structure. The PSD model only considers single harmonics of walking and states that higher harmonics do not invoke considerable vibrations, neglecting the energy and walking force from high-frequency components. The variability of the model is defined through the walking frequency, compared to Fourier approaches that consider the variability of DLF, walking frequency and walking speed.

Piccardo et al. [142] approximates the PSD of the modal force $S_{F_j}(\omega)$ assuming the randomness excitation is due to the walking frequency and phase angle, Eq 18. The model does not consider the variability of DLF as a parameter. Tubino et al. [143] and Piccardo et al. [142] contradict most models. They suggest that the walking speed and DLF, as random variables, have little impact on the mean, standard deviation, and peak acceleration factor. The PSD of the force-time history is defined through [143], considering N_p (number of people crossing the structure). The model only considers the variation in walking frequency as the principal component that causes variability in the model. Bassoli et al. [80] and Ferrarotti et al. [144] extend [143] by introducing the function $\chi(\beta, C)$, an admittance function to correlate the structural mode (β) and the pedestrian synchronisation (C).

$$S_{F_j}(\omega) \approx (W.DLF_m)^2 \frac{N_p}{4\beta} p_\omega(\omega)\chi(\beta, C) \qquad \text{Eq 18}$$

Ferrarotti et al. [144] coherence function is based on two factors: the positions of the pedestrian concerning the other pedestrian and the increase in pedestrian synchronisation

with increased pedestrian density. The model of Bassoli et al. [80], unlike other frequency-based models, includes methods for considering human structure interaction effects. The natural frequency and modal damping ratio of the structure are modified in the frequency response function to account for the effective increase or decrease in the parameters due to moving pedestrians.

Van Nimmen et al. [30] proposes extensions to [142] and [80] by providing provisions for arbitrary mode shapes such as torsional. A closed-form expression is then used to estimate the variance of the multi-modal response due to resonant and non-resonant loading considering human structure interaction effects. Van Nimmen et al. [30] propose a spectral force model considering the variance of the DLF inherently in the model, something previously unseen in spectral analysis. The model treats the DLF, weight, and walking frequency as independent random variables. The spectral force model of walking can thus be defined as:

$$S_{F_h}(\omega) = \sum_{h=1}^{m_h} \frac{N_p DLF_h^2 W^2 (1 + CoV^2)}{2} p_\omega(\omega) \left[\frac{1}{l_x l_y} \int_0^{l_x} \int_0^{l_y} \phi^2(x,y) dy dx \right] \quad \text{Eq 19}$$

The CoV is the coefficient of variance for each harmonic of the DLF. These values can be derived from the data provided previously in Section 2.1.2.3. $\phi^2(x,y)$is the two dimensional mode shape squared.

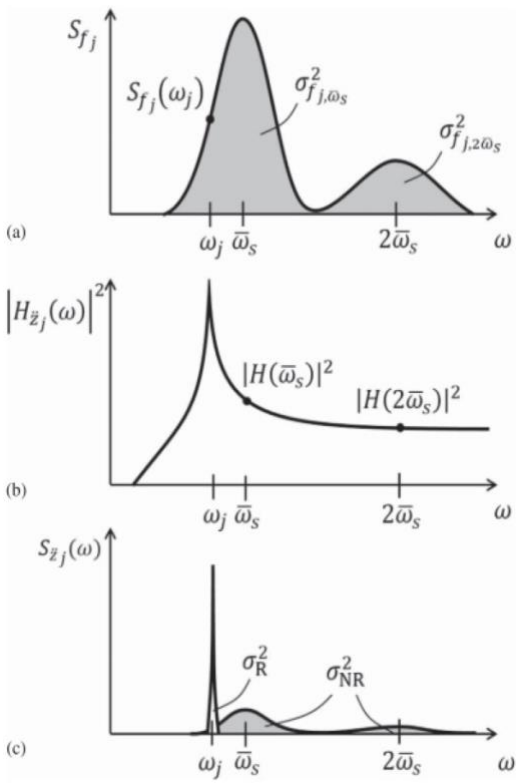

Figure 2.11 a)Schematic representation of PSD of walking load modelled as a narrow banded process b)Squared magnitude of the FRF c) PSD of the modal acceleration response, after [30]

The response of resonant loads can be defined through the simplified method proposed in Eq 12. The non-resonant response can be found through the numerical integration of Eq 11 considering angular frequencies away from the peak natural frequencies. A schematic of the procedure is given in Figure 2.11.

The spectral analysis of vertical walking loads has progressed since its first implementation by Brownjohn et al. [29]. The most all-encompassing spectral based model to date in the opinion of the author, is that of Van Nimmen et al. [30]. The model considers the various synchronisation of pedestrians, human structure interaction effects, walking frequency variation, DLFs, and finally, the resonant and non-resonant components of the acceleration response. The accuracy between numerically simulated and analytically predicted is "excellent", by Van Nimmen et al. [30]. However, the estimation of the structural acceleration provided by the framework is simultaneously conservative and an

overestimation. A load model representing all frequencies in the frequency domain for each walking frequency is yet to be seen.

2.3 Human Structure Interaction (HSI)

New insights and testing have shown that institutional guidance provides an overestimation of the expected acceleration response of a structure [9,24,34]. The discrepancy of predicted versus measured responses is primarily seen on flexible or lightweight structures. The shift to more slender and flexible structures has provided new challenges [81,91,145,146]. Structural masses have also tended to reduce, resulting in the pedestrian mass providing an increased contributing proportion to the overall mass of the structural system. However, when trying to simulate real moving walking loads on an analytically representative model, there is a reduction in vertical acceleration on the physical system compared to the analytical model [147–151]. Current guidance pertaining to the VSA dictates that the pedestrian is considered a massless moving vertical force on the structure [16,19,20,55] defined in Section 2.1 and Section 2.2. However, biomechanical research suggests that the human body is a dynamic system with perceptible vertical mechanical stiffness and damping [152–155]. Therefore, such reductions in the measured compared with predicted acceleration are attributed to so-called human structure interaction (HSI) effects. HSI fundamentally comprises of the dynamic interaction of two systems, the structure and the occupants. The two fundamental aspects of the relationship are the influence of perceptible vibrations on changes in human gait and the impact of the human body dynamics on the dynamic properties of the structure.

The dominant HSI effects manifest themselves as changes in the natural frequency and increased modal damping ratio of the human-structure system compared with the corresponding properties of the structure itself, resulting in erroneous predictions of the acceleration response [145,149,156,157]. The magnitude of such variations is attributed to a person's posture, mass or if they are walking or stationary [5,146,158–161].

The HSI principally is visible through modifications to the structure's mass, natural frequency and modal damping ratio when considering the human body's influence on the dynamic properties of the empty structure [10,34,158]. Regardless of their posture, humans will

increase a structure's modal damping ratio [162]. Depending on the person's stationary or moving nature, the structure's natural frequency can either decrease or increase, respectively [10,26]. The HSI feedback loop can also result in the structure affecting the human gait, Figure 2.12. The structure has an active effect on pedestrian walking due to the alteration of walking speed, walking frequency, DLFs and lock-in effects [26,81,160,163]. Lock-in is debatably linked only to the lateral direction of human walking [6,73,159,174]. Lock-in was famously demonstrated on the opening day of the London Millennium Bridge. The lateral vibration mode was excited due to the adaption of the human walking tendency to synchronise and produce a positive feedback loop that resulted in negative damping [6,73,160,172]. The pedestrians on the day changed their walking frequency to stay in phase with the lateral movement of the bridge. This action then increased acceleration response due to the resonant response to a fundamental lateral mode [6,7,77]. Deviating from the in-phase walking would cause a horizontal force on the pedestrian in the opposite direction to their motion, potentially causing them to lose balance and fall [160,175]. Macdonald [160] demonstrates that lock-in is not associated with vertical vibrations, whilst conversely, Milton et al. [164] and Bachmann and Ammann [66] indicate that vertical lock-in occurs when matching the vertical vibration of a surface with the walking frequency.

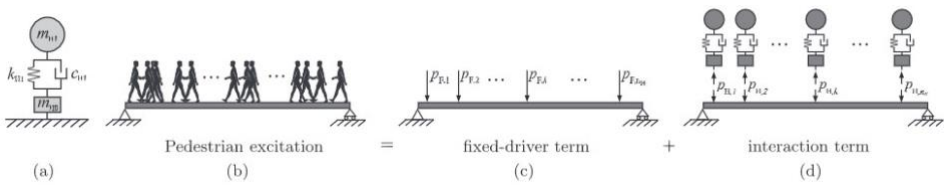

Figure 2.12 a) The human SDOF Spring Mass Damper (SMD) model b) Structure induced vibration by walking excitation of pedestrians c) Vertical ground force reaction due to footfall of each pedestrian due to rigid force d) interactive term due to HIS and relative movement of the structure and the SDOF SMD mass of the human, after [158]

The human walking force has been shown to change depending on the level of vibration perceived [78,169]. The prominence of HSI increases when the crowd-to-structural mass ratio grows [168]. Lightweight structures and structures prone to large crowds, such as stadia, are more susceptible to HSI effects [157,169,170]. This review focuses on the vertical direction only. The proceeding sections investigate the literature regarding the impact of HSI

effects on human gait (Section 2.3.1) and the modelling parameters for active and passive people (Section 2.3.2). Finally, an alternative approach to modelling HSI through inverted pendulums is reviewed (Section 2.3.2.3).

2.3.1 The HSI effect on the human gait

The vertical force can be split into two terms (Eq 20). The first is the fixed driver term ($F_{GFR}(t)$), resulting from the pedestrians' direct contact with a stiff structure. Such force measurements can be derived synthetically from models presented in Section 2.1. However, when the support structure is flexible, the resultant vertical force is modified by adding the interaction term ($F_{int}(t)$). The interaction term contains the movements of the human body and structure. Assuming both the human body and structure can be modelled as a single degree of freedom systems respectively, the total force is calculated as:

$$F(t) = F_{GFR}(t) + F_{int}(t) \quad \text{Eq 20}$$

$$F(t) = F_{GFR}(t) - m_h\ddot{x}_s + c_h(\dot{x}_h - \dot{x}_s) + k_h(x_h - x_s) \quad \text{Eq 21}$$

Subscript h denotes the human, whilst subscript s denotes the properties or response of the structure. m is the SDOF modal mass, c is the damping constant, and k is the vertical stiffness. Dot notation is the concerning derivative time, where x is the vertical displacement.

Ahmadi et al. [90] quantified the change in vertical walking forces for a specific footbridge with a natural frequency of 6Hz and maximum acceleration of 3.25m/s^2. Ahmadi et al. [90] noted a range of increases in the first DLF due to resonant walking of 2.3-6.3%. The non-resonant case of walking at the first harmonic showed variability, increasing and decreasing DLF values in some cases. For the second and third harmonics of walking in both the resonant and non-resonant cases, the DLF values decreased for all participants by a maximum of 8.1 percent and 30.4 percent (Figure 2.13).

Dang and Zivanovic [81] demonstrate that the interactive component of the force increased in magnitude with increased steady-state vibration on the structure. As such, conversely to Ahmadi et al. [90], Dang and Zivanovic [81] observed that the first DLF decreased in all cases by 21-53% due to the interactive term. An order of magnitude greater than that of

Ahmadi [90]. However, Dang and Zivanovic [81] footbridge possessed a natural frequency of 2.44Hz resulting in a resonant response by the first integer with a traditionally higher DLF value. Dang and Zivanovic [81] noted only minor changes to spatiotemporal parameters of walking due to the increased acceleration of the structure(Figure 2.14); only the interactive term of the walking force model resulted in statistically significant change. Archbold and Mullarney [171] note an increase in the peak force on a flexible structure compared to the rigid counterpart for all walking frequencies, conversely to Ahmadi et al. [90] and Dang and Zivanovic [81]. Archbold et al. [172] further demonstrate that the characteristic m shape of walking varies on a flexible surface compared to that on a rigid surface, with a relatively higher first peak and lower second peak. Thus, producing a different force characteristic on the structure and altered DLF values.

It is experimentally shown that the reduction in acceleration response becomes more prominent when a pedestrian excites a resonant mode of the structure [147,149,151,173,174]. Conveniently, the most considerable decrease in acceleration is seen when the structure is most susceptible to resonant responses. Therefore, carefully selecting the appropriate load model and human modal parameters become paramount to accurately modelling the acceleration response, with respect to the numerical analysis to the monitored response.

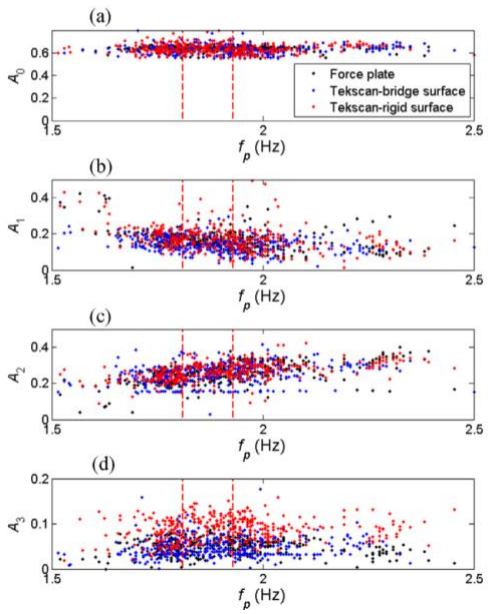

Figure 2.13 DLF of individuals at various pacing frequencies obtain on a flexible (Bridge) and rigid structures. After [90]

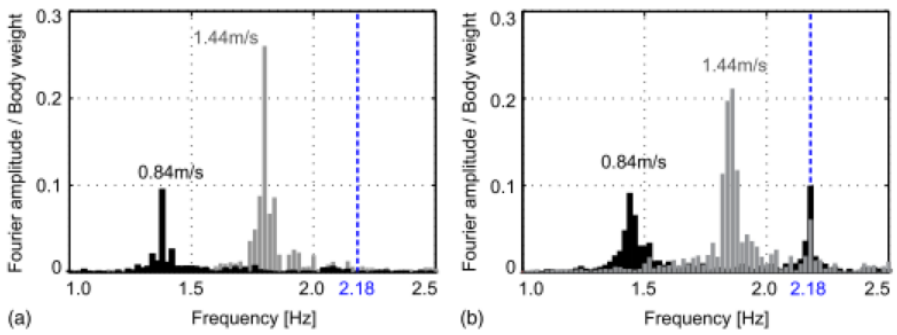

Figure 2.14 a) Fourier Amplitude of walking for a slow medium and fast velocity on a stiff surface b) Fourier Amplitude of walking for a slow medium and fast velocity on a vibrating surface subject to a steady state acceleration of 0.85 m/s2 at 2.18 Hz, after [81]

2.3.2 HSI effects on modal properties

Other than changing the gait of humans, HSI effects fundamentally change the modal properties of the structure. As mentioned above, principally, the effect is evident through the increase in modal damping ratio and modification of the natural frequencies. The values and

results further vary depending on the static or moving nature of the pedestrians; therefore, they are treated separately.

2.3.2.1 Stationary participants

Historically HSI effects were only evident when the modal mass of the structure was increased [108,175–177]. Such effects naturally lead to a lessened natural frequency. However, this method can result in overestimations of the natural frequency [157]. The reduction in natural frequency can be calculated (Eq 22) were μ_p is the ratio of pedestrian mass to structural mass.

$$\frac{1}{\sqrt{1+\mu_p}} \qquad \text{Eq 22}$$

Therefore, lightweight structures experience an increased reductions, such as fibre-reinforced polymer structures [178,179]. Lenzen [180] first noticed that such SDOF mass models negate the damping effects of the human body, noticing a factor of three increase in modal damping ratio from the presence of four people on a concrete floor. Brownjohn [181] and Zhang et al. [182] demonstrated that even a low mass ratio of a single human at the antinode of the first mode shape could result in a stark increase in modal damping ratio. An increased mass ratio also increases HSI effects, however not in a linear fashion [169], [170], [157]. Brownjohn [181] investigated other postures, such as standing, seated, and bent knees. The damping effect on the fundamental mode increased the modal damping ratio by 2.0%, 2.8% and 6.0%, respectively (Figure 2.15). Such passive effects are not cumulative. When comparing the FRF of a function hall, Brownjohn [181] notes that with 800 people sitting on the structure, the modal damping ratio increased, along with a reduced FRF peak value. Whilst this resulted in a lessened response than the empty state, the effects were not cumulative. Zhang et al. [182] also notes an initial increase in modal damping ratio for the structure for one person's first three vibration modes. However, the effect is not cumulative, and the modal damping ratio difference for additional people decreases (Figure 2.16). Shahabpoor et al. [183] and Van Nimmen et al. [146] conclude similar findings with the modal damping ratio of up to ten people (Figure 2.17), showing an asymptotic relationship of modal damping ratio to the number of people.

Matsumoto et al. [184], akin to the study of Dang et al.[81], modelled the varying modal properties due to different periodic accelerations on the body. In the bent-knee posture, the natural frequency of the human body decreases from 3.0Hz to 2.5Hz for increased accelerations. Similar findings are seen in the single leg and standing postures, with the natural frequency reducing. No other authors have commented on the changes in dynamic properties of the human body in civil engineering literature with various vibration levels. Alternative effects, such as the acceleration-based dependence on modal damping ratio, are also anticipated. Rapoport et al. [185] stated that constant mechanical stiffness might not apply to the human leg because joint stiffness is nonlinear due to modal damping ratio. As a result, a model that accounts for this modal damping ratio may improve the model predictions. As evidenced, no singular study addresses the needs of the research area. The effect of these parameters at varying acceleration levels is not demonstrated.

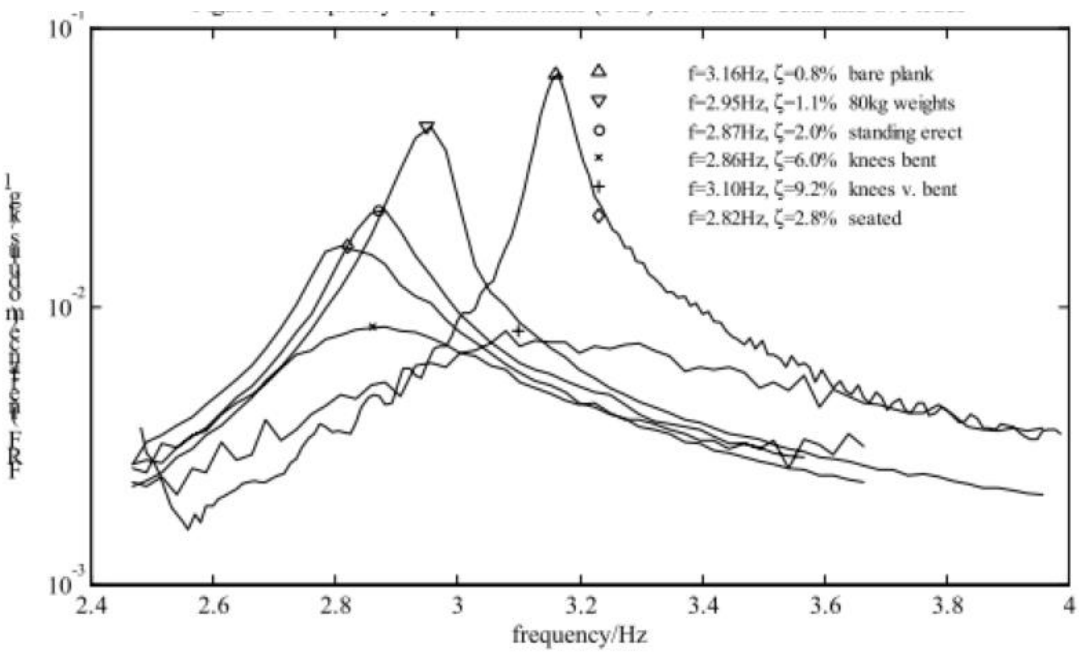

Figure 2.15 FRF for a bare plank, including the effects of a passive person in various postures given in the legend. After [181]

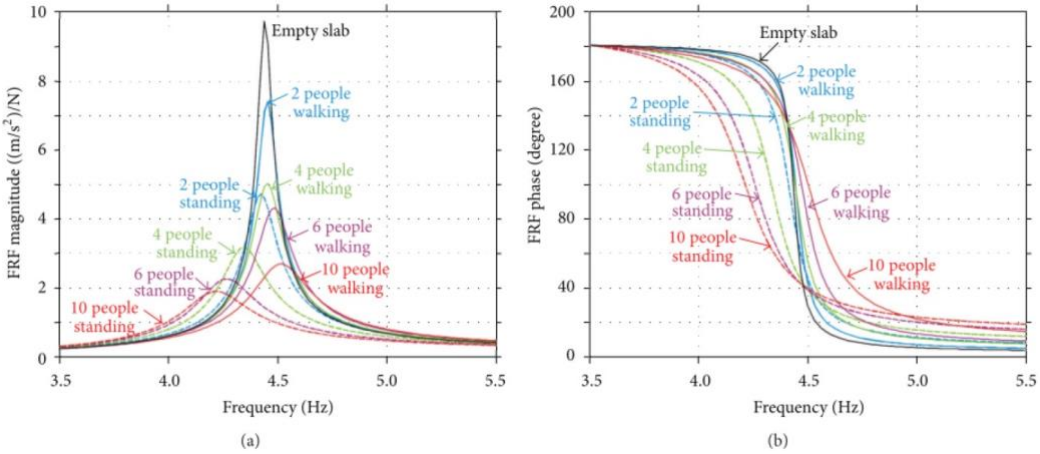

Figure 2.16 a) FRF magnitude for stationary and moving participants of various sizes b) Phase angles for stationary and moving participants of various sizes, after [168]

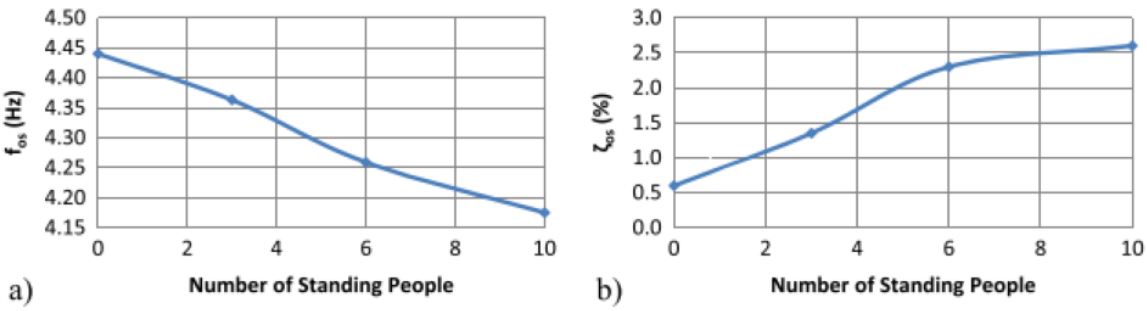

Figure 2.17 a) Reduction of the natural frequency of the structure with an increased number of passive participants, b) Nonlinear relationship of modal damping ratio with an increasing number of participants. After [183]

The stationary participant is often represented through a single degree of freedom (SDOF) [145,149,158,168,186,187] or multiple degrees of freedom system (MDOF) [157,188,189]. Some MDOF human models are often complex and overcomplicate the human-structure system [158]. Van Nimmen et al. [158] proposes an equivalent SDOF system representing the stationary human participant and the structural system. Proposing a modified representation of the coupled system by modifying the effective modal damping ratio and natural frequency of the linear SDOF structural system. Such work is beneficial because it can be extended to engineering practices in which simplistic methods can save time and produce accurate and meaningful results. That withstanding, Van Nimmen et al. [158] chose not to modify the SDOF modal mass of the system and only considered the empty mass of

the structure. This assumption and the modification of the other two parameters will provides close-consensus to monitored structures at near-resonant responses. Away from resonant frequencies, this methodology could lead to a deviation in expected results.

Table 2.8 provides values of natural frequency and modal damping ratio of stationary human in various postures derived from civil engineering structures. There is a clear consensus for the first mode of vibration of the human system. The natural frequency is approximately 5 Hz, with the modal damping ratio between 30 – 40%. Therefore, the human body can easily be excited in its first mode from other people walking. If a person is sitting or standing, the 2nd harmonic of walking can cause the resonant response of the body and absorb energy from the structural system. All modal values are achieved by comparing the vertical natural frequency response function through modal analysis. As all participants are static concerning their positions on the structure, accurate measurements of the human modal properties can be separated from the structural modes.

Table 2.8 SDOF SMD systems representing of the human body in various stationary postures.

Author	Natural Frequency (Hz)	Modal Damping Ratio (%)
Ellis and Ji [190] Standing	5.5-5.8	=
Shahabpoor et al. [183] Standing	5.17 - 5.44	43-57
Wei [191] Standing	4.67	49.4
Sachse et al. [192]	-	30-50
Coermann [193] Sitting	5.0	32
Zheng et al. [194] Standing	5.24 ± 0.4	39 ± 0.5
Sims et al. [195] seated men	5.1 S.D 0.58	31.1 S.D 10.11
Sims et al. [195] standing men	5.8 S.D 0.54	33.1 S.D 33.1
Sims et al. [195] seated women	5.3 S.D 1.06	38.5 S.D 14.90
Sims et al. [195] seated child	5.2 S.D 5.16	37.5 S.D 39.23

Brownjohn et al. [162] Standing	5.27	36
IStructE [196] Passive	5	40
Matsumoto et al. [184] Standing	5.25-6.75	69.4
Hashim [197] Standing	6.55- 6.67	21.1-21.9
Subashi et al. [198] Standing	5.63-6.39	-
Agu et al. [157] seated	5.222	34.5
Agu et al [157] standing	6.025	37.9
Brownjohn et al. [162] Standing	4.9	37
Van Nimmen et al. [146] standing	5.7 S.D.0.56	44 S.D. 0.07
ISO 5892:2019 [199] seated	5	-
ISO 5892:2019 [199] Standing	6.3	-

Table 2.8 presents a narrow range of values for both the modal damping ratio and natural frequency of the static human. Matsumoto et al. [184] provide a consistent natural frequency. However, the modal damping ratio is higher than others. It is the view of the author that choosing values with statistical properties provides better estimates than any precise point estimate. The natural frequency and modal damping ratio will vary due to the inherent varying compositions of each human. Therefore, no confident estimation of the most appropriate value is given until a comprehensive review of a diverse population set is analysed.

2.3.2.2 Moving participants

A walking pedestrian on the structure is characterised by constantly varying posture coupled with different muscular contractions, resulting in a continual change in the pedestrian's dynamic properties [152–155]. Research within mechanical and aerospace engineering has resulted in stationary biomechanical models simulating the effect of moving vehicles on

stationary bodies [191,200,201]. As a result, the static state of the human biomechanical model for various postures is known to a high degree of accuracy [167,202]. The variation of postures while walking results in only the average properties of the pedestrian being identified [145,174,203].

Simplifications of the walking pedestrians' SDOF natural frequency, modal damping ratio, and modal mass result in time-invariant properties due to the complexity of the dynamical response to perceptible vibrations on walking. As such, the HSI effects are simplified, and the dynamic changing of the systems' modal properties are modelled either through singular or MDOF spring mass damper (SMD) [145,198,202–207], Spring mass damper actuator (SMDA) [105,205], inverted pendulums (IP) [153,160,208–210] or modification of a structural system with additional equivalent modal damping ratio or mass [145,158].

The human body in the SMD and SMDA model is represented as a linear and time-invariant system. Such representations provide easy and convenient solutions to HSI representation by adding additional degrees of freedom per pedestrian to the typical approximated SMD structural systems. Table 2.9 estimates the active participant's SDOF SMD natural frequency, modal damping ratio, and modal mass. The properties are assumed to be time-invariant. The time-variant properties of the SMD models have not been researched. However, this is likely due to the complex nature of determining time-variant properties over shorter periods.

Mohammed et al. [35] show that a structure's FRF reduces nonlinearly with moving participants, similar to the static counterparts, and the reduction depends on the number of participants. Various trials conducting the same experiments produce different average properties for human stiffness and modal damping ratio over the experiment time frame. In the specific case of Mohammed et al. [35] with only two people, the FRF was reduced by 45% to the bare structure. When four people were on the structure, the FRF was reduced by a further 2% compared to the bare state. Shabahpoor et al. [183] conclude similar findings when a participant walks around in a tight circle at the antinode location compared to the quarter or random walking (Figure 2.18).

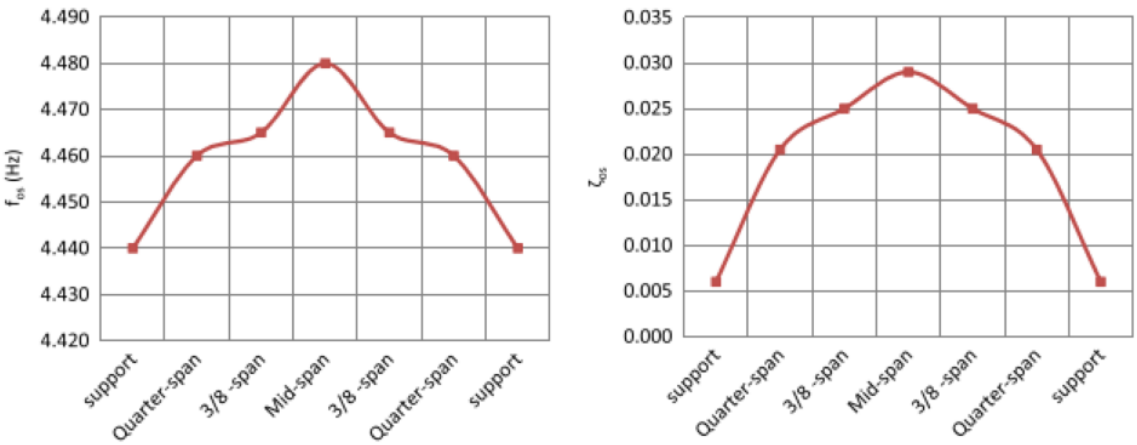

Figure 2.18 Change in natural frequency and modal damping ratio for people walking in tight circles at locations specified, walking at the support indicates no HSI effects. After [183]

Liang et al. [211] note a linear increase in the active participant modal damping ratio with increased walking frequency. The modal damping ratio increased from 28% to 32%, from 1.5Hz walking to 2.1Hz walking frequency. Furthermore, the first natural frequency of the active human body decreases, on average, with increased walking frequency. Liang et al. [211] further note the strong linear negative relationship between the human actual mass and the natural frequency. modal damping ratio showed no such dependency and is viewed as independent of the actual participants mass. Bertos et al. [212] and Kim et al. [213] observe how the modal properties are dependent on human walking parameters, increasing stiffness and modal damping ratio with increased walking speed.

Building on the moving modal properties of pedestrians presented in Table 2.9, DaSilva et al. [106], Toso et al.[54] and Pfeil et al.[214] provide estimates of the walking human properties through regression analysis of multiple input variables. DaSilva et al. [106] Eq 23-Eq 25 define the SDOF modal mass, m, damping constant, c, and the stiffness, k, through various nonlinear relationships dependent on the subject's actual mass, M and walking pace, f_p. DaSilva et al. [106], Toso et al.[54] and Pfeil et al.[214] conducted experiments on individuals walking on a stiff structure with their waist accelerations monitored. The result is participants' acceleration around the harmonics of walking; however, it is worth noting that the acceleration monitoring is subject to error, due to the device misaligning to the global vertical axis. Misplacement of the accelerometers results in other acceleration planes being

transformed into the vertical axis of the device, thus over- or underestimating the effects. Further to the above, DaSilva et al. [106] Eq 23-Eq 25, Toso et al.[54] Eq 26- Eq 28 and Pfeil et al.[214] Eq 29 – Eq 31 had low participation in their experiments and did not account for all walking frequencies. Therefore, misrepresenting the extreme values of walking frequency and participants actual mass results in negative modal parameter values in some instances. The models provide comparable higher estimates to other SDOF models presented in Table 2.9, with natural frequencies of walking pedestrians over 4Hz. Lastly, DaSilva et al. [106], Toso et al.[54] and Pfeil et al.[214] conducted their experiments with populations comprising of Brazilian people exclusively. Therefore, the parameters will be overfitted to the population characteristics. For all equations m is the participants actual mass, f_p is the walking frequency.

DaSilva et al. [106]

$$m_h = 97.082 + 0.2745m - 37.518f_p \quad \text{Eq 23}$$

$$c_h = 29.041m_h^{0.833} \quad \text{Eq 24}$$

$$k_h = 30351.744 - 50.261c_h + 0.035c_h^2 \quad \text{Eq 25}$$

Toso et al. [54]

$$m_h = -231.34 + 3.69m + 154.06f_p - 1.97mf_p + 0.005m^2 - 15.25f_p^2 \quad \text{Eq 26}$$

$$c_h = -1115.69 + 92.56m - 108.94m_h + 2.91mm_h - 1.33m^2 - 1.30m_h^2 \quad \text{Eq 27}$$

$$k_h = 75601.45 - 1295.32m - 33786.75f_p + 506.44mf_p + 3.59m^2 + 539.39f_p^2 \quad \text{Eq 28}$$

Pfeil et al. [214]

$$m_h = 0.874m - 9.142f_P + 12.940 \quad \text{Eq 29}$$

$$k_h = 360.3m_h - 1282.5 \quad \text{Eq 30}$$

$$\varsigma_h = -20.818f_{md} \quad \text{Eq 31}$$

Table 2.9 Natural frequency, modal damping ratio and Modal mass given as Percentage of actual mass of SDOF SMD systems representing the moving human body from various studies.

Author	Description of how parameters are obtained	Maximum acceleration (m/s^2)	Natural frequency of structure (Hz)	Population size	Natural Frequency (Hz) Mean, (standard Deviation)	Modal Damping Ratio (%) Mean, (Standard Deviation)	Modal mass given as Percentage of actual mass (%) Mean, (Standard Deviation)
Shahabpoor et al.[203]	Matching Frequency response Function of experiment acceleration to the analytical model	2.43	4.443	15	2.75-3.00	27.5-30.0	100 ()
Shahabpoor et al. mode 1 [215]	Matching Frequency response Function of experiment acceleration to the analytical model	2.43	4.443	15	2.85, 0.116	29.5, 0.047	100 ()
Matsumoto et al. [41]	Subjects on one leg, whole body vibrations from 0.5Hz to 30Hz	2	N/a	12	K = 279 N/mkg	C = 10.4 Ns/mkg	83.3 ()

Matsumoto et al. [202]	Subjects in bent leg posture, whole body vibrations from 0.5Hz to 30Hz	2	N/a	12	K = 508 N/mkg	C = 17.5 Ns/mkg	89.8 ()
Foschi [216]	N/a	N/a	N/a	N/a	3.3	33	100 ()
Jimenez-Alonso [189]	Match the minimum in natural frequency of the structure due to walking pedestrian decreasing the natural frequency	N/a	2.27	10	2.759, 0.165	47.175, 2.611	83.969 (1.05)
Gomez et al.[217]	Match the vertical acceleration of pedestrian COM with experimental data	5	2.15	3	2.51 2.29 2.52	12 18 12	100 ()
Zhang et al. [186]	Frequency response function matching of 5mm amplitude vibrations at various frequencies	n/a	n/a	10	1.85	30	100 ()

Wang et al. [205]	Ground force reaction (GFR) is monitored through insoles, acceleration response is taken as GFR minus weight of the pedestrian, all divided by mass. Velocity and displacement are inferred through numerical integration then linear SMD parameters are optimised.	N/a	N/a	56	$0.3049f_p$ +1.367	$-0.2116f_p$ + 0.8737	100 ()
Ahmadi et al. [145]	Optimisation of acceleration response of mid-span acceleration to match measured with numerical	2.2	2.4	23	Resonant Walking pace	0.38ln(m)-1.42	100 ()
Van Nimmen et al. [218]	Matching Frequency response Function of	N/a	N/a	6	3.06	35	100()

	experiment acceleration to the analytical model, one leg slightly bent						
Van Nimmen et al. [218]	Matching Frequency response Function of experiment acceleration to the analytical model, double stance phase	N/a	N/a	6	3.34	26	100()

The modal parameters are typically obtained through optimisation and minimisation of the structure's acceleration response [145,186,189,203,218]. The remaining researchers optimise the human body's approximate COM compared to a numerical estimation. Such an assumption causes uncertainty, as the actual location of the COM for each pedestrian is not precisely known. Thus, the locale of the position results in differing results. Furthermore, the human body is heterogeneous in composition, and body parts have differing modal properties. They can be excited at many different frequencies, resulting in a poor approximation of the human body being represented by a distinct mode of vibration.

Research exploring moving participants' influence on structures is a relatively new field, and there is little data that produces consistent results. The field requires an encompassing study to bring all finds together. The results of Table 2.9 do, however, provide some guidance on a sensible range of values. The selection of one value over another is unjustified due to the limited studies available. There is no systematic assessment of the existing HSI models' performance. Whilst many authors validate their models on a single structure from whose data the pedestrian dynamic models were initially derived, only a limited number provide estimates on new structures or compare concurrent models [145].

2.3.2.3 Inverted Pendulum Models

An alternative modelling approach in moving pedestrian scenarios is the inverted pendulum (IP) (Figure 2.19). Whilst bipedal pendulums have been present in biomechanical models, their use in civil engineering is scarce. The instantaneous load transfer mechanism of the IP to adjacent feet neglects the double stance phase of the leg swing [209,219]. An impulse must be applied at the beginning of every step to ensure the body's motion has the same initial conditions, ensuring stable walking.

The IP model is a mechanical model capable of generating step-by-step vertical force variation and time-dependent stiffness and damping changes. Bocian et al. [160] and Macdonald [220] introduced the IP model to structural engineering to counter the lack of HSI effects in vibration assessments. The model considered the centre of mass's rigid stiffness and that the additional variation between the actual response and the idealised is due to the

vibrations induced by the structure. Bocians et al. [160] assumed that vibrations of the structure are sinusoidal and undamped. The model is self-perpetuating, as no kinematic or potential energy is lost in the system. Biomechanical models can easily be adjusted to include spring stiffness and damping (Figure 2.19) to simulate natural walking characteristics [207,213,219].

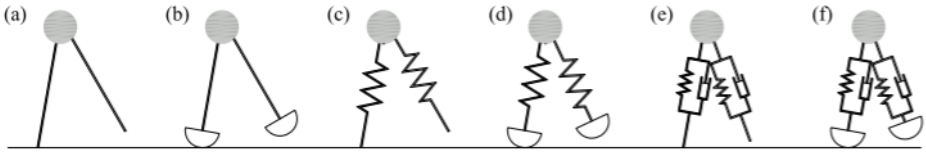

Figure 2.19 Visualisation of various IP models a)IP b)IP with rockers c) spring-mass d) spring-mass with rocker e)spring-mass-damper f) spring-mass-damper with rocker. After [221].

Historically, the damping and stiffness in IP models possess time-invariant properties. Qin et al. [210] produce time-dependent damping and stiffness of the leg cycle-by-cycle using a spring-loaded inverted pendulum [219]. External force must be applied to maintain a steady gait, as the model starts to yield unstable solutions on a high frequency or high amplitude structure [210]. Damping and direct energy input are required for the bipedal IP to regulate gait patterns on vibrating structures [209,210]. This demerit is the biggest obstacle to the model's uptake and the need for modelling and coding.

Lin et al. [209] parametrically analysed Qin et al. [210] stable gait production methods. Using such a compensation method, the IP model with damping and stiffness demonstrated that it could achieve stable gaits in the 1.6 -2.4 Hz walking frequency range and produce DLFs in the same region as Kerr's [45] results. Dang [221] provides an overview of the various inverted pendulum models. However, a perfect alignment is not seen when parametrically analysed. The IP model's angle of attack and leg length vary the first DLF [221] (Figure 2.20). Ruiz et al. [222] note that whilst the SMD bipedal model works well within normal walking ranges, outside of this (i.e., slow or fast walking), the model does not accurately represent DLF values. Furthermore, no studies compare the accuracy of such a model on the flexible surface to see its applicability to model HSI effects.

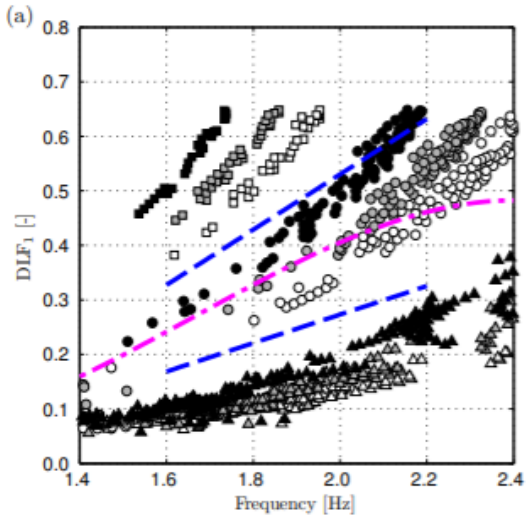

Figure 2.20 DLF_1 of force generated by spring mass damper IP with various leg lengths (black = 1.2, grey = 1.037 and no fill = 0.9 m) and angle of attacks (squares = 65°, circles = 70°, triangles = 75°) compared to Kerr mean, 5% and 95% model, after [221]

The practical use of IP is non-existent due to various energy correction methods requiring numerous simulation and coding to sustain a natural gait and produce meaningful VSA. The inverted pendulum does not create the characteristic m-shape GFR [219,223]. The widespread avoidance of such a model in industry is likely borne out of the time and skill required to get a single VSA.

2.4 Conclusions

The chapter reviews current and historical literature on the human walking force and its interactive effects on the structural system. Historically, vertical walking load models are based on deterministic integer value Fourier series. Newer models have been developed that synthetically describe the inter and intra-subject variation of actual walking loads [2,51,59]. Current industry models lack the fundamental intra-subject variation at each walking frequency, preferring an expected value of parameters throughout. This conformity fundamentally alters the VSA and negates the probable range of accelerations likely to be seen on a structure. Current industry models [16,19–21,28] provide a split in vertical load models based on the structure's natural frequency. This artificial split is shown to be a direct

result of previous models being constructed on biased data. The fundamental process of walking does not change on high-frequency structures, nor does the vertical walking force. New models [2,51,59] can contain DLF and phase angle content across all frequency ranges, thus giving a complete informative signal, contrasting to older models that only include information at integer values of harmonics of walking up to a truncated harmonic. Larger quantities of data are currently available [38,52,59] so more accurate models are being produced compared to sampled signals of vertical walking forces. Using such models removes the artificial split in structures and creates a universal load model. However, no publication explicitly recommends which current model best represents vertical walking loads.

The frequency domain-based models provide inferior results and present themselves sophisticatedly. This procedure is laborious compared to the partner time domain models. Whilst some models claim to provide “accurate’ acceleration results compared to real walking, this is not conclusively proven. A common theme seen through new time and frequency domain models is a lack of appreciation for the end users. Whilst producing representative synthetic signals is the goal of academia, the industry requires a model that can be easily used, interpretable and, crucially, produce accurate acceleration outputs that mimic the real structure. There exists a disconnect between industry and academia regarding the needs and demands of the respective groups.

Furthermore, the dissemination of knowledge in the industry is severely lacking. The latest publication of new industry guidance, AISC Design Guide 11 [16], published in 2016, still uses deterministic values of DLF not correlated with walking frequency. This is a step backwards from current best practices.

The HSI effects have been shown to play a clear and imperative role in a structure's vertical force and acceleration response. Including HSI effects can reduce acceleration response and provide a closer match to the acceleration output of a structure. The topic is still in its infancy, even after the public opening of the London Millennium Bridge triggered a increase in research efforts. Parameters for the moving human natural frequency and damping are unknown with much certainty due to the complex procedure of their time-varying properties.

Furthermore, no formal guidance is given on including the HSI dyad. Currently, these issues are dealt with in isolation. Finally, no study provides a conclusive set of natural frequency and damping parameters that can be confidently used in all scenarios. There exists sufficient scope to conduct further research into the most applicable full-scale VSA, including accurate walking load models, all HSI effects, and statistical representation of various input parameters (e.g., walking velocity, walking frequency and pedestrian weight).

Table 2.5 and Figure 2.6 highlight the inherent variability in current vertical walking load models. As demonstrated, there is no clear consensus on the accurate representation of the DLF, and as such the vertical walking force. This current lack of unification provides uncertainty into the design of pedestrian structures. The ramifications of which, provide practicing engineers with an unknown level of accuracy with respect to the acceleration response of the structure to the vertical walking load. As illustrated in Table 2.5 for a given walking frequency (2.5Hz) a 600% difference in DLF value is seen. For a structure idealised by a single lightly damped mode, this corresponds to a steady state acceleration response varying by 600% too. The variation of the vertical walking force representation provides a barrier to the accurate prediction of the acceleration response. Coupled with the increased complexity and uncertainty of the HSI effects, the accurate prediction of a structure's response has thus far eluded engineers. As the VSA is performed before the construction of the structure, assumptions of the modal damping ratio, vertical walking force and HSI parameters must all be assumed and provide some level of accuracy and redundancy. Whilst the accurate VSA is paramount, over reliance on older vertical load models may result in inaccurate assessment that provide overly conservative results. Thus, leading to unnecessary design decisions.

Current widely used Fourier based models [19,20,28,45,53,65,68,103] are derived from single footfall data, thus such data could be assumed biased. Therefore, an area of further research is identified through the modification of the Fourier series model to include updated parameters based on continuous measurements of multiple footsteps. Furthermore, the accuracy of current synthetic realisations of vertical walking forces has not been assessed against their real counter parts. Therefore, an investigation is required to compare current models and their real measured counterparts to deduce which vertical walking load model

provides the most accurate representation of walking. Finally, the inclusion of HSI effects is infrequently seen within VSA, thus adding additional layers of both complexity and uncertainty to the VSA. Furthermore, the accurate estimation of the HSI representation of the human body as a SDOF SMD system has not established. Whilst several authors have provided estimates of the various parameters (Table 2.8, Table 2.9), the validity of the estimates is not currently tested. The results of Table 2.8, Table 2.9 are not seen within each study and are taken in isolation with respect to each other. Therefore, the accuracy and validity of both the parameter estimations and their assumptions must be trialled independently before any recommended use of one set of parameters is given.

Chapter 3 Fourier series approximation of vertical walking forces

For structures subjected to human walking activities, the resonance between a harmonic walking load and one or more natural vibration modes of the structure can result in a significant acceleration response. Such responses can produce acceleration magnitudes that result in discomfort to human occupants and thus cause the structure to fail in its serviceability limit state (SLS). Therefore, the accuracy of such vertical walking loads is paramount to the overall structure's SLS requirements. However, the issue of prescribed SLS limits is a complex topic due to the several interpersonal factors affecting a person's ability to perceive vibrations. As seen from Chapter 2, current vertical walking loads do not provide a universal consensus of the parameterisation or mathematical representation of the load and exhibit numerous approximations. This is primarily attributed to poor-quality data and ill-posed assumptions.

This chapter aims to develop and improve current Fourier-based vertical walking load models. The main objective is to provide updated Fourier series parameters, namely the DLF and phase angle values. The presented models explore the inter-subject variation of the DLF and phase angles. Additionally, intra-subject variation of the DLF and walking frequency are analysed to provide a comprehensive vertical load model. This chapter leverages the dataset of Racic and Brownjohn [52], which amounts to 10.5 hours of walking force time histories of multiple subjects walking on an instrumented treadmill. The size and diversity of the dataset are unmatched in research and therefore lend themselves to provide a generalised representation of the vertical walking load model.

The chapter is organised as follows: Section 3.1 explains the data collection process, experimental setup and methodology. Section 3.2 details the method of extraction of crucial parameters of the data. Section 3.3 explores the inter- and intra-subject variation of the key Fourier series parameters in detail and their co-dependent relationships whilst also investigating the presence of differences due to the sex of the participant.

The proceeding Chapter is an extension of the publication:

Peters, A.E., Racic, V., Živanović, S. and Orr, J., 2022. Fourier Series Approximation of Vertical Walking Force-Time History through Frequentist and Bayesian Inference. Vibration, 5(4), pp.883-913.

3.1 Data Collection of vertical walking forces

Data acquisition was performed on an instrumented treadmill at the Light Structures Laboratory at the University of Sheffield in 2010 and 2011 by Dr Vitomir Racic, Figure 3.1. Specifics of the experimental campaign can be found in Racic et al. [52]. The raw data was then passed to the author in 2020 [224]. Only the vertical force measurement is of interest, with the longitudinal and lateral forces beyond the scope of the thesis. The velocity of the treadmill ranges from 0.1-10km/h. However, the entire range of the treadmill velocity was not utilised due to participants transitioning to jogging and running motions.

The experimental setup allowed measurements of the left and the right foot vertical forces to be simultaneously acquired over multiple footsteps. During each walking trial, the speed of rotation of the treadmill belts (referred to as "treadmill speed") was fixed and controlled by the data acquisition system. Treadmill speeds started at 2km/h, then at least 64 steps were taken before a period of rest, and then the procedure was repeated at 0.5km/h faster speed. The process continued until the participant started to jog. The treadmill speed is taken as the average walking speed, whilst variations may exist due to the participant moving up and down the belt. However, these variations are considered negligible. The population of the treadmill participants ranged from students, academics, and technical staff at the University of Sheffield. A total of 80 volunteers (55 males and 25 females, mass 76.1 ± 15.3kg, height 174.8 ± 8.1cm, age 29.7 ± 9.3 years) performed the experiment, resulting in 824 total vertical walking time histories summing to 10.5 hours of continuous force time measurements. The

data was acquired at 200Hz sampling to stop aliasing of the signal. Therefore, all information below 100Hz can be fully reconstructed due to the Nyquist sampling theorem. Each participant's weight, speed, sex, height, age, and triaxial force measurements of each foot were recorded. The triaxial force is measured in units of Newtons (N).

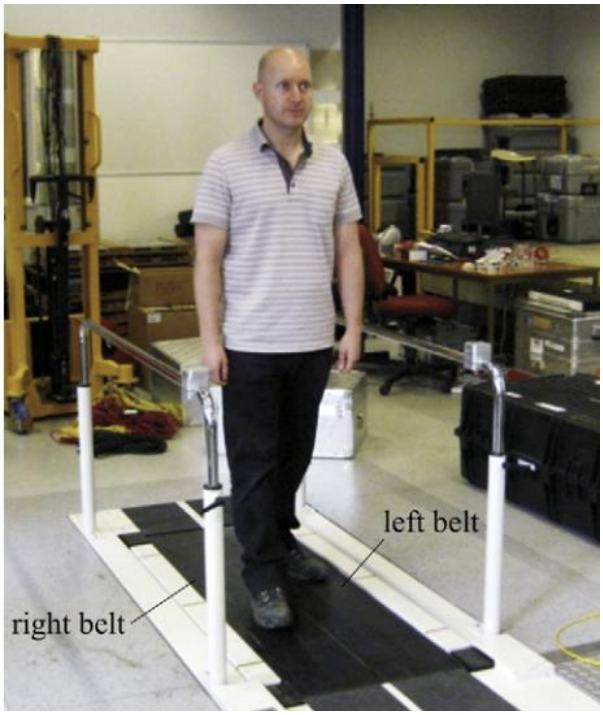

Figure 3.1 Experimental setup of typical participant on the dual treadmill walkway, after [52]

3.2 Data Processing

The proceeding section outlines the various pre-processing and processing steps required to format the force time histories in a usable format. From this, the data can be inferred to establish and form multiple relationships of the DLF, walking frequency, phase angle, and walking velocity.

3.2.1 Pre-processing

The separate left and the right vertical footfall force-time histories are summed to obtain the total vertical walking force signal for each force-time history, Figure 3.2. As demonstrated experimentally in Racic and Brownjohn [52] the DLF value and the body weight can be decoupled as they are proven independent of each other. This is visually inspected in Figure 3.3 when comparing DLF_1 to the body weight, where no known relationship or distribution is evident.

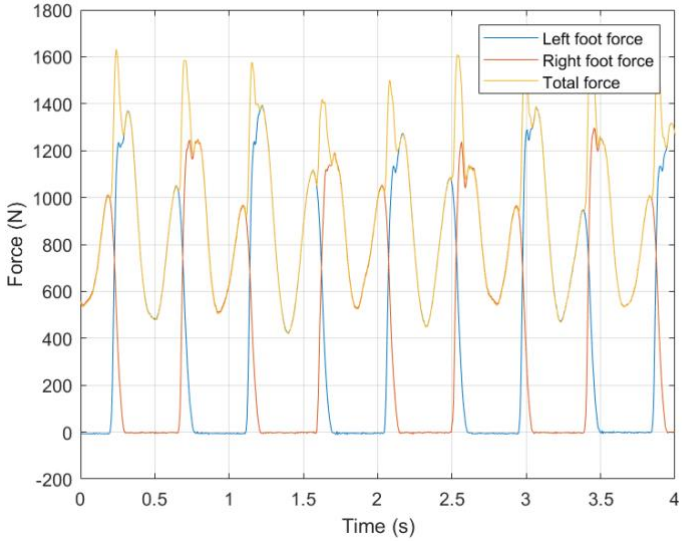

Figure 3.2 Sample vertical force-time history (participant's weight=937N, pacing frequency=2.21Hz, treadmill speed=2.00m/s)

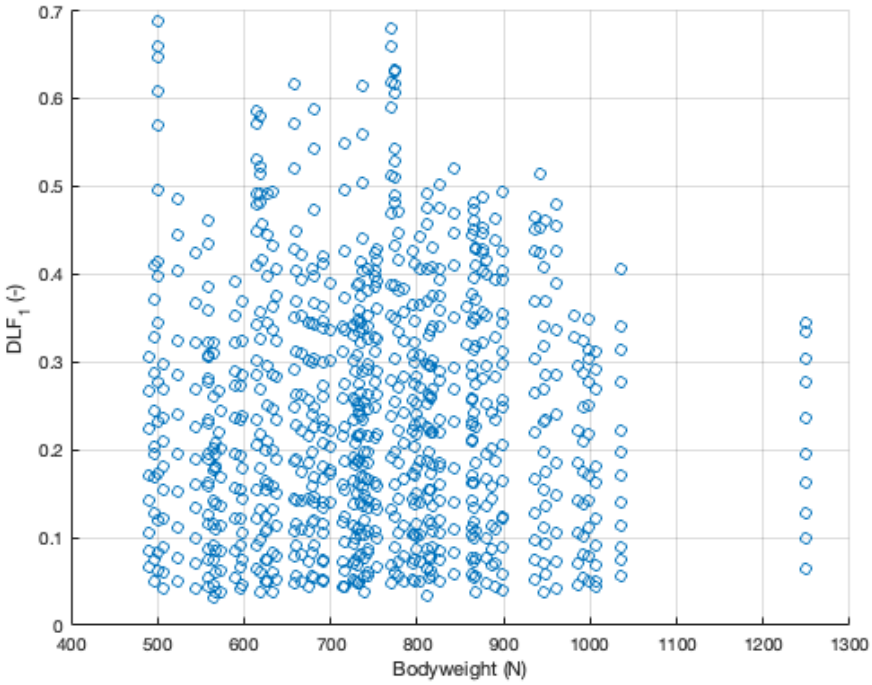

Figure 3.3 Bodyweight vs DLF1extracted from [52]

The body weight representing the static component of the signal is removed, as the force function is only concerned with the dynamic portion of the signal. The body weight is taken as the mean value of the signal. The resulting dynamic signals are then normalised by the

body weight, leaving a signal as a proportion of body weight. Hence the signal is now represented through a dimensionless unit signal. Due to the duality of the frequency and time domain, coupled with the quasi-periodic nature of walking, the signal ($x(t)$) can be approximated through a Fourier series as the sum of all the periodic frequencies up to 100Hz:

$$x(t) = \sum_{n=0}^{100} DLF_n \sin\left(2\pi f_n t + \theta_n\right) \qquad \text{Eq 32}$$

Such a model presents the discrete information of a signal at regular frequency intervals from 0Hz to the aliasing frequency (100Hz). The average frequency resolution of the signals in the data varies from 0.01-0.05Hz depending on the length of the signal considered. The frequency resolution of the frequency content of the signal is given as follows:

$$\Delta f = \frac{f_s}{N} \qquad \text{Eq 33}$$

Were f_s is the sampling frequency (200Hz), and N is the number of samples in the signal.

A usable vertical load model must have certain physical and practical limitations. As stated previously, the usable content of the signal is only up to 100Hz. Typical Fourier load models only model DLF values at integer harmonics of the walking frequency [16,19,20,45,55]. This is primarily a result of the signal only providing higher DLF values at the integer values of the walking frequency corresponding to the forcing frequency of the signal. As seen in Figure 3.4 there is scarce information evidenced in the frequency domain outside the integer values of walking frequency. Bands of information are evidenced within the immediate vicinity of the integer of walking frequency. This information is described in Chapter 2 section 2.1.2.1 and is attributed to the intra-subject variation of walking frequency and DLF values, resulting in a narrow-band signal, as seen in Figure 3.4.

As the discrete-time signals of the vertical force are presented through the time domain, and walking is described as a narrow-band process [38,52,139], the duality of the time and frequency domain can be leveraged to provide further analysis of the time signals through the

Fourier transform. The Fourier transform decomposes a periodic signal into constituent parts of a complex Fourier series. For each frequency, an associated magnitude and phase offset is assigned through the complex components of a signal. Concerning the signal, the magnitude of the Fourier transforms, and phase offset represents the DLF and phase angle, respectively. As the vertical force time histories in question are presented as a finite set of equally spaced samples, the discrete Fourier transformation (DFT) is utilised. The frequency domain representation of N number samples of a complex series $\{x_n\}$ to its frequency domain representation $\{X_k\}$ is formed as:

$$X = \mathcal{F}\{x\} \qquad \text{Eq 34}$$

$$X_k = \sum_{n=0}^{N-1} x_n . e^{\frac{-i2\pi kn}{N}} \qquad \text{Eq 35}$$

$$X_k = \sum_{n=0}^{N-1} x_n . \left[cos\left(\frac{2\pi}{N}kn\right) - i.sin\left(\frac{2\pi}{N}kn\right)\right] \qquad \text{Eq 36}$$

Where N is the total number of samples, n is the nth number of samples, k is the kth frequency, and i is the imaginary unit. The Fast Fourier transformation (FFT) is used in place of the DFT due to the FFT's faster computational time and efficiency. These terms are often used interchangeably as the FFT is used more frequently than its DFT counterpart for discrete-time signals. Figure 3.4 presents a typical FFT of a 937N participant walking at 2.21Hz up to 30Hz.

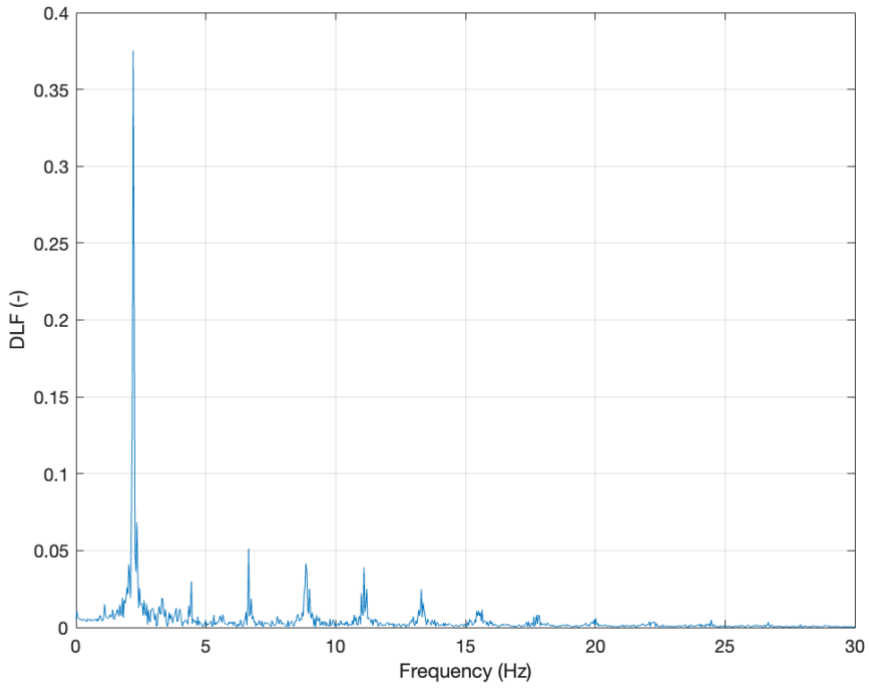

Figure 3.4 FFT of time signal from Figure 3.2(participant's weight=937N, pacing frequency=2.21Hz, treadmill speed=2.00m/s), signal is shown as continuous but is discrete in nature. The continuous line of the frequency domain representation is only used for easier visualisation.

From Figure 3.4, peaks in the frequency domain can be seen accompanied by the associated energy leakage around each integer of the walking frequency. Outside of the peaks the signal contains little information, with the remaining signal seen as zero magnitudes or a white noise process. Therefore, only modelling near the walking frequency integer has become common practice and is justified. The average walking frequency of each signal is taken as the frequency of the first peak in the frequency domain of the signal.

3.2.2 Data processing

The first step is curtailing the number of walking time histories to ensure a standard range of walking frequency is used and any extreme data points do not bias or alter the findings. In line with Chapter 2 Section 2.1.2.1, all signals outside the walking frequency range of 1.5-2.5Hz are discarded because they are deemed exceptionally fast or slow walking frequencies

[4,53,70,71,73]. This selection reduces the content from 824 to 672 measured force-time histories.

Figure 3.5 provides the histogram of average walking frequencies of the signal pre-and post the limitation of walking frequencies. To confirm the normally distributed nature of the average walking frequency, the one-sample Kolmogorov-Smirnov test was performed using the standard normal curve as a reference, i.e., ~ N (0,1)(Mean, Variance) [225].

The one-sample Kolmogorov-Smirnov test is a non-parametric test that quantifies the distance between the sampled and reference distribution [225]. The test provides a metric of the distance between cumulative distribution functions (CDF) and an associated p-value. The Kolmogorov-Smirnov (KS) test is used in place of the student t-test or other normality test due to the KS test's robustness against differences in the mean and variance of the data against the reference case [225]. Furthermore, the student t-test only considers the normal distribution as the reference case. The KS test can be altered to measure parametric or non-parametric cumulative distribution. The relative distance between the cumulative distributions is given as follows:

$$D_{n,m} = sup|CDF_1(x) - CDF_2(x)| \quad \text{Eq 37}$$

Where sup is the supremum function and CDF is the empirical cumulative distribution functions of inputs x. n and m represent the size of the first and second cumulative distributions. The null hypothesis is rejected at a level α if:

$$D_{n,m} > \sqrt{-ln\left(\frac{\alpha}{2}\right).\frac{1+\frac{m}{n}}{2m}} \quad \text{Eq 38}$$

The null hypothesis statement is that the data is drawn from the reference distribution, which is a standard normal distribution. The alternative hypothesis is that the error does not come from the distribution at a significance level of p= 5% [78].

The z score of the walking frequencies is first determined to transform the data to the same length and scale as the standard normal distribution. The z score is formed through Eq 39

where $WF_{norm}$is the normalised walking frequency, $\overline{\mu_{WF}}$ is the sample mean walking frequency and $\overline{\sigma_{WF}}$ is the sample standard deviation of the walking frequency. Performing the one-sample Kolmogorov-Smirnov test, it is confirmed that the average walking frequencies are indeed normally distributed and are defined through the normal distribution ~ N (1.85, 0.1241). The p-value of the one-sample KS test is 0.34. Thus, the test presents evidence not to reject the null hypothesis. Figure 3.5 presents the histogram of results before and after limitation, Figure 3.6 illustrates the CDF of the normalised data and the standard normal distribution N (0, 1).

$$WF_{norm} = \frac{WF - \overline{\mu_{WF}}}{\overline{\sigma_{WF}}} \qquad \text{Eq 39}$$

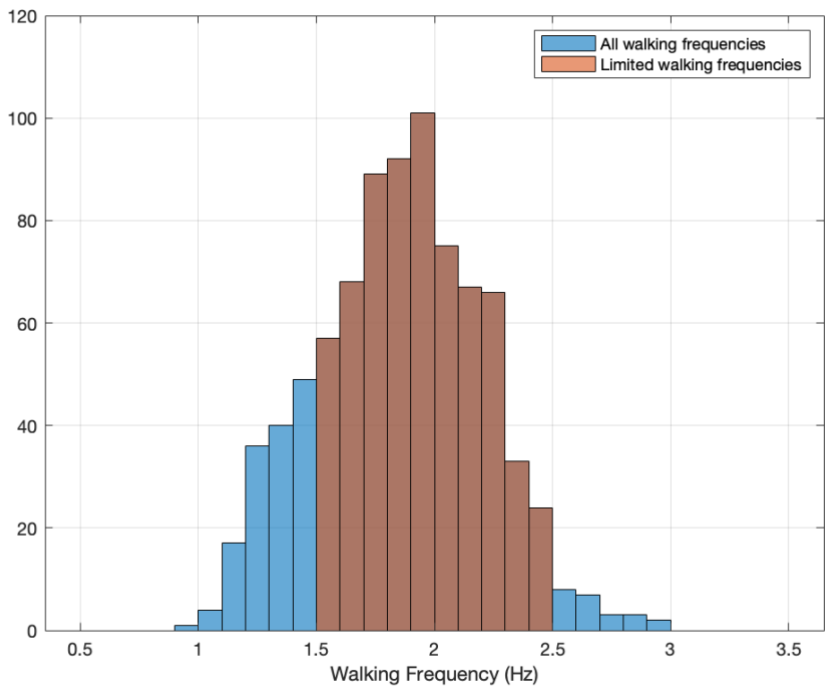

Figure 3.5 Histogram of walking frequency showing walking frequencies pre (Blue) and post-limitation (red), bin widths = 0.1Hz

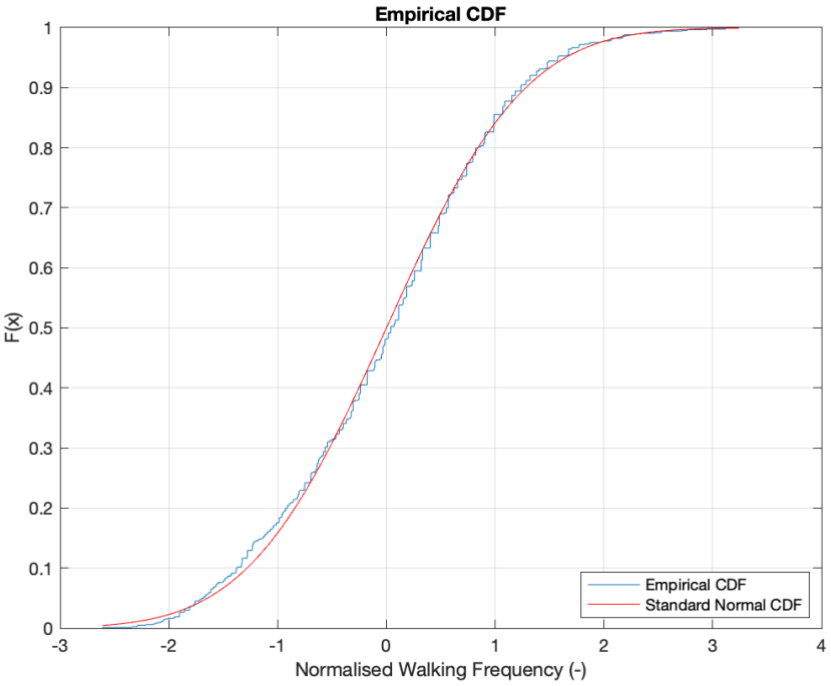

Figure 3.6 CDF of normalised walking frequencies compared to the standard normal distribution

The distribution of walking frequencies is biased and forced. As the walking velocity was controlled, it forced participants to walk at a frequency dictated by the treadmill's speed. As the experimental campaign proceeded through various walking speeds incrementally, participants were forced to increase their step length or walking frequency. Therefore, using such instrumentation forces participants into an irregular pattern of walking. Measurements must be taken when participants are walking at a self-guided frequency and speed to determine the actual distribution of walking frequencies. The distribution of free walking on a structure is anticipated to be statistically different from the instrument distribution. Such an experimental campaign is not assessed in this thesis and is the major limitation of the thesis.

Traditionally, peak picking the DLF value at the integer harmonics approximates the entire signal. As seen in Figure 3.4, DLF values exist around the integer value. Thus, such magnitudes of DLF leakage, along with the off-frequency forces, can result in an increased or decreased signal value in the time domain compared to just selecting the peak values. This chapter seeks to produce a novel method of extraction.

To determine the equivalent DLF, a bandpass filter is used at each harmonic with upper and lower frequency range limits at plus or minus a percentage of the walking frequency. One low pass and one high pass filter are simultaneously used to provide the limiting effect within the given frequency limits. The low pass filter has a frequency limit equivalent to the ith integer of the walking frequency plus some percentage of the walking frequency. Counter to that, the high pass filter has a frequency limit equivalent to the ith integer of the walking frequency minus some percentage of the walking frequency. The percentage of walking frequency is taken as 5-50% to ensure no overlapping of the signals is seen, therefore ensuring components of the signal are not double counted.

Figure 3.7 provides an example of the filter at the first harmonic of walking with a high and low pass at 50% of the walking frequency. The bandpass filter attenuates and rejects frequencies outside of the range. However, the bandpass filter is imperfect, and regions adjacent to the proposed frequency range are not rejected but attenuated. This is deemed 'the filter roll off'.

What remains is the filtered signal around the harmonic, considering all frequencies and DLF values around it. Taking the average of the peaks of the filtered signal reconstructed to the time domain (Figure 3.7), an estimate of the DLF in each harmonic is made. The process is repeated for all force time signals considering an upper and lower limit of the filter plus or minus 5-50% of the walking frequency for each harmonic.

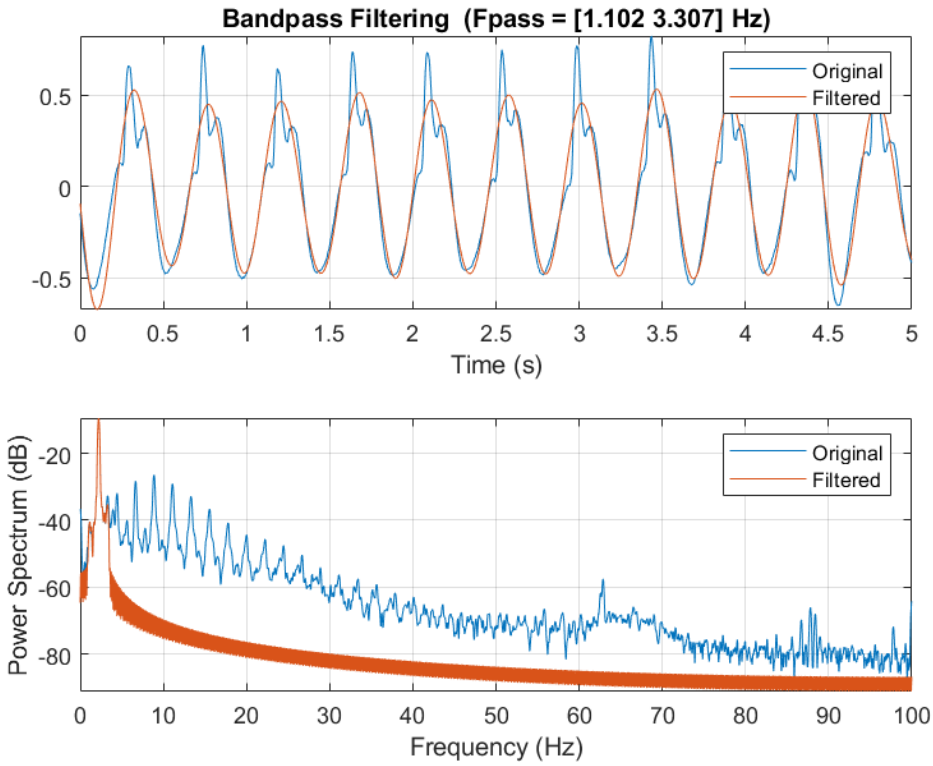

Figure 3.7 a) Time domain representation of Bandpass filter on the signal of Figure 3.4 at the first integer value of walking, with frequency limits equal to plus or minus 50% of the walking frequency. b) PSD representation of a)

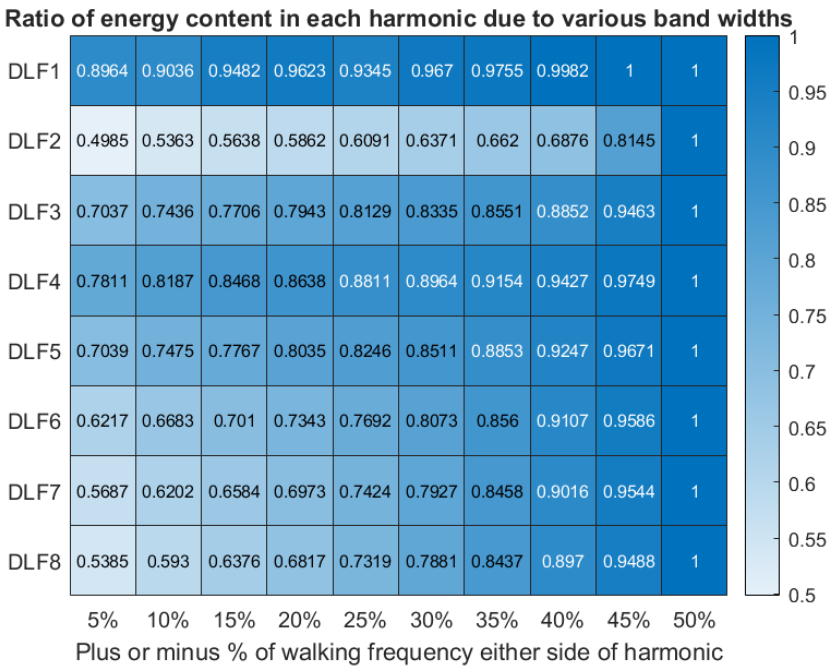

Figure 3.8 Ratio of energy content in each harmonic compared to total (+/- 50% of walking frequency) energy content in each harmonic for the average result.

Table 3.1 Percentage change in DLF over all DLFs compared to peak picking for various percentages of walking frequency bandwidth.

+/- Percentage of walking frequency considered	5%	10%	15%	20%	25%	30%	35%	40%	45%	50%
Average percentage change in DLF values from selecting peak (%)	23	31	33	34	34	36	36	37	37	39

Figure 3.8 shows the integral of the PSD (energy) variation in each harmonic when considering the various frequency bandwidths around the peak harmonic walking frequency. Most energy is in the first harmonic and distributed close to the peak value. After the first harmonic, the energy content of the signal starts to dissipate over a more considerable amount of frequency range. Most energy (89.6% in Figure 3.8) is within a bandwidth of 5% of the walking frequency on either side of the first harmonic. This indicates that the first harmonic has a sharp peak consistently across all the results. Thus, the energy content of the signal is seen to act predominantly at the integer harmonic. However, other harmonics have larger relative energy spreads.

There is no indication of a correlation between increased energy spread around the harmonic and increased integer harmonic (i.e., the second harmonic of walking has the largest relative energy spread, not the eighth, Figure 3.8). Table 3.1 presents the average percentage variation

in DLF1 with different bandwidth sizes (i.e., frequency filters) around the peak value. The peak-picking method produces the lowest DLFs in all scenarios. The value of DLF tends to stabilise after the 10% filter and remains relatively constant throughout, barring rare exceptions. The signals are filtered to ±50% of the walking frequency due to the marginal change in DLF after 10%, and thus choosing 50% ensures all energy influences around a harmonic are considered. As demonstrated in Table 3.1, filtering the signal around the harmonic of walking produces a DLF value greater than just selecting the peaks. Thus, the energy leakage around the harmonics creates a more representative DLF value.

Taking only the peak would sometimes negate 40% of the DLF value due to energy leakage and intra-subject variability. Thus, taking a filtered estimate provides an artificial degree of representation of the narrow-band nature of walking. Figure 3.9 presents the filtered data vs the peak picking method for DLF_1, thus indicating the filtered method results in a reduced DLF value compared to selecting the peak value.

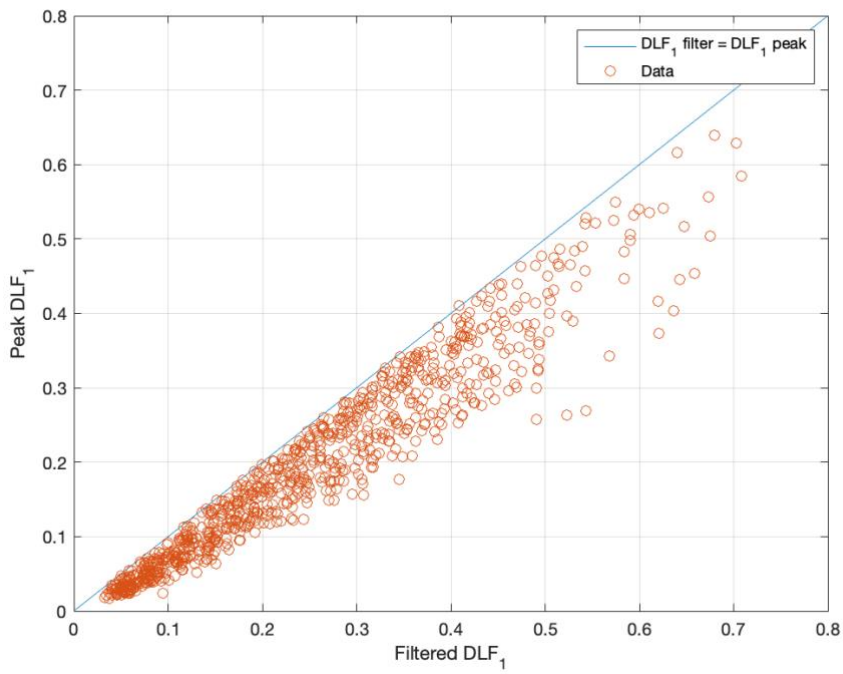

Figure 3.9 DLF_1 peak vs DLF_1 filter using method described in Section 3.2.2 (plus or minus 50% filter)

As seen in Chapter 2 Section 2.1.2.3, Fourier models are often curtailed at a frequency that is deemed to represent the transition from a resonant to an impulsive-like response to the load. Therefore, a criterion is necessary to assess the limit of integer harmonics of the new proposed walking force model. To this end, Figure 3.4 presents the FFT of a typical signal. Visually only the 8th or 9th harmonic of walking is distinguishable from that of a white noise process. Based on the author's experience, it is postulated that most pedestrian structures exhibit fundamental modes below 20Hz. Therefore, due to the lack of notable DLF values seen above 20Hz in the frequency domain and limited structures providing dominant modes of vibrations above 20Hz, only information up to the eight harmonic of walking is considered. The DLF values observed for the 9th and 10th harmonic range are all below 0.005, which accounts for 120 times less than the typical DLF value of the first harmonic.

It was determined the DLF model would be curtailed at the 8th harmonic and have a bandwidth of plus or minus 50% of the walking frequency. For each DLF one to eight, a corresponding walking frequency is known. It has been historically demonstrated that the DLF and walking frequency have a strong dependent relationship, Chapter 2 Section 2.1.2.3. Whilst other authors have attempted to provide alternative relationships, such as independent distributions [4], or velocity-based inputs[63], the use of the walking frequency-based relationship offers a more accessible interpretation of a model, as the forcing frequency itself is used to define the state of a resonant or non-resonant like response.

3.3 A statistical representation of vertical walking force

The proceeding section provides a statistical overview of the data to represent the data used through the lens of inter- and intra-subject variability. Principally the variation is evident through the inter- and intra-subject variation of the walking frequency and DLF. Other characteristic variations of the inter-subject variation are further considered. Finally, an assessment of bias in the data due to the sex of each participant is explored to determine if walking spatiotemporal parameters are statistical dependant on the sex of the participant.

3.3.1 Walking Frequency

The critical determinant of the resonant response of vertical walking is when the walking frequency, or a harmonic integer of, matches with a natural mode of the structure. The Fourier series models presented in research and industry [16,19,20,28,53,55] show the walking frequency as the average walking frequency. The subject of the inter-subject variation of walking is discussed in Section 3.2.2. The proceeding sub-section outlines the intra-subject variation of walking frequency.

3.3.1.1 Walking frequency intra-subject variation

To deduce the variation of walking frequency on a step-by-step basis, the same method for extracting DLF values is used, as noted in section 3.2.2. However, instead of taking the average DLF value between the peaks, the time between each peak of the first integer of walking is monitored. Then, the reciprocal of the time between successive peaks is seen as the intra-subject walking frequency. From the example, in Figure 3.7, the following histogram of walking frequencies is seen in Figure 3.10a. To compare all subject intra-subject variability, each participant's estimated intra-subject walking frequency is normalised by the average walking frequency and divided by the standard deviation, thus producing results normalised to unity and in the same length scale as the normal distribution, Figure 3.10b).

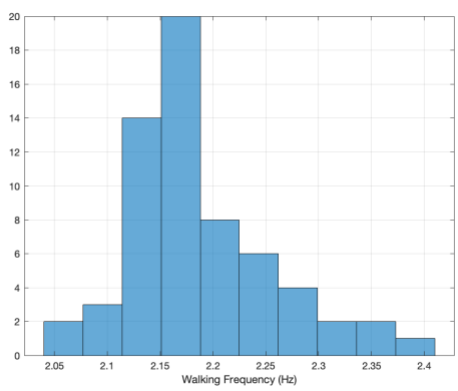

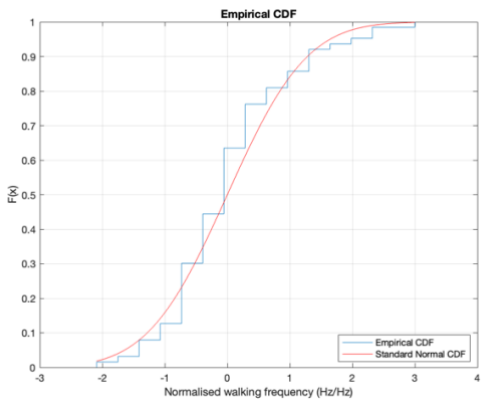

Figure 3.10 a) Intra-subject variation of subject 842 b) normalised values of intra-subject walking frequency cumulative density function compared to the standard normal distribution.

The intra-subject variation of walking in the example (Figure 3.10) and within the dataset appear to follow a normal distribution. The likeliness of fit of the standard normal distribution of the intra-subject walking frequency is assessed through the one-sample Kolmogorov-Smirnov test using the standard normal curve as a reference distribution, i.e., ~ N (0,1)[225].

The one-sample Kolmogorov-Smirnov test is performed for all samples. The null hypothesis is that the normalised intra-subject variation is described through a standard normal distribution at an alpha level of 5%. It is shown that 618 of the 672 (92%) walking time histories demonstrated failure to reject the null hypothesis of a standard normal distribution of intra-subject walking frequencies. Therefore, the null hypothesis is accepted, and it is reasonable to assume that all the 672 examples can be described by the standard normal distribution N (0,1).

As each intra-subject walking frequency is normalised to the standard normal distribution, the process can be further examined through the coefficient of variation (CoV) (Eq 40) representing the mean and standard deviation of the data. As indicated, many results appear from a standard normal distribution when standardised. Therefore, the CoV should appear similar for all values of the intra-subject variation across all walking frequencies.

$$CoV = \frac{\bar{\sigma}}{\bar{\mu}} \qquad \text{Eq 40}$$

Where $\bar{\sigma}$ is the sample standard deviation and $\bar{\mu}$ is the sample mean. Figure 3.12 presents the transformation results concerning the walking frequency. Figure 3.12 indicates no dependency on the walking frequency with the CoV, and it is evident that the results show a single dominant value estimate. The mean value of the intra-subject walking frequency CoV is 0.0185.

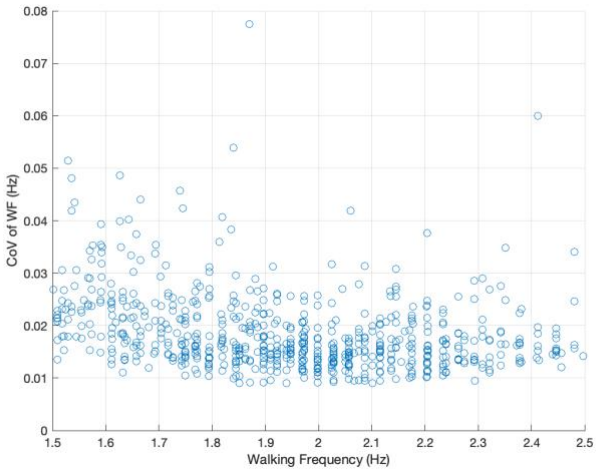

Figure 3.11 CoV of the intra-subject variation with respect to the walking frequency

Figure 3.13 presents the histogram of CoV. The distribution of the CoV is well modelled through the gamma distribution due to the non-negative nature of the CoV. The CoV is fitted to the gamma function using the MLE and is defined through the parameters a = 8.286 and b = 0.0022. For a complete overview of the gamma distribution, the reader is guided to [109].

Such a CoV for intra-subject variation of walking frequency is similar to that of Brownjohn et al. [29] and Chen et al. [4], who both indicate that the CoV of intra-subject variation of walking frequency is 3% - 3.25%. The data provided in the chapter suggests a 1.2% decrease in the overall mean CoV value. Chen et al. [4] only used double footfalls for the data acquisition, and participants had to walk multiple times at the same frequency to determine the "intra-subject" variation. However, it is the view of the author that this is not genuinely intra-subject because the walks occurred at different times and are not from successive footsteps. Therefore, a bias or difference in results is anticipated due to this experimental limitation.

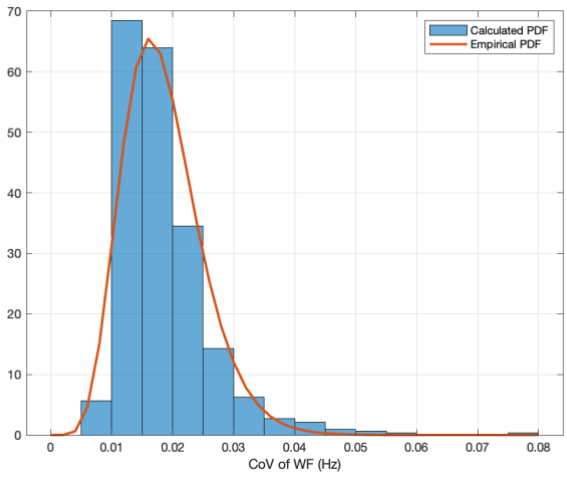

Figure 3.12 Calculated and empirical PDF of CoV for the intra-subject walking frequency

Finally, the autocorrelation of the successive walking frequencies is investigated to determine if the intra-subject walking frequencies are a random or autoregressive process. Autocorrelation is the correlation of a discrete-time signal convolved with a lagged version of itself, thus determining if reoccurring patterns or correlation occurs within a signal. To provide meaning to autocorrelation, the normalised autocorrelation is used to bring the output of the function in the scale of -1 and 1. A value of 1 indicates a strong positive correlation, with -1 indicating a strong negative correlation. The normalised auto-correlation, ρ_{xx}, of a stochastic process is defined as:

$$\rho_{xx} = \frac{\sum_{i=1}^{N-k}(x_i - \mu_x)(x_{i+k} - \mu_x)}{\sum_{i=1}^{N}(x_i - \mu_x)^2} \qquad \text{Eq 41}$$

Where N is the number of discrete values, k is the lag, x_i is the ith value of the series x and $\mu_x$is the mean of the series x. Figure 3.13 present a random selection of the 672-time series occurrences and the normalised auto-correlation of the intra-subject walking. Assuming a maximum lag of N-1, it is shown that many of the samples demonstrate uncorrelated behaviour and thus exhibit a random process. While subject 222 provides a strong autocorrelation, it is seen as an exception of the data, with only a limited number giving similar results.

Table 3.2 further supports this claim of the non-autoregressive nature, with only 1% of all autocorrelation values being above an absolute autocorrelation value of 0.5. Table 3.2 further demonstrates that, even at a low level of correlation (e.g., 0.25). Therefore, due to the low percentage of auto-correlation values showing any dependency, the intra-subject variation of walking frequencies can be considered a random process.

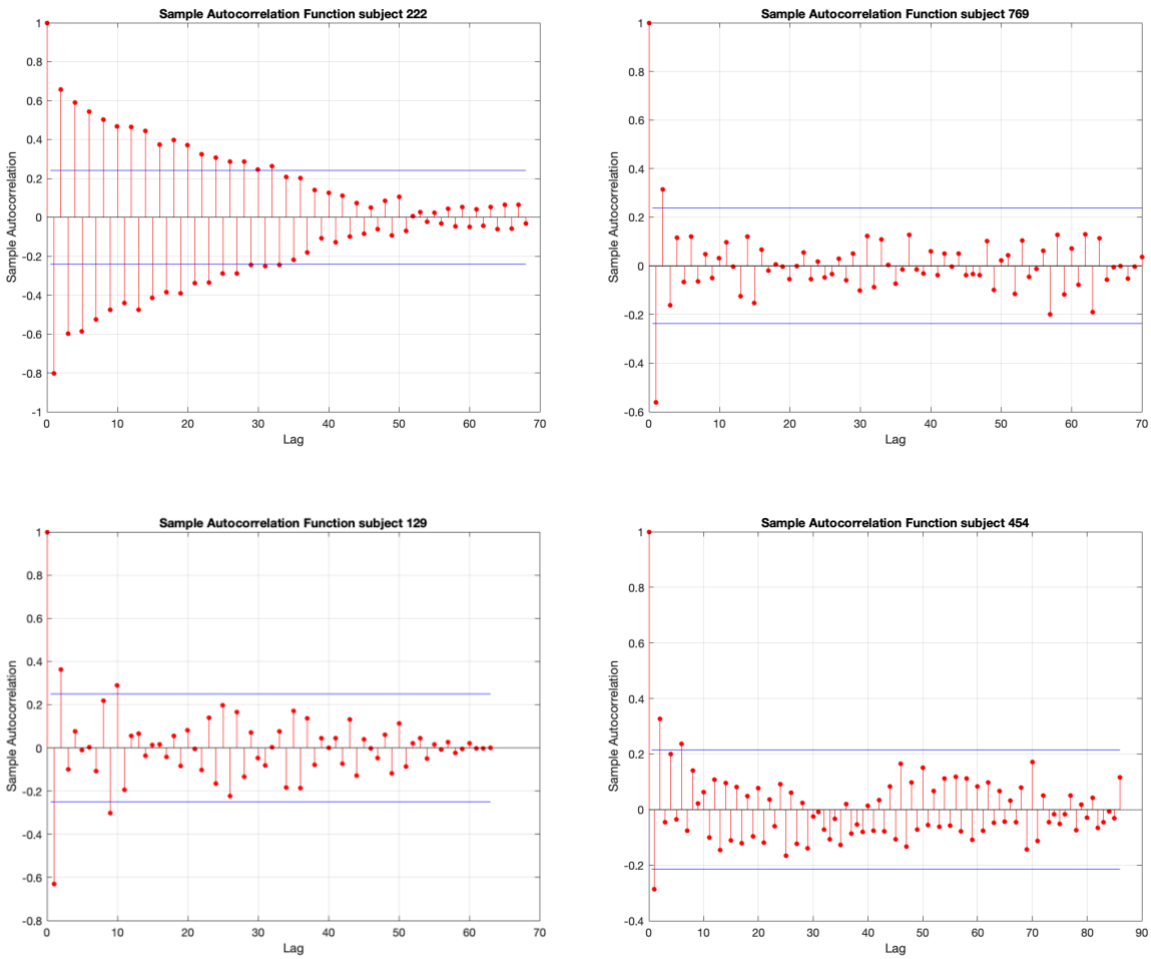

Figure 3.13 Auto-correlation of a random sample of participant's intra-subject variation of walking frequency

Table 3.2 Percentage of auto-correlation values above a specific threshold for all signals

Correlation value (Absolute magnitude)	Percentage of values of the intra-subjection variation of walking frequencies over correlation value (%)
0.25	5
0.375	2
0.5	1
0.75	0.1

This section provides evidence to conclude that the intra-subject variability of walking frequencies is taken from a normal random distribution defined through its CoV. The CoV is sampled from the gamma distribution with shape and scale parameters a = 8.2865 and b = 0.0022, and successive samples of the walking frequency are uncorrelated.

3.3.2 DLF

The largest variation of all Fourier models arises from the inter-subject variation of the DLF values of each harmonic, and only a few researchers have attempted to determine or incorporate the intra-subject variation of walking. Section 3.3.2.1 explores the inter-subject variation of the DLF relationship with the walking frequency presented through a Frequentist and Bayesian perspective. Finally, the intra-subject variation of the DLF values is explored in the same vale as the walking frequencies in section 3.3.1.

3.3.2.1 DLF inter-subject variation

From the methodology outlined in section 3.2.2, the corresponding DLF values for all eight harmonics of walking are known, along with their associated walking frequency values. Therefore, within section 3.3.2.1 various machine learning methods are trialled to find the representation of the DLF walking frequency relationship with respect to both a Frequentist

and Bayesian statical analysis that minimises the error between predicted function versus measured DLF. Further, several data processing steps are introduced to provide a robust and generalised approximation of the data.

Partitioning the data is critical in providing robustness for regression analysis and preventing overfitting. To ensure any machine learning method is robust to generalisation on unseen data, the initial subsection of 672 DLF and walking frequency data is further subdivided. Representing approximately 10% of the data, 67 random sets are set aside and used to validate the accuracy of each of the models for all eight DLF values. The test set is only used to measure and determine the model accurately; it is not used for training. The remaining 90% of the data is used to train each method to provide a regression model. The accuracy of each model is measured and defined herein as the squared Euclidean distance, commonly known as the root mean squared error (RMSE), between the predicted acceleration response of the real load versus the synthetic.

Further to sub-setting the training and testing data, each method is cross validated. Cross-validation, specifically k-fold cross-validation, is the process of resampling the data into k different sets and holding out one of the k sets. The model is then successively trained separately at k other times, producing k different parameters for the single methodology. Then, on the held-out test data, the test data is processed by all k models and then concatenated to provide an average regression result. Cross-validation aids in the process of inspecting overfitting. Overfitting is the process by which the training data and model parameters provide bias and do not generalise to new data. Overfitting is characterised by high accuracy on training data and comparatively low accuracy on new data. Overfitting is to be avoided because it will bias future unseen examples, thus rendering the model ill-suited for the task.

Fundamentally and philosophically, two schools of thought for statistical inference exist Frequentist and Bayesian [109]. Within academic and professional civil and structural engineering, statistical inference is often viewed monolithically through a Frequentist approach. Whilst Frequentist statistics are taught due to their popularity and ease of use, benefits can be gained from using Bayesian statistics or a combination of both [226,227].

To determine the suitability and accuracy of the regression models, the RMSE of the predicted versus actual DLF values is compared on the held-out test set. Table 3.3 provides the RMSE of all three regression models (Linear [110], Gaussian Process [228] and Neural network [110,229]) subject to Bayesian optimisation [230–232]. Specifics of each method can be found in the given references. Figure 3.14-Figure 3.16 visually represents the DLF relationships for each method.

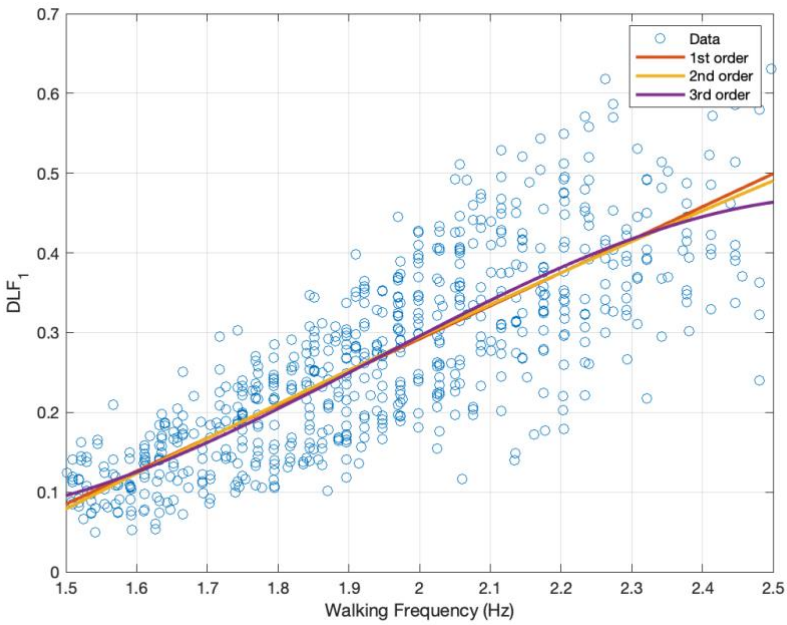

Figure 3.14 Linear and Polynomial fit of DLF_1 with respect to the walking frequency

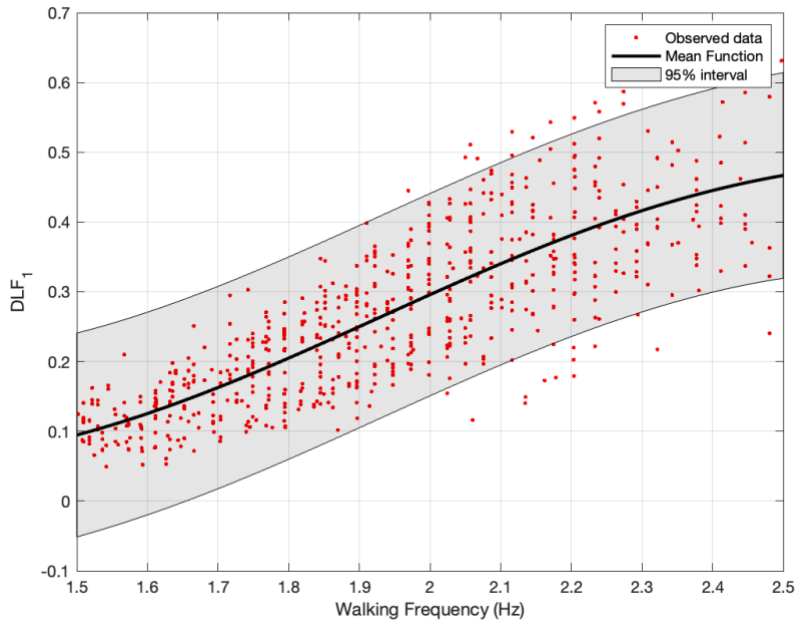

Figure 3.15 Bayesian optimised GP of DLF_1 with respect to the walking frequency

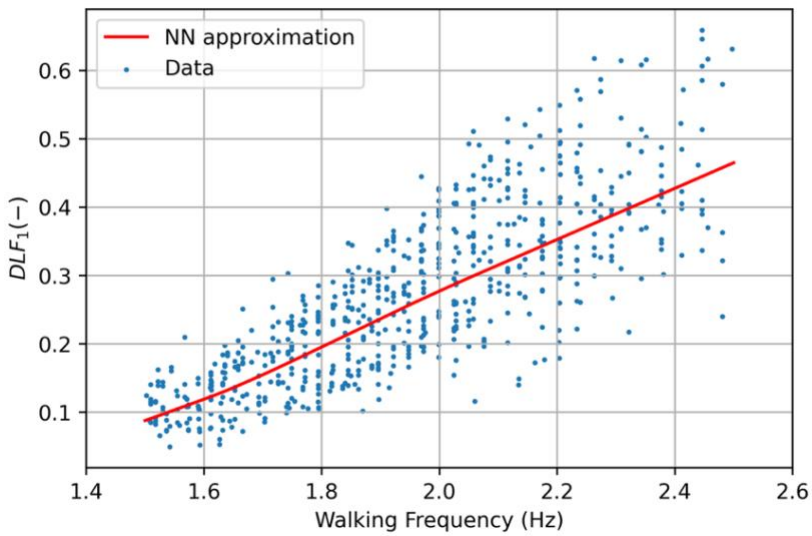

Figure 3.16 NN representation of DLF_1 with respect to the walking frequency

Table 3.3 RMSE of DLF_1 based on various modelling techniques on a held-out set.

Model	1st order Polynomial	2nd order Polynomial	3rd order Polynomial	GP	NN
RMSE	0.0742	0.0746	0.0746	0.0743	0.0687

The NN provides the lowest RMSE of all the models for DLF_1, second only to linear regression. The RMSE of the first DLF is the accuracy metric due to the wide variety of values compared to any other harmonic of the walking integers. Whilst the NN is viewed as the most accurate, the usability of the NN model could be improved. Other than the visual interpretability of the NN, using the NN in any scenario other than software applications provides limited uses of the model. The linear regression is less accurate than the NN; however, the ease of interoperability and the ease of use is a beneficial factor. As stated in the objectives of this thesis, the goal is to provide a new load model for industrial use. To achieve this objective, metrics beyond measurable ones must be considered, such as useability and the experience of users. Visual differences in the relationship of various other DLF models are evident. As the models are typically presented as linear functions, comparing the function values with the polynomial model over the NN counterpart will be more accessible.

The proceeding sections, 3.3.2.1.1 and 3.3.2.1.2, provide an overview of the walking frequency and DLF models presented in this thesis in the context of the frequentist and Bayesian perspectives, respectively. The validation of each model's assumptions is tested to ensure the models are correct and justified. Section 3.3.2.1.3 compares the Bayesian and frequentist linear models concerning themselves, with section 3.3.2.1.4 comparing the presented models with historic and modern DLF models for the Fourier representation only considering the inter-subject variation.

3.3.2.1.1 Frequentist representation of DLF inter-subject variation

The Frequentist approach assumes the parameters to be fixed and the data random. The fixed nature of the parameters means probabilities cannot be assigned to parameter values. The

parameter value can only be estimated through sampling the data, but the parameter's actual value is unknown as only sample subsets of populations are trailed. Therefore, long-running repeatable experiments are required to determine a parameter value based on the assumption that the population subset is representative to combat ill-poised statistics. Frequentist statistic are fundamentally only associated with repeatable events.

The primary method of frequentist inference is performed through the maximum likelihood estimation (MLE) of parameters. The MLE is a method of approximating point estimations of parameters $\emptyset$ or statistical tests of interest. It is first assumed that a set of observations of data D are independent and identically distributed, where $D = \{D_1, D_2, .., D_n\}$. The random variable D has a univariant density function of $f(D, \emptyset)$. The function $f(D, \emptyset)$ is determined via the data and or model assumptions. Typical functions include the Normal or Poison distribution. The likelihood function is a product of the data given the parameters of the density functions.

$$P(D|\emptyset) = \prod_{i=1}^{n} f(D, \emptyset) \qquad \text{Eq 42}$$

The maximisation of Eq 42 therefore, produces the MLE, given formally as:

$$\widehat{\emptyset}_{MLE}(D) = arg \max_{\emptyset} P(D|\emptyset) \qquad \text{Eq 43}$$

Where $\widehat{\emptyset}_{MLE}$ is the set of most likely parameters. It is often mathematically more convenient to transform the likelihood function with the natural logarithm. Since the logarithm is a monotonic function, the maximisation of $P(D|\emptyset)$ occurs at the exact locations as the log of the function. A necessary condition of the location of maximisation is for the likelihood function derivatives concerning the parameters to be zero. From this, the location, or locations, of maximisation can be found.

Further fundamental tools of Frequentist inference are *p*-values and null hypothesis testing. Null hypothesis testing determines whether sufficient evidence from the data supports a hypothesis. Often the measure of such a test is selected from the *p*-value, a measure from 0-1.

The *p*-value is the probability of obtaining a test result as extreme or more extreme than the given null hypothesis.

Researchers commonly use *p*-values to conclude statistically significant results. Calculating the *p*-value implies statistical significance when a *p*-value is sufficiently small compared to some predefined value α = 0.05, 0.1. Using an alpha value is a fictitious limit on a rejection policy. Using 0.05 results in a 1-in-20 chance that the result is a false positive. The historic dictation of the significance being 0.05 is not founded on mathematical rigour but on human decisions[233]. This highlights the main downfall of the *p*-value, if a value is above or below the limit, they are immediately deemed opposite in result and provide concurring findings. Cowles and Davis [233] offers a historical overview of Fishers' decision to select p = 0.05 as the standard practice.

Using a metric like the *p*-value has created controversy in recent years [234]. The *p*-value does not establish a probability of a hypothesis. It is a tool for the user to determine if they should reject or accept the null hypothesis. It has been criticised that authors often categorically state statistical significance merely by having a *p*-value less than a particular alpha value provided. Over the past century, since its inception by Ronald Fisher, the scientific community has used it as a definitive metric of significance.

Finally, results are often misrepresented due to the weight the *p*-value holds within the academic community for statistically significant results. Simonsohn et al.[235] analysed several *p*-values from published psychology papers. They concluded that a suspicious proportion of published *p*-values are clustered around 0.05. It has been long conjectured that such *p*-hacking practices have occurred throughout the research. *p*-hacking is the process of curating the data in such a way that it reinforces the authors' hypothesis.

As the training set of walking frequencies and DLF values confirms that the linear model produces a representative model, the held-out set is concatenated to provide the complete dataset of 672 examples and used for inference on the selected model. The underlying classical assumptions of linear regression must be assessed to ensure the linear regression model is an appropriate estimator of the walking frequency and DLF relationship. The assessment is performed in the context of the ordinary least squares (OLS) and, coincidently,

the Maximum Likelihood Estimation (MLE) approach to parameter estimation first. The classical assumptions of the OLS are:

- The regression model is linear in the coefficients and the error term.
- The error term has a population mean of zero.
- All independent variables are uncorrelated with the error term.
- Observations of the error term are uncorrelated with each other.
- The error term has a constant variance (no heteroscedasticity).
- The error term is normally distributed.

As presented in Figure 3.18, the data is visually linear in the walking frequency, validating the linearity requirement of the linear model. The normal distribution of the errors is assessed through the one-sample Kolmogorov-Smirnov test using the standard normal curve as a reference, i.e., $\varepsilon_i \sim N(0,1)$ [225]. First, a pre-processing step is performed on the raw residuals of each DLF. The Z-score of each residual is taken to normalise the data into the same length scale as the standard distribution, Eq 39. As the actual population mean and standard deviation are unknown, the sample mean $\bar{\mu}$ and standard deviation $\bar{\sigma}$ is used instead. The null hypothesis for each DLF is stated as the normalised errors of each DLF model come from a standard normal distribution. Four out of eight DLF errors provide strong evidence to fail to reject the null hypothesis, coming from a DLF_2, DLF_3, DLF_7, and DLF_8 coming from a standard normally distributed. Therefore, for a random process such as walking, a linear model approximates the data well. The mean error values for each of the harmonics: are 0.0008, 0.0032, 0.0014, 0.00006, 0.0001, 0.0004, 0.0008 and 0.0011, respectively. Whilst the mean values are not exactly zero, the magnitude of the mean is negligible compared to the magnitude of the DLFs they represent. Therefore, the residuals can be assumed to be sampled from a zero mean Gaussian function. Figure 3.17 presents the cumulative distribution functions of the normalised data for each DLF compared to the standard normal distribution.

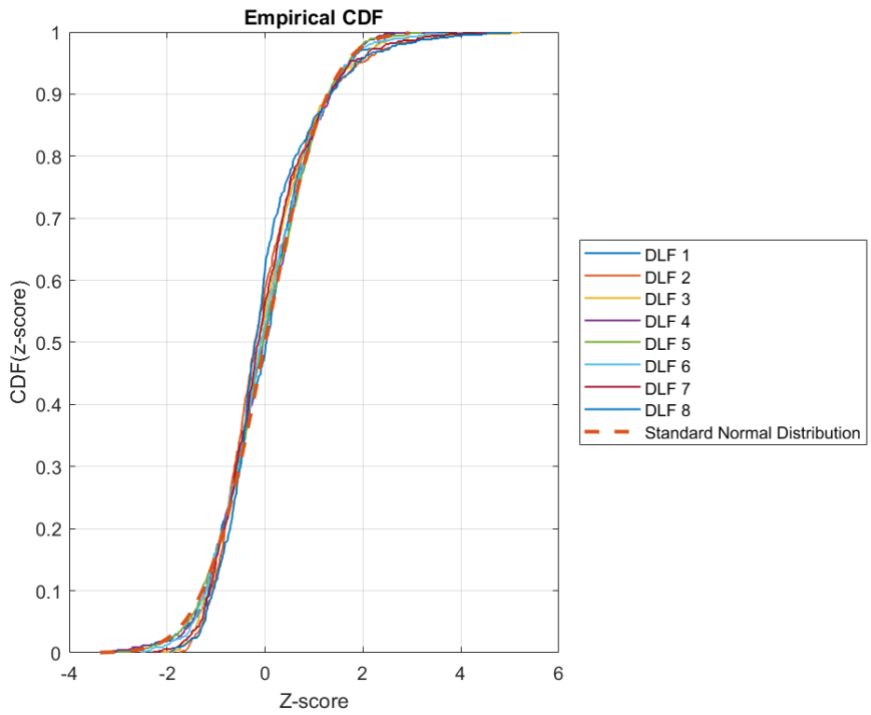

Figure 3.17 Cumulative density function of the residuals of DLF_1 to DLF_8 compared to the standard normal distribution.

The assumption of data homoscedasticity is central to linear regression models and entails the errors having a constant variance, being independent of the input variable and non-autoregressive [236]. To determine if the data is autoregressive and conditionally heteroscedastic, the Engle test [237] is performed. The null hypothesis is that the residual errors come from a heteroscedastic series. The test fails to reject the null hypothesis. The Engle test provides strong evidence (P = 0.34, compared to the significance value of 0.05) that the data is heteroscedastic.

The consequence of heteroscedasticity means the OLS estimator is not the best linear unbiased estimator, and the variance of the errors is not the lowest of all the unbiased estimators. The presence of heteroscedasticity does not cause the parameters, but instead the error variance, to be biased. Weighted least square regressions are employed to address heteroscedasticity [238]. Each observation is weighted using a diagonalised matrix to bias results closer to the mean and penalise results far from the mean before the normal equation,

or maximum likelihood estimation is performed [238]. The weight is taken as the reciprocal of the variance of each measurement to the mean value, thus providing a penalty for results that are not well represented by the mean.

Figure 3.18 presents the weighted linear regression through the lens of Frequentist statistics. Each DLF is mapped to the various integer walking harmonics from 1 to 8, along with the associated equations for each DLF.

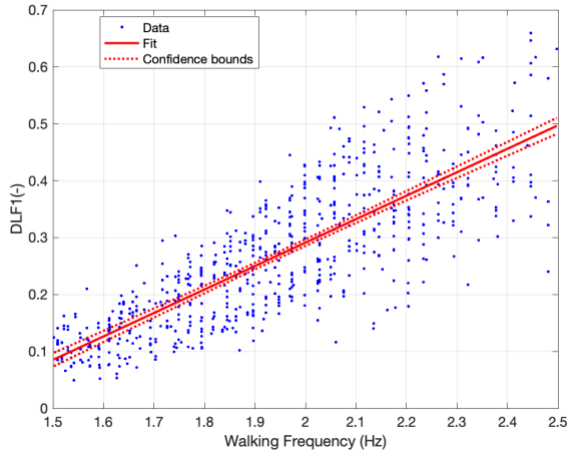

$DLF_1\ (f_p) = 0.41212\ f_p - 0.5331 + N\ (0.0008,\ 0.0055)$ Eq 44

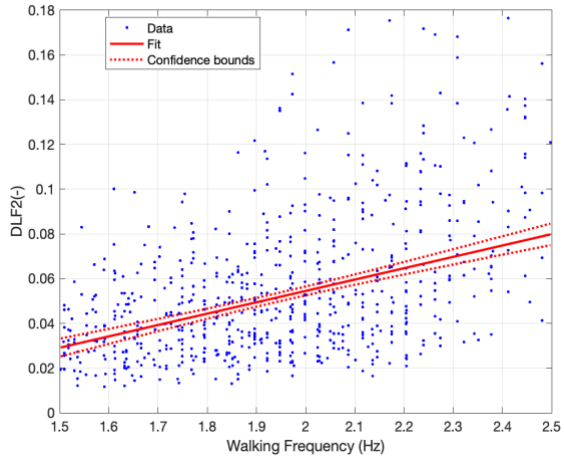

$DLF_2\ (f_p) = 0.0508\ f_p - 0.0471 + N\ (0.0032,\ 0.00077)$ Eq 45

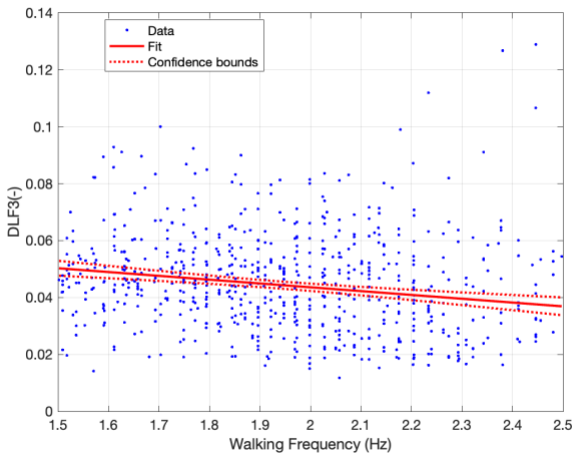

$DLF_3\ (f_p) = -0.0135\ f_p + 0.0704 + N\ (0.0014,\ 0.00077)$ Eq 46

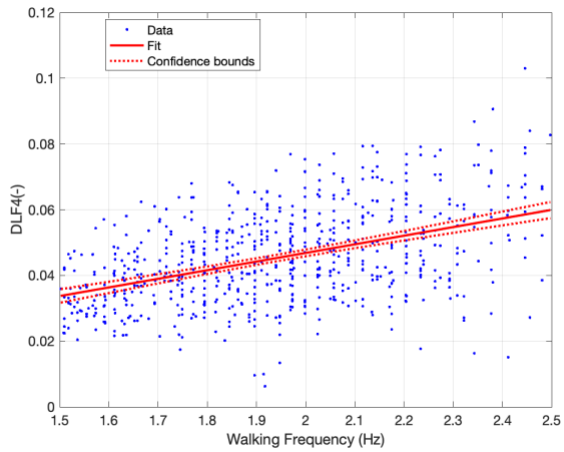

$DLF_4\ (f_p) = 0.0264\ f_p - 0.0056 + N\ (0.00006,\ 0.00016)$ Eq 47

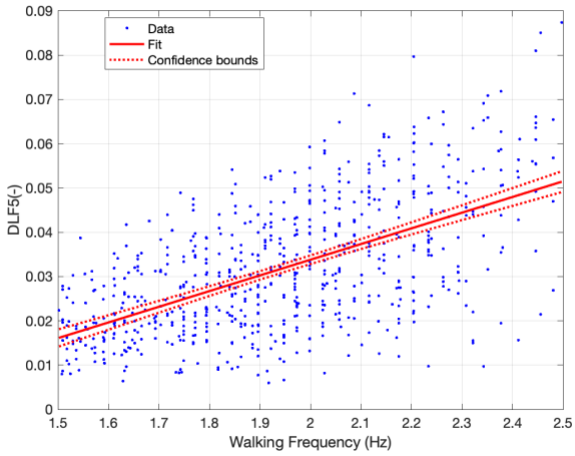

$DLF_5\ (f_p) = 0.0355\ f_p - 0.0370 + N\ (0.00001,\ 0.0001)$

Eq 48

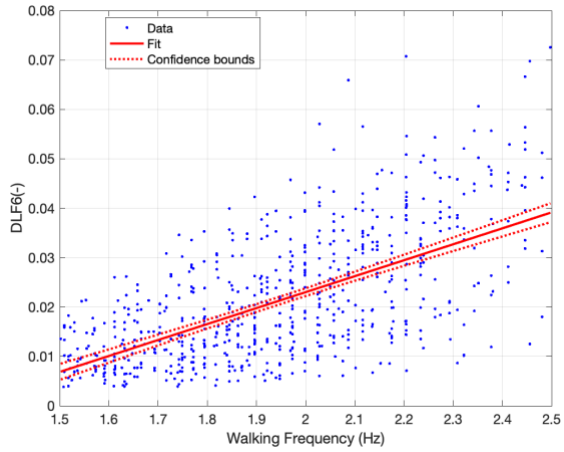

$DLF_6\ (f_p) = 0.0324\ f_p - 0.0416 + N\ (0.0003,\ 0.0001)$

Eq 49

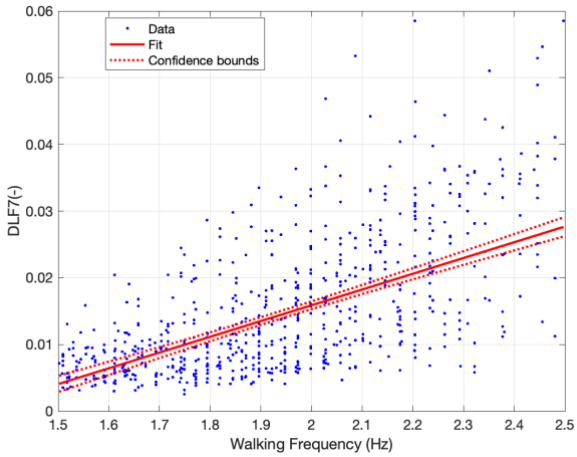

$DLF_7\ (f_p) = 0.0238\ f_p - 0.0314 + N\ (0.0008,\ 0.00006)$

Eq 50

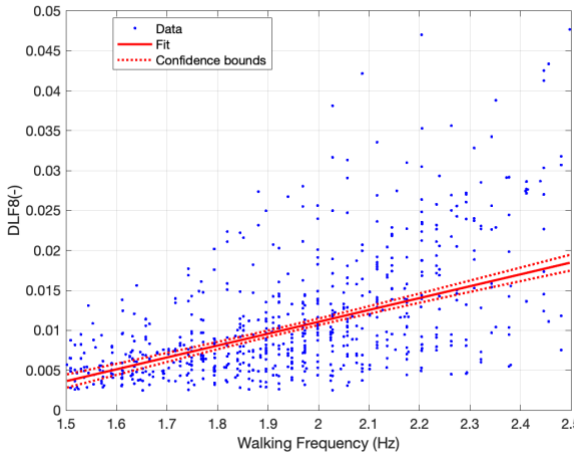

$DLF_8\ (f_p) = 0.0152\ f_p - 0.0187 + N\ (0.0011,\ 0.00004)$

Eq 51

Figure 3.18 Frequentist representation of the functional mapping of each $DLF_{1\text{-}8}$ given the average walking frequency presented through a linear function and the error estimation. Confidence intervals show the 95%, N (mean, std)

3.3.2.1.2 Bayesian representation of DLF inter-subject variation

In Bayesian inference, the parameter value is defined through a probability distribution, even though the parameter's actual value is fixed and static [239]. Moreover, Bayesian inference provides a framework to interpolate the parameter given prior belief and knowledge of the parameters. As more data becomes available, the probability distribution over the parameter estimation changes and alters the prior belief. Thus, the posterior distribution is gained via [109]:

$$P(\emptyset|D) = \frac{P(D|\emptyset)P(\emptyset)}{P(D)} \qquad \text{Eq 52}$$

Where $P(\emptyset)$ is the prior probability estimate of the model parameters $\emptyset$ before any data D is observed. $P(D|\emptyset)$ is the likelihood function. It represents the likelihood of the data given the parameters. Finally, $P(D)$ is the marginal likelihood and is the distribution of the observed data marginalised over the parameters. This denominator ensures the posterior distribution integrand integrates to 1, giving a complete probability distribution. Often the proportionate relationship between the likelihood and prior probabilities is used instead of the entire posterior probability distribution.

$$P(\emptyset|D) \propto P(D|\emptyset)P(\emptyset) \qquad \text{Eq 53}$$

Firstly, the prior belief of the parameters $P(\emptyset)$ must be established. This can be done by two methods: either using an informative or noninformative prior [226]. The latter is considered uniform over the entire parameter space and provides no insight into the current problem. Providing a uniform prior reduces the posterior distribution to wholly dictated by the likelihood function. Thus, the intuition of previous data or *a priori* knowledge is ignored. The assignment of a prior distribution is a difficult task as the process is entirely subjective, and no correct answer is the actual prior of the data; the prior distribution reflects an author's belief in the problem *a priori*. The formal distribution of the informative prior can take any form, be it Normal, Poison or uniform. As priors can fall within any range of an infinite set, it is dictated by the researcher where the unknown value is assumed to lay. A subset of the data can be used to form a preliminary analysis for the priors to facilitate Bayesian reasoning

when no prior knowledge is known. However, such subsets should not be used in calculating the final likelihood function or marginal likelihood as this results in double dipping of data.

The marginal likelihood arises to ensure the posterior distribution is complete, with integral sums to 1. For continuous random variables, Bayes theorem is written as:

$$P(\emptyset|D) = \frac{P(D|\emptyset)P(\emptyset)}{\int P(D|\emptyset)P(\emptyset)d\emptyset} \qquad \text{Eq 54}$$

The integration of the marginal distribution can provide challenges the function is high dimensional, and various known or unknown distributions are used to describe either the prior or likelihood function. Due to the unknown nature of some distributions or the intractability of closed-form solutions, numerical integration techniques must be employed.

Due to the often-multi-dimensional nature of marginal distributions and sparsity of the probability density functions, Monte-Carlo integration methods are employed. More specifically, a class of Monte Carlo integration methods has prevailed, known as Markov chain Monte Carlo (MCMC) algorithms [226,227]. Several commonly used algorithms include: Metropolis-Hastings[240,241], Hamiltonian Monte Carlo[242] and Gibbs Sampler[243].

MCMC simulations are preferred over Monte Carlo Integration methods, as MCMC produce successive autocorrelated samples based only on the previous sample. As the number of samples increase in a MCMC chain the more the distribution will converge to the stationary distribution of the target distribution or some unnormalized version of the distribution $q(\emptyset|D)$.

$$P(\emptyset|D) = \frac{q(\emptyset|D)}{\int q(\emptyset|D)d\emptyset} \qquad \text{Eq 55}$$

Practically the MCMC chain starts at a set of arbitrarily chosen points and seeks to move and sample the parameter $\emptyset$, such that each successive sample of $\emptyset$ contributes a high proportion of the posterior distribution. Traditional Monte Carlo methods tend to become increasingly inaccurate at higher dimensions [244], therefore the various algorithms of MCMC are

preferred to the increase in speed and efficiency required to obtain the stationary target distribution or a unnormalized variant. Further details of MCMC algorithms are given in Gelmann et al. [244].

A different approach to performing inference of a dataset is through conjugate distributions. A conjugate distribution occurs when the prior and the posterior distributions arise from the same parametric probability family. A parametric probability family is a set of distributions with the same functional form. As such, closed-form solutions of the posterior can be directly inferred from the prior distribution and data, and thus the posterior distribution is from a known PDF that can be easily sampled. The use of conjugate distributions provides computational and mathematical simplicity. Schoot et al. [226] and Gelman et al. [244] provide a broad overview of Bayesian inference topics and give an exhaustive list of conjugate pairs of distributions.

First, to provide a Bayesian estimation of the linear regression parameters, the prior distribution of the parameters must be assigned, namely the gradient term $\emptyset_1$, intercept term $\emptyset_2$ and variance term σ^2. As with the Frequentist model, the ordinary linear regression problem is formed as the conditional probability:

$$P(Y|x,\theta) \sim N(x\theta, I\sigma^2) \qquad \text{Eq 56}$$

Where Y is the target variable, in this instance the DLF, and x is the independent variable, walking frequency. θ represents the set of parameters that define the model, namely in the thesis the gradient and intercept terms. The standard deviation of the error is conditionally zero mean homoscedastic and multiplied by the identity matrix, I. Gelman et al. [244] provides an overview of the topic of Bayesian inference and the estimation of the linear regression. The procedure outlined in [244] is used throughout the proceeding section. The complexity of the procedure is found in the estimation of marginal likelihood:

$$P(Y) = \int P(Y|x,\theta,\sigma)P(\theta,\sigma)\, d\theta d\sigma \qquad \text{Eq 57}$$

The prior distribution of the gradient and intercept terms are taken from the multivariant Gaussian distribution. The prior distribution will be taken as the average estimate from Concrete society estimate of the linear model of each DLF, where the upper harmonics are not given, a mean value of zero for both parameters is chosen. The variance is described through the identity matrix times 0.1. Thus, it is assumed that the parameters' distribution is initially uncorrelated. The inverse gamma function is used for the prior distribution of the standard deviation of the error, the inverse gamma function is described through the shape and scale factors (a,b). The values of a and b are set such that the mean value of the distribution is the MLE of the variance from the frequentist representation, with the mean value of the inverse gamma distribution given by

$$\mu = \frac{b}{a-1} \qquad \text{Eq 58}$$

Whilst conjugate pairs can be used for performing inference as the conjugate pair of the multivariant Gaussian distribution is a conditional student-t distribution, numerical methods described earlier utilising MCMC methods, specifically Gibbs sampling are used to demonstrate the generality of the method.

Figure 3.19 presents the trace plots of each chain of the MCMC for the intercept, gradient and standard deviation of the error for DLF_1 only. A burn in of 400 samples was used to thus ensure that distribution of the posterior was indeed stationary, and that the stationary target distribution had been reached.

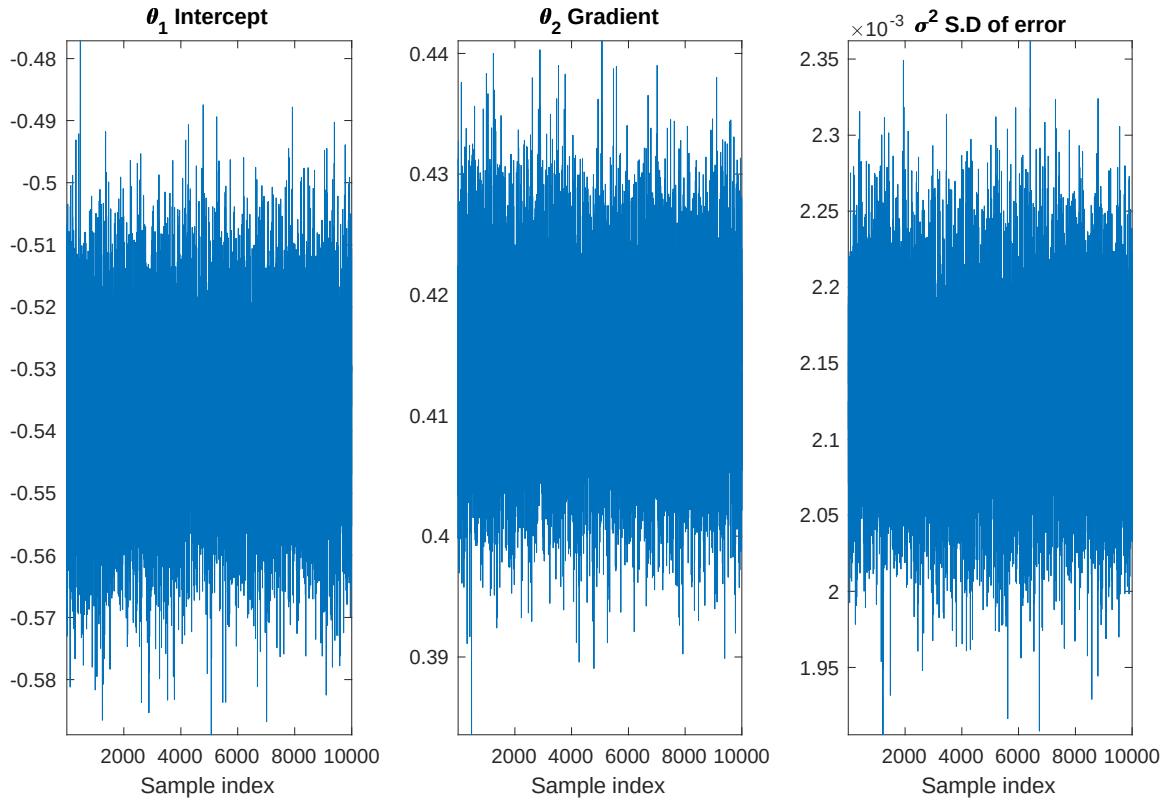

Figure 3.19 Trace plot of MCMC chains using Gibbs sampler with a 400 sample burn in (not shown) for all parameters of the linear regression model, only shown for DLF_1 model

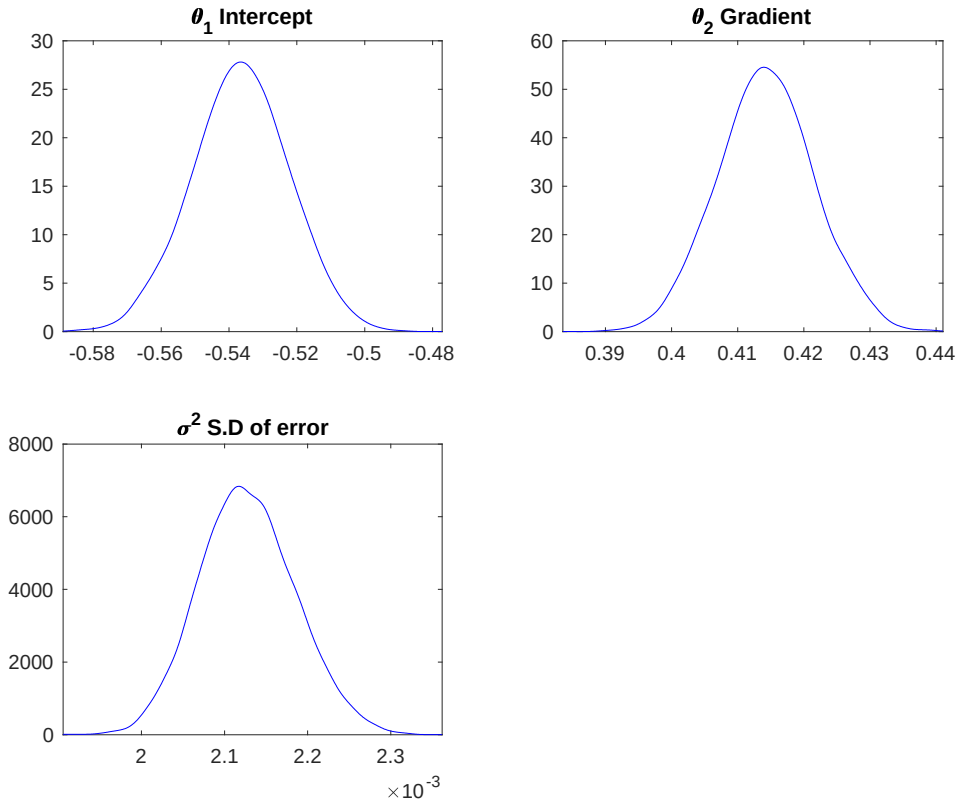

Figure 3.20 Marginalised posterior distribution for all parameters of the linear regression model, only shown for DLF1 model

Figure 3.20 presents the univariant distribution of each parameter, as demonstrated the distributions appear well conditioned with clear and defined peaks at the mean values. Figure 3.20 was constructed marginalising over the other parameters, to integrate out the other distributions. This can be represented as:

$$P(\theta_1|Y) = \int P(\theta|Y)\ d\theta_2 d\sigma^2 \qquad \text{Eq 59}$$

$$P(\theta_2|Y) = \int P(\theta|Y)\ d\theta_1 d\sigma^2 \qquad \text{Eq 60}$$

$$P(\sigma^2|Y) = \int P(\theta|Y)\ d\theta_1 d\theta_2 \qquad \text{Eq 61}$$

Figure 3.21 presents the moving average of each parameter over a 500-sample period, the results indicate a stable and stationary distribution of the mean results.

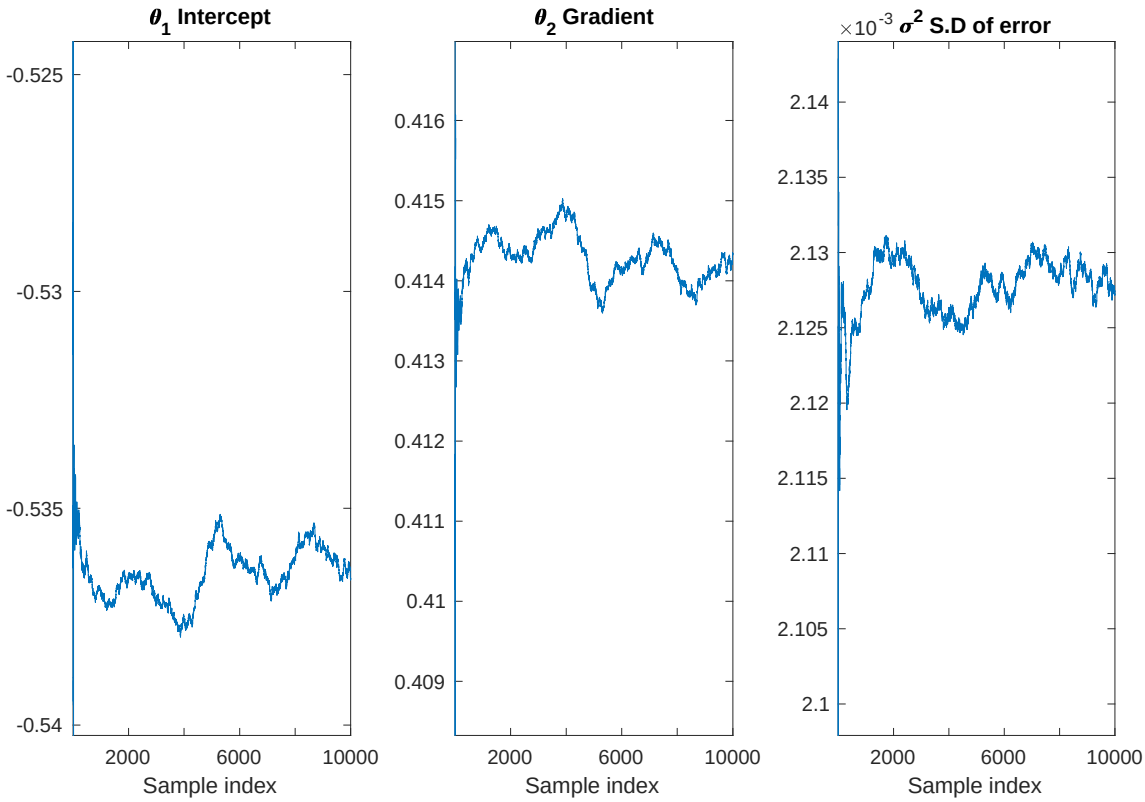

Figure 3.21 Moving average for all parameters of the linear regression model, only shown for DLF1 model, averaging over 500 sample period

The posterior distribution of the parameters is given in Table 3.4. The covariance matrix values indicate that the gradient and intercept terms exhibit co-dependent behaviours.

Table 3.4 Mean, covariance and variance of the error distributions for Bayesian linear models $DLF_{1\text{-}8}$

DLF	Mean values (Intercept, Gradient) μ	Covariance (Intercept, Gradient) Σ	The variance of error (a, b)σ^2
1	$\begin{bmatrix} -0.5360 \\ 0.4140 \end{bmatrix}$	$\begin{bmatrix} 0.0776 & -0.0393 \\ -0.0393 & 0.0203 \end{bmatrix}$	$[1336 \quad 0.3523]$

2	$\begin{bmatrix} -0.0598 \\ 0.0295 \end{bmatrix}$	$\begin{bmatrix} 0.0800 & -0.0203 \\ -0.0203 & 0.0052 \end{bmatrix}$	$[1336 \quad 0.7960]$
3	$\begin{bmatrix} 0.0609 \\ -0.0026 \end{bmatrix}$	$\begin{bmatrix} 0.0805 & -0.0136 \\ -0.0136 & 0.0023 \end{bmatrix}$	$[1336 \quad 0.9082]$
4	$\begin{bmatrix} -0.0050 \\ 0.0065 \end{bmatrix}$	$\begin{bmatrix} 0.0806 & -0.0102 \\ -0.0102 & 0.0013 \end{bmatrix}$	$[1336 \quad 0.9485]$
5	$\begin{bmatrix} -0.0367 \\ 0.0071 \end{bmatrix}$	$\begin{bmatrix} 0.0807 & -0.0082 \\ -0.0082 & 0.0008 \end{bmatrix}$	$[1336 \quad 0.9533]$
6	$\begin{bmatrix} -0.0429 \\ 0.0055 \end{bmatrix}$	$\begin{bmatrix} 0.0807 & -0.0068 \\ -0.0068 & 0.0006 \end{bmatrix}$	$[1336 \quad 0.9666]$
7	$\begin{bmatrix} -0.0348 \\ 0.0037 \end{bmatrix}$	$\begin{bmatrix} 0.0808 & -0.0058 \\ -0.0058 & 0.0004 \end{bmatrix}$	$[1336 \quad 0.9789]$
8	$\begin{bmatrix} -0.0242 \\ 0.0023 \end{bmatrix}$	$\begin{bmatrix} 0.0808 & -0.0051 \\ -0.0051 & 0.0003 \end{bmatrix}$	$[1336 \quad 0.9870]$

Figure 3.22 presents the joint PDF of DLF_1. As demonstrated, the relationship exhibits a high degree of correlation. Figure 3.22 presents the typical multivariant distribution of the gradient and intercept term for DLF1, the figure presents the degree of conditional probability each parameter has unto each other. Rather than the typical frequentist assumption of a single point estimate of inference for new data points, Bayesian methods allow the quantification of the uncertainty in the inference of new data points to the linear regression X_{new} is given through the conditional probability $P(Y_{new}|Y, X_{new})$ by marginalising over the parameters. The posterior predictive distribution is written as:

$$P(Y_{new}|X, Y, X_{new}) = \int P(Y_{new}|\theta, X_{new})P(\theta|X, Y)\ d\theta \qquad \text{Eq 62}$$

Where $P(\theta|Y, X)$ is the posterior distribution of the parameters given the inputs X and targets Y Eq 46 inferred through Gibbs sampling, and $P(Y_{new}|\theta, X_{new})$ is the likelihood estimation of the new inputs given the parameters and new inputs. Thus, integrating over the parameters

marginalises the distribution to allow the uncertainty in the new outputs given the training inputs, targets and new inputs.

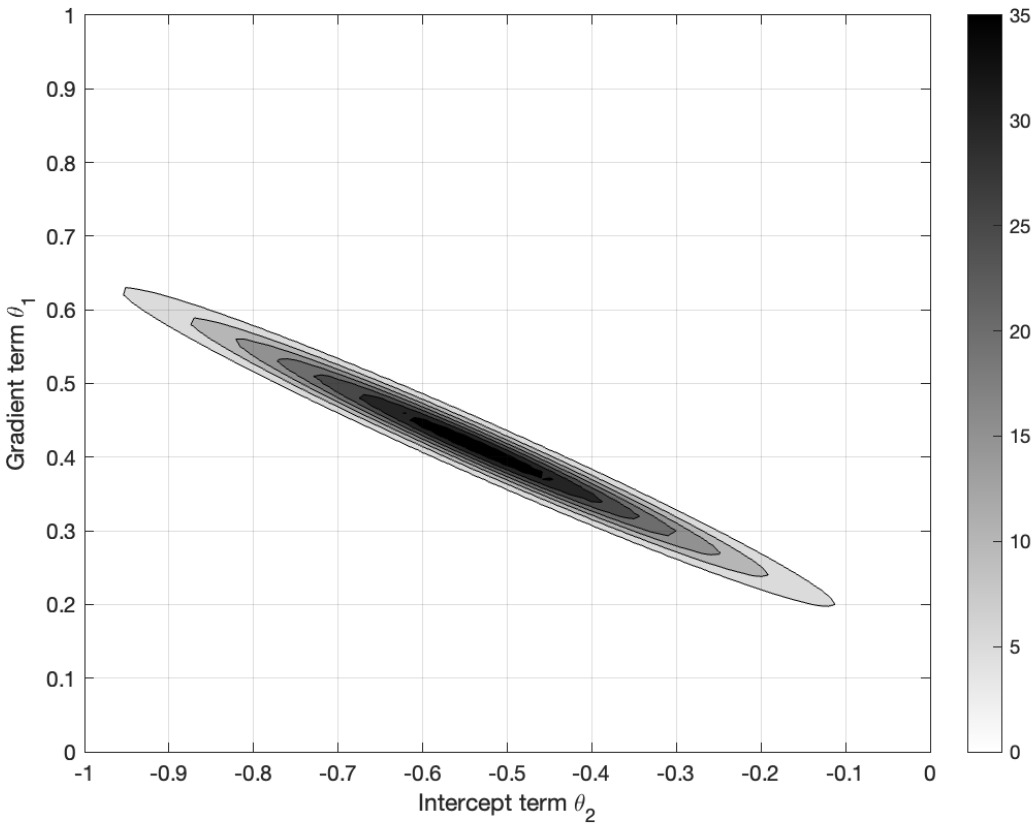

Figure 3.22 Joint PDF of the intercept and gradient term of DLF_1

3.3.2.1.3 Comparison of Bayesian and frequentist DLF models

This section presents a retrospection of the outputs from the regression inference from the previous sections for the Frequentist and Bayesian perspectives. The Frequentist philosophy of statistics does not provide a probability distribution over the parameters but instead the data. Therefore, only a single estimation is given. Conversely, the Bayesian analysis assumes the data is fixed, and there is uncertainty over the parameters. The maximum a posteriori (MAP) can be used to determine the most likely singular parameter value for the Bayesian perspective. The MAP is obtained by maximising the posterior distribution of the parameters. The maximisation procedure can be further simplified as the marginal likelihood is always

positive, has no bearing or dependency on the parameter set $\emptyset$, and can be ignored in the optimisation of obtaining the MAP. The marginal likelihood is achieved by integrating out the parameters $\emptyset$ of the likelihood and prior function. Such integration is only known for a few conjugate prior functions, and numerical integration is often required. The MAP of the parameters ($\widehat{\emptyset}_{MAP}$) is given as the maximisation of the likelihood and prior functions [109]:

$$\widehat{\emptyset}_{MAP}(D) = arg \max_{\emptyset} P(D|\emptyset)P(\emptyset) \qquad \text{Eq 63}$$

The MLE and MAP values of the model parameters for DLF_1 -DLF_8 are shown comparatively in Table 3.5. The values coincide well, with only a few varying by 10^{-4} in most scenarios. Such a variation is negligible compared to the values they represent and can therefore be considered approximately similar. When sampling the Bayesian approach 100 times and comparing it to the Frequentist model of DLF_1 (Figure 3.23), the model estimates align and represent the data similarly.

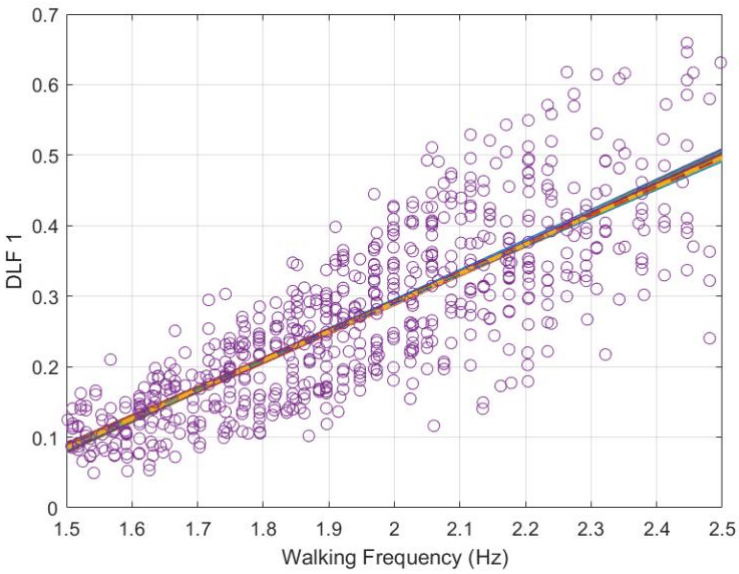

Figure 3.23 Frequentist value of the parameters (single dashed) vs the sampled (100 times) Bayesian approximation of the parameters (solid line) for walking frequency vs DLF_1

Visually the MLE and MAP converge to similar estimates as exhibited for the parameters of DLF_1 in Figure 3.24. The MAP, MLE, and posterior distribution all provide plausible solutions to parameters and a consistent range of results.

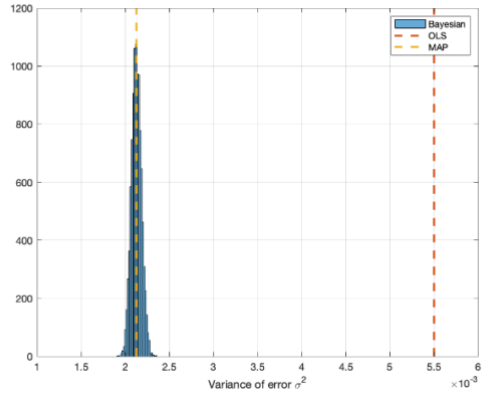

a)Marginalised posterior distribution of variance of errors compared to MAP and MLE estimations for DLF_1

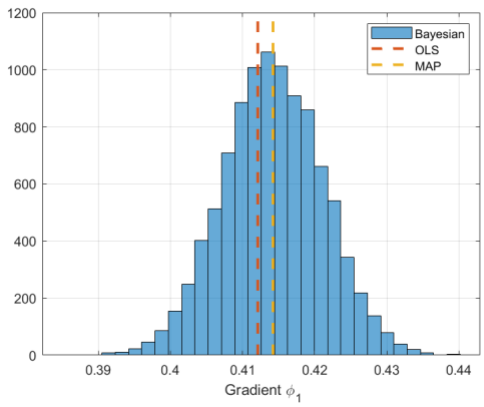

b) Marginalised posterior distribution of gradient parameter compared to MAP and MLE estimations for DLF_1

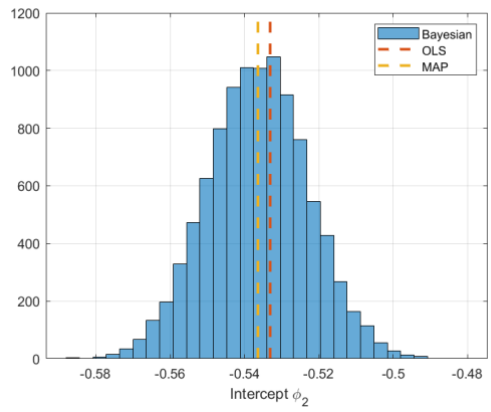

c) Marginalised posterior distribution of intercept parameter compared to MAP and MLE estimations for DLF_1

Figure 3.24 Marginalised posterior distribution of parameters compared to MAP and MLE estimations for DLF_1

The MLE and Bayesian estimate converges when larger amounts of data are available. Taking the log of Eq 63 does not affect the properties of the maximisation but allows the separation of the terms. As the log function is monotonic, the maximisation of $\emptyset$ occurs at the exact location as the non-log function. The MLE arises plus a regularisation term, $\log(P(\emptyset))$ (log of the prior distribution):

$$\widehat{\emptyset}_{MAP}(D) = arg \max_{\boldsymbol{\theta}}[\log\big(P(D|\emptyset)\big) + \log(P(\emptyset))] \qquad \text{Eq 64}$$

Thus, the MLE and MAP will eventually coincide when more data is present, and the prior is not biased. Moreover, the Bayesian MAP will become a more data-centric estimation of the parameter rather than the prior when sufficient data is collected [66]. The covariance of the gradient and intercept term increases resulting in a slender joint probability density function and less variance of the sampled function of the posterior distribution of DLF_1.

Table 3.5 Comparison of MLE and MAP estimates of DLF1-DLF8 for gradient and intercept terms

DLF	MLE	MAP
1	$\begin{bmatrix}-0.5331\\0.4121\end{bmatrix}$	$\begin{bmatrix}-0.5360\\0.4140\end{bmatrix}$

2	$\begin{bmatrix}-0.0471\\0.0254\end{bmatrix}$	$\begin{bmatrix}-0.0598\\0.0295\end{bmatrix}$
3	$\begin{bmatrix}-0.0704\\-0.0045\end{bmatrix}$	$\begin{bmatrix}0.0609\\-0.0026\end{bmatrix}$
4	$\begin{bmatrix}-0.0056\\0.0066\end{bmatrix}$	$\begin{bmatrix}-0.0050\\0.0065\end{bmatrix}$
5	$\begin{bmatrix}-0.0370\\0.0071\end{bmatrix}$	$\begin{bmatrix}-0.0367\\0.0071\end{bmatrix}$
6	$\begin{bmatrix}-0.0416\\0.0054\end{bmatrix}$	$\begin{bmatrix}-0.0429\\0.0055\end{bmatrix}$
7	$\begin{bmatrix}-0.0314\\0.0034\end{bmatrix}$	$\begin{bmatrix}-0.0348\\0.0037\end{bmatrix}$
8	$\begin{bmatrix}-0.0187\\0.0019\end{bmatrix}$	$\begin{bmatrix}-0.0242\\0.0023\end{bmatrix}$

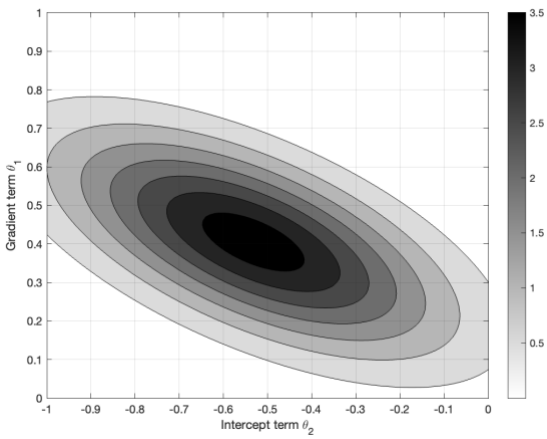

a)Posterior Distribution after 10 data points

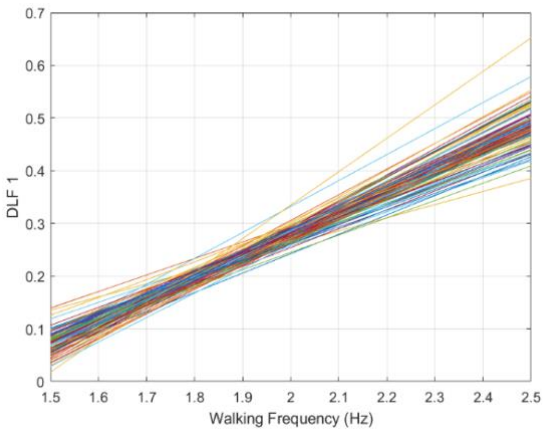

b) 100 samples of the linear relationship after 10 datapoints

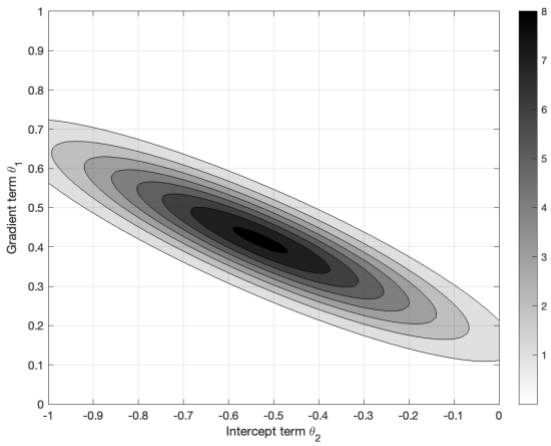

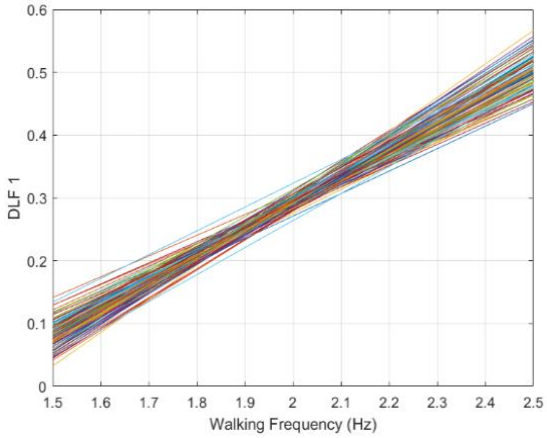

c) Posterior Distribution after 50 data points d) 100 samples of the linear relationship after 50 datapoints

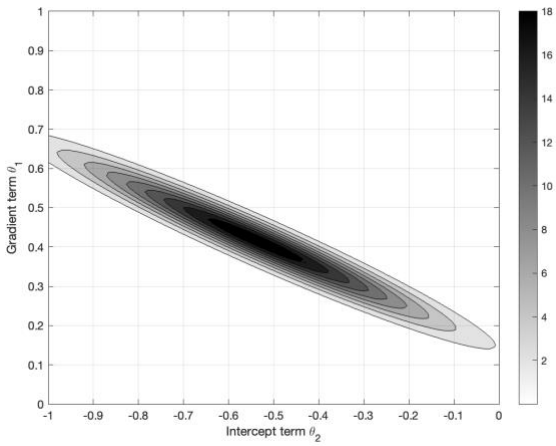

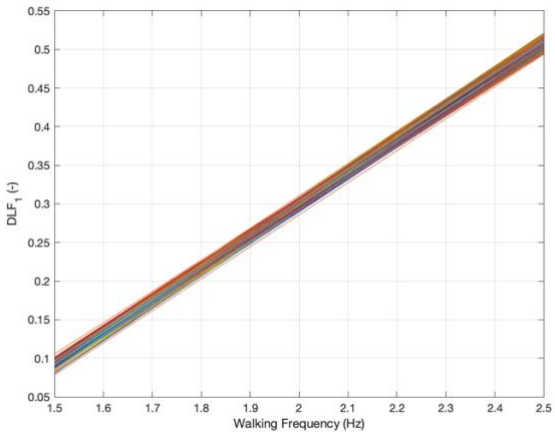

g) Posterior Distribution after 250 data points h) 100 samples of the linear relationship after 250 datapoints

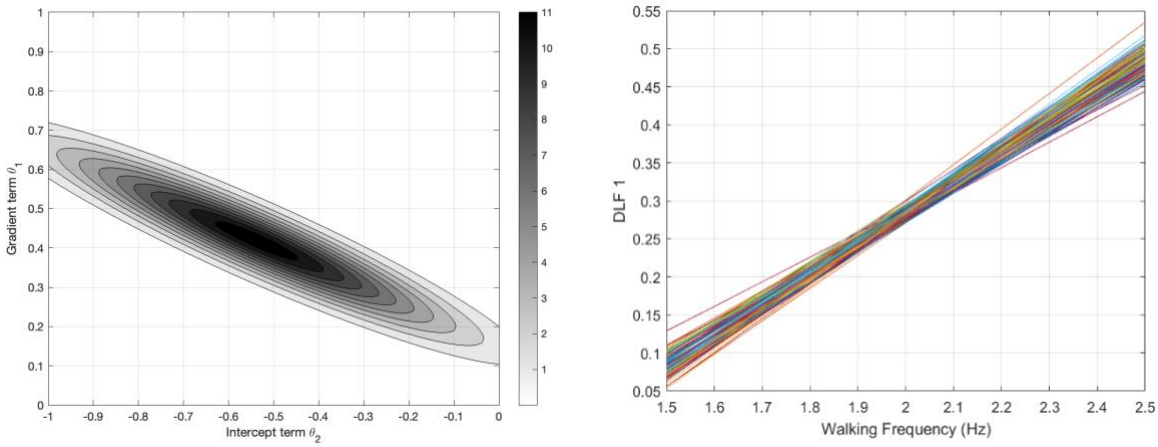

e) Posterior Distribution after 100 data points f) 100 samples of the linear relationship after 100 datapoints

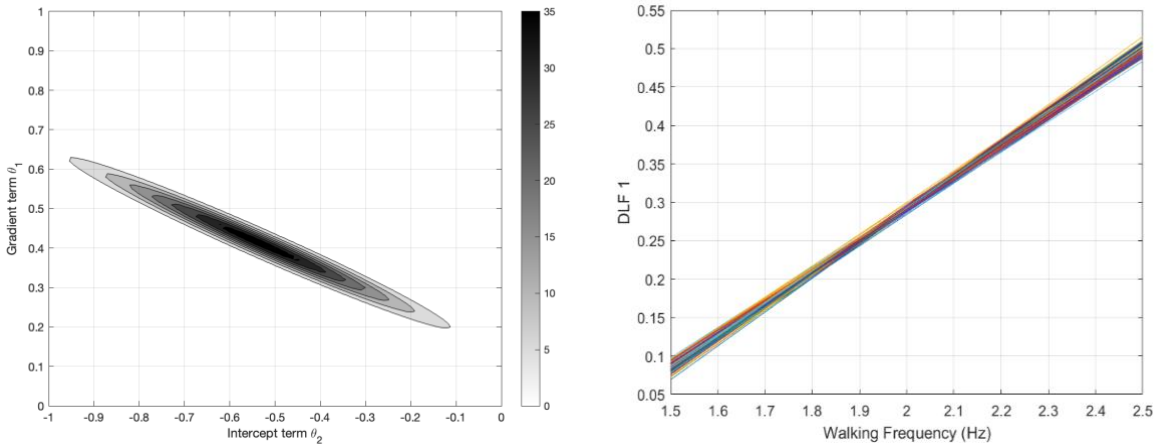

i) Posterior Distribution after all data points j) 100 samples of the linear relationship after all data points

Figure 3.25 Informative prior used to infer posterior distribution for 0,10,50,100,250 and all data points for DLF_1, each posterior distribution is then sampled 100 times.

The error variance is the only inconsistency between both methodologies, as illustrated in Figure 3.24 and Table 3.5. In DLF_1, the variance of the error of the Bayesian model is estimated to be about half as much as the Frequentist approach. This result arises due to the variance of the models being heteroskedastic. The preferred use of one model over the other

is, therefore, down to the discretion of the user and their philosophical view of statistics, as both models provide comparatively similar representations of the data, with each statistical viewpoint providing almost identical mean values of each parameter.

3.3.2.1.4 Comparison of historic DLF models

The formulated models previously seen in sections 3.3.2.1.1 and 3.3.2.1.2 are compared in Figure 3.26 to the existing Fourier series models [4,19,21,45,46,63,64] deemed state-of-the-art [5,31]. Table 3.6 present the limiting walking frequency ranges of each Fourier-based model.

Table 3.6 Limits on walking frequency ranges for each Fourier series model

Model	Walking frequency limits (Hz)
AISC Design Guide 11 [16]	1.6-2.2
ISO 10137 [21]	1.2-2.4
Technical report 43 appendix G [28]	1-2.8
CCIP Mean value [20]	1-2.8
CCIP design value [20]	1-2.8
SCI P35[19]	1.6-2.2
SETRA [55]	1.6-2.4
Varela et al. [64]	1.4-2.6

Numerous industrial vertical load models provide a range of feasible walking frequencies; however, researchers have continually provided evidence that walking occurs through a normal distribution centred at 1.8-2Hz and can exhibit 1 – 3Hz [53,70,71]. It is seen in Figure 3.26 that the greatest DLF values are seen at 2.5Hz. Thus the models of AISC Design Guide

11 [16], ISO 10137 [21], SCI P35[19] and SETRA [55] all do not consider the highest values of DLF. The curtailment of walking frequency is concerning since the data used to model the DLFs of the limited models are derived from the data of Kerr [45], where walking frequencies from 1-3Hz are monitored. It is further exhibited in Figure 3.26 that the limited models provide, on average, a poor estimation of the DLF values producing continually higher results of DLF values for the limited number of harmonics they model compared to the data and this thesis.

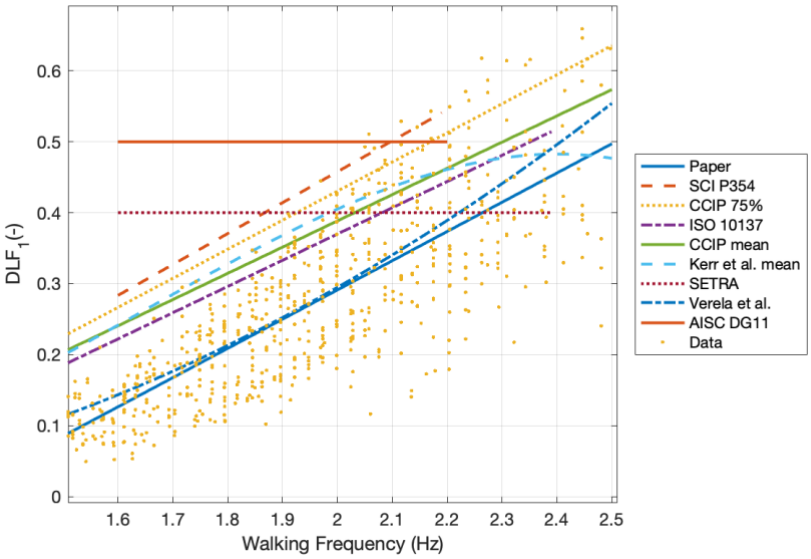

a) DLF_1 data points collected using the methodology outlined in section 3.2.2 compared to models of section 3.4.2.1.1 and [16,19–21,45,64]

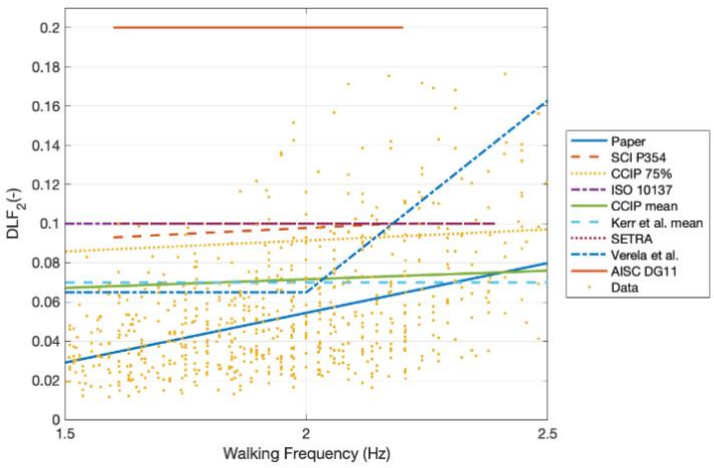

b) DLF2 data points collected using the methodology outlined in section 3.2.2 compared to models of section 3.4.2.1.1 and [16,19–21,45,64]

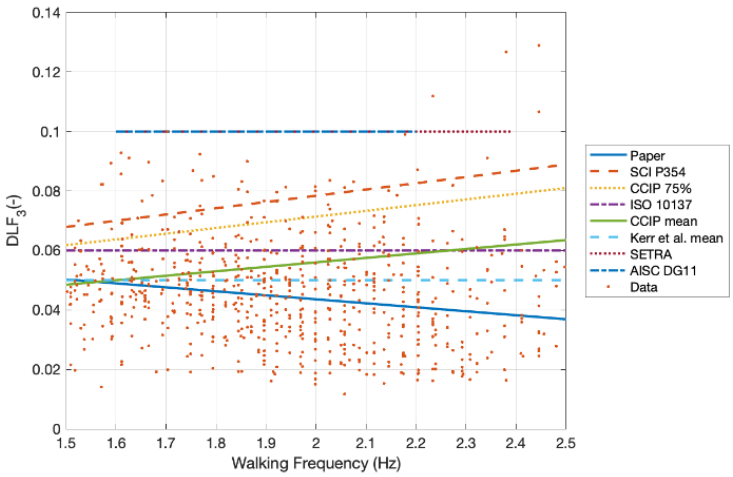

c) DLF_3 data points collected using the methodology outlined in section 3.2.2 compared to models of section 3.4.2.1.1 and [16,19–21,45,64]

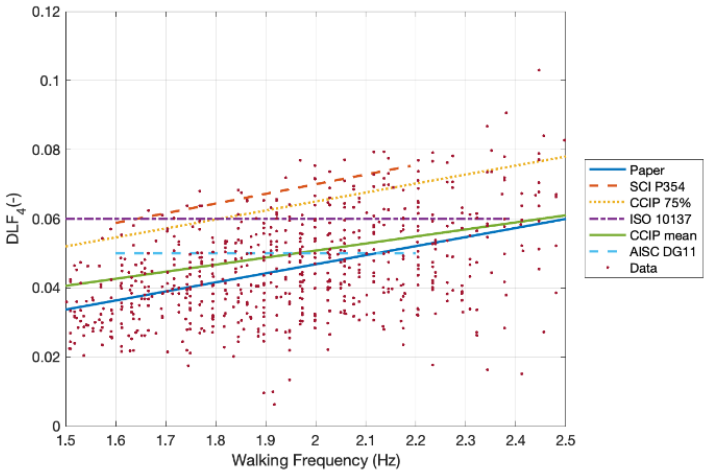

d) DLF_4 data points collected using the methodology outlined in section 3.2.2 compared to models of section 3.4.2.1.1 and [16,19–21,45,64]

Figure 3.26 Comparison of DLF_1 to DLF_4 of the presented models against historical models of [16,19–21,45,64] against the background of the current set of data

The formulated model of this thesis results in a lower magnitude of DLFs than all the other models, barring that of DLF_2 above 4.8Hz. Varela et al. [64] demonstrates a close representation of the first integer of walking. The model closely resembles that of the proposed model for the first integer. The results of Varela et al. [64] start to diverge in the successive integers and only represents a limited number of harmonics. Varela et al. [64] suggests DLF values be elevated at lower and higher walking frequencies compared to the presented model in the first harmonic. However, the data points within the thesis do not indicate as such, with the data more accurately represented through a 1st order linear regression. As walking frequencies are normally distributed, less information is available at the extreme high and low walking frequencies. Coupled with the heteroscedastic nature of walking, the precise nature of the DLF at higher walking frequencies is not known with confidence. AISC DG 11 [16] model provides a oversimplification and overestimation of the first, second, and third harmonic and represents a poor estimation of the dataset. At higher harmonics of walking, DLF values of industry models provide a similar magnitude of responses to the data points. This results from the relatively low values of the DLF. However, there are significant percentage error differences. Figure 3.27 shows a historical trend of walking forces having higher DLFs. This could be speculatively attributed to several issues: "white coat syndrome", making people walk unnaturally, the short lengths of older force plates making participants target footfalls on the force plates, thus creating unnatural force waveforms, improper modelling due to heteroscedastic data, improper inference or lack of error estimation, test subject population differences, bias population or bias results due to a low number of data points recorded by force plates, the bias of results due to replication of force-time histories to produce higher resolution results, etc.

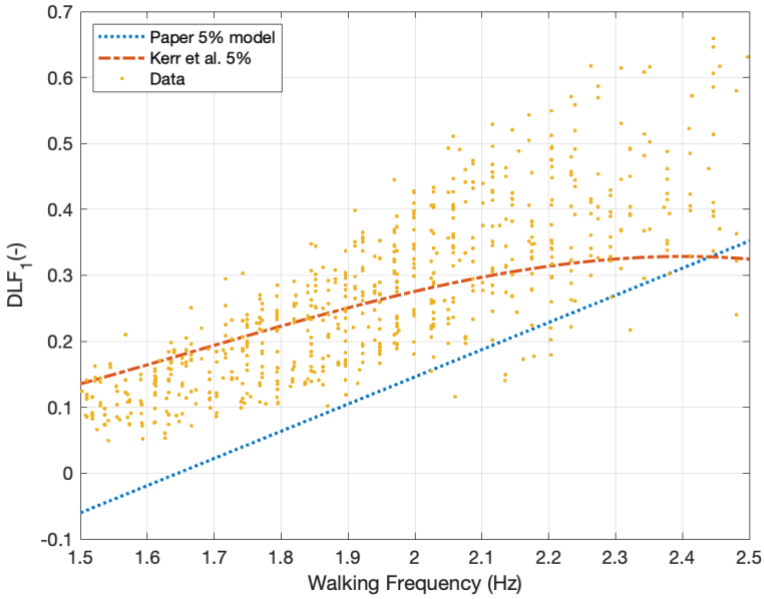

a) Comparison of results based on 5% error estimation compared to [45] and data points obtained in Section 3.2.2.

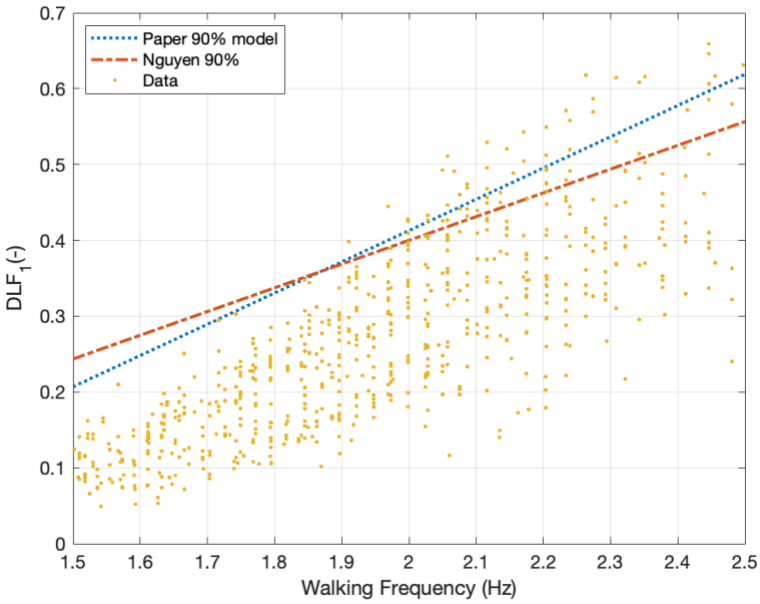

b) Comparison of results based on 90% error estimation compared to [46] and data points obtained in Section 3.2.2..

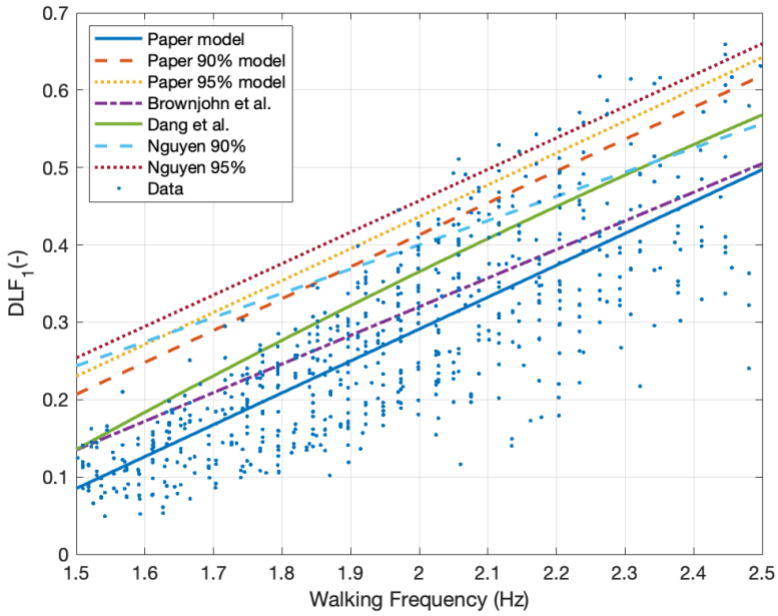

c) Comparison of results based on data collected by a treadmill and data points obtained in Section 3.2.2. [29] [46] [245]

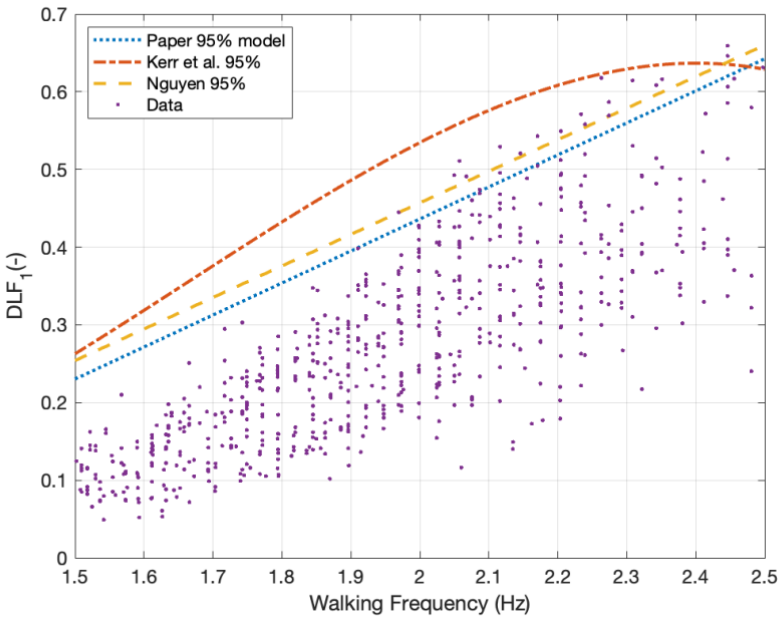

d) Comparison of results based on 95% error estimation and data points obtained in Section 3.2.2. [46], [45]

Figure 3.27 Comparison of historical models of DLFs (using the treadmill, force plate and various percentiles of parameters) with the current set of data

The results of Figure 3.27 indicate that even when differing modelling methodologies are used, similar results are found for models derived from treadmill data. All the results coincide and produce lower magnitudes of DLF_1 than the force plate measurements (Figure 3.27). Noting that Brownjohn et al. [29] data is limited to three subjects, the results are not as statistically comparable to the present study. The results' consensus indicates that the presented models align well with historic treadmill data for similarly obtained results. As such, the multiple-step measurement of vertical walking forces allows for a more representative representation of the mean properties of walking compared to their single-step counterparts.

In the case of Kerr's models [45], the equation of DLF for the 5% error model appears to fit the mean value of the proposed DLF model rather than the 5% error of the data. This again shows the historically high DLFs derived from force plate data compared to the current treadmill data [52] (Figure 3.27a and d). In the case of the 95% model, the equation does not represent the shape of the data. As seen in Figure 3.27 the cubic nature of the data misrepresents the approximately linear data. Along with the improper use of statistics, the DLF values are clearly misrepresented through their statistics. It is noted that the population samples are both different in size and people. Therefore, some variation may be a result of fundamentally different walking attributes.

Due to the variance and heteroscedasticity, the error in the present linear models produces negative values of DLFs at low values of walking frequency for the 5% error model (Figure 3.27a). This is not feasible and shows where the proposed model breaks down. Due to the data-dependent variance, the overall estimation of the error is varied in regions of the model than is presented in the data.

Nguyen's [46] 90% and 95% confidence interval validates the results of the 90% and 95% of the Frequentist and Bayesian models presented in the paper (Figure 3.27c and d). However, Nguyen [46] used only single footfall measurements and temporally shifted the wavelet to provide a complete force-time history.

The historic overestimation of vertical walking load models further suggests that the data is statistically different from the presented study or that the data acquisition and modelling

methodology resulted in differences. Figure 3.9 shows the variation of DLF_1 using the filtered method in the thesis compared to peak picking. As shown in Figure 3.9, using the peak-picking method on the data results in lower magnitudes of DLF than the filtered method. Therefore, compared to previous models' peak picking, the resultant DLFs would produce a force-time history of even lower magnitude than the proposed model in sections 3.3.2.1.1 and 3.3.2.1.2. It is posited that the variation of DLFs concerning previous models results from the quality of the data and the inclusion of the intra-subject variation of the data. Therefore, the intra-subject variation of data plays a crucial role in selecting an appropriate DLF value.

In the statistical inference of a regression model, it is necessary to estimate the error in the model. Such an error is not from the incapability of the model but instead, errors arising from unobservable differences in the data. Therefore, the error of any model's output is independent of the model parameters themselves. As such, the inclusion of any error estimation will merely linearly increase or decrease the output value and does not affect the actual parameter values. Examples of misuse of the error and confidence bands are exhibited in [20,45]. Both models use confidence intervals over parameters, not the error estimation of DLF values.

3.3.2.2 DLF intra-subject variation

The intra-subject variation of the DLF is determined using the same process as Section 3.3.1. However, the peak values of the signal are taken as the DLF amplitude on a step-by-step basis. The one-sample Kolmogorov-Smirnov test determines if the intra-subject DLF is taken from a normal distribution. The z-score of the DLF values is used as a pre-processing step to ensure all values are within the same length and scale as the normal distribution. The null hypothesis is that the normalised intra-subject data of each walking history comes from a standard normal distribution. Performing the one-sample Kolmogorov-Smirnov test on the normalised data, the results conclude evidence to fail to reject the null hypothesis, thus suggesting that the intra-subject variation of the DLFs comes from a normal distribution. 78% of all intra-subject DLFs provide sufficient evidence to indicate they are from a normal standard distribution when the data is normalised. Such a high value offers substantial

evidence to conclude the intra-subject variation is described primarily through a normal distribution.

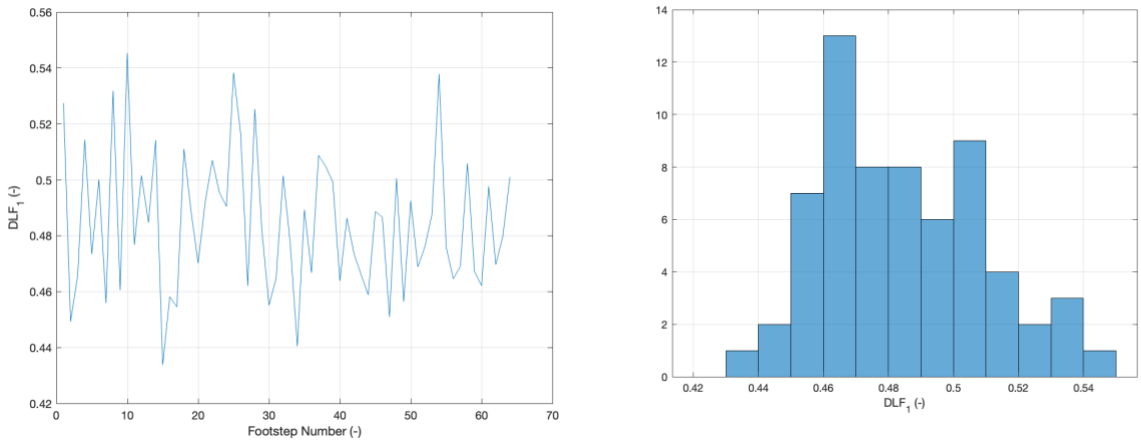

Figure 3.28 Intra-subject variation of DLF_1 values for subject 842 along with the histogram of results with 0.1 bin widths.

To compare any dependency, the data of the average DLF is compared to the DLF of including intra-subject variation cases at each footstep walking frequency. As seen in Figure 3.29 including the intra-subject variation increases the magnitude of the overall variance of the data. Figure 3.29 appears heteroskedastic, with an increased variance and an increase in the independent variable. The heteroskedastic nature of the data appears in both the mean and intra-subject variation of the data. However, it seems more prominent in the intra-subject inclusion. The intra-subject variation of DLF values thus provides a more appropriate representation of the walking frequency – DLF relationship, demonstrating the full spectrum of possible DLF values. Of noteworthiness is the DLF values at 2.5Hz walking frequency. DLF values are seen in a range of 0 up to 0.9 when the intra-subject variation is included. Whilst the probability of such values occurring is small, the figure provides an illustrative example of the data's lack of consistency with the historic models presented in Chapter 2 Section 2.1.2.3. Figure 3.28 and Figure 3.29 only show the information for DLF_1, with the remaining harmonics presenting similar conclusions. Excluding the intra-subject variation of the walking force model limits the natural variation of DLF values, resulting in a narrower range of plausible values, thereby underrepresenting the true vertical walking forces.

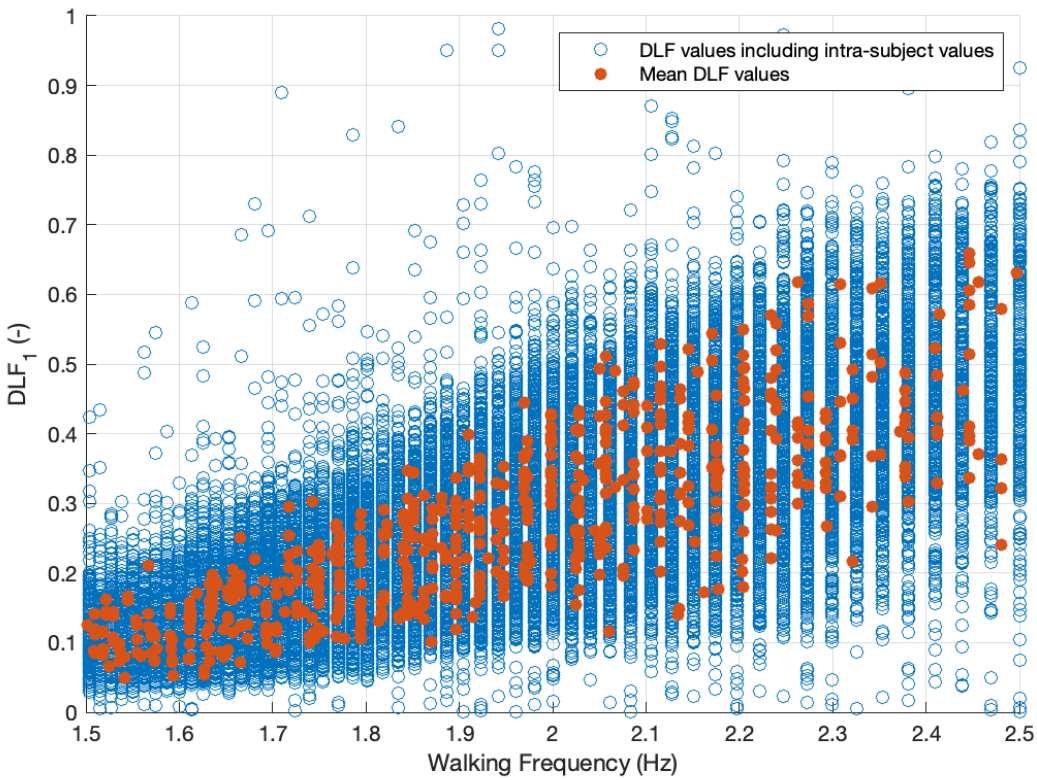

Figure 3.29 DLF_1 inclusion of intra-subject variability vs intra subject variation of DLF_1 with respect to the walking frequency

As the data appears heteroskedastic, the CoV of the DLF intra-subject variation is examined in Figure 3.30. As anticipated, the CoV remains monotonic around a static distribution. It is only natural that the variance would increase with increased walking frequency due to the CoV remaining a constant value of the mean. This is because the DLF values depend on the walking frequency value (e.g., for DLF_1, the CoV exhibits a mean value of 0.125). Therefore, at 1.5Hz, the mean DLF and standard distribution is 0.0987 and 0.0123, respectively. At 2.5Hz, the mean and standard distribution of DLF values is 0.512, 0.065. The above further demonstrates the heteroscedastic nature of the data. The CoV of walking appears independent of the walking frequency. As such, the heteroscedastic nature of the data is a result of the constant CoV throughout walking and not the data itself being heteroscedastic.

Table 3.7 compares CoV of each harmonic of DLF with the mean results from Chen et al.[4] and Garcia-Dieguez et al. [63]. The results of this thesis demonstrate an increase in CoV

compared to that of Chen et al.[4], with the stark comparison of DLF_2 of the former being ten times the CoV of the latter.[4]. The results of Chen et al.[4] were obtained by a participant walking at the same walking frequency over two force plates multiple times, and the intra-subject variation was taken over the total number of repeats. In the truest sense of walking, the instances were performed separately. They cannot be reliably called intra-subject variation. In the author's view, intra-subject variation of DLF values can only be monitored through the same act of walking. Repeating the same walking frequency is practically impossible due to deviations in results.

In contrast, Chen et al.[4], the results of Garcia-Dieguez et al. [63] provide a good consensus of results within the thesis, sometimes within a few thousand of a decimal place. The data collection of Garcia-Dieguez et al. [63] is identical to the thesis with a dual treadmill used with multiple individual steps monitored but different populations. Garcia-Dieguez et al. [63] however, notes a parabolic relationship between the CoV of intra-subject DLF for DLF_1 and the pedestrian velocity. This result is not founded in the thesis, with the velocity shown to be a linear transformation of the walking frequency Section 3.3.3. The second harmonic of walking CoV of the intra-subject DLF is close to double that of Garcia-Dieguez et al. [63] which may be attributed to population differences or DLF extraction methods. The similarity of results is anticipated due to the use of similar data; however, it is seen that DLF_2 possess a stark increase in the variance of the DLF over the walking frequencies.

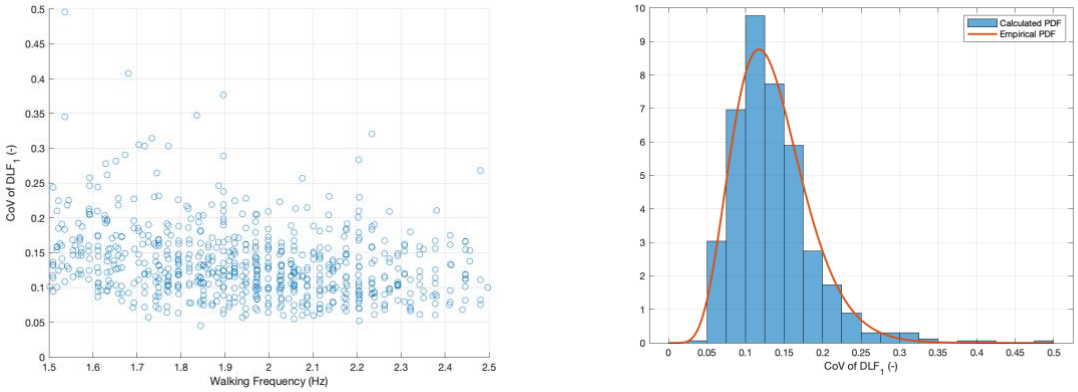

a) Distributions of the CoV for DLF_1 comparing the emperical relationship to the estimated histogram with 0.025 bin widths.

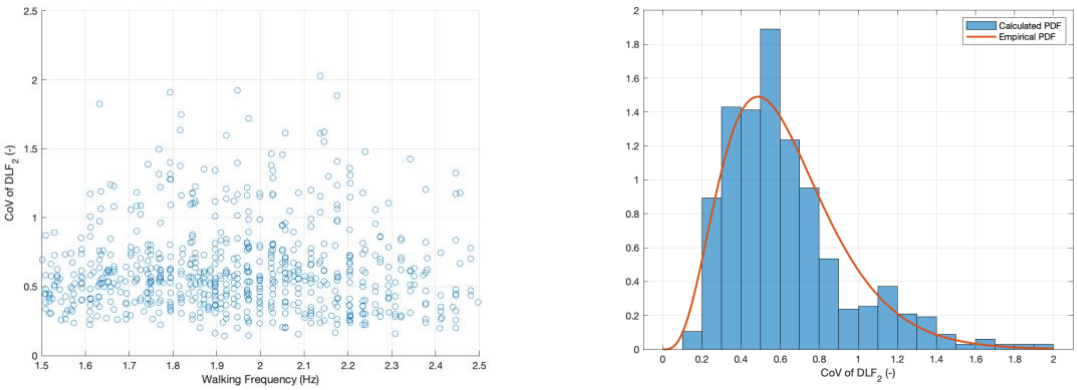

b) Distributions of the CoV for DLF_2 comparing the emperical relationship to the estimated histogram with 0.1 bin widths.

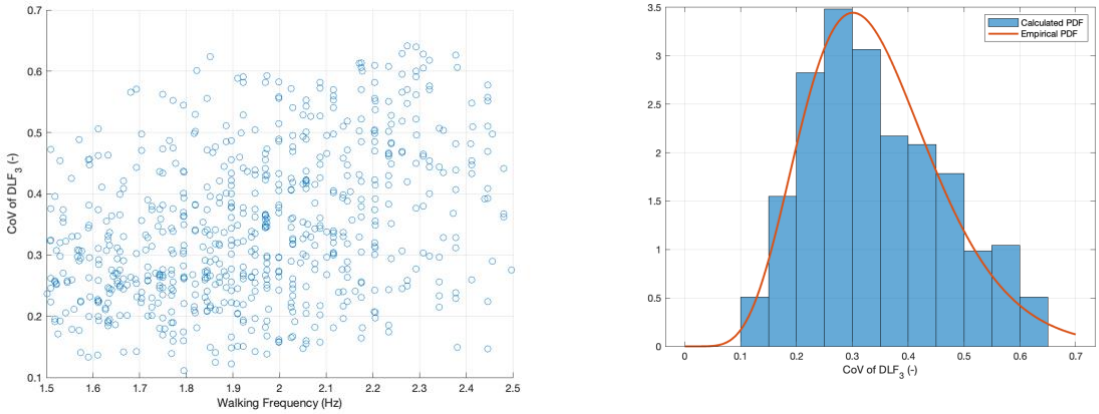

c) Distributions of the CoV for DLF_3 comparing the emperical relationship to the estimated histogram with 0.05 bin widths.

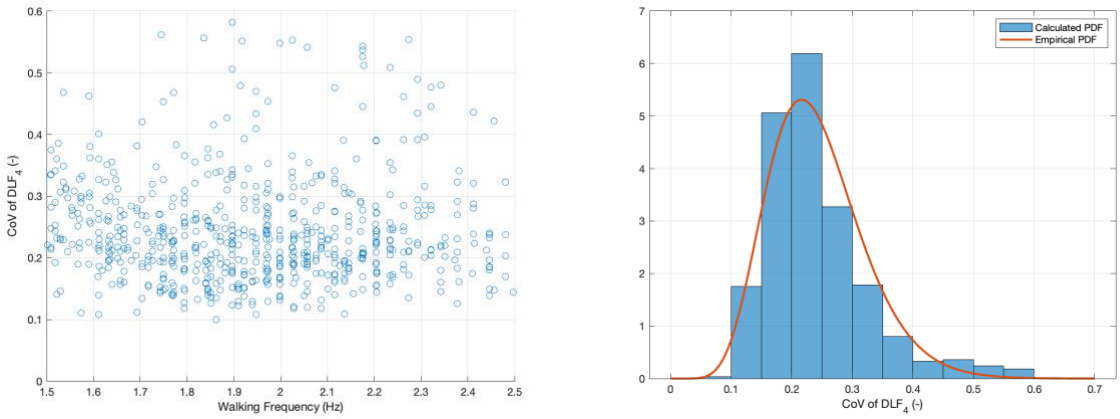

d) Distributions of the CoV for DLF_4 comparing the emperical relationship to the estimated histogram with 0.05 bin widths.

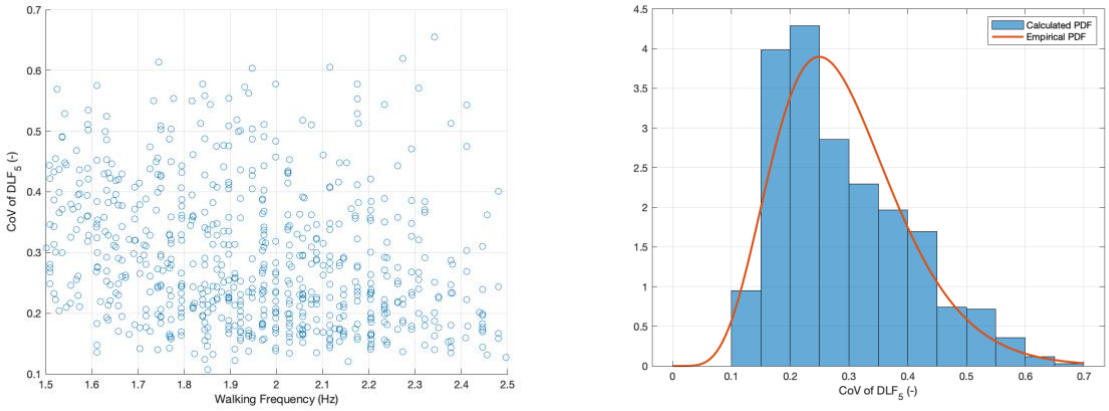

e) Distributions of the CoV for DLF_5 comparing the emperical relationship to the estimated histogram with 0.05 bin widths.

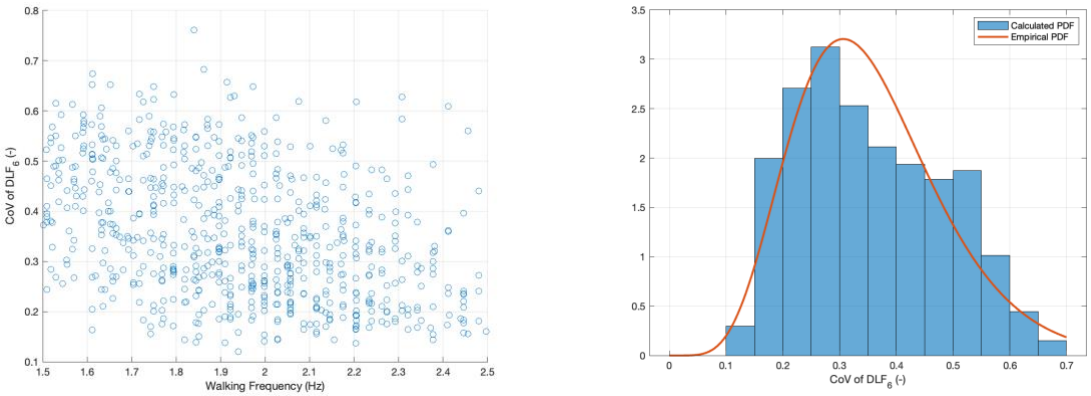

f) Distributions of the CoV for DLF_6 comparing the emperical relationship to the estimated histogram with 0.05 bin widths.

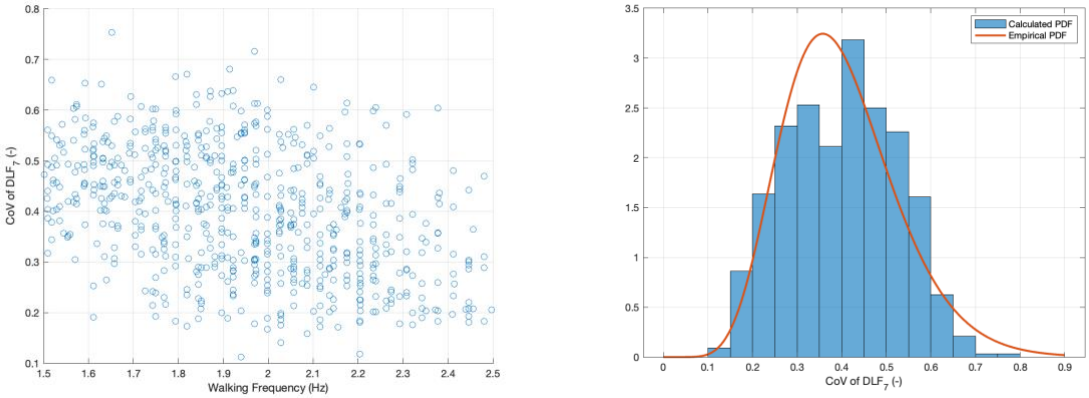

g) Distributions of the CoV for DLF_7 comparing the emperical relationship to the estimated histogram with 0.05 bin widths.

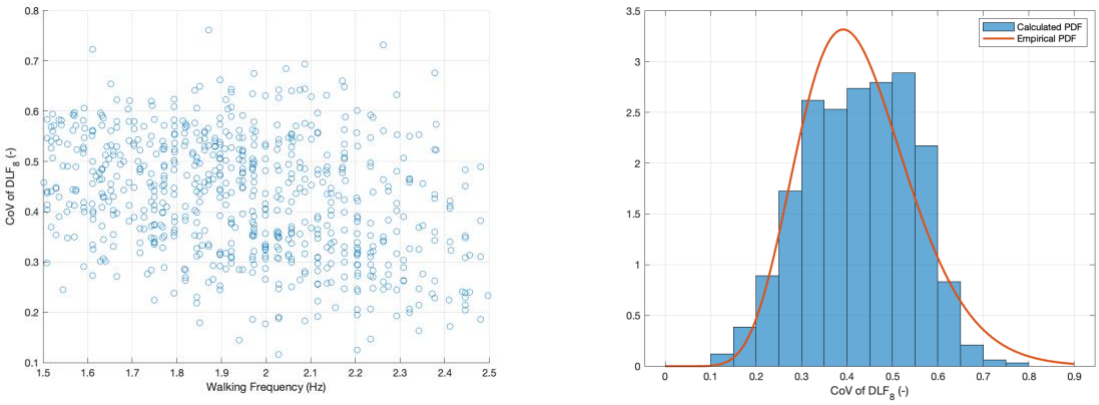

h) Distributions of the CoV for DLF_8 comparing the emperical relationship to the estimated histogram with 0.05 bin widths.

Figure 3.30 Distribution of CoV for DLF_1-DLF8 concerning the walking frequency and univariant distribution of each DLF

Table 3.7 Gamma distribution parameters and mean values of CoV of intra subject variation of DLF, compared to Chen et al.[4] and Garcia-Dieguez et al. [63]

DLF	Gamma a parameter of CoV of intra-subject variability	Gamma b parameter of CoV of intra-subject variability	Mean CoV Value	Mean CoV Chen et al. [4]	Mean CoV Garcia-Dieguez et al. [63]
1	7.831	0.017	0.135	0.123	0.099-0.297
2	4.651	0.129	0.601	0.059	0.381
3	7.925	0.044	0.345	0.101	0.311
4	9.460	0.026	0.242	0.158	0.269
5	7.110	0.041	0.290	0.202	0.326
6	7.233	0.049	0.356	0.296	N/a
7	9.623	0.042	0.399	0.363	N/a
8	11.770	0.036	0.428	0.378	N/a

Finally, the autocorrelation of the DLF values is examined to determine if the successive intra-subject DLF values are autoregressive or a random process. The four random subjects used in Figure 3.31 are again used for conciseness. The autocorrelation values presented in Table 3.8 it is demonstrated that the intra-subject variation of DLFs is a random process and little evidence is given that the DLF series is autoregressive. Only 4% of the autocorrelation values are above an absolute value of 0.25. The various thresholds demonstrate only a limited instance of potential auto-regressive behaviour. There is insufficient probable cause to state that the intra-subject DLF values are anything other than a random process.

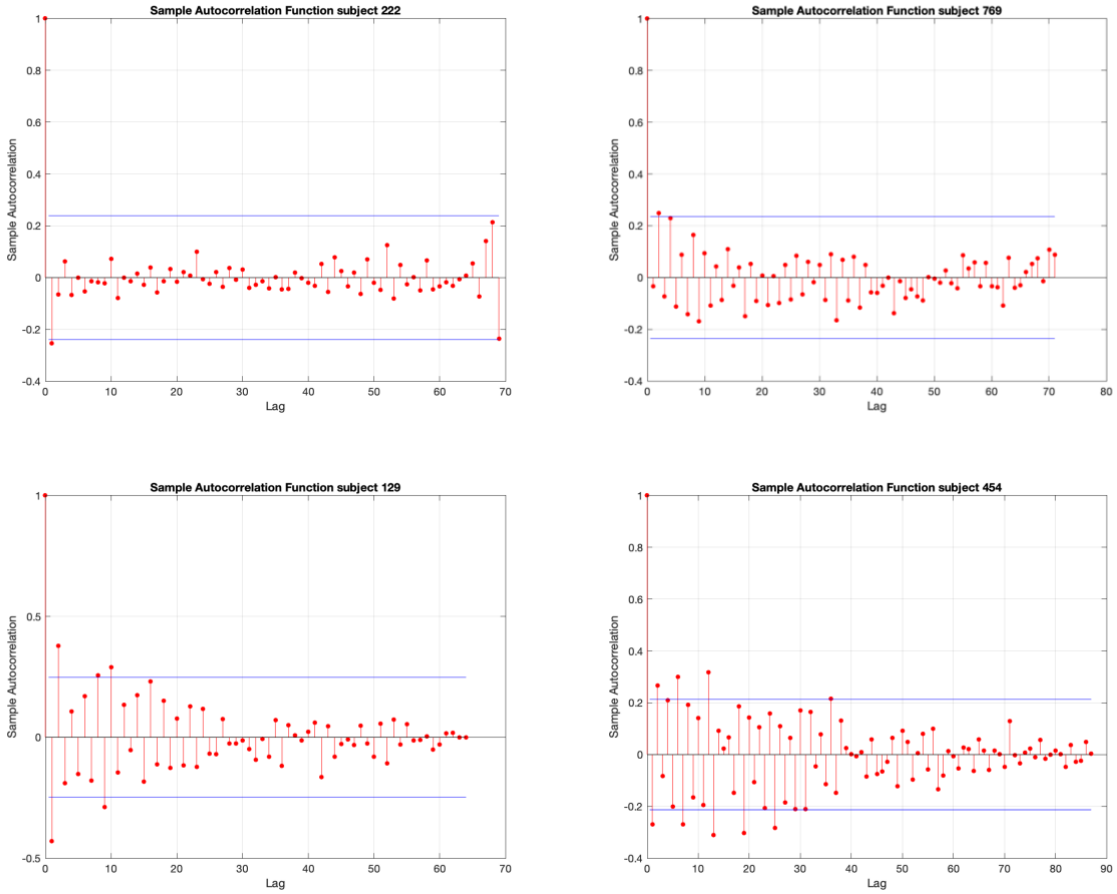

Figure 3.31 Autocorrelation of 4 random samples of intra-subject variation of DLF_1 values

Table 3.8 Percentage of auto-correlation values above a specific threshold for all intra-subject DLF values

Correlation value (Absolute magnitude)	Percentage of values of the intra-subjection variation of DLFs over correlation value (%)
0.25	4
0.375	2
0.5	1
0.75	0.1

The inclusion of the intra-subject nature of the DLF values is modelled through a normal distribution. With a mean of the average DLF values and the standard deviation given through the CoV, each CoV is taken from sampling the gamma function of the respective intra-subject CoV for each DLF from Table 3.7.

3.3.3 Velocity

Whilst velocity is not directly involved in the Fourier series representation, the velocity of the pedestrian is required to know their exact location as they traverse a structure at any time. As seen in Chapter 2 Section 2.1.2.5, the velocity is either inferred through the known walking frequency and sampled step length or through a dependent relationship between walking frequency and velocity. Figure 3.32 presents the linear relationship between average walking frequency and average velocity from the given dataset. The linear approximation produces a plausible relationship; however, the relationship only holds for the values of walking frequency from 0.9 to 3Hz. Furthermore, various walking velocities can occur due to the same walking frequency. To account for such an error in the line regression model, the error distribution is sampled from a zero mean normal distribution with a variance of 0.049m/s.

Outside the limits of 0.9-3Hz, the relationship between walking frequency and walking velocity does not hold, and the physical meaning of the equation breaks down. At walking frequencies less than 0.82Hz, the average velocity would be negative. As the velocity was the controlled variable, no statistical representation can be inferred regarding velocity. Whilst other researchers have used velocity-based inputs for DLF models [63], the mathematical and interpretive nature of the models falls short compared to walking frequency-based models. Limited research has been published on the velocity of pedestrians on structures, and to use velocity-based models, the velocity is often inferred from walking frequencies. As such, the walking frequency inevitably dictates the models' use. Furthermore, walking frequency-based load models are preferred due to their ease of interpretability in defining scenarios of resonant response. However, such information is not readily available from the velocity information.

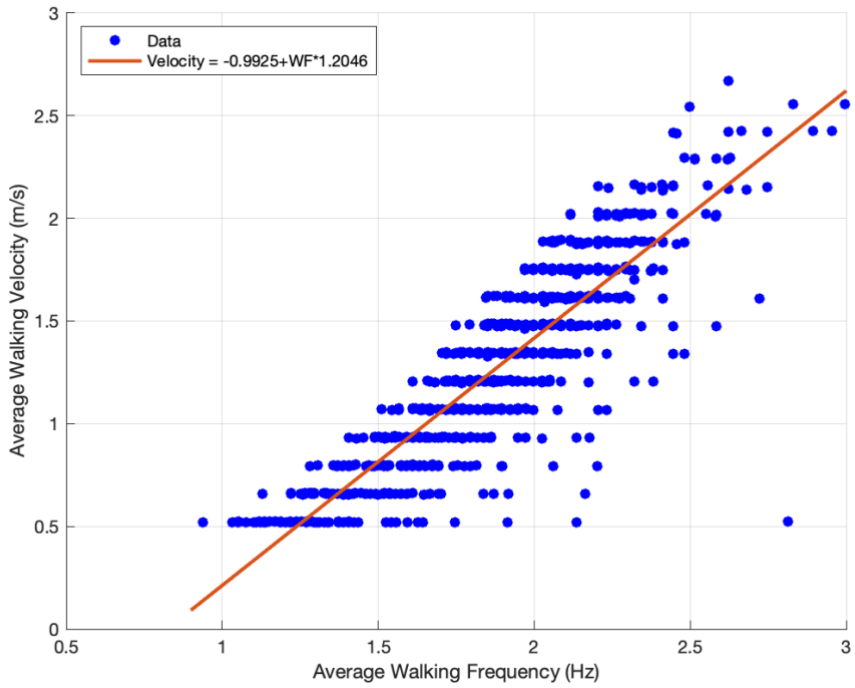

Figure 3.32 Linear relationship of average walking speed to the average walking frequency

3.3.4 Phase Angle

The phase angle associated with each harmonic of the Fourier series is often assumed to be a fixed value [16,19–21] or uniformly distributed in the range [-π, π] [52,246]. In the case of resonance by a singular harmonic, the phase angle does not influence the response calculations. However, when the response is composed of multiple modes, phase angles possess fundamental properties to determine if the signals can be constructive or destructive to each other, resulting in an increase or decrease in magnitudes of the force-time signal. Figure 3.34 presents the histograms of the phase angles taken at each of the eight walking harmonics derived from the 842 vertical force-time records.

Figure 3.34 confirms the uniform random nature of the phase angles for each harmonic. Figure 3.33 further provides evidence of a lack of correlation between phase angles at each harmonic. Therefore, phase angles of each harmonic can be assumed to follow uniform random distribution on [-π, π] interval independent of each other.

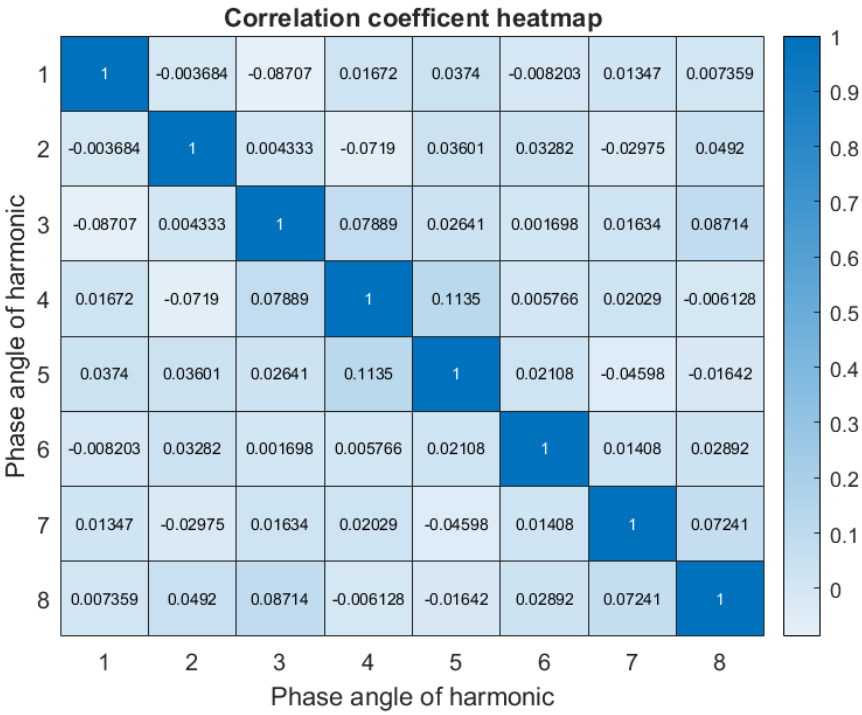

Figure 3.33 Correlation matrix of the phase angles for harmonic 1 – 8

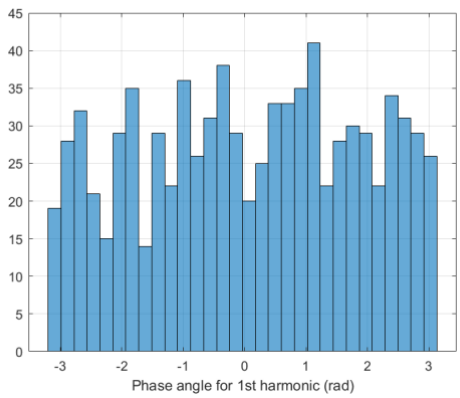

a) Distribution of phase angles at the first harmonic

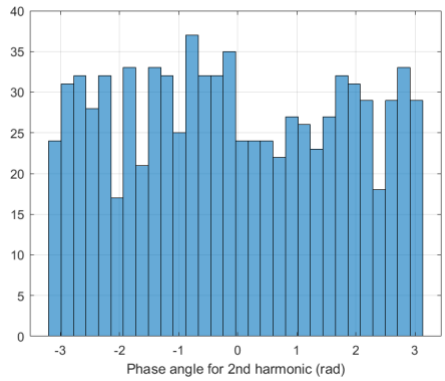

b) Distribution of phase angles at the second harmonic

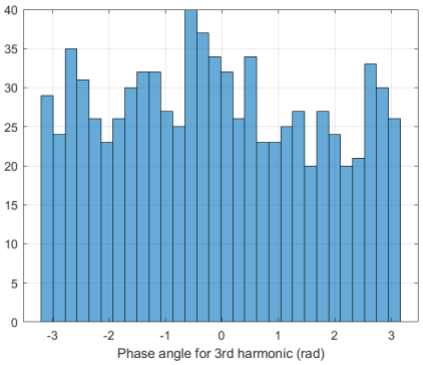

c) Distribution of phase angles at the third harmonic

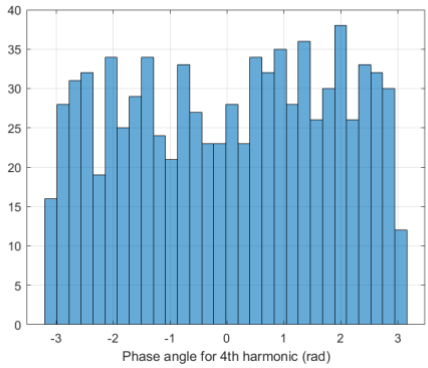

d) Distribution of phase angles at the fourth harmonic

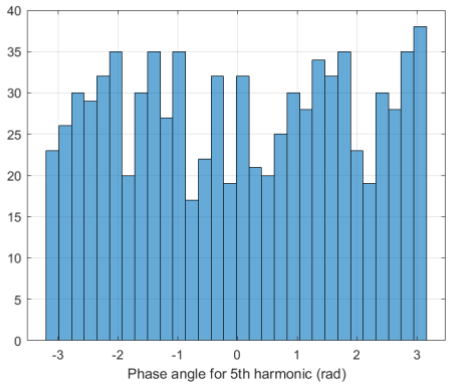

e) Distribution of phase angles at the fifth harmonic

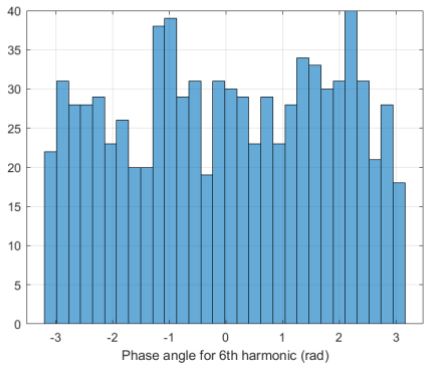

f) Distribution of phase angles at sixth harmonic

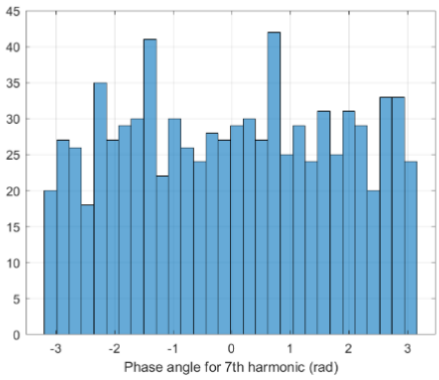

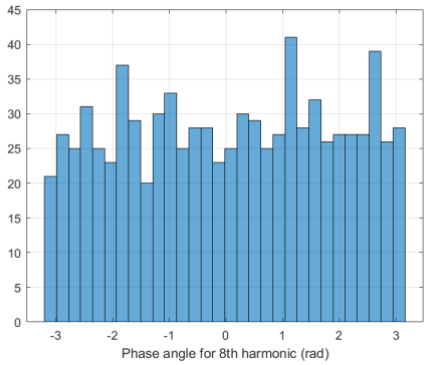

g) Distribution of phase angles at seventh harmonic h) Distribution of phase angles at eighth harmonic

Figure 3.34 Distribution of phase angles of each walking harmonic

3.3.5 The difference in walking characterisations due to sex

The proceeding section seeks to identify if the two binary sexes of the population sampled in the data exhibit different statistical characterisations of walking. Sex in this scenario is taken from the UK government division of national statistics as: "*biological aspects of an individual as determined by their anatomy, which is produced by their chromosomes, hormones and their interactions*" [247]. Therefore, the two options of sex are given as male or female. In the experiment, each participant was asked about their sex before participating. The experimental data shows 55 males and 25 females. Thus, females are underrepresented in the data compared to global averages. Of the 842 force time history records, 674 are male records, and 168 are female force time histories. Therefore, some bias in results may exist due to the limited female data (20%).

The proceeding subsections explore the variation of the vertical walking force through the lens of the Fourier representation of the force as a male or female. Section 3.3.5.1 provides an overview of the walking frequency variation in the context of inter- and intra-subject differences. Section 3.3.5.2 explores the interpretation of DLF values for both the inter and intra-subject variation. Finally, 3.3.5.3 provides a statistical overview of the variation in the inter-subject velocity.

The two-sample Kolmogorov-Smirnov test is conducted to determine if the two distributions of a feature are drawn from similar sample populations [225]. The two-sample Kolmogorov-Smirnov test, identical to the one-sample test, is a non-parametric measure of the similarity between two underlying one-dimensional probability distributions. The null hypothesis is that the samples come from the same distribution. Therefore, the samples are tested for any violation of the different medians, variances, or distributions.

3.3.5.1 Walking Frequency

Figure 3.35 visually represents the two distributions of each sex compared to the overall distribution. Performing the two-sample Kolmogorov-Smirnov test, with the null hypothesis that the two distributions are drawn from identical distribution, a p-value of 0.037 is given. It is concluded that the null hypothesis is rejected in favour of the alternative that the results come from different statistical representations. The difference in the CDF of the walking frequencies can be seen in Figure 3.35. The one-sample Kolmogorov-Smirnov test is then performed to determine if the distributions of walking frequency for each sex can be modelled through a normal distribution. Both sex fail to reject the null hypothesis, indicating they are from normal distributions with p-values of 0.57 and 0.48, for male and females respectively. The inter-subject variation of the walking frequencies for males and females is given by the normal distributions described in Table 3.9.

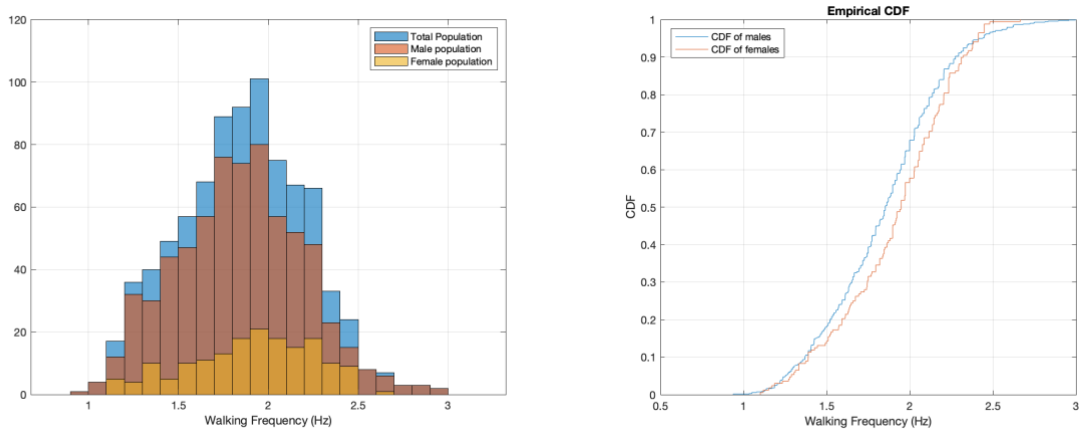

Figure 3.35 a) Probability distribution of walking frequency for males and females with 0.1 Hz bin widths b) cumulative density functions (CDF) of both male and female walking frequencies

Table 3.9 Mean and standard deviation of male and female walking frequencies

Sex	**Mean (Hz)**	**Standard Deviation (Hz)**
Male	1.844	0.354
Female	1.905	0.341

Table 3.9 and Figure 3.35 indicate that females, on average, walk at a higher average walking frequency. The result is sustained by [71,79], both showing the same elevated mean walking frequency of females compared to males.

Separating the intra-subject variation of the walking frequencies into their constituent parts, the null hypothesis is tested that the distribution of each intra-subject variation for each sex are drawn for separate but normal distributions. Each sex fails to reject the null hypothesis, evidenced that the male population's intra-subject variation is characterised by a normal distribution 91% of the time and females 92%. Therefore, there are a few discrepancies in the statistical distribution of the intra-subject model of the sexes.

As described in section 3.3.1.1, the distribution of the intra-subject variation can be conveyed through the CoV distribution. It is determined that the gamma distribution provided an adequate fit for the overall data of the walking frequency. The two-sample Kolmogorov-Smirnov test is used to determine the closeness of the CDF of the CoV for males and females.

The null hypothesis is tested that the two sexes intra-subject variation of walking frequency CoV is drawn from the same distribution. The test indicates a *p*-value of over 0.85, thus failing to reject the null hypothesis providing compelling evidence that the distribution of the CoV for the intra-subject walking frequencies is fundamentally similar. As such, the intra-subject variation of the walking frequency is shown to be invariant to sex. It is human nature that provides a natural variation in intra-subject walking frequencies. It is prudent to consider that the population in this experiment is not representative of the wider global audience. Variations in walking characteristics based on location, age, and demographic are complex issues that have yet to be studied. These issues are not addressed in the thesis but are noted for their source of variation in data.

3.3.5.2 DLF

Figure 3.36 presents the variation of DLF_1 to DLF_8 for both male and female participants. DLF_1 exhibits the largest magnitude of DLF change, with females producing a marked reduction in DLF value. This reduction is most prominent at higher walking frequencies, with 0.1 less DLF value for females. Therefore, the female will produce a lessened force for the equivalent male and female of the same weight or mass. Such a reduction is tenuously attributed to variations in the biomechanics of both sexes. However, a concrete rationale is not found. Further investigation of key biomechanical metrics would need to be addressed to provide a sound rationale for such a phenomenon.

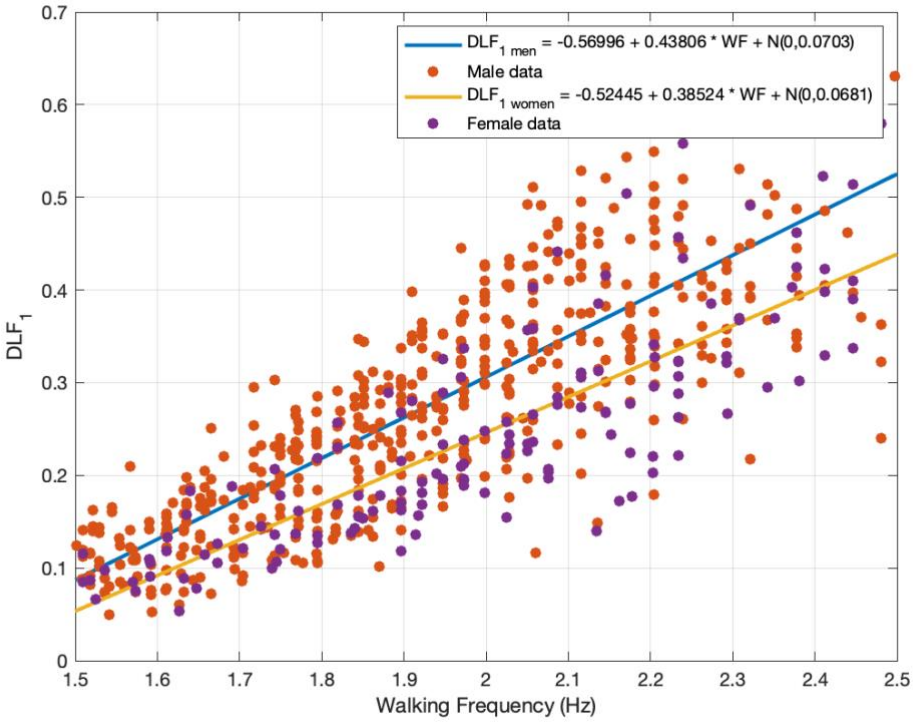

a) Comparison of DLF_1 for male and female participants with respect to average walking frequency

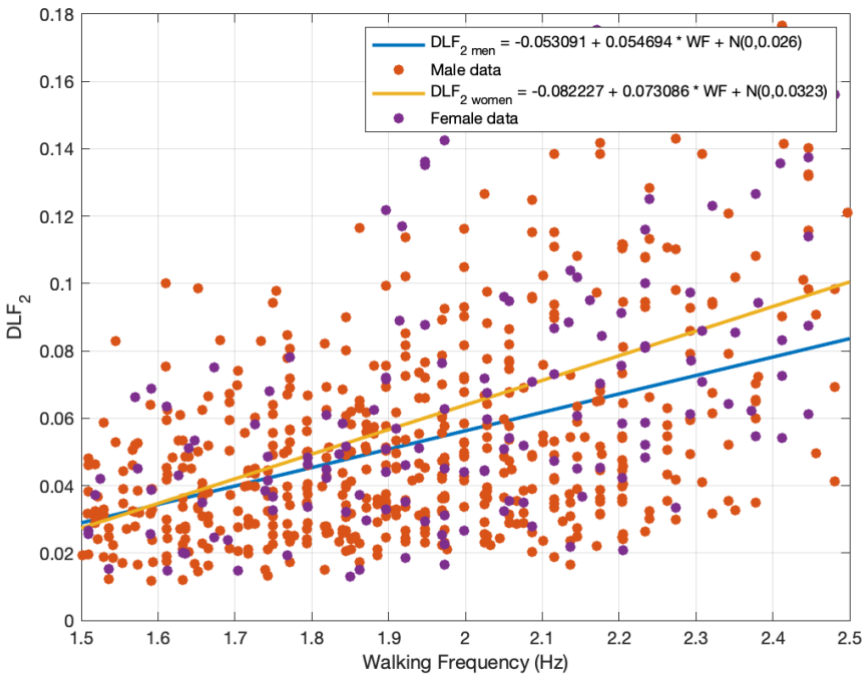

b) Comparison of DLF_2 for male and female participants with respect to average walking frequency

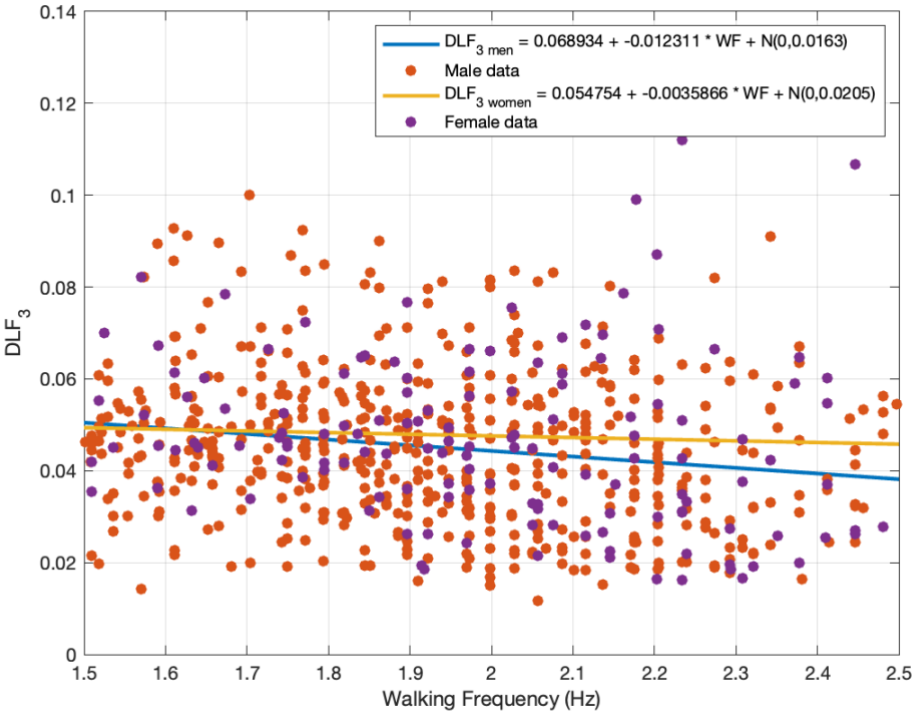

c) Comparison of DLF_3 for male and female participants with respect to average walking frequency

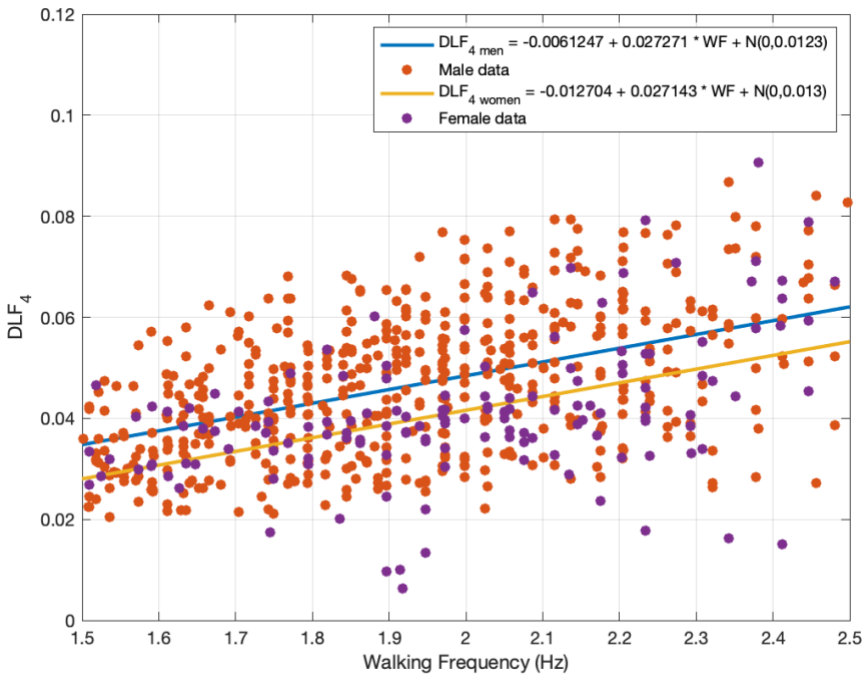

d) Comparison of DLF_4 for male and female participants with respect to average walking frequency

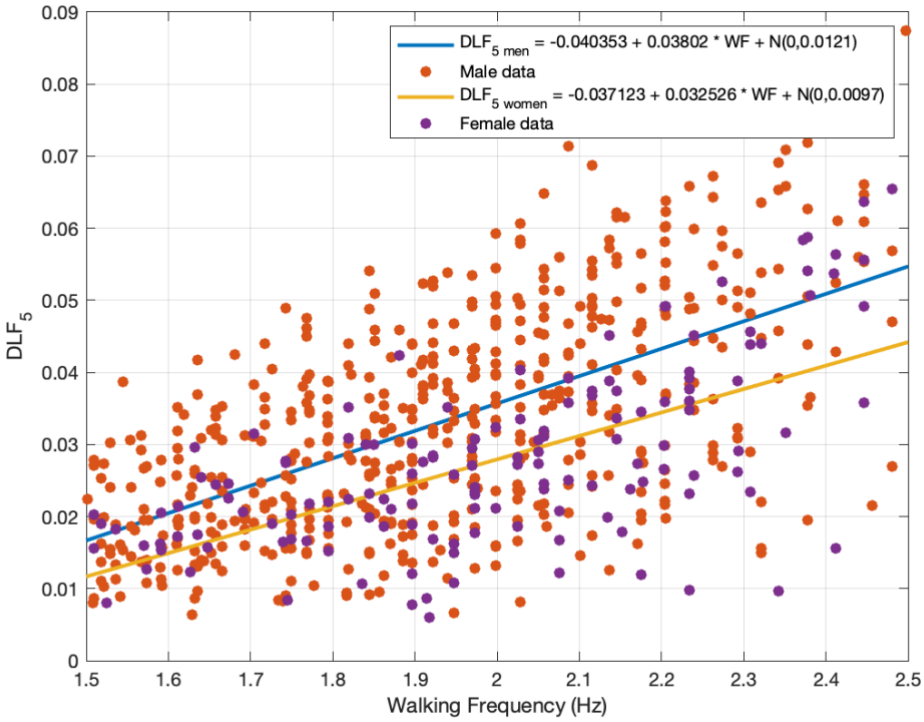

e) Comparison of DLF_5 for male and female participants with respect to average walking frequency

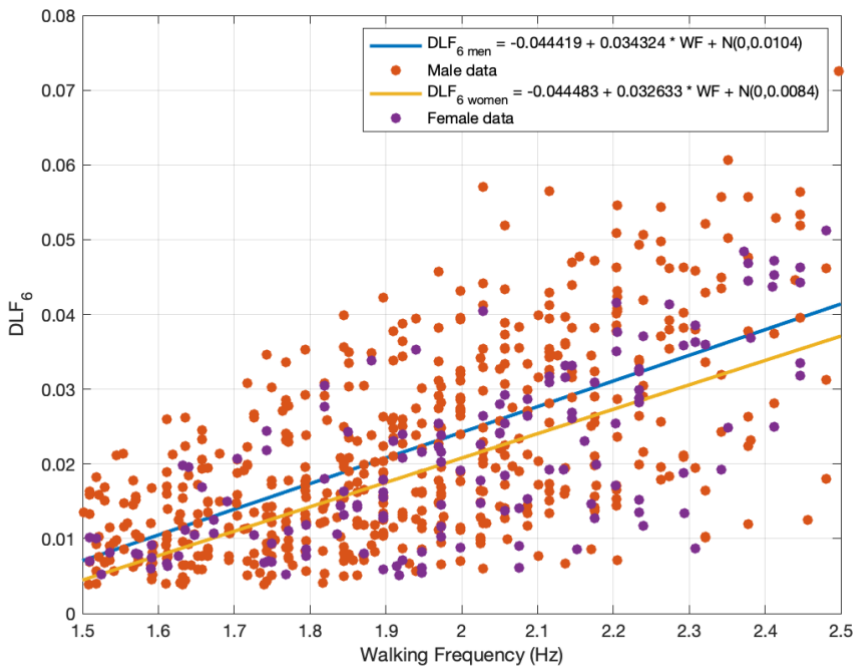

f) Comparison of DLF_6 for male and female participants with respect to average walking frequency

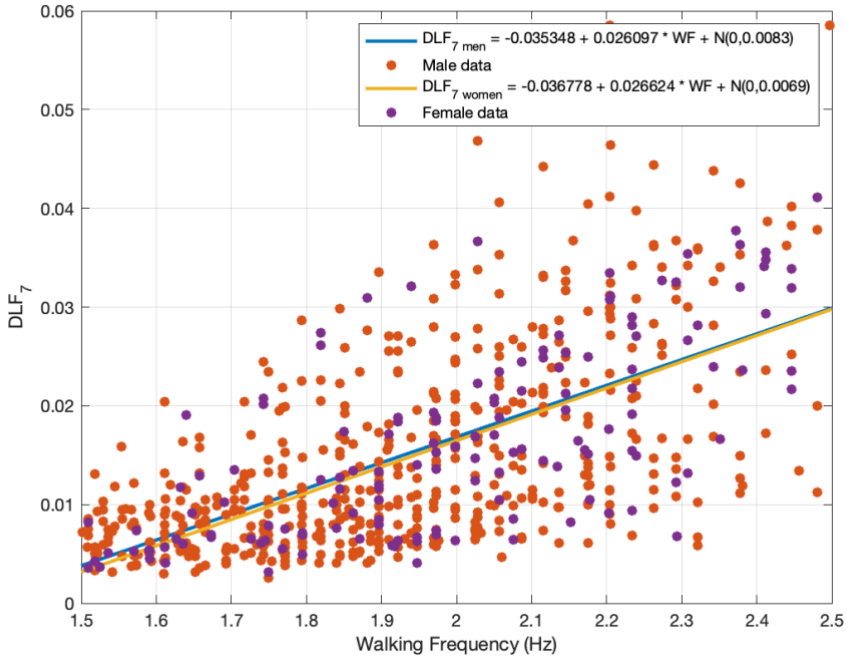

g) Comparison of DLF_7 for male and female participants with respect to average walking frequency

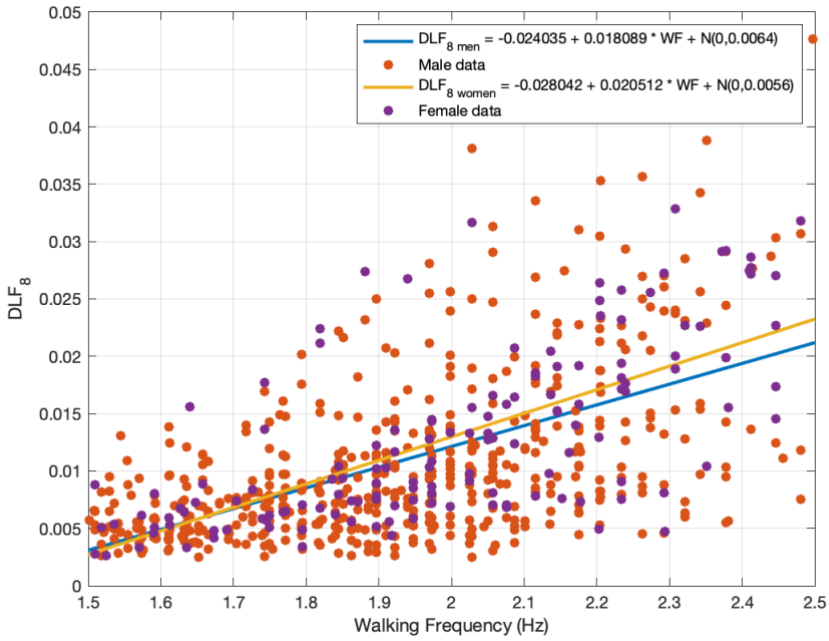

h) Comparison of DLF_8 for male and female participants with respect to average walking frequency

Figure 3.36 Comparison of male and female DLF values for DLF_1 - DLF_8 with respect to average walking frequency

The standard deviation of the error for both sexes appears similar and does not exhibit any distinguishing features. A two-sample Kolmogorov-Smirnov test is performed with the null hypothesis that the distributions of the errors of each DLF come from the same distribution. The result is that only DLF_1 indicates a *p*-value less than 0.05, thus providing evidence to reject the null hypothesis. Whilst the variation of DLF values on average are lower for females at higher harmonics, the variation is only minor compared to the magnitude of DLF_1. The maximum variation of the mean response outside of DLF_1 is 0.02, only 20% of the magnitude of DLF_1. Thus, it is DLF_1 that provides the most variation and consideration for designers. Figure 3.36 provides evidence to support the segregation of male and female walking DLF values. Including such will give a more accurate response of the structural response compared to its conjoined counterparts investigated in section 3.3.2.

Like the walking frequency, the intra-subject variation of the male and female data for DLF_1 – DLF_8 appear to be described through similar normal distributions. The one-sample Kolmogorov-Smirnov test of both males and females indicates strong evidence to support the null hypothesis that the distributions come from the standard normal distribution, with respective *p*-values of 0.846 and 0.784. The CoV of DLF_1 – DLF_8 intra-subject is used as a unique identifier of each walking instance. Section 3.3.2.2 shows the distribution follows a gamma function with the various parameterisations defined in Table 3.7. When the CoVs are separated into their male and female constituent parts and compared in their likeness through the two-sample Kolmogorov-Smirnov test for each DLF, it is shown that half of the distributions provide evidence to reject the null hypothesis, and the other half fail to reject the null hypothesis that they are from similar distributions based on an alpha value of 0.05. There appears to be a polarisation of results and no clear indication of resounding consensus that the CoV occurs in different distributions for male and female populations.

The DLF values of the population exhibit apparent differences in values based on the sex of participants and is a topic that is yet to be explored in the context of structural engineering.

Evidence supports that the DLF value of females is lower in magnitude than the equivalent male most of the time. In some instances, there is a reduction of 0.1 in magnitude or a decrease of 20% in magnitude. The mechanism by which this reduction occurs is not known but is anticipated to be biological. The intra-subject variation of males and females is similar in distribution, and evidence supports that the distribution of the intra-subject variation is from similar distributions. However, the CoV used to identify the intra-subject variation of the DLF is unclear. There exists evidence to both support and deny the claim they are similar for males and females.

3.3.5.3 Walking Velocity

Observing the variation of walking velocity concerning the input for both sexes in Figure 3.37, there are demonstrable differences between each sex. Females are evidenced to walk at higher frequencies for the given walking velocity. The consequence is that if a male and female walk together at the same speed, the female, on average, would have to walk at a higher walking frequency to match the velocity. The variation of the relationship becomes more pronounced at higher walking frequencies. The expected rationale for this finding is that females are, on average shorter than males and have shorter limbs (i.e., shorter legs).

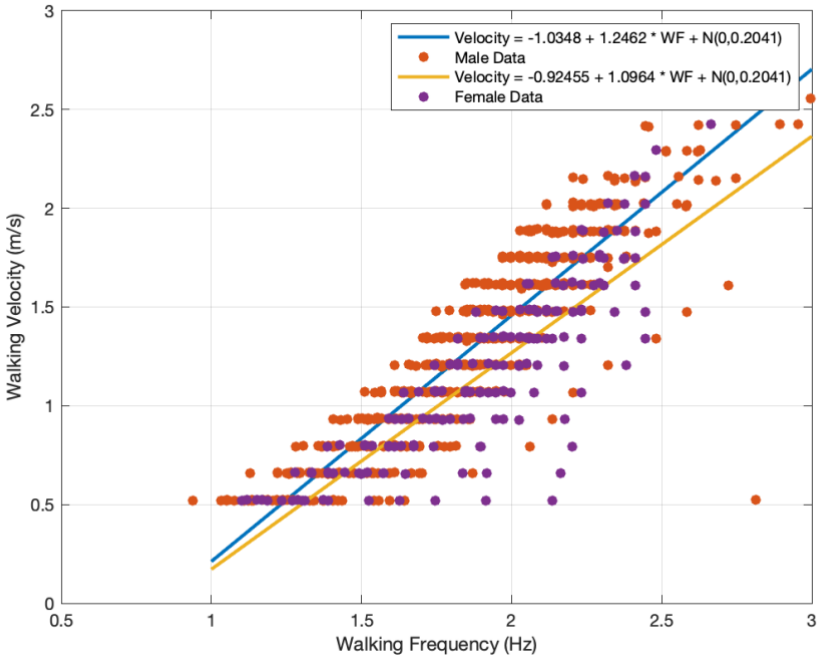

Figure 3.37 Inter-subject variation of walking speed as a function of walking velocity for males and females

To further investigate the effects of sex on velocity, the DLF values of each sex are examined concerning the velocity. As females walk at higher walking frequencies for a given walking velocity and have a lower DLF for the corresponding walking frequency, it is expected that the results of the DLF of the males and females would align concerning the walking velocity.

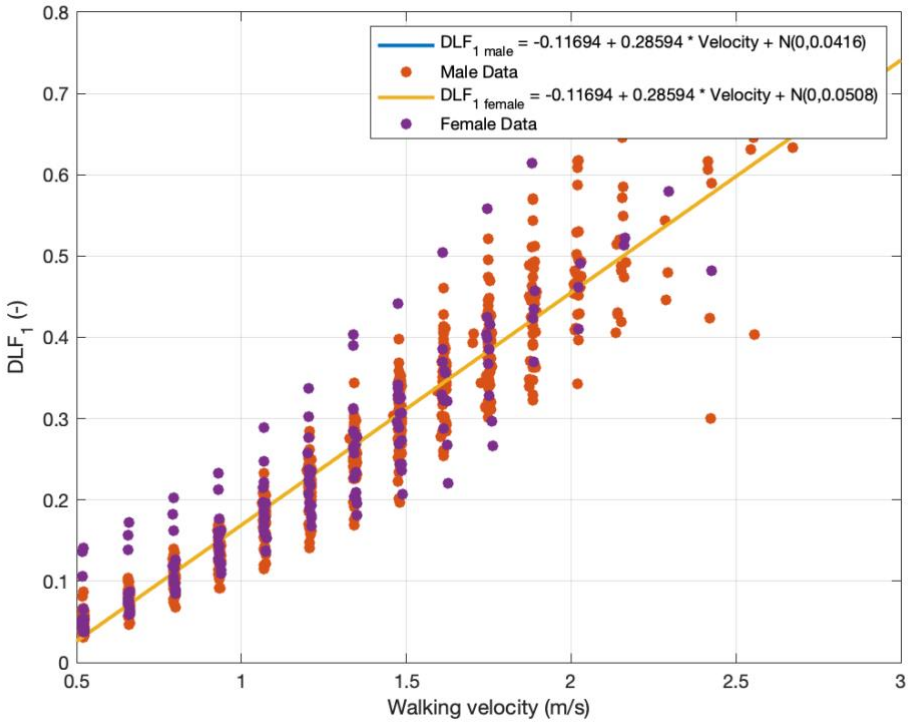

Figure 3.38 DLF_1 with respect to the average walking velocity for each sex

Figure 3.38 presents a similar linear model of DLF_1 for the walking velocity of both sexes. Similar results of DLF_2 – DLF_8 are seen but are omitted for conciseness. It is demonstrated that the two sexes align perfectly, barring the standard deviation of the error, which diverges. The parameterisation of the linear models produces identical values of the gradient and intercept terms. Therefore, males and females moving at the same velocity will have identical DLF values. However, if either sex attempts to step in phase with their counterpart, they will produce a variation in DLF values. The exact reasoning for the velocity aligning can only be hypothesised in this thesis and is thought to be attributed to walking velocity being the driving force of walking and not walking frequency. It is assumed that people tend to match a particular velocity of walking with others, not the walking frequency. Intuitively this hypothesis applies when considering groups of people walking together. Due to the natural variation in step length, the walking frequency of the participants varies depending on the dictated walking velocity.

3.4 Example use of Chapter 3 load model

The proceeding section provides guidance on the explicit methodology of sampling the models defined in Chapter 3, including both the provisions for the inclusion and exclusion of intra-subject variation.

3.4.1 Inter-subjection variation model

The model that excludes intra-subject variation is akin to those currently used in industry [16,19–21,28]. No variation in between each new footstep is seen with respect to the walking frequency or DLF values, with the reconstructed signal being perfectly periodic to the walking frequency f_p.

Firstly, either the desired walking frequency is chosen or is sampled from a known probability density distribution referenced in Section 2.1.2.1 and Table 2.2. Walking velocity, v is then inferred through the relationship defined in 2.1.2.5 or through Section 3.4.3 and Figure 3.29. The limiting time, t_{lim}, or more aptly, the time taken to cross the structure is inferred through the known structure length or walking path length divided by the average velocity. The discretisation of the time steps is then chosen to provide an adequate representation of the force function, it is suggested 0.05s increments. The DLF value of all eight harmonics is then inferred through the relationships defined in Figure 3.19 or Table 3.4 depending on the use of either the Frequentist or Bayesian interpretation. Next, the phase angle for each harmonic is sampled from the uniform distribution given in section 3.4.4. Finally, the superposition of all eight harmonics is performed, representing a vertical walking function for eight harmonics, until a defined stop time of t_{lim}. Figure 3,39 represents a flow chart of the procedure.

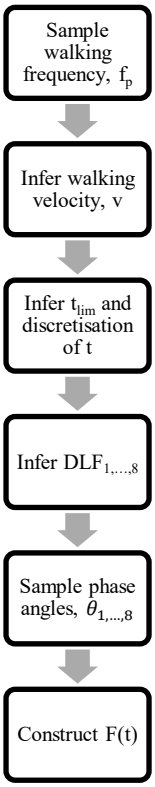

Figure 3.39 Flow chart of procedure to reconstruct vertical walking load model for inter-subject variation.

3.4.2 Intra-subjection variation model

The inclusion of intra-subject variability is seen as an essential step to present a narrow-banded vertical walking force signal. The procedure for determining the inter-subject variation is identical to that in Section 3.5.1 and Figure 3.36. The intra-subject variation is injected through the variation of the DLF and walking frequency for each new step. The intra-subject variation of the walking frequency is determined by first, sampling the CoV of the intra-subject variation of walking frequency defined in Section 3.4.1.1 through a gamma distribution. As the average walking frequency is known, the standard deviation of the intra-subject variation can be inferred through the CoV. This relationship of the mean and standard deviation can then define the normal distribution of the intra-subject variation of walking. Samples of the walking frequency are successively drawn, along with its reciprocal the time period, till enough samples are drawn such that the sum of all time periods exceeds the time

to cross the structure t_{lim}. All n samples of walking frequencies and time periods are then stored. A similar procedure is then performed to determine the n number of different DLF values for all eight harmonics of walking. The CoV of each DLF is defined in Section 3.4.2.2 and Table 3.7. As the mean DLF is known from the inter-subject model, n number sample for each new footstep is sampled for each DLF defined through the respective normal distributions.

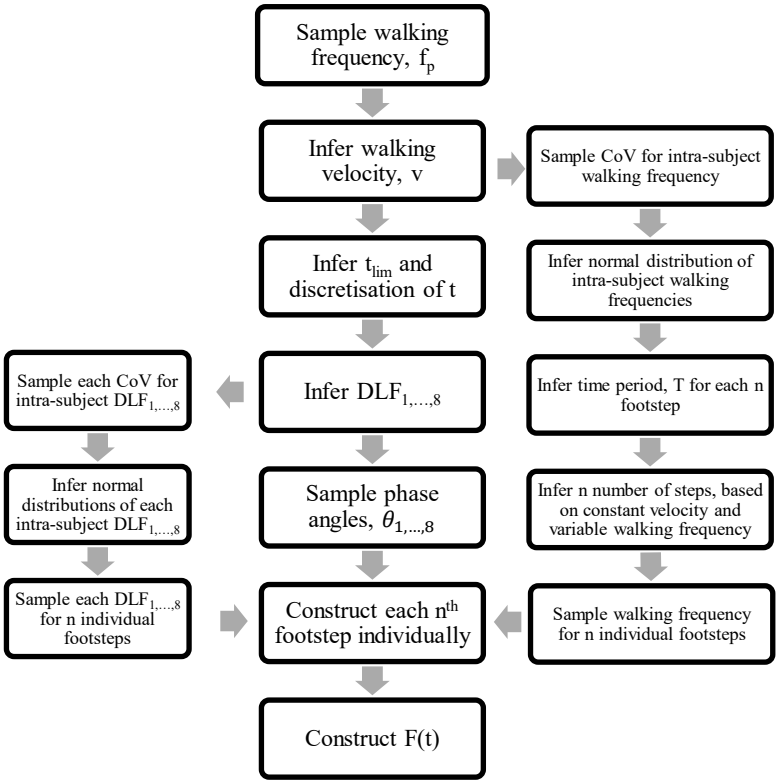

Figure 3.40 Flow chart of procedure to reconstruct vertical walking load model for inter and intra-subject variation.

The reconstruction of each footstep can now occur for each nth step. The phase angle of each signal must remain the same to ensure signals align at each new period. As the period of each step is known, along with the specific DLF and walking frequency, the force function for each step can be reconstructed using the superposition of all eight harmonics of the Fourier series approximation. Each footstep is then stitched together and adjusted to ensure the

gradients of the force function for the last-time discretisation of the previous step, and first-time discretisation of the next step are approximately similar. This process ensures that no unusual artefacts in the frequency domain occur and taint the signal's ability to reconstruct representative walking functions.

3.5 Conclusion

A new vertical load model is proposed through a Fourier series approximation, including inter- and intra-subject information regarding the DLF and walking frequency values. Further, the inter-subject variation of the phase angles and walking velocity are explored. A novel methodology is presented for extracting the DLF values, which are demonstrated to be consistent with other DLF values of treadmill data. The extraction method allows the DLF information of surrounding frequencies to influence the DLF values and not solely rely on a single peak value of DLF. The DLF values proposed in this chapter are a function of the walking frequency, and the models are parameterised in a Bayesian and frequentist fashion. The DLF models result in values consistently lower than those proposed previously. The intra-subject variation of the DLF models is presented through an independent normal distribution defined through the CoV. The CoV is shown to have a well-defined gamma distribution. Including the intra-subject variation of the DLF values also presents a broader range of DLF values for a given walking frequency.

Akin to the intra-subject nature of the DLFs, the walking frequency intra-subject variation is proven to be modelled as a normal distribution. The CoV of the intra-subject variation is defined through a gamma distribution. The phase angles of all harmonics are proven to follow a uniform random independent distribution, with no interconnected behaviour of any harmonics. Finally, the walking velocity to walking frequency relationship provides consistent results with Chapter 2 Section 2.1.2.5.

The final portion of the chapter investigated the variation of walking due to sex differences. It is shown that females walk at higher frequencies concerning male counterparts. The DLF values of females are shown to be lower on average than their male counterparts, and, in some instances, this reduction is 20%. Finally, it is evidenced that females walk at higher

walking frequencies concerning the same walking velocity as males. It was further seen when considering the DLF values concerning walking velocities both sexes produced identical models of the DLF values.

Chapter 4 Comparison of vertical walking force models

As demonstrated in Chapter 2 Section 2.1.2-2.1.4, the vertical walking force is represented through several parametric formulations. However, only a few studies have investigated the most appropriate and accurate formulations. Several published and viable models provide various vertical walking force functions within industry and academia. Muhammad et al. [24] compared the acceleration response of three structures and provided estimates of the acceleration response with the predicted response of five load models used in industry [16,19,20,28,133]. No individual load model provided a conclusive estimate; however, the HIVoSS [133] load model consistently produced a constant overestimation [24]. Muhammad and Reynolds [24] provide a limited account of all vertical load models, negating many current published models and any human structure interaction effects. Furthermore, this study only considers three different natural frequencies and modal damping ratio. Hence, the applicability of a reliable model across all possible walking frequencies and modal damping ratio is not considered.

The preceding chapter of this thesis seeks to provide a robust comparison of the currently published and industry-used vertical walking loads. A series of fictitious, simply supported structures are modelled with incremental modal damping ratios and natural frequencies of the fundamental vibration mode. Each identified load model will then be used to estimate the mid-span acceleration of an idealized walking participant. The results of each model were compared to the dataset of Racic et al. [52] when each of the recorded individual force time histories was applied to the fictitious structures. Therefore, each load model was compared in terms of the mean and variance of the mid-span acceleration response compared with the values produced by the actual vertical walking forces measured.

Section 4.1 describes the methodology used in this study. Section 4.2 provides a comparison of the mean acceleration responses. Section 4.3 provides a comparison of the variance in the acceleration response. Section 4.4 is a discussion of the results in Sections 4.2 and 4.3. Finally, Section 4.5 presents the conclusions of the study.

4.1 Methodology and assumptions of dynamic analysis

Current industry-used load models are presented as reconstructions from the measurements of walking force signals, and limitations arise owing to the data quality. Historically, only a small number of studies have recorded force data for singular [4,45], double [4], and several [53,139] footfalls, thus providing incomplete representations compared to continuously monitored walking force signals. Advancements in measurement techniques have enabled the direct recording of continuous walking from treadmills [52,63] and insoles [90], which can capture an unlimited number of steps. More reliable footfall data can be utilized to produce models that accurately describe the true narrowband random process of walking [139]. The current load models used in industry [19–21,28] are derived from the historical data of [45], consisting of single footfall force records only. Therefore, they lack the natural intra-subject variation of individual footfalls because the data are derived from a limited number of footfalls (approximately 1000 steps). Other researchers have presented findings from datasets containing approximately 1.7 million individual footsteps [52].

The following sections aim to establish a robust methodology for comparing all available vertical walking load models. Section 4.1 provides the methodological steps of the assessment, outlining the relevant tests and metrics of evaluation, along with the identified models of interest. Section 4.1, also provides the structural assumptions of the fictitious structures used. Finally, Section 4.1.2 provides the mathematical procedure for solving the dynamic systems.

4.1.1 Methodology of comparison

The 19 load models chosen for this comparison study include current academic and industry load models and are presented in Table 4.1. Each model was selected based on its everyday use in practice or as a result of recent research trends [23,24,27,248]. The HIVoSS model

[133] was not used in this study because it overestimated the acceleration response in previous studies [24]. Chapters 2 Section 2.1.2 and Chapter 3 Section 3.4.1 and Section 3.4.2 . provide explicit details of each model and various nuances.

Table 4.1: Vertical walking load models under investigation

Vertical load model name
SCI P354 low frequency [19]
SCI P354 high frequency [19]
SETRA [55]
concrete and cement industry publication (CCIP) design low frequency [20]
concrete and cement industry publication (CCIP) design high frequency [20]
concrete and cement industry publication (CCIP) mean low frequency [20]
concrete and cement industry publication (CCIP) mean high frequency [20]
Technical report 43 appendix G [28]
ISO 10137 [21]
AISC Design Guide 11 low frequency [16]
AISC Design Guide 11 high frequency [16]
Inter variation model of Chapter 3 Section 3.4.2
Inter and intra-subject variation model of Chapter 3 Section 3.4.2
Zivanovic et al. [34]

Muhammad et al.[51]
García-Diéguez et al. [63]
Racic et al. [52]
Varela et al. [64]
Mohammad et al. [17]

Industry-used load models are typically presented with corresponding high- and low-frequency components based on the natural frequency of the structures. Chapter 2 Section 2.1.1 provides in-depth insights into the rationale and methodology for such a decision. When models are comprised of separate high and low-frequency load models [16,19,20,28], the appropriate model is used up to the given boundary (Table 4.2). Therefore, the Fourier-based models are only used up to their limited integer walking frequency, after which the corresponding impulse model is used, if applicable. Table 4.3 presents the limits of the walking frequency for each model, as not all models consider the same range.

Table 4.2: Cut-off frequency from low to high-frequency load models

Load Model	Low to high-Frequency limit (Hz)	Model frequency content limit (Hz)	Separate High-frequency load model
AISC Design Guide 11 [16]	8.8	40	Yes
ISO 10137 [21]	8-10	12	No
Technical report 43 appendix G [28]	11.2	40	Yes
CCIP Mean value [20]	11.2	40	Yes
CCIP design value [20]	11.2	40	Yes

SCI P35[19]	8.8	40	Yes
SETRA [55]	7.2	7.2	No
Thesis Chapter 3	N/a	20	No
Zivanovic et al. [62]	12.5	12.5	No
García-Diéguez et al.[63]	13	13	No
Racic et al. [52]	N/a	100	No
Muhammad et al.[51]	N/a	100	No
Varela et al. [64]	7.8	7.8	No

Table 4.3: Limits of walking frequency for each model

Model	Walking frequency limits (Hz)
AISC Design Guide 11 [16]	1.6-2.2
ISO 10137 [21]	1.2-2.4
Technical report 43 appendix G [28]	1-2.8
CCIP Mean value [20]	1-2.8
CCIP design value [20]	1-2.8
SCI P35[19]	1.6-2.2
SETRA [55]	1.6-2.4
Thesis Chapter 3	1.5-2.5
Zivanovic et al. [62]	1.5-2.5

García-Diéguez et al.[63]	1.5-2.6
Racic et al. [52]	1.5-2.5
Muhammad et al.[51]	1.5-2.5
Varela et al. [64]	1.4-2.6

The 19 synthetic models were compared against the baseline-recorded signals of Racic and Brownjohn [52]. While no dataset of overground direct walking force measurements exists (to the authors knowledge), the dataset of Racic et al. [52] acquired on a treadmill was used as a surrogate. Semaan et al. [249] demonstrates that treadmill walking and overground walking possess statistically similar spatiotemporal parameters and can be used interchangeably. First, 864 vertical walking time signals were examined to select only signals within a normal range of walking frequencies (1.5Hz to 2.5 Hz) [4,43,53,70,71,250]. Each signal is then categorized into one of 11 walking frequency bands in the 1.5-2.5 Hz range at 0.1 Hz intervals. The distribution of walking frequencies in the dataset is shown in Chapter 3 Section 2.1.2.1. The division of 0.1Hz was chosen to allow sufficient data in each category. If the division is determined to be any smaller, numerous walking frequencies are populated with singular values, resulting in an ill-posed statistical representation of the loads.

The weights of the pedestrian and DLF are uncorrelated [52]. Therefore, each signal from the dataset was divided by the participant's weight and then multiplied by 750 N, corresponding to the average pedestrian weight in the UK [86]. While the average weight of pedestrians varies globally and locally [23,51], the constant value used throughout the study was selected to provide a baseline estimation of the structural response to compare the synthetic load models. It is further assumed that pedestrians walk at a constant velocity dictated by the walking frequency. The relationship formed in Chapter 3 Section 2.1.2.5 for the walking velocity was used to estimate the average constant velocity of each pedestrian.

For low-frequency and high-frequency load models, the vertical force is represented in a numerical time-step manner. A modal force was applied to a single-degree-of-freedom (SDOF) spring mass damper system representing the first structural vibration mode to calculate the acceleration output. The 1s-RMS acceleration was chosen as the comparison metric because of its frequent use in VSA [16,19,20,24,28,55]. Each walking load model was

sampled 100 times for models founded on stochastic processes to provide an adequate approximation of the statistical representation at each walking frequency.

Because of the two categories of high- and low-frequency load models, each category was assessed individually within its appropriate range and provided a comparison of the dataset [52]. The likeness of each vertical load model was evaluated using two assessments. First, the maximum 1-second Root Mean Squared acceleration (1s RMS) was investigated. The 1s RMS is used as the acceleration metric because of its frequent use within the VSA [16,19]. The use of the 1s RMS acceleration also smooths singular high instantaneous peaks. For a rigorous comparison of the load models to occur, a variety of fictitious structures incrementally increasing in natural frequency from 0.5 to 20Hz in 0.25Hz steps are modelled or up to the limiting bounds of the model's applicability concerning the walking frequency or cut-off limit. The structure is then subjected to walking paces ranging from 1.5Hz to 2.5Hz or the limited range of models-defined walking frequencies (Table 4.3). Finally, the max 1s RMS acceleration variation is examined for all stochastic or probabilistic models using the same numerical procedure described before discussing all possible ranges of the walking load model's response.

For a direct comparison of the vibration output, an idealized single-degree-of-freedom structural system was used. It represents a 50-metre-long simply supported structure with a modal mass of 10,000 kg and modal damping ratios of 0.5%, 1%, 2%, and 5%. The length of the structure was chosen to ensure that a resonant response could be built due to the low-frequency walking modes. The structure is assumed to behave linearly, and the first vibration mode dominates the dynamic response. Various modal damping ratios are chosen because damping and the force input have a non-linear relationship with the resultant acceleration response. The range of modal damping ratios was selected to mimic typical structural modal damping ratios published [19,82,133].

Whilst HSI effects will likely become instrumental in an actual structure [89,149,190,218], in the present chapter, it is ignored. The study is focused on determining the most accurate representation of situations where structural vibrations do not affect the pedestrian gait. Once this baseline knowledge is established, further studies on the effect of the HSI on vibration response can be carried out (Chapter 5). Accuracy within this context is defined as the

minimisation of the maximum acceleration response of the structure less that of the acceleration of the synthetic load models.

The results of the mean and variance of the structures' response are presented as both the relative error and percentage error. The relative error is defined herein as the output of real walking results minus the output of the synthetic signal result. The percentage error is the relative error divided by the real signal times 100. Positive results indicate an underestimate, and negative results indicate an overestimation of the acceleration response. In the cases of Racic and Brownjohn [52], Muhammad and Reynolds [51] and the Chapter 3 Section 3.41 and Section 3.4.2 models, the models present information up to the defined system limit of 20Hz. Therefore, the models are artificially split into the constitutive parts separately for comparison, with low-frequency responses deemed up to 10Hz and high after that. By doing so, the models can be independently assessed for their high and low-frequency content qualities. The artificial separation of the models is only done to provide a like-for-like comparison. The location (walking frequency and natural frequency of the structure) and magnitude (1s-RMS acceleration error and percentage error) of the over and underestimation for both the relative error and percentage error are given to provide context and identify key locations of poor estimations of the model.

The midpoint of the walking path is chosen as the location of the 1s RMS acceleration response measurement, as this is the antinode of the first mode shape. Each walking load model will be simulated on 316 structures (Natural frequency 0.5Hz-20Hz in 0.25Hz increments and modal damping ratio 0.5-5%) at 11 different prescribed walking frequencies (1.5Hz-2.5Hz in 0.1Hz increments). The maximum 1s RMS acceleration at the midpoint of the structure for each of the load models is noted. This response is compared to the acceleration responses of the real walking load signals from [52] walking on the same structure. The comparison of the mean and the variation of the maximum 1s RMS acceleration response for each synthetic load model versus the real walking forces are then performed based on the metrics above.

4.1.2 Dynamic analysis

The equation of motion of a structure subject to the vertical walking force $F(t)$ is defined through the set of linear second-order differential equations, assuming that a structure exhibits viscous damping. It is further assumed that a reduced-order modal analysis is sufficient to describe the response of a structure to an arbitrary force. The equation of motion for one mode of a structure is written as follows:

$$M_{sn}\ddot{q}_{sn} + C_{sn}\dot{q}_{sn} + K_{sn}q_{sn} = F(t) \qquad \text{Eq 65}$$

WhereM_{sn}, C_{sn} and $K_{sn}$are the modal mass, damping and stiffness of the nth structural mode, subscript s denotes the structure. $\ddot{q}_{sn}$, $\dot{q}_{sn}$ and q_{sn} represents the generalised modal acceleration, velocity and displacement, respectively. Dot notation is taken as the time derivative concerning the variable. Thus, the modal properties of the system approximating the SDOF system are calculated as follows:

$$C_{sn} = 2\xi_{sn}M_{sn}\omega_{sn} \qquad \text{Eq 66}$$

$$K_{sn} = \omega_{sn}^2 M_{sn} \qquad \text{Eq 67}$$

$\xi_{sn}$is the modal damping ratio of the nth mode and $\omega_{sn}$is the natural angular frequency of the nth structural mode. To determine the overall approximation of the structure's response, the modes under consideration are summed with the appropriate mode shape, thus producing the response concerning the structure. However, in the specific example only one mode is considered, therefore the entire response is seen through only one mode.

Eq 65 can be solved using time integration methods, convolutional methods, closed form analytically in unique instances, or converted to a state-space representation and solved numerically. The latter option is preferred for discrete-time problems. It is used throughout this thesis to solve the linear sets of differential equations. First, a set of state variables $\boldsymbol{U}$ is introduced as:

$$\boldsymbol{U} = \begin{Bmatrix} U_1 \\ U_2 \end{Bmatrix} = \begin{Bmatrix} q_{sn} \\ \dot{q}_{sn} \end{Bmatrix} \qquad \text{Eq 68}$$

With its associated derivatives denoted as:

$$\dot{\boldsymbol{U}} = \begin{Bmatrix} \dot{U}_1 \\ \dot{U}_2 \end{Bmatrix} = \begin{Bmatrix} \dot{q}_{sn} \\ \ddot{q}_{sn} \end{Bmatrix} \qquad \text{Eq 69}$$

Eq 65 can then be rewritten to satisfy Eq 69, thus producing the state-space representation:

$$\dot{\boldsymbol{U}} = \begin{bmatrix} 0 & I \\ -KM^{-1} & -CM^{-1} \end{bmatrix} \boldsymbol{U} + \begin{bmatrix} 0 \\ F(t)M^{-1} \end{bmatrix} \qquad \text{Eq 70}$$

Where I is the identity matrix, Eq 70 can therefore describe the standard state-space discrete time-invariant system with state vector ***U(t)*** and output vector ***Y(t)*** defined through the state matrix $\boldsymbol{A}$, input matrix $\boldsymbol{B}$, output matrix $\boldsymbol{C}$, feedthrough matrix $\boldsymbol{D}$ and ***w(t)*** the input vector.

$$\dot{\boldsymbol{U}}(\boldsymbol{t}) = \boldsymbol{AU}(\boldsymbol{t}) + \boldsymbol{Bw}(\boldsymbol{t}) \qquad \text{Eq 71}$$

$$\boldsymbol{Y}(\boldsymbol{t}) = \boldsymbol{CU}(\boldsymbol{t}) + \boldsymbol{Dw}(\boldsymbol{t}) \qquad \text{Eq 72}$$

For the case when the acceleration is the state of interest, the output vector is written as:

$$Y(t) = \ddot{q}_{sn}(t) = [-KM^{-1} \quad -CM^{-1}] \begin{Bmatrix} q_{sn} \\ \dot{q}_{sn} \end{Bmatrix} + F(t)M^{-1} \qquad \text{Eq 73}$$

Thus, the state vector $\boldsymbol{U}$ must be first solved to obtain the solutions to the output acceleration. Whilst it may be feasible to provide an analytical solution, multiple instances of solving an ordinary differential equation for the application of the thesis occur. Thus, a more efficient and robust methodology is required when the functions and boundary conditions of the differential equations repeatedly change. Furthermore, the actual function of the output is not of interest, only the values of the function at the discrete time intervals. Therefore, a numerical analysis of the ordinary differential equation is used. First, the initial value problem is formed:

$$\dot{U}(t) = f(t, U(t)) \quad \text{Eq 74}$$

$$U(t_0) = U_0 \quad \text{Eq 75}$$

WereU_0 is the set of initial conditions. The simplest of all the numerical methods is Euler's Method. For simplicity, the time variable is formed of evenly spaced samples defined as:

$$t_n = t_0 + nh \quad n = 0,1,\dots,N \quad \text{Eq 76}$$

Where t_0 is the initial time, and h is the time increment. Euler's forward difference approximation is derived from the standard derivative approximation:

$$\dot{U}(t) \approx \frac{U(t+h) - U(t)}{h} \quad \text{Eq 77}$$

As such, this approximation is rewritten to form the Euler forward method:

$$U(t+h) \approx U(t) + h\,.\dot{U}(t) \quad \text{Eq 78}$$

The function $U(t+h)$ is approximated considering the tangent to the function at $U(t)$. Therefore, errors will propagate the approximation when larger values of *h* are chosen, leading to a small value of *h* required to provide stability to the approximation. The local truncated error, i.e., the error with every new step, is found to be [251]:

$$LTE = O(h^2) \quad \text{Eq 79}$$

Where *O()* denotes the order of complexity of the function for the input, the error of the numerical solution is poor. To increase the accuracy of a solution, the number of steps between the start and end of the function needs to be increased by the same proportion of the required increased accuracy. Other methods, such as the Runge-Kutta, provide increased accuracy and use larger step sizes. Therefore, throughout the thesis, the Runge-Kutta method is used explicitly. The Runge-Kutta methods are a family of techniques that interpolate a function to provide approximations of the higher-order derivates of the function, thus providing increased accuracy. The most used method is the 4th order method, commonly referred to as RK4. The technique is formed as follows:

$$U(t+h) = U(t) + \left[\frac{k_1}{6} + \frac{k_2}{3} + \frac{k_3}{3} + \frac{k_4}{6}\right] \quad \text{Eq 80}$$

Where:

$$k_1 = h.f(t, U(t)) \quad \text{Eq 81}$$

$$k_2 = h.f\left(t + \frac{h}{2}, U(t) + \frac{k_1}{2}\right)$$

$$k_3 = h.f\left(t + \frac{h}{2}, U(t) + \frac{k_2}{2}\right)$$

$$k_4 = h.f(t + h, U(t) + k_3)$$

From the Eq 80 and Eq 81 values of $U(t)$ can be found for all the time increments and, as such $\dot{\boldsymbol{U}}(\boldsymbol{t})$ can be found for all time instances through Eq 70 or Eq 73. Therefore, the accelerations of a structure's response can be readily found for any unique force function represented through a discrete time interval series. The local truncated error of RK4 is $O(h^5)$, thus several orders of magnitudes better than Euler's method. The improvement of the estimate of the gradient-based method of RK4 is principally seen through consideration for the derivate of $U(t)$ at various points between time instances *t* and *t*+*h*. As such, more accurate representations can be approximated of the function, and larger time steps, *h*, can be taken.

4.2 Mean acceleration response

Using the methodology laid out in Section 4.1, the 1s RMS mean acceleration response of the synthetic load models of a 750N pedestrian walking at the 11 predefined walking frequencies (1.5Hz to 2.5Hz at 0.1Hz increments) on the structures of various natural frequencies (0.5Hz to 20Hz at 0.25Hz increments) and modal damping ratio (0.5%, 1%, 2%, 5%), are compared to the real measured vertical walking forces obtained by Racic et al. [52].

4.2.1 Mean 1s RMS acceleration for low-frequency models

Table 6.1 to Table 6.4 of Appendix A provide the analysis for the low-frequency model of the vertical walking signals. The relative error is defined herein as the 1s RMS acceleration

output of real walking on the structure minus the output of the synthetic walking loads. The percentage error is the relative error divided by the real walking forces times 100. Positive results indicate an underestimation, and negative results indicate an overestimation of the synthetic loads. Where models comprise of high and low-frequency functions, each is used up to its associated limit (Table 4.2). In the cases of Racic and Brownjohn [52], Muhammad and Reynolds [51] and Chapter 3 Section 3.41 and Section 3.4.2 models, the models present information up to and surpassing the upper limit of the highest natural frequency (20Hz). Therefore, the models are artificially split into low and high-frequency constitutive parts for comparison. The cut-off frequency is artificially chosen as 10Hz, thus ensuring the models can be independently assessed for their low and high-frequency load models compared to similar walking models.

Table 4.4: Summary ranking of low-frequency models based on the minimum range of relative error and percentage error for each modal damping ratio scenario.

		Maximum relative error				Maximum percentage error			
Model number	Load model	0.50%	1%	2%	5%	0.50%	1%	2%	5%
1	AISC Design Guide 11 [16]	13	13	13	13	14	14	14	14
2	ISO 10137 [21]	7	7	6	14	13	13	12	7
3	Technical report 43 appendix G [28]	12	9	7	8	10	11	11	11
4	CCIP Mean value [20]	10	8	11	7	9	10	9	10
5	CCIP design value [20]	14	13	13	11	12	12	13	12
6	SCI P354 [19]	11	11	12	8	7	5	4	4
7	SETRA [55]	8	10	7	12	11	9	10	13
8a	Chapter 3 Section 3.4.1 inter-subject	6	6	5	1	3	3	3	2
8b	Chapter 3 Section 3.4.2 inter-subject plus walking frequency and	3	2	2	1	2	2	2	3

	DLF intra-subject								
9	Zivanovic et al. [62]	5	5	7	10	5	6	7	9
10	García-Diéguez et al. [63]	1	1	3	4	4	4	5	5
11	Racic et al. [52]	4	2	1	3	1	1	1	1
12	Muhammad et al.[51]	2	2	3	5	6	7	6	6
13	Varela et al. [64]	9	11	10	6	8	8	8	8

Table 4.4 provides a summative ranking of the low-frequency models based on the relative and percentage error range, with the full degree of information given in Appendix A. Whilst the ranking is objective, specific subjective merits must be considered. For the percentage error, each location refers to different scale ranges. However, the ranking is used to measure the results objectively. From Table 4.4 Racic et al. [52], García-Diéguez et al. [63] and the intra-subject model of Chapter 3 Section 3.4.2 provide the consistent top performers occupying the first, second and third positions in most of the categories. This is demonstrated through the similar range of over and underestimation errors. All provide overestimates consistently at a 2.5Hz walking pace, with Racic et al. [52] and the intra-subject model occurring at a resonant walking frequency. However, García-Diéguez et al. [63] model overestimates the error off-resonant at 2.75Hz natural frequency.

Racic et al. [52] percent error are consistently narrower than the Chapter 3 intra-subject model Section 3.4.2 and García-Diéguez et al. [63], producing a maximum percentage error of overestimation at 40% and 35%. Whilst García-Diéguez et al. [63] has a maximum percent error of overestimation of 94% and underestimation of 89%. The intra-subject variation model of Chapter 3 Section 3.4.2 provides a maximum over and underestimation of 51% and 59%, respectively. The intra-subject model produces a median value between Racic et al. [52] and García-Diéguez et al. [63]. However, the values of the percent error correspond to different harmonics of walking. Racic et al. [52] provides the largest percentage error at consistently the exact location of the second harmonic of walking at 2.5Hz walking frequency. The intra-subject model consistently demonstrates an underestimate at 10 Hz natural frequency and 1.5 Hz walking, corresponding to the 6.67 harmonic range. However, the actual magnitude of the 1 RMS is negligible. Therefore, any perturbation is exacerbated.

Compared to García-Diéguez et al. [63] largest percentage overestimation is often seen at 9 Hz natural frequency and 2.5Hz walking. This location corresponds to a subharmonic between the 3rd and 4th harmonic, explicitly modelled in García-Diéguez et al. [63]. Therefore, systemic misrepresentations exist in all three models' ability to represent the load.

One major drawback of García-Diéguez et al. [63] is the limited harmonic representation. The model includes up to the 5th harmonic of walking, but resonant-like responses are seen far beyond this limit [17]. Racic et al. [52] and the Chapter 3 intra-subject model Section 3.4.2 represent information beyond this, with Racic et al. [52] providing information up to 100Hz and the intra-subject variation model up to 20Hz.

A caveat to Racic et al. [52], Muhammed et al. [51] and the models of Chapter 3 Section 3.4.1 and Section 3.4.2 is that the models are derived from the data used to establish the baseline. That withstanding, any model derived from the dataset of [52] could potentially overfit the data and have an inherent bias. Alternatively, due to the largest and diverse dataset, the conclusions may provide a generalised representation of real walking. Such hypotheses cannot be tested until further measurements, similar-sized datasets are made, and statistical testing is completed on the datasets. [63] produced a similar smaller dataset of treadmill walking forces and used the walking data of [52] to validate their model. The results of [63] made similar findings compared to [52] thus validating that the two datasets produce similar walking characteristics.

The next set of smallest error models are that of Muhammad et al.[51] and the inter-subject variation model of Chapter 3 Section 3.4.1. At the highest modal damping ratio of 5%, the inter-subject model of Chapter 3 Section 3.4.1 rivals the Racic et al. [52] model and bests the intra-subject counterpart, producing the joint lowest range of error and larger percentage error. Again at 2% and 1% modal damping ratio, the inter-subject Chapter 3 Section 3.4.1 model performs better than Muhammad et al.[51] in all categories. However, in the extremely low modal damping ratio scenario, Muhammad et al.[51] model provides a superior performance over the inter-subject variation model of this thesis, providing a marginally smaller range of error. Both the presented inter-subject model and Muhammad et al.[51] give the greatest overestimation at the first harmonic of walking at 2.5Hz. As evidenced in Chapter 3 Section 3.3.1, there are fewer participants walking at 2.5Hz walking frequency.

Therefore, misrepresentations of the data and poor generalisation can occur at extremely high and low walking frequencies.

The next set of models produce higher errors than that of of Muhammad et al.[51] and the inter-subject variation model of Chapter 3 Section 3.4.1, are [64] and [62]. Both provide similar values of error and percentage error for under and overestimation. However, the location of the error for [62] differs. [62] shows a constant overestimation at low walking paces in the first harmonic and high underestimations in the 4th harmonic at high walking paces. Akin to the previously discussed minimum error load models, the largest overestimation of acceleration comes at the first harmonic of walking at the extremes of walking pace for both [64] and [62] at 1.5Hz and 2.5Hz, respectively. Again, this may be attributed to a lack of data at the extremes of walking paces, a persistent issue for all reviewed load models. [62] demonstrates that the model exhibits singular errors as the location of the maximum error and percentage error align. [64] location of percentage errors varies and does not provide anyone with the unanimous location of weakness.

The remaining models are ranked in ascending order as ISO 10137 [21], CCIP Mean value [20], SCI P354 [19], Technical report 43 appendix G [28], CCIP design value [20], SETRA [55] and AISC Design Guide 11 [16] performing the worse. The last seven, and not coincidently all industry models, are all derived from the data of [45]. The industry model of ISO 10137 [21] is the most reliable, providing a low range of percentage error than some of the academic counterparts in multiple modal damping ratios. The relative error always remains higher than in every research model.

As seen in Chapter 3 Section 3.3.2.1.4, the Fourier series models derived from Kerr [45] have DLF values larger than those derived from treadmill data, thus resulting in larger overestimations of the vibration response. The largest overestimation of all industry models came at the first harmonic of walking. In the case of the AISC Design Guide 11 [16], the model produced a 119% (over double the actual acceleration) overestimation at a resonant walking and natural frequency of 2Hz with a 0.5% modal damping ratio. This error is likely a result of AISC Design Guide 11 [16] only providing a single deterministic value of each DLF, irrespective of the walking frequency. AISC Design Guide 11 [16] also provides a limited use of the model by only defining the walking frequency in the 1.6Hz to 2.2Hz. Thus, negating a proportion of the plausible walking frequencies. Furthermore, as the model only

considers four harmonics of walking, no meaningful predictions can be achieved above four times the walking frequency. Similarly, as seen in Table 4.4 baring that of [20] mean and design values, all industry models provide a limited range of walking frequency.

As anticipated, CCIP [20] design values exacerbate the over and underestimations of [20] mean value, resulting in larger ranges of errors, both percentage and relative. Using the model's 75% probability negates the true DLF relationship to walking frequency. No industry model (models from guidance and institutions, models 1-7) performed well compared to current academia-based models (models 8-13). No new VSA guidance has been released since 2007, barring the AISC Design Guide 11 [16] published in 2016. That withstanding, AISC Design Guide 11 [16] is shown to provide the lowest rank estimates concerning both the error range and percentage error. This shows a passive academic impact on the industry and a disconnect within the civil engineering community [9,23].

Of the 13 models in the low natural frequency models, five present methodologies for including the intra-subject variability and narrow-banded nature of walking [34,51,52,63] and Chapter 3 Section 3.4.2 intra-subject model. Whilst they are all high ranking concerning the mean 1s RMS acceleration, the inter-subject model of Chapter 3 Section 3.4.1 gave a narrower range of results of the mean compared to Zivanovic et al. [62], Muhammad et al. [51] and García-Diéguez et al. [52] in some instance, Table 6.1-Table 6.4. With the cases of high modal damping ratio, the inter-subject variation model of Chapter 3 Section 3.4.1 provides a close second-best model estimate with respect to minimising the error. Therefore, the necessity of providing intra-subject variation in load models versus correctly approximating the amplitude of the frequency content of walking is questioned. The inter-subject variation model of Chapter 3 Section 3.4.1 demonstrates that minimal error walking loads can be achieved without adding intra-subject variation. Current industry models present as Fourier series akin to the inter-subject variational model. However, the approximations of the industry's low-frequency models all provide unreliable and lower-ranking models. Previous researchers suggest that the intra-subject variation is a defining feature lacking in current models [23,27]. However, the largest difference seen through the models is due to the variation of the data sources, with Racic et al. [52]. García-Diéguez et al.[63] and Muhammad et al.[51] and Zivanovic et al. [62] all obtained results from treadmill data.

The largest acceleration response is dominated by the resonant response of the first harmonic, providing a larger 1s RMS acceleration response (4 times the acceleration response of any other harmonic and above 10 times for higher modal damping ratio) than that of any other harmonic. When low modal damping ratio are present, the flaws of any model are exacerbated due to the resonant build-up. Therefore, examining each model more intimately at 0.5% modal damping ratio can provide further insights into the specific local regions where models begin to break down.

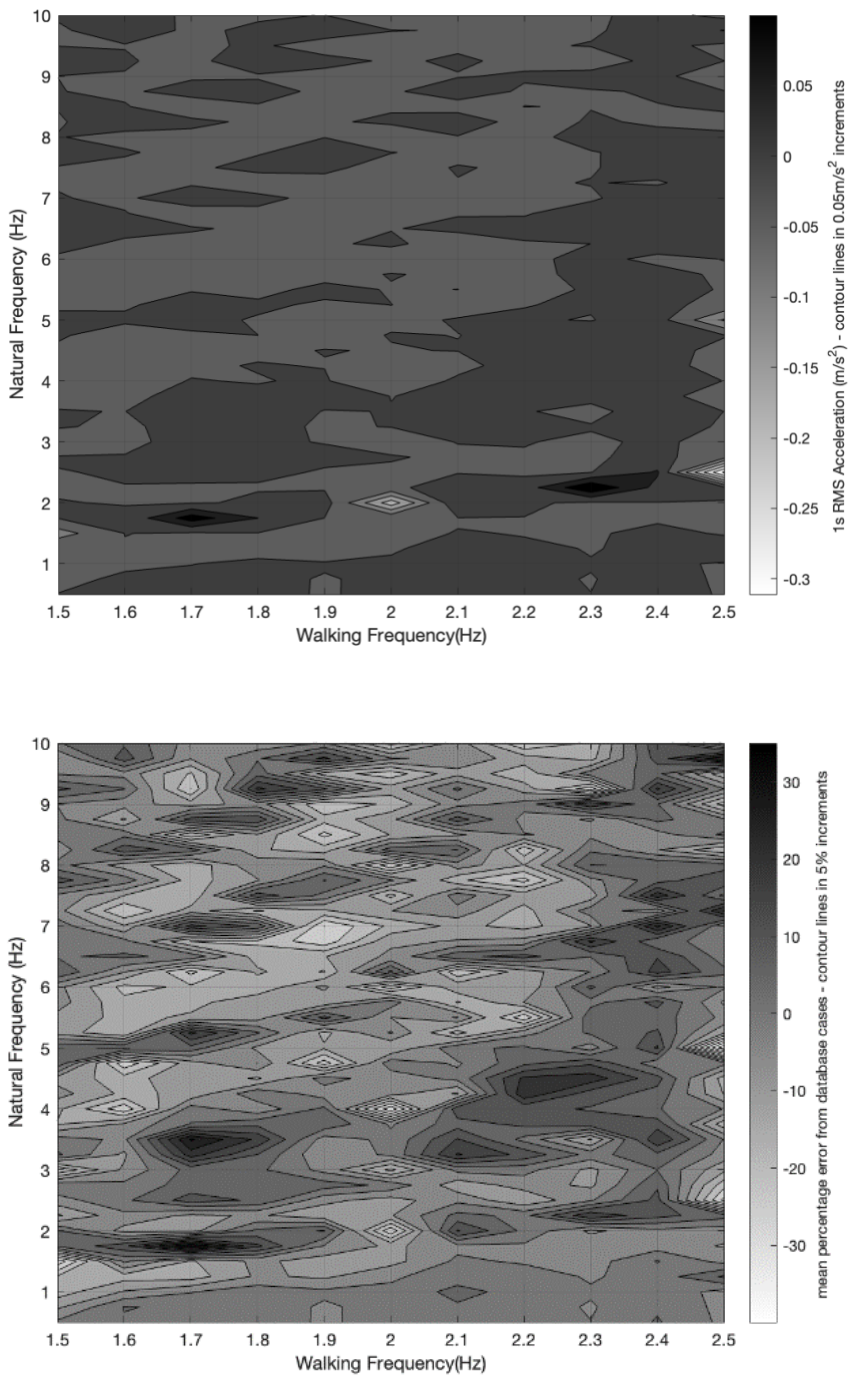

Figure 4.1: Racic et al. [52] 1s RMS acceleration response minus mean real walking at 0.5% modal damping ratio, displaying both the relative error and percentage error.

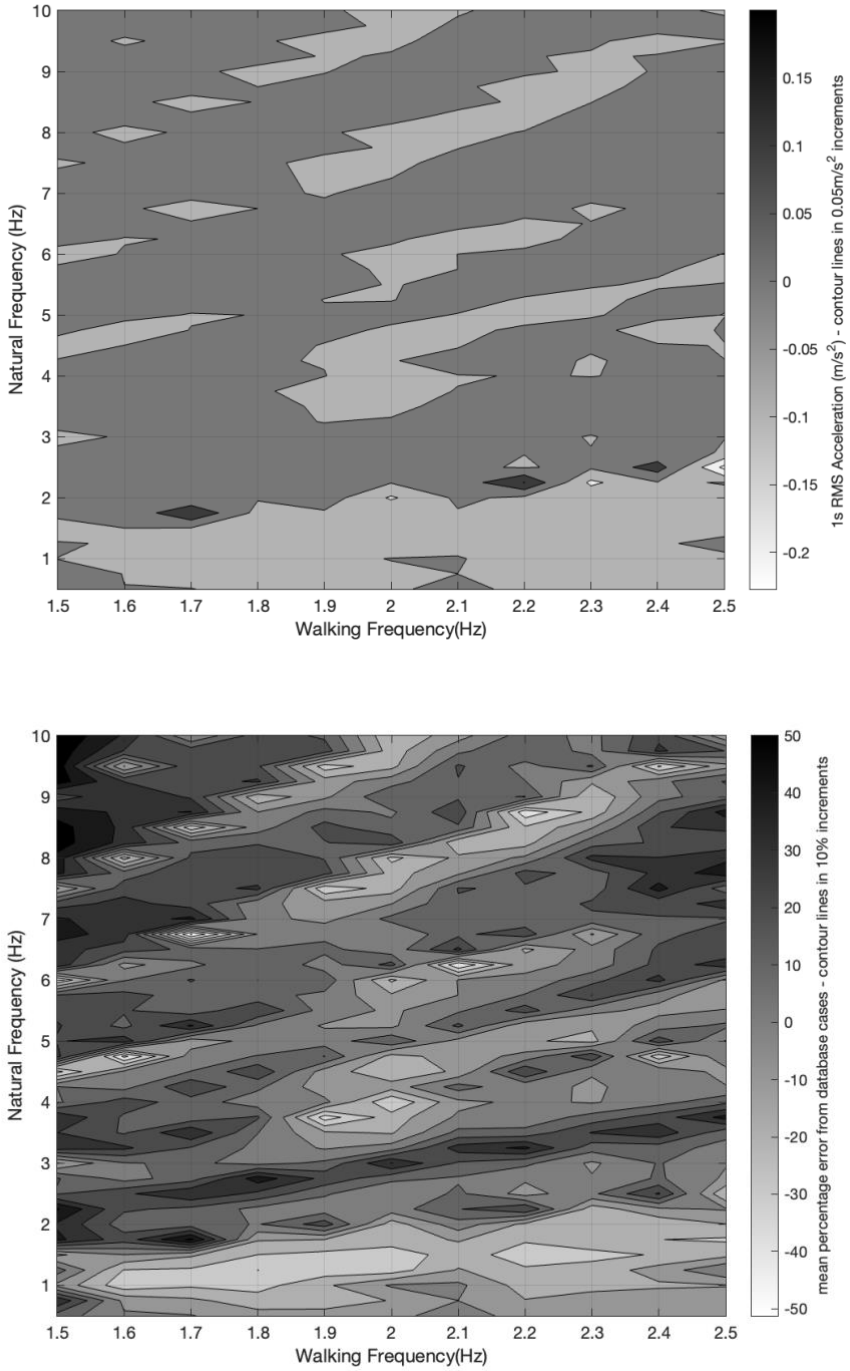

Figure 4.2: Intra-subject model of Chapter 3 Section 3.4.1 1s RMS acceleration response minus mean real walking at 0.5% modal damping ratio, displaying both the relative error and percentage error.

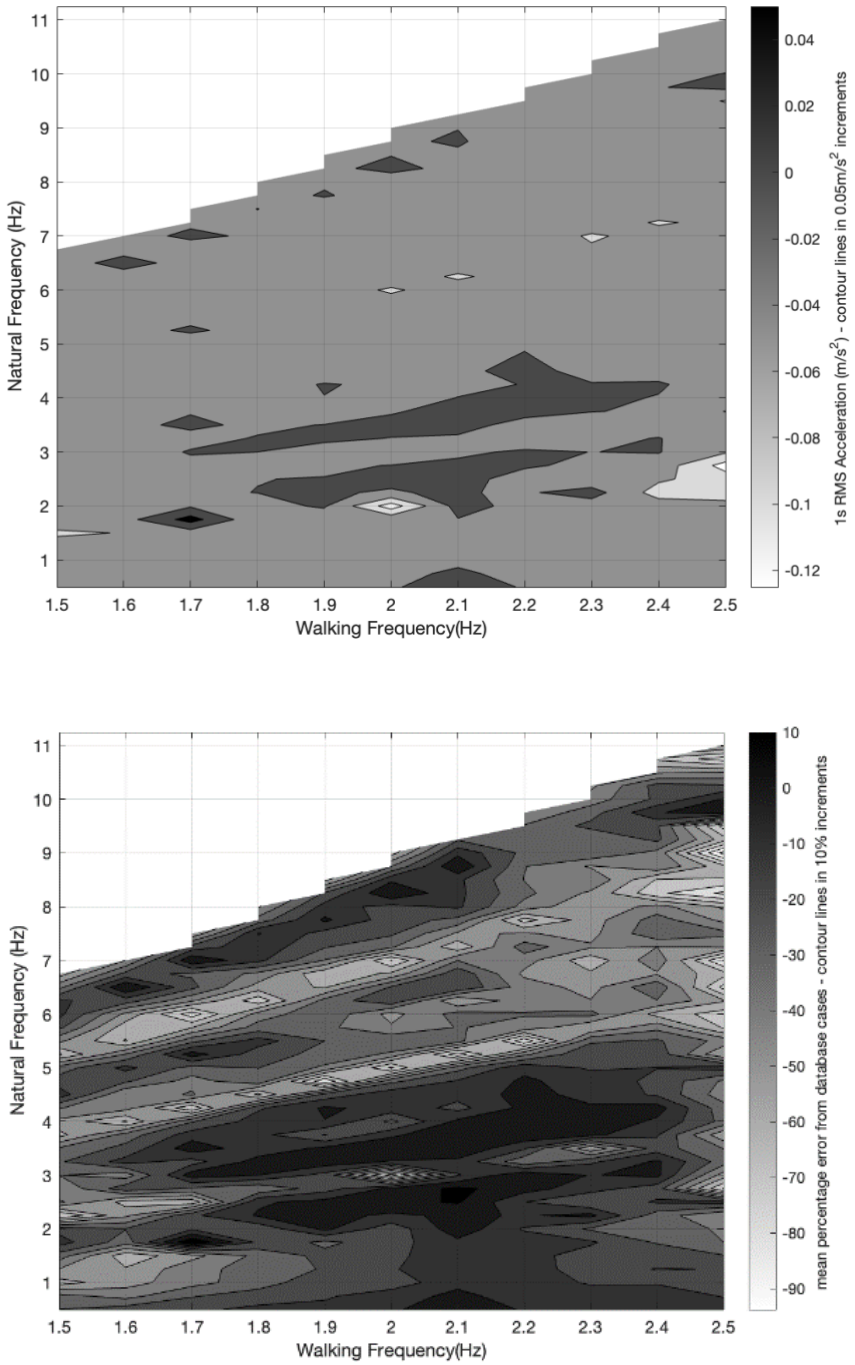

Figure 4.3: García-Diéguez et al.[63] 1s RMS acceleration response minus mean real walking at 0.5% modal damping ratio, displaying both the relative error and percentage error.

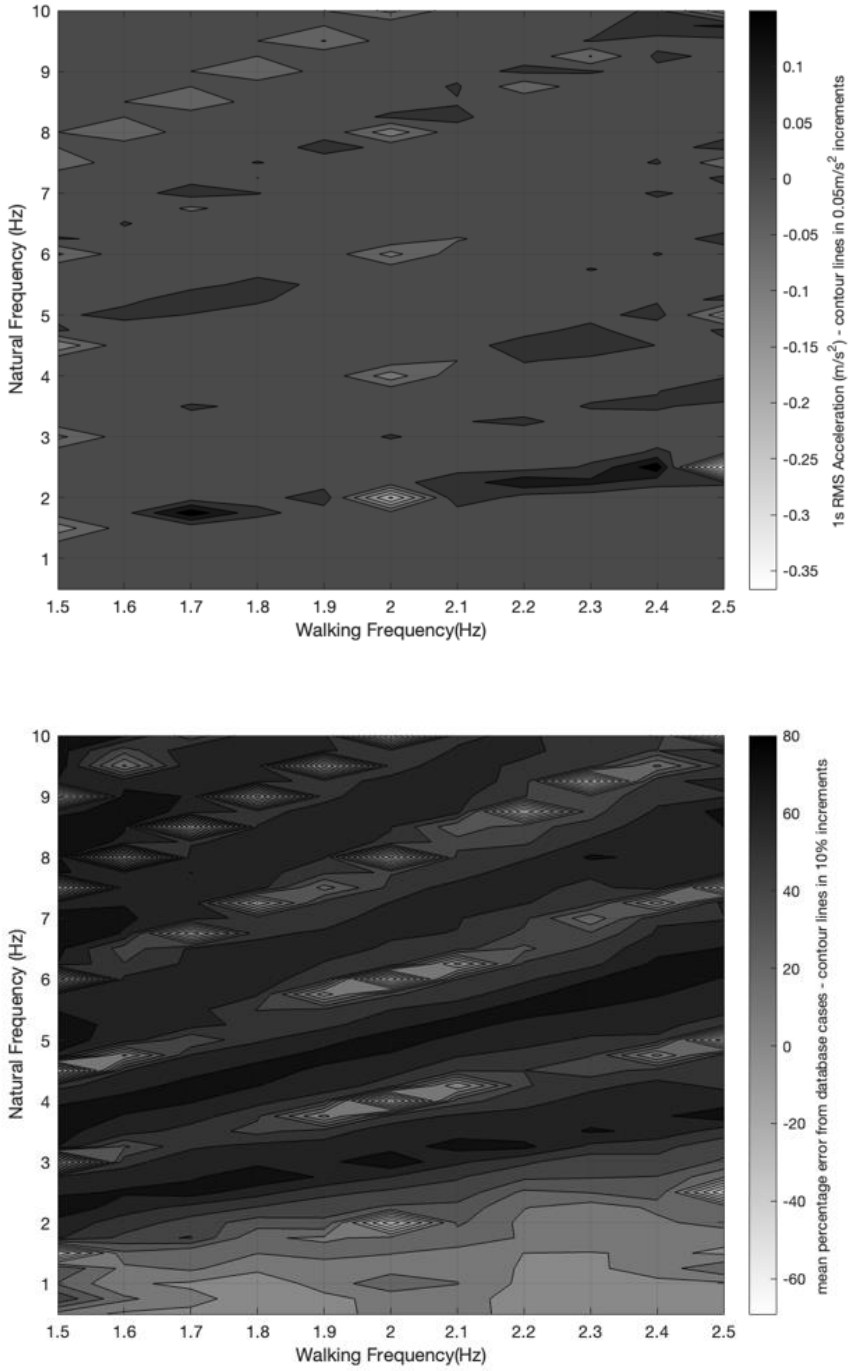

Figure 4.4: Inter-subject variation model of Chapter 3 Section 3.4.1 RMS acceleration response minus mean real walking at 0.5% modal damping ratio, displaying both the relative error and percentage error.

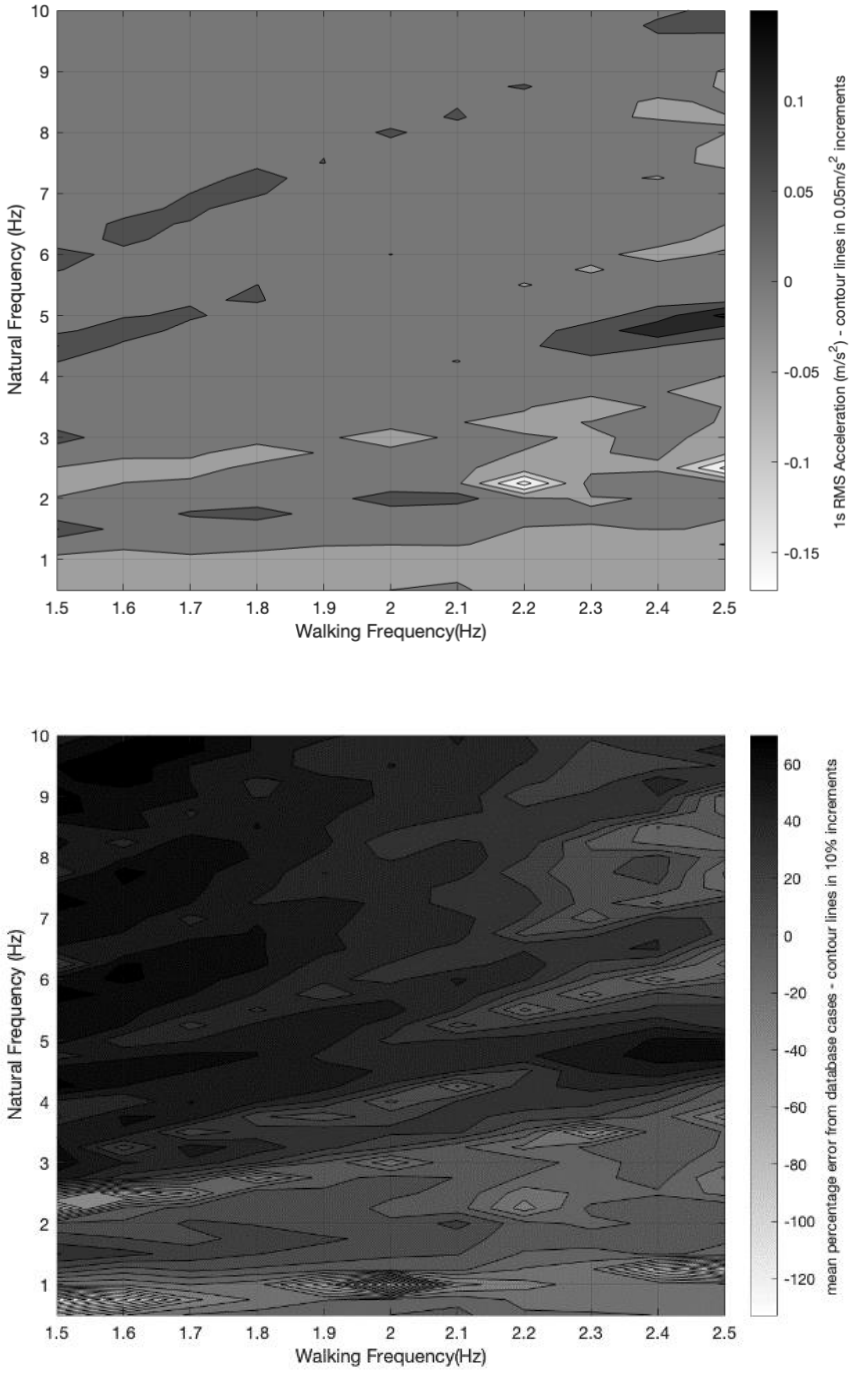

Figure 4.5: Muhammad et al.[51] 1s RMS acceleration response minus mean real walking at 0.5% modal damping ratio, displaying both the relative error and percentage error.

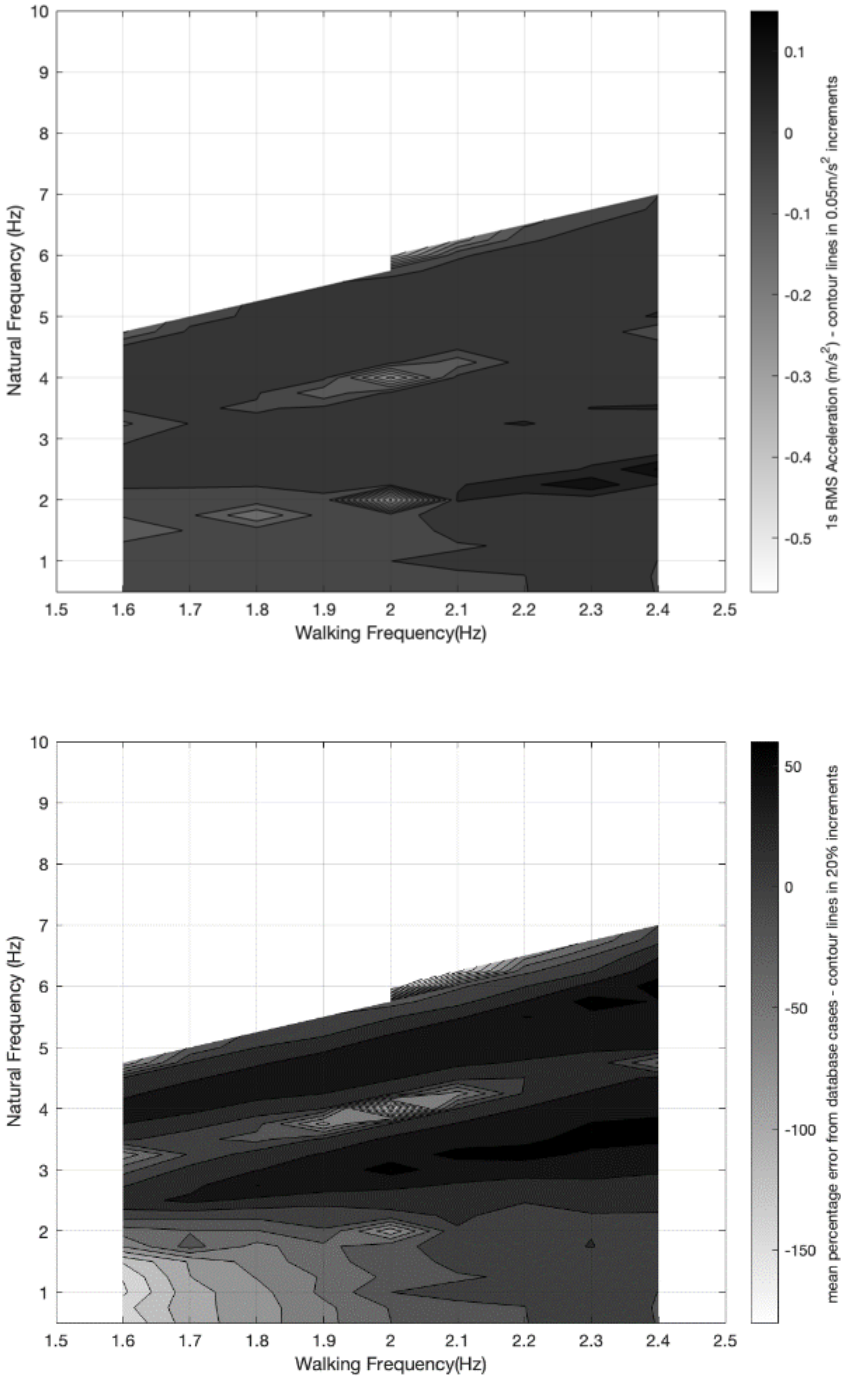

Figure 4.6:Setra [55] 1s RMS acceleration response minus mean real walking at 0.5% modal damping ratio, displaying both the relative error and percentage error

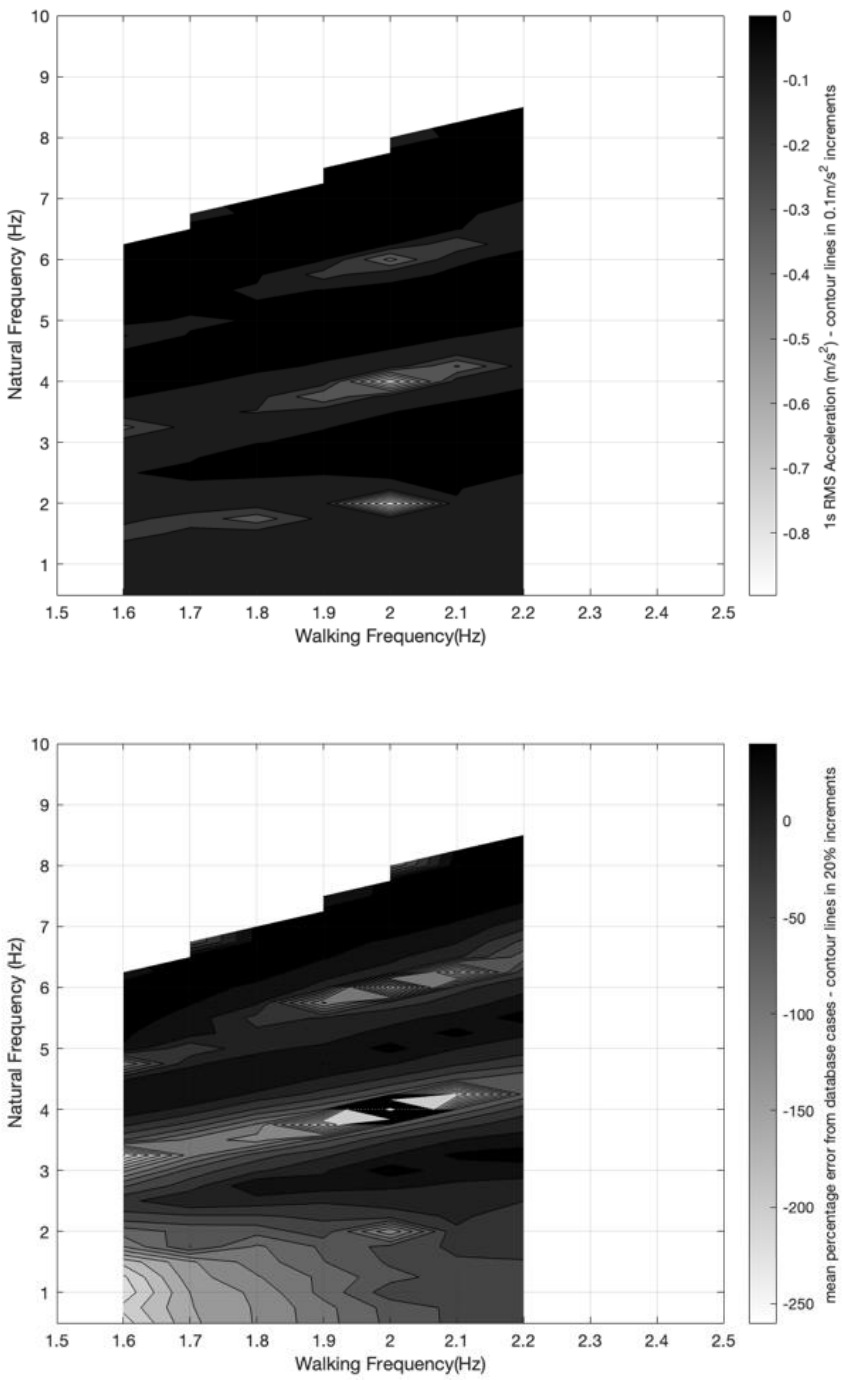

Figure 4.7: AISC DG 11 [16] 1s RMS acceleration response minus mean real walking at 0.5% modal damping ratio, displaying both the relative error and percentage error

Figure 4.1-Figure 4.7 demonstrate a selection of each model's error and percentage error. As seen with Racic and Brownjohn [52] and the intra-subject model of Chapter 3 Section 3.4.2, no distinguishing error features occur. Compared to AISC DG 11[16] and Setra [55], each harmonic of walking can be demonstrated due to the larger error and percentage error across all harmonics. Furthermore, comparing Figure 4.1-Figure 4.5 to Figure 4.6 and Figure 4.7, the lack of range some industry models possess becomes apparent. As noted in [31,62,70,71] the walking frequency is described as a normal distribution. However, the limited walking frequencies provide a narrow range not representative of real walking. Figure 4.6 and Figure 4.7 present clear instances where each harmonic provides an over and underestimation of the results, with little consistency. The major error of the two worse models is seen through the first harmonic of walking. Therefore, the models present the worst estimation and largest deviation from the results at the points where the largest DLF values occur.

The expected acceleration result for the 0.5% modal damping ratio, Figure 4.8, shows the presence of low magnitude sub-harmonics between the first and second, and second and third integer harmonic. This resonant-like response of the sub-harmonics is only visible at low levels of modal damping ratio due to the small magnitude the Fourier amplitudes sub-harmonics possess. Furthermore, the sub-harmonics are only visible at higher walking frequencies, where walking is more energetic. Limited models provide provisions accounting for sub-harmonics [43,51,52,63]. The requirement of sub-harmonics beyond the second to third integer of walking is not crucial, as the relative 1s RMS acceleration response is indistinguishable from that of the non-resonant response of integer values of walking (Figure 4.8). Sub-harmonics arise due to asymmetry in walking gait and are the most prominent for persons with a lower limb injury, poor form, or a medical condition [79,223]. Asymmetry is evident in healthy individuals, but such gait asymmetries are subtle. The necessity of explicitly modelled subharmonics is questioned when the inter-subject model of Chapter 3 Section 3.4.1 provides a better approximation in specific scenarios than models that specifically model them.

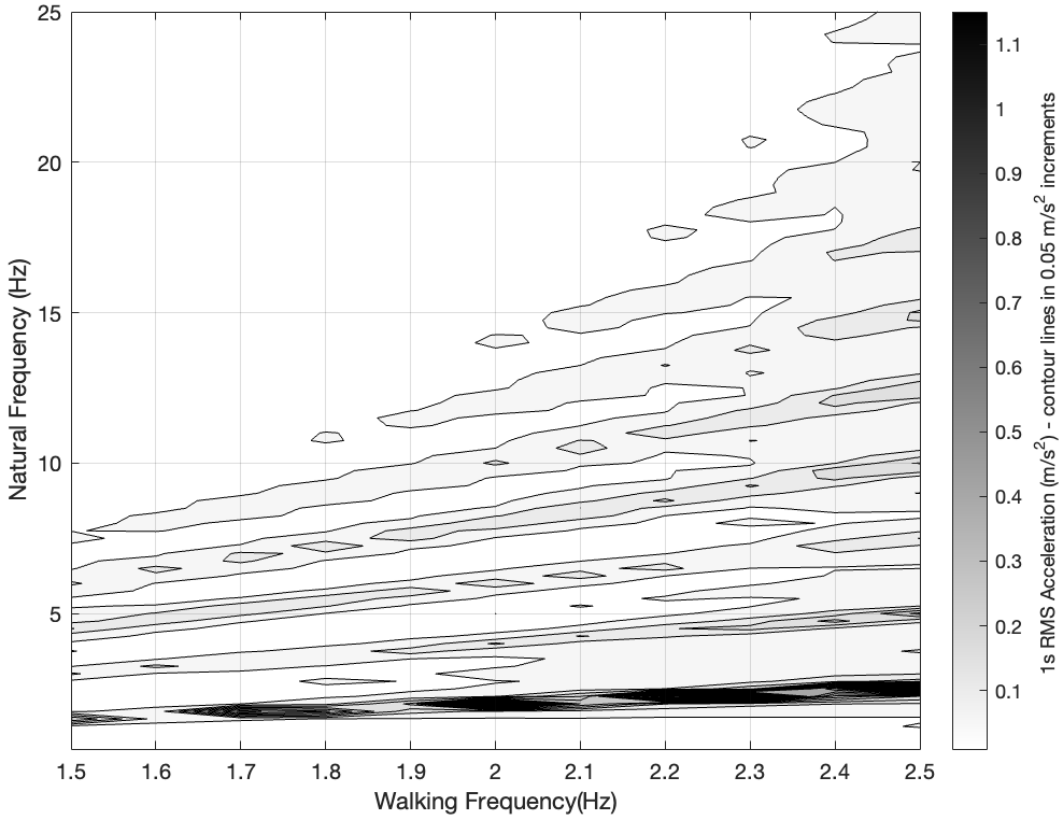

Figure 4.8: 0.5% modal damping ratio, 1s RMS mean acceleration response to real walking loads.

The mean 1s RMS acceleration response analysis shows that current industry models [16,19–21,28,55] provide a higher overestimation than the selected academic models of [52,63,64] and Chapter 3 Section 3.4.1 and Section 3.42 models whilst concurrently producing the largest underestimates too. Although the current industry models have been regularly used in practice, it is perceived that more reliable models are available in academic literature. The models of [52], [63], [51] and Chapter 3 Section 3.4.1 and Section 3.42 models are viewed as the top-performing models from the analysis of the mean 1s RMS acceleration compared to real walking for low-frequency structures. This is primarily seen through the top ranking each model achieves in Table 4.4. The best-ranked model in the industry, with respect to minimising the error, is ISO 10137[21]. However, [52], [63], [51] and Chapter 3 Section 3.4.1 and Section 3.42 models provide smaller errors in all scenarios. In the case of 0.5% modal damping ratio the best-ranked model, with respect to minimising the error of acceleration, of [52], [63], [51] and Chapter 3 Section 3.4.1 and Section 3.42 provide errors more than half that of the industrial load model best of ISO 10137[21].

4.2.2 Mean 1s RMS acceleration for high-frequency models

Table 6.5 to Table 6.8 of Appendix B compare the high-frequency content of load models compared to the database walking loads. The lower limit of each synthetic model is given in Table 4.2 with an upper limit of 20Hz due to the infrequency of typical fundamental structural modes being above the limit. The models under consideration for the high-frequency content are: AISC Design Guide 11 [16], CCIP mean and Design [20], SCI P354 [19], inter- and intra-subject models of Chapter 3 Section 3.4.1 and Section 3.42, Racic et al. [52] and Muhammad et al. [51], whilst Technical Report 43[28] provides a high-frequency load model it is identical to that of CCIP.

Table 4.5: Summary ranking of high-frequency models based on the minimum range of relative error and percentage error for each modal damping ratio scenario.

		Maximum relative error				Maximum percentage error			
Model number	Load model	0.50%	1%	2%	5%	0.50%	1%	2%	5%
1	AISC Design Guide 11 [16]	7	2	7	4	6	6	6	6
4	CCIP Mean value [20]	6	1	8	6	5	5	5	5
5	CCIP design value [20]	5	3	5	7	3	7	7	7
6	SCI P354 [19]	1	8	5	8	8	8	8	8
8a	Chapter 3 inter-subject Section 3.4.1	8	7	3	3	7	4	4	4
8b	Chapter 3 inter-subject plus	3	5	2	2	4	3	3	3

	walking frequency and DLF intra-subject Section 3.4.2								
11	Racic et al.[52]	2	4	1	1	1	1	1	1
12	Muhammad et al. [51]	4	6	4	4	2	2	2	2

Table 4.5 provides an approximate ranking of the high-frequency load models concerning each modal damping ratio scenario for the relative and percentage error, with the full information given in Appendix C. At low levels of modal damping ratio, the industrial models provide the lowest error representation of high-frequency walking load response concerning the relative error. However, the percentage difference is larger and increases in magnitude with increased modal damping ratio compared to academic models that regress and provide smaller ranges of error and percentage error.

Racic et al. [52] provides the most accurate model concerning the lowest error of magnitude and percentage error and is further evidenced in

Table 4.5 with a consistent top ranking, demonstrating a maximum percentage error of overestimate of 23% and an underestimation of 34%. However, as seen in Figure 4.9-Figure 4.11 the magnitude of accelerations in the high-frequency range (i.e. 10 -20Hz for Racic et al.[52]) is small, compared to the first harmonic of walking. Therefore, any change can result in a larger percentage change, as seen in the industry models. Racic et al. [52] performs the best, with respect to minimising the error of acceleration, in the high-frequency range. However, the location of over and underestimate of error and percentage error remain consistent concerning different modal damping ratio. Thus, this indicates the model is misrepresented in these ranges. The overestimated positions are at a natural frequency of 10Hz and a walking pace of either 2 or 2.2Hz. Therefore, the 5th integer of walking and the subharmonic between the 4th and 5th harmonic presents an uncharacteristically higher value,

with the largest underestimate seen at 12.25Hz natural frequency and 2.5Hz walking frequency corresponding again to the fifth harmonic of walking. The largest percentage error underestimations are consistently evident at 19.75Hz natural frequency and 2.4Hz walking frequency. However, this is at the 8.23 harmonic. As such, there is no clear indication if this arises due to some low-lying subharmonic or another characteristic feature of walking that is not present in models.

The second-best model, with respect to minimising the error of acceleration, oscillates between the intra-subject model of Chapter 3 Section 3.4.2, Muhammad et al.[24] and that of the inter-subject variation model of Chapter 3 Section 3.4.1, as evidenced by

Table 4.5 with consecutive high rankings concerning relative and percentage error. At higher modal damping ratio, both models of Chapter 3 provide the superior estimation, with a narrower range of error and comparatively similar percentage error difference. In the case of 5% modal damping ratio, both Muhammed et al. [51] and the inter-subject model provide only an underestimate and no overestimate. In the 2% modal damping ratio case, Muhammad et al. [51] provides only an underestimation with a range larger in magnitude and percentage than both models of Chapter 3. However, the range of the error magnitude is smaller for the intra-subject model. Like Racic et al. [52], both Muhammad et al. [51] and both models of Chapter 3, over and underestimations appear in the same positions of natural frequency and walking frequency across all modal damping ratio, again suggesting natural limits of the model's predictive abilities.

Both models in Chapter 3 consistently overestimate the 10.75-11.5Hz natural frequency at 2.2Hz and 2.3Hz walking. Therefore, the expected value of walking at the 5th harmonic at both 2.2Hz and 2.3Hz is larger than real walking consistently. This can be attributed to the modelling technique used by the Chapter 3 models. Consistent underestimations are again evident on the 5th harmonic of walking at 2.5Hz walking. As seen in Chapter 3 Section 3.2.2 , very little data is available at 2.5Hz. Therefore, the information can be easily malformed from the true value. Muhammad et al. [51] provides the greatest error at the subharmonic between the 12th and 13th harmonic. As the error is of smaller magnitude, compared to the first harmonic of walking, and percentage error at 6% and 12%, respectively, it is deemed unimportant. Like the models of Chapter 3, Muhammad et al. [51]. the fifth harmonic of walking at 2.5Hz also provides an underestimation point. Both models use the same dataset to

produce their respective models. Hence it appears to be a systematic misrepresentation of the data resulting in consistent underestimations.

From

Table 4.5, the current industry load models used for high-frequency structures, AISC DG 11[16], CCIP[20], Technical report 43 Appendix G[28] and SCI P354[19] provide a mixture of results. The models offer a close estimate of real walking at low modal damping ratio. However, the percentage error of each model is consistently in the lower half and bottom of the rankings. Similar conclusions from the data derived from [45] are made in the high-frequency range, as highlighted in the low-frequency range. All the industry models exhibit underestimation at the 4th harmonic integer of walking at 2.5Hz. As seen with the low-frequency content in Appendix A Table 6.1 to Table 6.4 of Appendix A provide the analysis for the low-frequency model of the vertical walking signals. The relative error is defined herein as the 1s RMS acceleration output of real walking on the structure minus the output of the synthetic walking loads. The percentage error is the relative error divided by the real walking forces times 100. Positive results indicate an underestimation, and negative results indicate an overestimation of the synthetic loads. Where models comprise of high and low-frequency functions, each is used up to its associated limit (Table 4.2). In the cases of Racic and Brownjohn [52], Muhammad and Reynolds [51] and Chapter 3 Section 3.41 and Section 3.4.2 models, the models present information up to and surpassing the upper limit of the highest natural frequency (20Hz). Therefore, the models are artificially split into low and high-frequency constitutive parts for comparison. The cut-off frequency is artificially chosen as 10Hz, thus ensuring the models can be independently assessed for their low and high-frequency load models compared to similar walking models.Table 4.4 of the same models, the extreme walking pace of 2.5Hz produces erroneous results that are both under and overestimated. The largest percentage errors of the industry models are demonstrated at the extremes of the walking pace, either 1.5Hz or 2.5Hz. Therefore, the data collected from [45], combined with the modelling methodologies adopted in industry, provide statistically different characteristics than the results of the treadmill database at these extremes.

Current industry high-frequency load models are ranked low in

Table 4.5, utilising the impulse method of vertical walking loads. However, Fourier series models, such as that of the inter-subject model of Chapter 3 Section 3.4.1, demonstrate that the method of a Fourier series reconstruction at harmonic integers can provide a reliable level of structural acceleration at higher natural frequencies compared to real walking signals. This statement is further backed by Figure 4.9-Figure 4.11 demonstrating clear resonant responses at integer values of the walking frequency. If an impulse-like response was seen, the maximum acceleration response should be virtually identical for the same natural frequency across all walking frequencies.

Comparing the 1s RMS response of real walking (Figure 4.11) to AISC DG 11[16] at 0.5% modal damping ratio (Figure 4.12), the underlying assumption of non-resonant response above the cut-off frequency does not hold. The resonant-like response is evident along multiple integer values of walking frequencies. As all industrial models use the impulse model to respond, the only variation arises from the coefficient A, given in Chapter 2 Section 2.1.5. The impulse formulation does not provide provisions for a resonant response. The last division of load models based on natural frequency is inconsistent in both the high and low-frequency ranges. Whilst [52] produces the most reliable high-frequency structures response, current industry load models provide a varying degree of reliability estimation across differing modal damping ratio and natural frequencies. More consistent responses are seen from the models of [52] closely followed jointly by [51] and Chapter 3 models. All four models in [52], [51] and Chapter 3 models provide lower ranges of error and percentage error compared to industry models. In a limited number of scenarios, the industry models of [20] mean value and [19] provide superior responses concerning the error. However, they then provide the worst estimation of the models in other scenarios. Thus, using the industry model in the high-frequency range can result in an unreliable prediction.

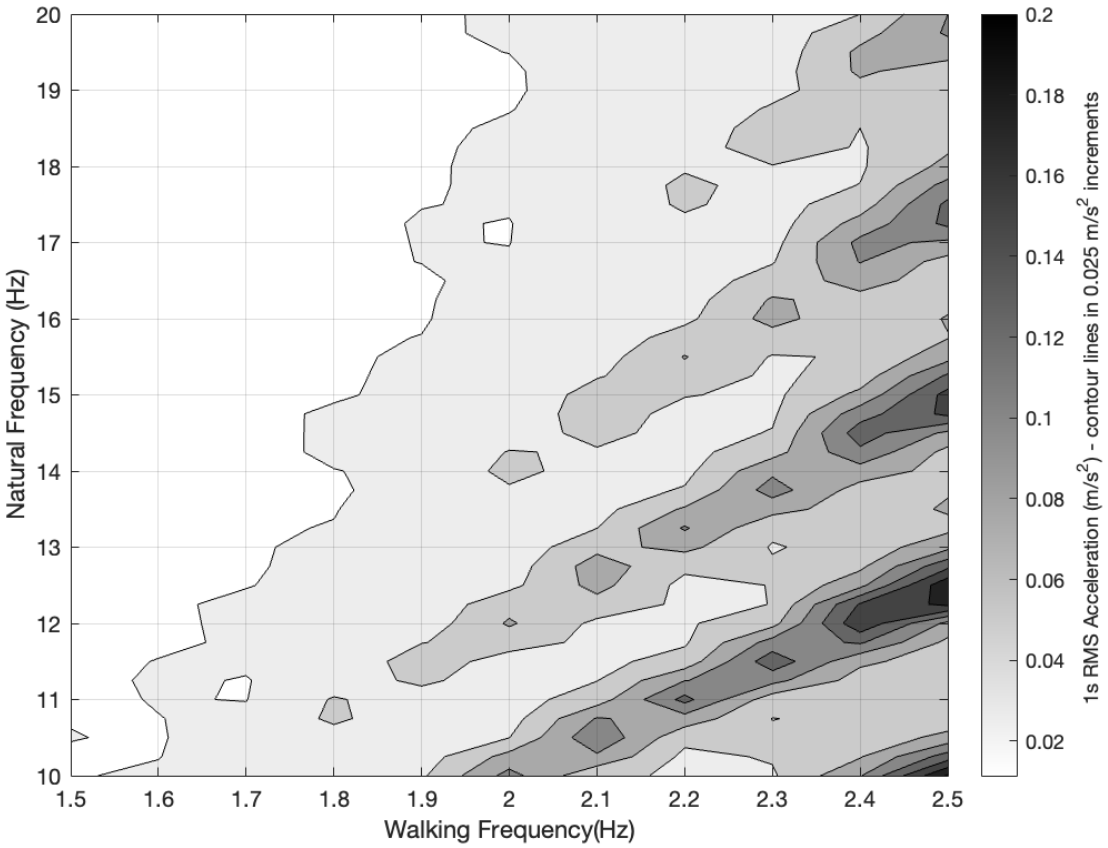

Figure 4.9: 1s RMS acceleration of high-frequency structures subjected to real walking loads at 0.5% modal damping ratio.

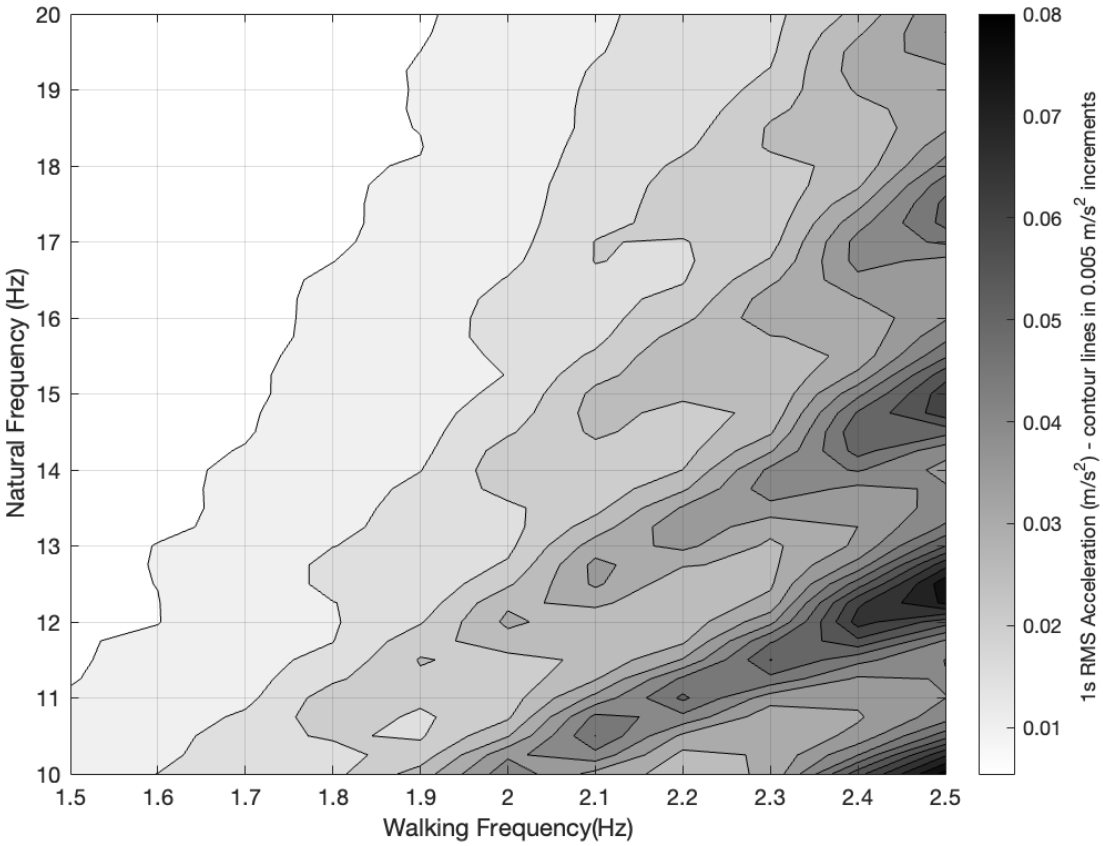

Figure 4.10: 1s RMS acceleration of high-frequency structures subjected to real walking loads at 2% modal damping ratio.

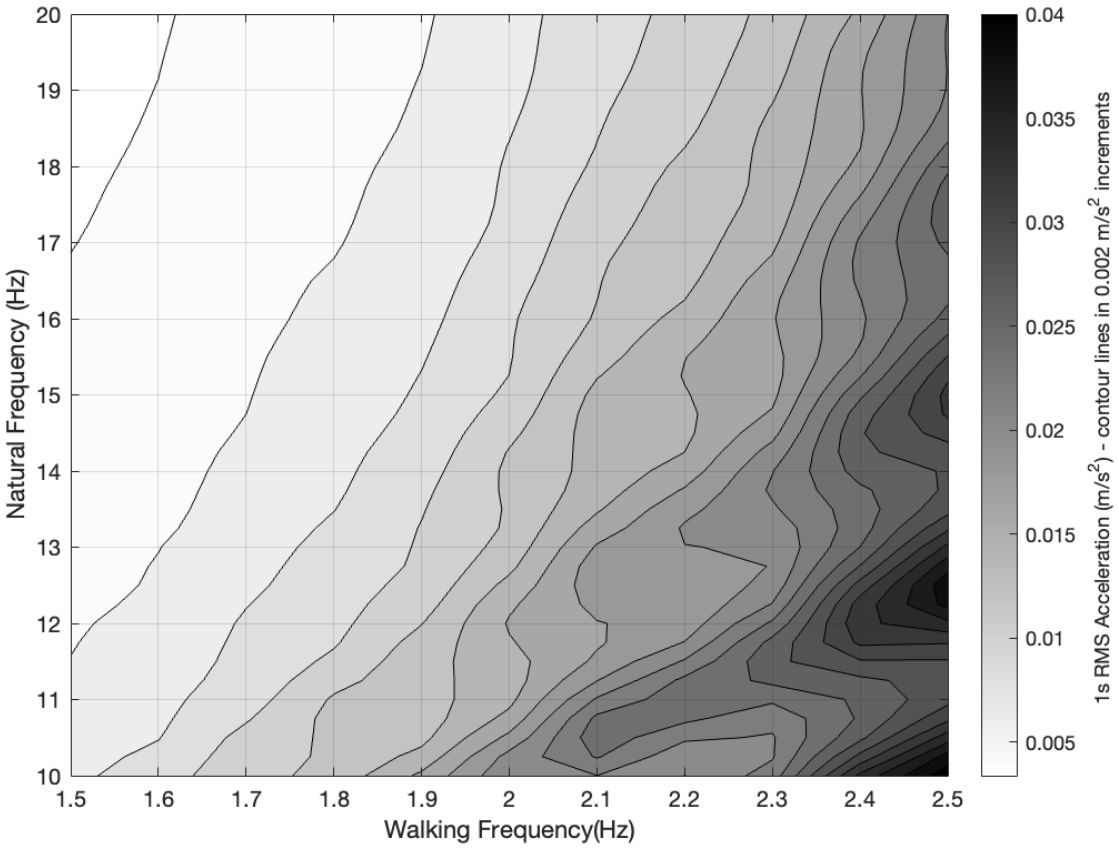

Figure 4.11: 1s RMS acceleration of high-frequency structures subjected to real walking loads at 5% modal damping ratio.

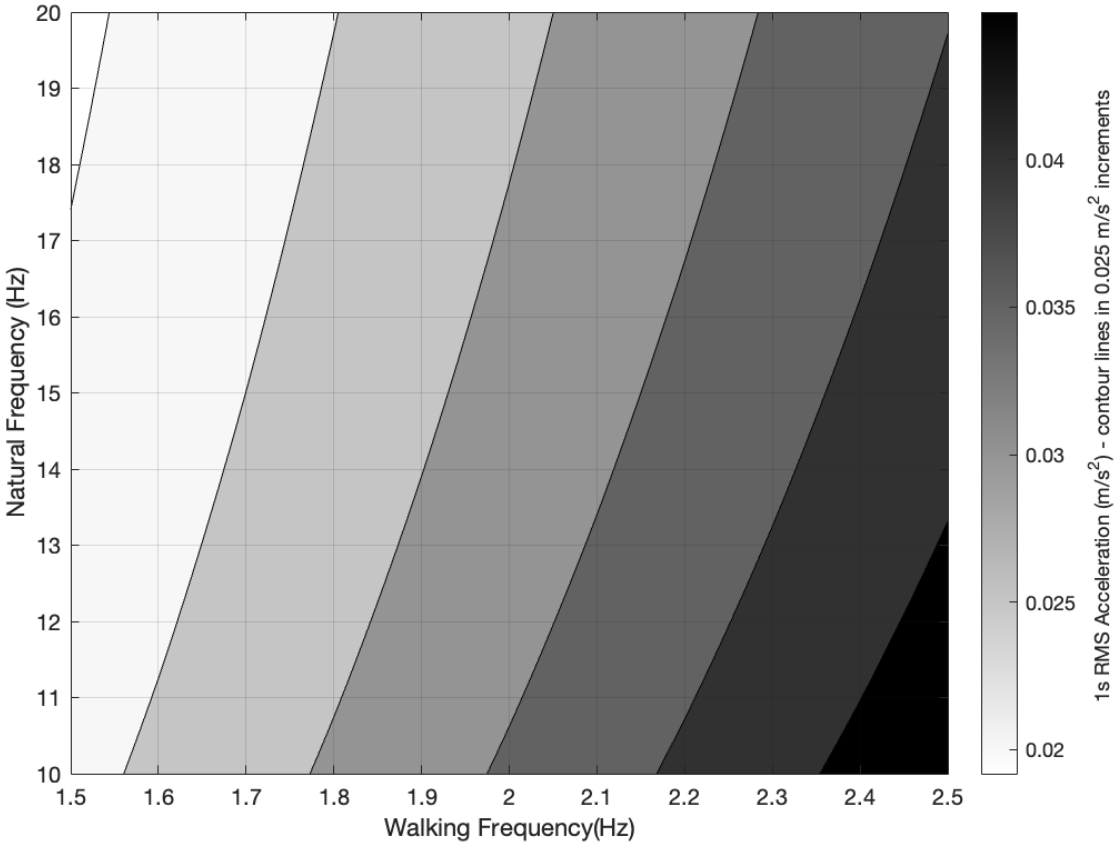

Figure 4.12: 1s RMS acceleration of high-frequency structures subjected to AISC DG 11 [16] loads at 5% modal damping ratio.

4.3 The variance of acceleration response

For models with a stochastic nature, each synthetic walking load is sampled 100 times at each walking frequency. This methodology is used to demonstrate the variability of the model's output. Table 6.9 presents the maximum and minimum error of variance, percentage error, and associated locations of the errors. The following models provide a deterministic force representation. They thus cannot be assessed for their variance: CCIP Mean and design value [20], AISC Design Guide 11 [16], ISO 10137 [21], SCI P354 [19] and SETRA [55] and Verela [64]. Due to the few models that provide a range of results, the high and low-frequency models are considered together. The models are used in their associated limits concerning walking frequencies and walking integer values.

Table 4.6: Summary ranking of the variance of each appropriate model based on the minimum range of relative error and percentage error for each modal damping ratio scenario.

		Maximum relative error				Maximum percentage error			
Model number	Load model	0.50 %	1%	2 %	5 %	0.50 %	1 %	2%	5 %
3	Technical report 43 appendix G [28]	5	1	1	4	1	1	1	1
8a	Chapter 3 inter-subject Section 3.4.1	7	4	5	5	3	5	4	5
8b	Chapter 3 inter-subject plus walking frequency and DLF intra-subject Section 3.4.1	5	7	7	7	5	4	2	3
9	Zivanovic et al. [62]	3	5	3	5	4	3	5	6
10	García-Diéguez et al. [63]	2	3	5	2	7	7	7	7
11	Racic et al. [52]	4	6	2	2	2	2	3	2
12	Muhammad et al.[51]	1	2	3	1	6	6	6	4

Table 4.6 provides a summative ranking of each appropriate model based on the maximum error range and percentage error. Technical report 43 appendix G [28] consistently ranks the top performer for the smallest range of error and percentage error, with Racic et al. [52] providing a consistent second-best performer, with respect to minimising the error of acceleration. Whilst García-Diéguez et al. [63] and Muhammad et al.[51] often provide top-ranking relative error estimates, they consistently produce the worst percentage errors. This disparity in error is attributed to the low value of the 1s RMS acceleration. Therefore, any small variance in error results in a percentage difference.

All models that can describe the variance of the load produce a small error compared to the mean error and percentage error of the respective models. The larger percentage errors are due to the small scale of the acceleration measurements, causing a larger percentage error, compared to the first harmonic of walking. It is difficult to distinguish one better model, as the range of over and underestimating the variance and percentage errors constantly changes with different modal damping ratio values. Contrary to the low ranking mean 1s RMS acceleration response of technical report 43 appendix G [28], it provides a superior variance approximation of the 1s RMS acceleration. Thus, the model offers a precise cluster of estimates but misplaced measurements of the 1s RMS acceleration compared to the acceleration response of the real loads. The reduction in error of [28] is principally demonstrated through using a larger and more diverse dataset, over the current singular or double footfalls on force plates used to model the DLF values.

Figure 4.13-Figure 4.16 illustrates the variance of 1s RMS acceleration becoming negligible with increased modal damping ratio, resulting in the variance only becoming prominent in the first integer of walking. The 5% modal damping ratio case's maximum variance is 2% of the maximum mean value. The variance of the load becomes insignificant and provides minimal variation in acceleration output. Comparatively, the 0.5% modal damping ratio produces a variance of 9% of the mean 1s RMS acceleration. Therefore, the variance of the load models becomes significant in low- modal damping ratio scenarios. That withstanding, all models

that provide statistical description adequately model the variance of walking loads. The variance of the 1s RMS acceleration is a critical component of the VSA that is currently overlooked in guidance. Current guidance only pertains to the average human scenario and a structure's mean response; however, incorporating the variance can allow additional information to be founded and provide a fully statistical approach to the VSA.

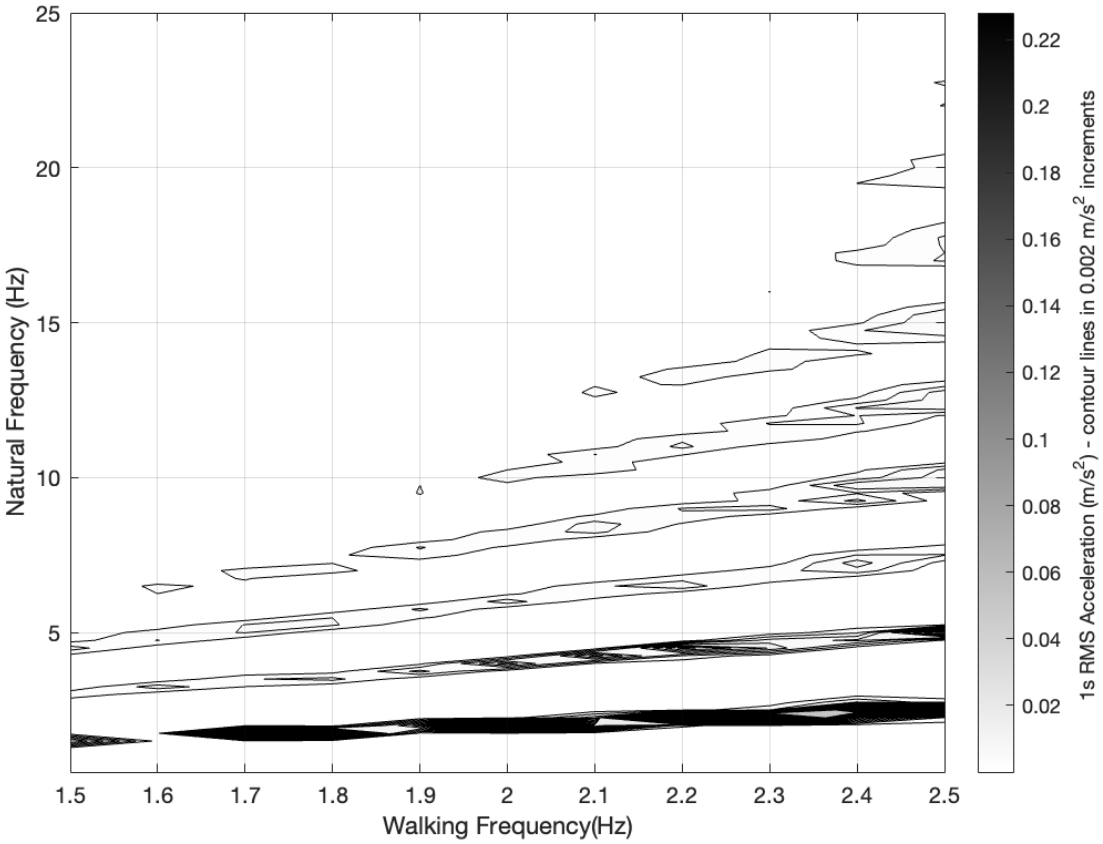

Figure 4.13: 1s RMS acceleration variance of real walking load at 0.5% modal damping ratio.

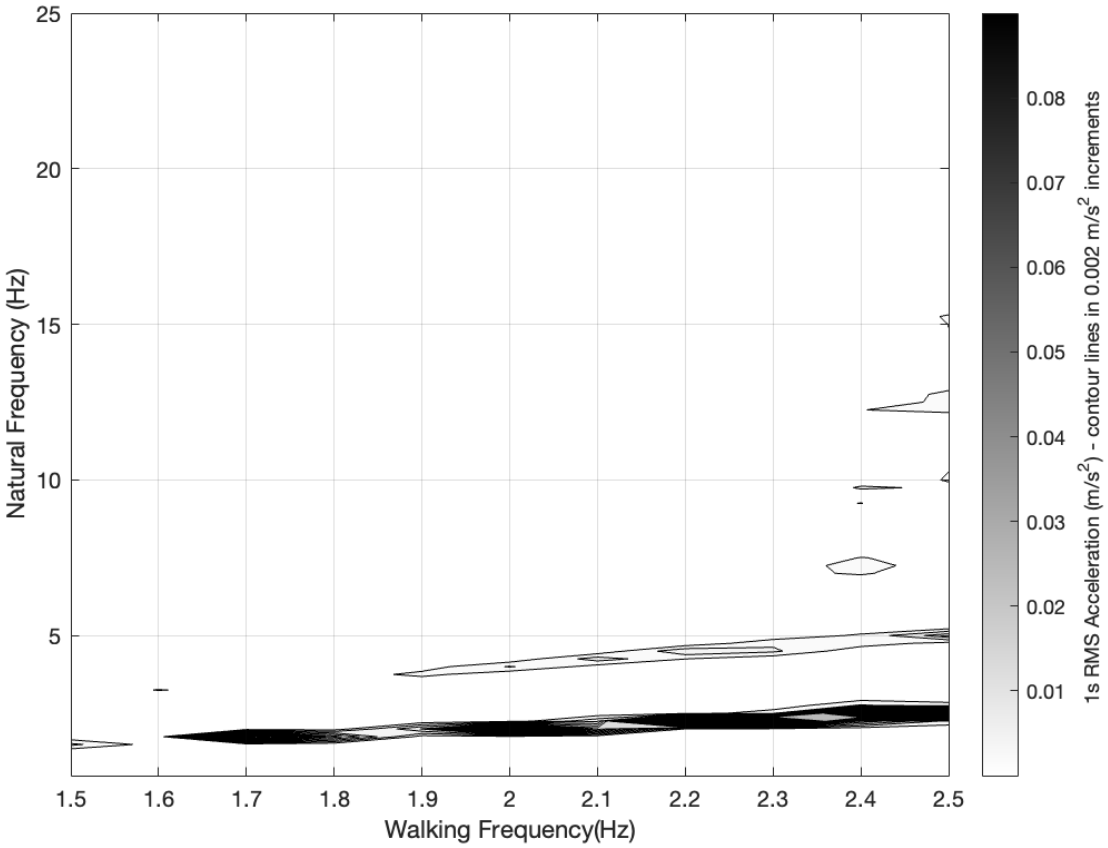

Figure 4.14: 1s RMS acceleration variance of real walking load at 1% modal damping ratio.

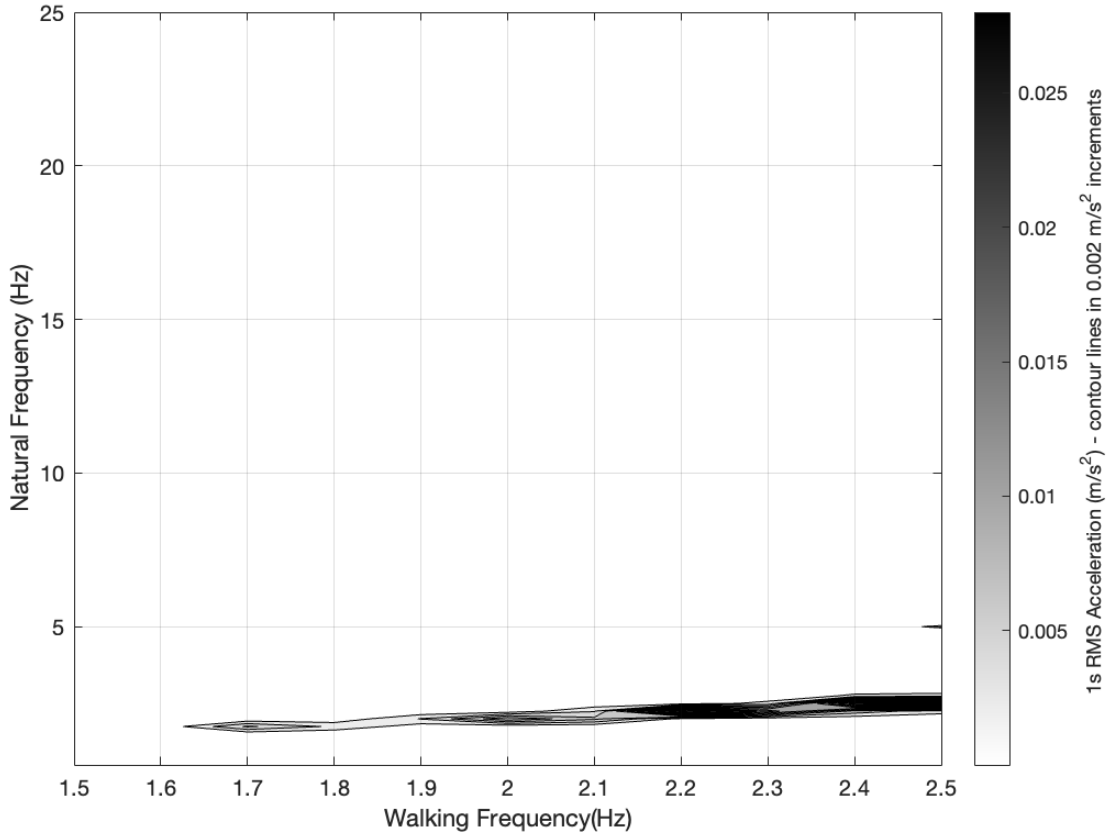

Figure 4.15: 1s RMS acceleration variance of real walking load at 2% modal damping ratio.

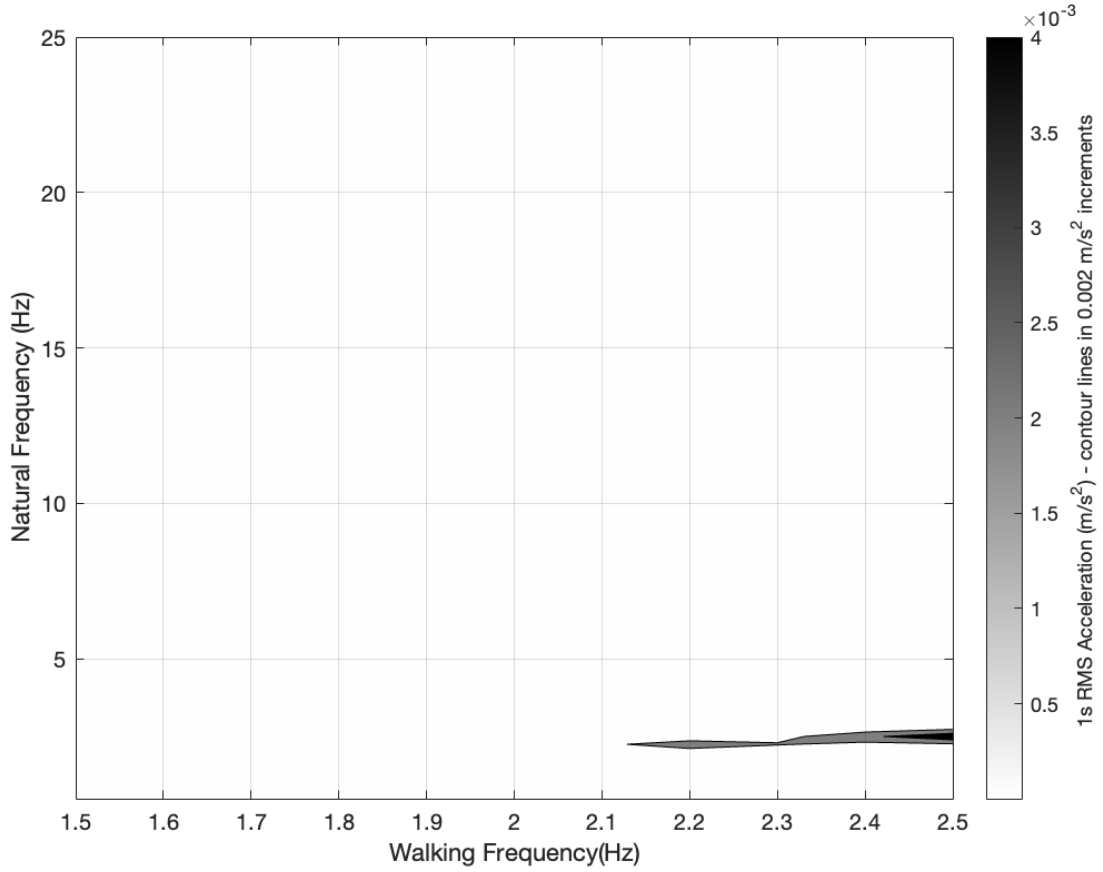

Figure 4.16: 1s RMS acceleration variance of real walking load at 5% modal damping ratio.

4.4 Discussion

The bedrock of industry models is based on the data of Kerr [45], which was deemed state-of-the-art in 1998. The methodology of expanding the single footfall force time history temporally negates any intra-subject variability. This results in an unnatural frequency domain representation compared to the treadmill data of [52] and [63]. Models 1-7 (Table 4.4) are founded from this data, and all the above models produce inconsistent results. This result is further seen in Sections 4.2.1 and 4.2.2 when all models derived from Kerr [45] provide the largest error ranges in different scenarios. Chapter 3 Section 3.3.2.1.4

demonstrates that this result is due to the increased and inconsistent DLF values from Kerr [45] compared to such data used by biomechanics researchers from as early as 1982 [48–50]. Therefore, more advanced data should have circulated within civil engineering publications before [45].

Technical report 43 appendix G [28], CCIP Mean value [20], AISC Design Guide 11 [16], ISO 10137[21], SCI P354 [19] and SETRA [55] all propose deterministic phase angles for each harmonic of the Fourier series integers. However, [43,52] propose that phase angles exist over a uniform distribution [-π, π] and are uncorrelated. The analysis in Chapter 3 Section 3.3.4 further backs this. The deterministic nature of phase angle is a direct result of previously available data [45]. Whilst phase angles do not provide any additional information in singular dominate modes of vibration when a structure has a multi-modal response to a load or multiple simultaneous walking loads, the relative phase angles can cause an increase or decrease in the acceleration magnitude.

Both models of Chapter 3, technical report 43 appendix G [28], Zivanovic et al. [62] provide probabilistic ranges for DLFs. However, due to the nature of normal distributions, the value of DLF can be negative. The negative values exist due to the variance seen in DLF values concerning the walking frequencies and low mean DLF values at higher harmonics. Negative DLF values are not seen in practice and limit how physical systems are modelled empirically. The heteroskedastic nature of the DLF results in the data variance having flawed assumptions. The largest variance is evident in higher walking frequencies; however, the error distribution will be underestimated at this location and overestimated at low walking frequencies where a smaller variance is evident.

Velocity input-based models such as García-Diéguez et al. [63] and Muhammad et al. [51] do not precisely match the walking frequency used to categorise the various input frequencies as the walking velocity is sampled. Current methods only dictate the linear mapping of walking frequency to velocity. As each band of walking frequencies covers a 0.1Hz range, various walking frequencies and force magnitudes can occur due to the rounding of imprecise

walking frequencies. This inexact matching may result in errors that bias results. Similarly, as the walking data used for the baseline cases are subject to the same categorisation, errors may exist due to a coarse range of walking frequencies within each bandwidth. A smaller bandwidth of walking frequency is required to produce more precise estimations. However, if the baseline data were categorised into 0.05Hz bandwidth instead of 0.1Hz, the resulting distribution of force time histories would result in some categories only containing one force time history.

4.5 Conclusions

Sections 4.2.1 and 4.2.2 show that current in-use industry models do not adequately represent the vertical walking loads of the database case. Whilst deviations are expected due to differences in population, such poor estimates are likely attributed to different walking representations. It is acknowledged that the dataset used is the largest of its kind, but is only a population subsection and may have inherent imperfections associated with the database. Such a statement could not be validated until a similar size dataset was acquired.

The lack of variance in the response is concerning as designers falsely understand that a structure has a single output to walking when an entire range is possible due to variations in the loads and/or weight of pedestrians. Whilst all models are evaluated to provide a range of over and underestimation, the current in-use industry models offer the largest range of error and percentage error. Thus, current structures will have been overdesigned to accommodate this poor correlation with real walking. As demonstrated for low-frequency structures in

Table 6.1-Table 6.4 along the first harmonic integer of walking, the largest overestimates of 1s RMS acceleration can be seen for industry models. Therefore, misclassification of the VSA will have historically occurred, resulting in the unnecessary design of stiffer or heavier structures. Furthermore, current industry-used models present themselves in a limited fashion of walking frequencies.

Whilst it was demonstrated that academic models produce more consistent and reliable results, no academic model is currently used in industry to the author's knowledge. [52] provides a favourite for the best overall model concerning high and low-frequency content, with respect to minimising the error of acceleration, supported by the result of section 4.2. However, the application and uptake of the model are lagging, as the article was published over 10 years ago. A similar point is made for [62] having published the model five years earlier than [52]. Therefore, a disconnect lies between research and industry. The dissemination of knowledge to the industry is lacking, and practising engineers are using old and outdated information. More research must be engaged via industry and professional institutes to provide updated guidance on research best practices. A gap in the market arises for new guidance to be published to provide up-to-date information on vibration serviceability assessments.

There may be bias in the results from [52], [51] and both Chapter 3 models due to the models being derived from the baseline data. Such a bias is unavoidable as no other dataset is comparable. Similarly, [63] provides low error acceleration response through their walking loads using different methodologies and still produces similar results to [52]. Whilst [63] is comparable to [52],[51] and Chapter 3 models, the model only provides information up to the 5th harmonic. Hence it provides no provisions for high-frequency load models.

The Fourier series nature of [16,19–21,28,55,64] and the inter-subject model of Chapter 3 Section 3.4.1 allows for quick hand calculations of acceleration in a closed-form solution. [52], [51], [34] and the intra-subject model of Chapter 3 Section 3.4.2 models are random processes that can only be defined statistically and cannot provide a closed-form solution. Therefore, a hierarchical approach is suggested conditioned on the outcomes of Section 4.2. When the overall accuracy (with respect to monitored acceleration responses of real structures) is the key driver and not time, the model [52]should be used. When quick calculations or closed-form solutions are required, the inter-subject mode of Chapter 3 Section 3.4.1should be implemented.

Section 4.2 provides evidence to suggest that current in-use industry models for vertical walking forces do not provide the minimum error (relative or percentage) of the mean acceleration response or in measurement of variance in acceleration response. The models of [52], [51], [63] and Chapter 3 models provide models with the minimum error of the mean and variance estimation of the acceleration response in the low-frequency estimation compared to other vertical load models (Table 4.4). [52], [51] and Chapter 3 models consistently provide the most reliable estimations in the high-frequency range concerning the error and percentage error (

Table 4.5). In a few low modal damping ratio scenarios, current industrial impulse high-frequency load models [19,20,28] provide comparably good relative errors, yet they consistently provide the lowest rank with concerning percentage error. Therefore, current industry models can be unreliably combined with varying results.

The assumption of two distinct load models for high and low-frequency structures is questioned; clear harmonic peaks can be seen up into the 7th harmonic of the baseline data. Additional care must be taken when using any synthetic load model at low modal damping ratio levels due to such a scenario providing the largest deviation of error of any model. Continued research on vertical walking is required to provide an even larger database of continuous walking. Suppose such a dataset occurred with a larger representation of locations, ethnicity, and a fairer representation of sex. In that case, such force time histories could be used instead of producing synthetic counterparts.

This Chapter presents findings to conclude that the current industry-used vertical walking load models are only fit for purpose in some scenarios. It is demonstrated that research models exist that produce smaller errors in acceleration response compared to real walking loads for over a decade, but current engineers need to be made aware of the models. The intra-subject variation model of Chapter 3 Section 3.4.2 presents a reliable alternative and produces a superior estimation in several scenarios with respect to minimising the error. The

closeness in both models, Racic et al. [52] and the intra-subject variation model of Chapter 3 Section 3.4.1, is often indistinguishable.

Chapter 5 Estimation of the moving human structure interaction parameters on a flexible structure.

Structures that undergo excitation due to walking forces will, to some degree, be affected by the interaction of the human and the structure. The magnitude of this complex interaction is multifaceted. The principal effect of humans traversing a structure is the altering of the natural frequency and modal damping ratio of the structure, leading to a reduced acceleration response. The counter-effect, the structural effect on the human, is the structural accelerations altering the human walking gait. Current industry guidance pertaining to the assessment of human excitation on structures needs to provide more guidance on the implementation and effects of the human structure interaction (HSI). The inclusion of such effects in the mathematical representation of the dynamic system not only improves the accuracy of the acceleration estimation compared to the monitored acceleration, but also are seen to reduce the acceleration of the structure (Chapter 2 Section 2.3). Whilst several researchers provide estimations of the moving human and mechanical systems, a current study needs to provide a detailed comparison of the existing parameters on a flexible structure, where the acceleration response can be significant compared to the acceleration due to gravity.

The present Chapter is organised as follows: Section 5.1 details the experimental methodology of determining the modal properties of the flexible structure, and Section 5.2

describes the experimental campaign's methods to determine the structure's acceleration response subjected to various walking frequencies. Section 5.3 compares the effects of the HSI. Section 5.4 compares current moving HSI parameters and their effects on the structure through its mathematical representation compared to the actual acceleration output of the experimental campaign in Section 5.3. Finally, Section 5.5 derives estimations of the moving HSI parameters through an inverse analysis and optimisation procedure.

5.1 Estimation of modal properties of GFRP bridge

To establish the degree and validity of HSI effects, a glass fibre reinforced polymer (GFRP) bridge was designed and built at the University of Warwick in 2019 to exhibit an acceleration response comparably close to the acceleration due to gravity [252], due to the low density and high strength characteristics of GFRP. The structure was designed as lightweight as possible while fulfilling all strength and safety requirements [178], thus, a pultruded GFRP design with a shallow truss design was adopted. The truss depth is 475mm between chord centre lines, spanning 16.8m. Full details of the structural layout are given in [178].

Figure 5.1 presents an isometric view of the GFRP bridge. The bridge is supported on 4 steel bearings with one end on a roller support to mimic supported conditions.

Figure 5.1: Photograph of GFRP bridge used to obtain experimental acceleration responses

5.1.1 Modal analysis due to chirp excitation

Modal testing was carried out in 2019 by Russel et al. [252] at the University of Warwick, the result of which was received by the author in 2022 [253]. Table 5.1 provides the modal properties of the GFRP bridge up to a limiting frequency of 25Hz.

Table 5.1: Natural frequencies of empty FRP footbridge [252]

Mode Description	Frequency (Hz)
Vertical bending 1st	2.53
Torsional 1st	3.36
Vertical bending 2nd	8.48
Torsional 2nd	11.3
Vertical bending 3rd	15.8
Torsional 3rd	21.9

The finite element analysis (FEA) conducted by Russel et al. [252] validated the modal assessment's natural frequency and modal mass of the structure. It is demonstrated that the vertical mode shapes align with integer values of the sine function [252]. The first vertical mode's modal mass is 650kg from FEA.

The first vertical bending mode appears at the extreme limit of typical walking frequencies [70,71,73,74,246] (Table 5.1). Therefore, the first vertical bending mode can be excited by resonant walking at 2.5Hz. The first torsional mode can be excited by the second harmonic of walking at 1.68Hz.

5.1.2 Non-linear modal properties due to free decay response

To investigate f_n and ζ_n over a range of possible vibration amplitudes, a free decay analysis was performed on the structure. As this chapter focuses on the HSI effects, consideration of the non-linear representation of the modal parameters must be investigated to ensure any changes in the modal properties result from the moving participants and not the structure itself. To monitor the non-linear relationship of f_n and ζ_n, three free decay tests were performed, and the resulting mid-span accelerations were recorded on either side of the bridge. Dr Stana Zivanovic performed all three free decay tests, and the raw data was shared with the author in 2022 [253]. Free decay tests are conducted when an individual walks along the structure and the steady state acceleration response is monitored from when the individual leaves the structure. The log-decrement method [254,255] is utilised from the acceleration time histories to determine the modal damping ratio on a cycle-by-cycle base. To ensure the response is generalised and no local variations occur, the modal damping ratio is taken over a 10-cycle period.

$$\delta_n = \frac{1}{10}\ln\left(\frac{a_n}{a_{n+10}}\right) \qquad \text{Eq 82}$$

$$\zeta_n = \frac{1}{\sqrt[2]{1+\left(\frac{2\pi}{\delta_n}\right)^2}} \qquad \text{Eq 83}$$

a_n is the acceleration of the nth peak and a_{n+10} is the acceleration at the nth + 10 peak. The acceleration-based natural frequency of the structure is taken as the reciprocal of the time period between the 10 successive peaks divided by 10.

Before each free decay acceleration signal is analysed for the non-linear modal properties, each signal is passed through a bandpass filter to isolate the first mode contribution to the decaying response. The filtered frequencies are set at a lower limit of 0.5Hz and an upper limit of 2.8Hz. The lower limit was established to ensure the removal of low-frequency noise. The upper limit was chosen to remove contributions of the higher modes and high-frequency noise. Figure 5.2 provides a visual representation of the effect of the bandpass filter.

In the specific example of Figure 5.2, the free decay of the bridge response can be seen from approximately 33 seconds and starting at a magnitude of 4m/s^2.

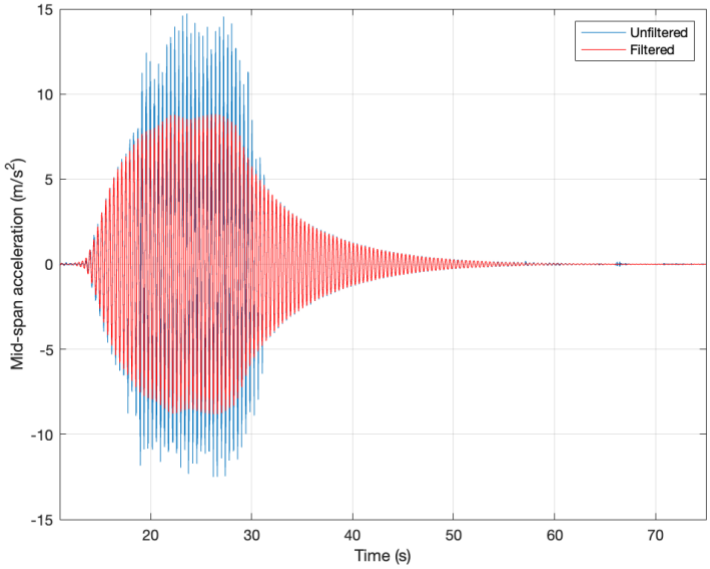

Figure 5.2: Free decay acceleration response of the unfiltered and filtered bandpass signal at mid-span subjected to 2.5Hz average walking frequency.

The maximum likelihood estimator was then used to perform curve fitting of the data for both the natural frequency and the modal damping ratio, Figure 5.3 and Figure 5.4respectively. The absolute magnitude of the acceleration is used as the input to provide a smooth function. The exact damping mechanisms are assumed to occur at the negative acceleration values. For each free decay, the average acceleration time history for the left and right side of the mid-span is averaged to provide a single value and remove any torsional mode effects.

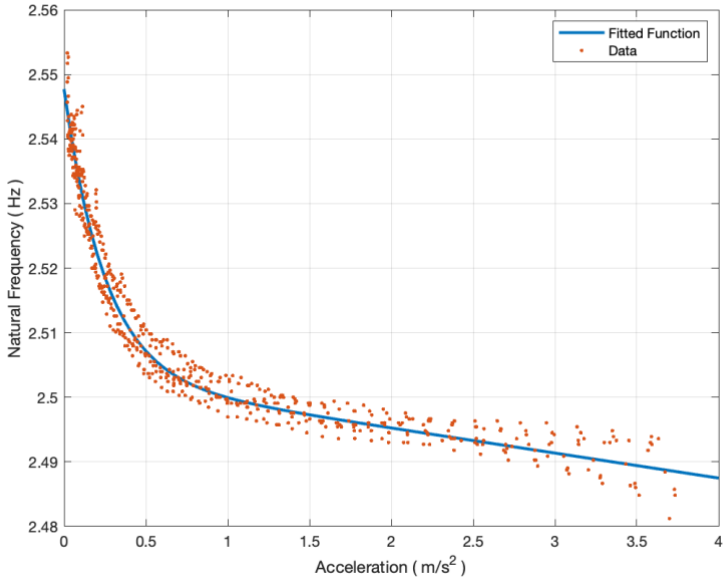

Figure 5.3: Non-linear acceleration dependent natural frequency of the first vertical bending mode

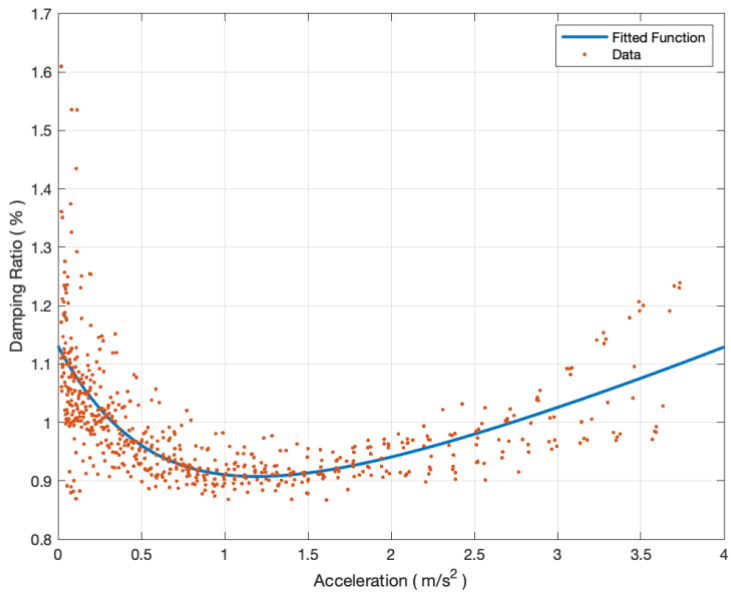

Figure 5.4: Non-linear acceleration dependant modal damping ratio of the first vertical bending mode

The nonlinear modal damping ratio for the first vertical mode of the structure is approximated as follows:

$$\xi(a) = 0.003685e^{-1.688\,a} + 0.007624e^{0.0981a} \quad \text{Eq 84}$$

Where a is the absolute magnitude of the acceleration at the midspan of the structure in m/s^2. The non-linear relationship for the fundamental natural frequency of the structure is given as follows:

$$f_n(a) = 0.04472e^{-3.981\,a} + 2.503e^{-0.001554a} \quad \text{Eq 85}$$

The first mode's natural frequency and modal damping ratio can only vary marginally.

5.2 Experimental methodology of determining the acceleration response of the GFRP bridge subjected to walking

To conclude the HSI effects on lightweight structures, a series of physical measurements are required to compare and investigate the acceleration response of humans walking on a structure. Section 5.2.1 presents the methodology to measure the acceleration response of the physical system, whilst section 5.2.2 presents the numerical formulation of the combined human and structural model. The numerical representation can then be used to estimate the acceleration response of the structure, subjected to synthetic vertical walking forces and estimated moving human parameters.

5.2.1 Determination of acceleration response of GFRP (Physical)

Dr Stana Zivanovic conducted the experimental campaign, and the raw data was sent to the author in 2022 [253]. To ensure the estimations of the human dynamic properties are robust to all cases of resonant and non-resonant walking forces, 56 volunteers walked at 4 prescribed walking frequencies [1.5Hz, 1.9Hz, 2.3Hz, 2.5Hz] twice with the aid of a metronome. Before each volunteer walked over the structure, the participant's mass was taken. Each volunteer then performed a traverse of the structure before a period of rest, the walking frequency is repeated, or the walking frequency is increased to the next increment if two successive traverses of the same walking frequency occur.

The acceleration responses are monitored at the quarter, half and three-quarter lengths of the structure described in Section 5.1. The accelerometers are located on either flank of the bridge or the top side of the GFRP decking, however, only the mid-span acceleration is used throughout this chapter because it is the location of the antinode of the first mode. As the structure's first vertical and torsional modes are close in natural frequency, acceleration measurements are taken from the flank. The raw signals will have additional acceleration from the torsional natural frequency. To mitigate and remove such effects, the average response of the left and right accelerometers is taken to negate the influence of the first torsional mode at the mid-span location. A low pass filter is then set with a limit of 8Hz, thus ensuring the acceleration signal is purely a combination of the first vertical mode of the structure and not the second vertical mode at approximately 8.48Hz, and only considers the influence HSI walking effects and the forcing frequencies of the walking force signal. The moving HSI parameters are shown in Chapter 2 Section 2.3.2.2 to be lower than 8Hz. Therefore, no information is lost through filtering. At a minimum, the third harmonic of walking will be included in the presented information, with a maximum of the 5th harmonic seen for lower walking frequencies.

The first vertical mode of the structure is the only mode of consideration in this Chapter. As seen in Chapter 3 Section 3.3 the first harmonic of walking presents higher DLF values. It is, therefore, more susceptible to a larger acceleration response than any other mode. All other vibration modes present resonant cases with higher integer values of the walking frequency, which naturally have a lessened DLF value and, thus, a lessened acceleration response compared to the first harmonic of walking. The resonant response of the first mode at 2.5Hz walking will produce a larger structural acceleration response than any other walking frequency.

Figure 5.5 illustrates the effects of the low pass filter for two of the four walking frequencies. At 1.5Hz walking frequency, clear peaks in the frequency domain occur at integer values of 1.5Hz walking frequency. The second vertical mode of the structure would not be detected, as the mid-span location is a perfect nodal point for this mode. Finally, the remnants of a resonant response with the 3rd vertical mode and the 11th integer of walking frequency can be seen in the unfiltered signal. A larger proportion of the mid-span 1s RMS is attributed to frequencies above the cut-off frequency of 8Hz. In the instances of 2.5Hz walking frequency, a clear resonant response of the first and third vertical modes is seen from the frequency analysis.

Figure 5.5 presents a limitation of the study. Whilst a low pass filter at 8Hz is used, the frequency domain representation of the acceleration time history clearly shows content in higher-order frequencies. The limitation is a result of the mathematical representation of the filter. The low pass filter does not block frequencies above the limit but attenuates the signal, therefore, the roll-off of the signal results in some information passing through.

From the presented pre-processing steps of Section 5.1 and Section 5.2.1; the modal mass of the structure, non-linear natural frequency and modal damping ratio, filtered acceleration response, and mass of each participant are known for all 448 acceleration time histories.

Therefore, all the required information is founded to numerically estimate the structure's response for each walking frequency and pedestrian.

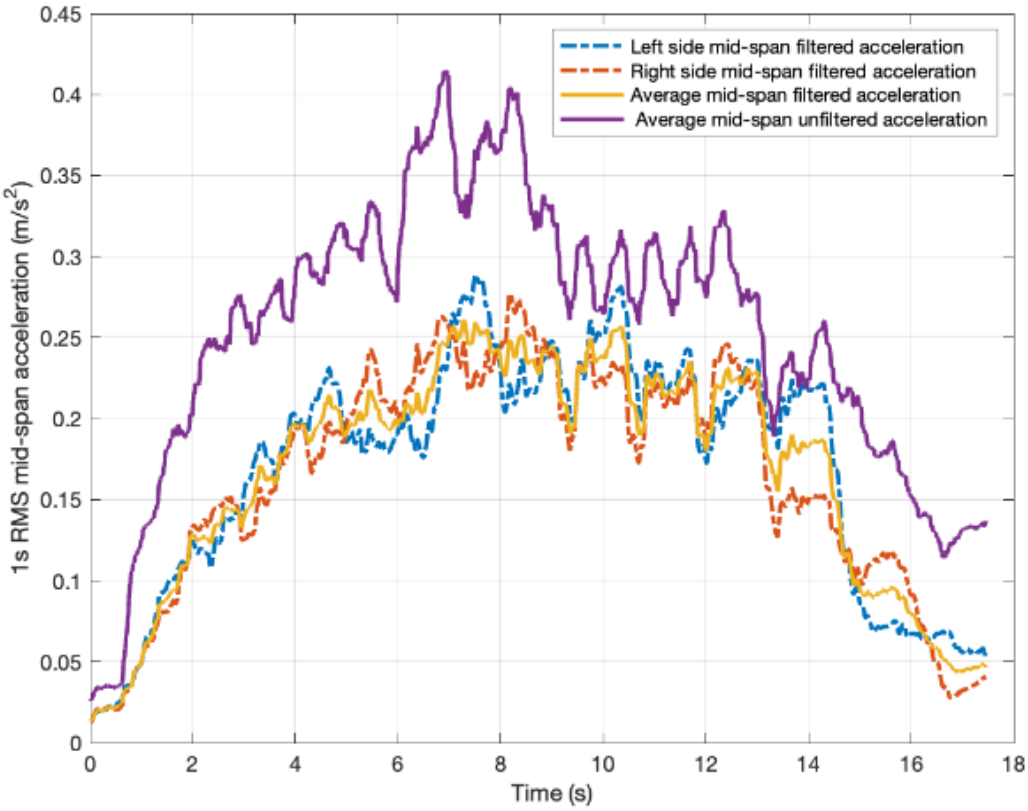

a)1s RMS mid-span acceleration of the filtered and unfiltered signal of a 100Kg participant walking at 1.5Hz walking frequency

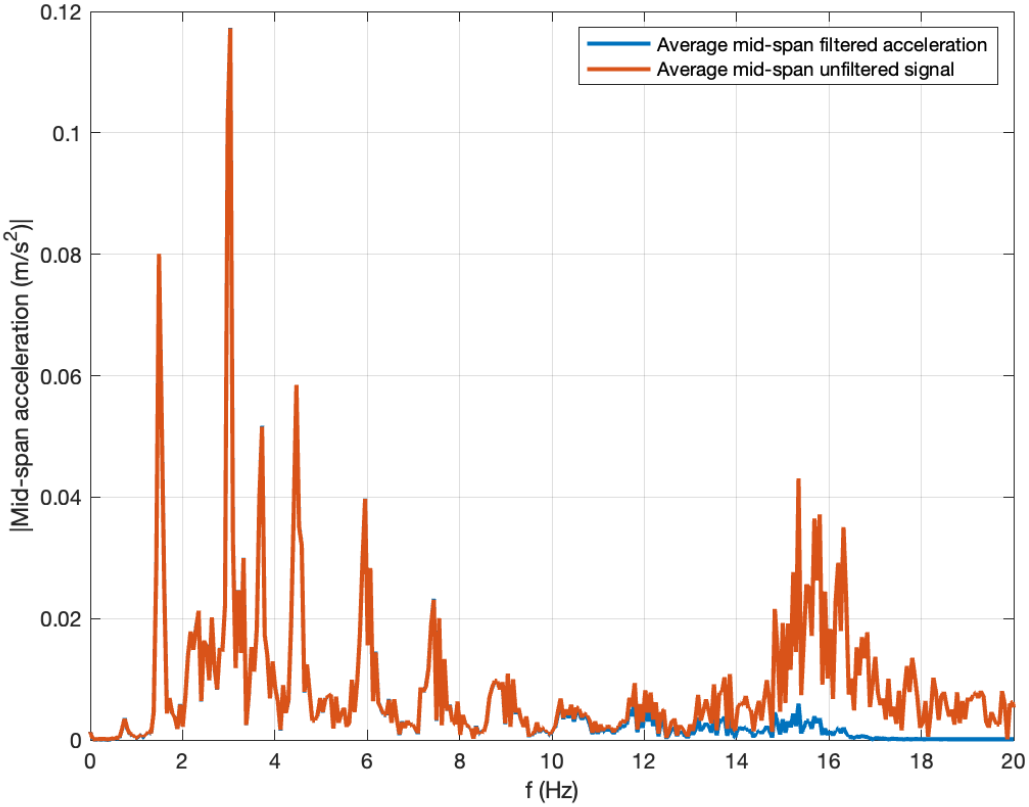

b) Frequency domain representation of filtered and unfiltered mid-span acceleration of a 100Kg participant walking at 1.5Hz walking frequency

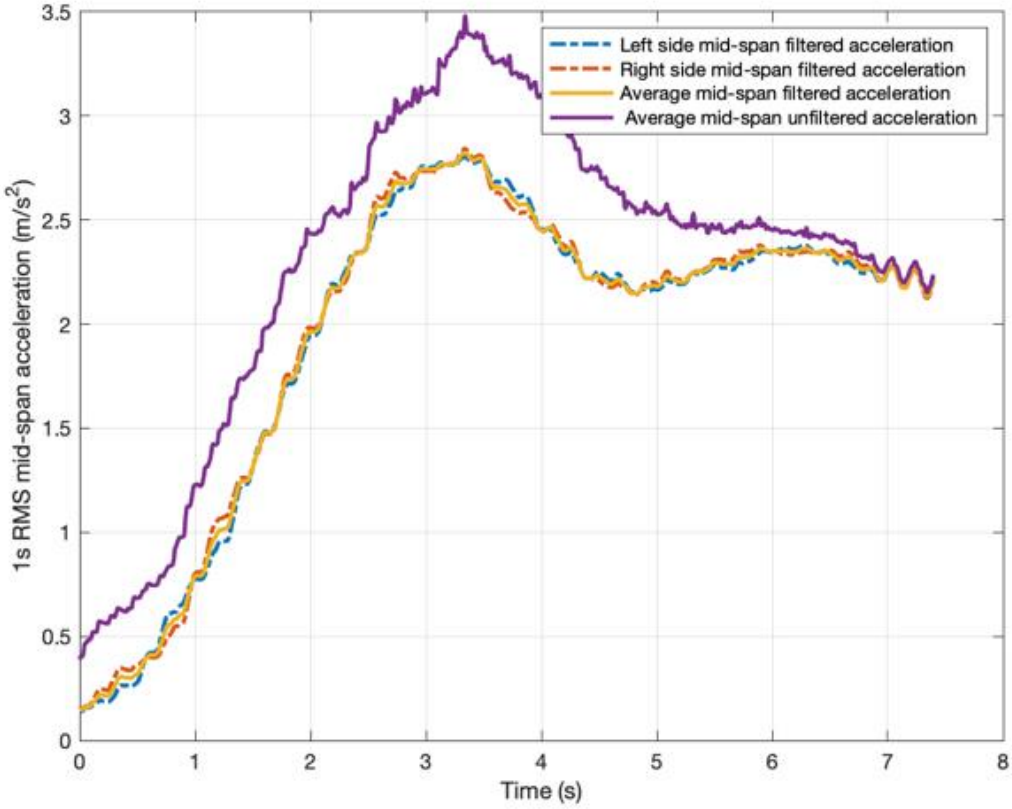

c)1s RMS mid-span acceleration of the filtered and unfiltered signal of a 100Kg participant walking at 2.5Hz walking frequency

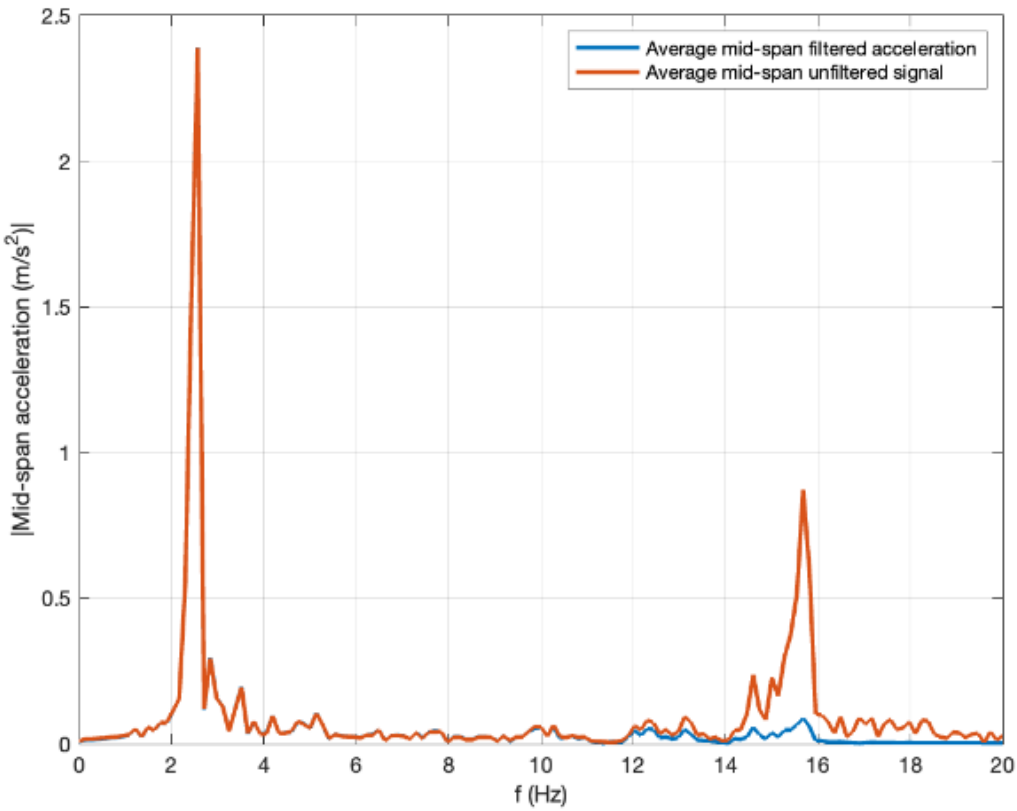

d) Frequency domain representation of filtered and unfiltered mid-span acceleration of a 100Kg participant walking at 2.5Hz walking frequency

Figure 5.5: Time and frequency domain representations of filtered and unfiltered signals at 1.5Hz and 2.5Hz walking frequencies

5.2.2 Determination of acceleration response of GFRP (Numerically)

To provide a comprehensive comparison of the current and historic moving HSI parameters, namely the SDOF SMD modal mass, natural frequency and modal damping ratio (Chapter 2 Section 2.3.2.2), to the measured results of section 5.2.1, a multi-degree of freedom (MDOF) model is constructed. The MDOF model is constructed through the respective mass, stiffness, damping and force matrices:

$$\boldsymbol{M} = \begin{bmatrix} M_{hn} & 0 \\ 0 & M_{sn} + \phi(t) M_{hn} \phi(t) \end{bmatrix} \quad \text{Eq 86}$$

$$\boldsymbol{K} = \begin{bmatrix} K_{hn} & -K_{hn}\phi(t) \\ -K_{hn}\phi(t) & K_{sn} + \phi(t) K_{hn} \phi(t) \end{bmatrix} \quad \text{Eq 87}$$

$$\boldsymbol{C} = \begin{bmatrix} C_{hn} & -C_{hn}\phi(t) \\ -C_{hn}\phi(t) & C_{sn} + \phi(t) C_{hn} \phi(t) \end{bmatrix} \quad \text{Eq 88}$$

$$\boldsymbol{F(t)} = \begin{bmatrix} 0 \\ \phi(t) F(t) \end{bmatrix} \quad \text{Eq 89}$$

Were M_{hn} is the SDOF modal mass matrix of the human due to the nth vertical, $M_{sn}$is the modal mass of the structure due to the nth vertical mode shape, $\phi(t)$ is the nth vertical mode shape. The stiffness and damping coefficient of the nth mode is given as:

$$K_n = M_n \omega_n^2 \quad \text{Eq 90}$$

$$C_n = 2\xi_n \omega_n M_n \quad \text{Eq 91}$$

Where $\omega_n$is the natural angular frequency and $\xi_n$is the modal damping ratio of the mode of vibration. From the analysis of Section 5.2.1, the non-linear modal properties of the structure are known, along with the accompanying inputs of the walking frequency and actual mass of the participant. Therefore, each walking force can be taken from the model of Racic and Brownjohn [52], due to its superior likeness in producing synthetic walking forces compared to real loads, as demonstrated in Chapter 4 Section 4.5. The SDOF representation of percentage of modal mass compared to actual mass, modal damping ratio, and natural frequency of the moving pedestrian can be obtained from Chapter 2 Section 2.3.2.2 and summarised in Table 5.2. It is further assumed that each participant has a constant average

velocity and is linearly mapped to the average walking frequency through the relationship given in Chapter 3 Section 3.3.3.

With the above information, the MDOF system of linear ordinary differential equations is solved at each time step using the method presented in Chapter 4 Section 4.1.2 with the appropriate initial conditions. Before each timestep, the non-linear modal properties of the structure are updated based on the acceleration of the previous time step. The horizontal position and modal force are then updated to the current time step. This process is recursively performed until the time elapses for the pedestrian crossing the structure. It is acknowledged that there will be a lag in results due to the modal properties being updated based on the acceleration of the previous time step.

The full acceleration time history of a pedestrian walking on the first vertical mode of the structure can be approximated and compared to the physical results of Section 5.2.1. The location of interest for the acceleration response is the mid-span 1s RMS acceleration. Therefore, the acceleration is multiplied by the appropriate 1st vertical mode shape to achieve the physical acceleration response from the modal acceleration response.

5.3 Investigation into the effects of moving participants on the structure

A numerical and physical examination of the structure subjected to walking pedestrians is performed to assess the HSI effects' prominence. Hypothetical if HSI effects play no role in affecting a structure's modal properties and acceleration response, the filtered measured acceleration response (Section 5.1 and Section 5.2.1) of the structure will be closely approximated by an SDOF linear structural system not considering HSI effects. The numerical model will approximate each pedestrian crossing at the corresponding walking frequencies, only considering the first vertical mode of vibration.

As the exact vertical walking time histories are unknown for each individual, Racic and Brownjohns' [52] vertical walking model is sampled 100 times for each participant crossing. The maximum 1s RMS mid-span acceleration response is then noted for each sample. The distribution of the acceleration responses for both the numerical and filtered measured accelerations are summarised in Figure 5.6. The physical measurements are up-sampled 100 times to provide the same number of data points as the non-HSI effect model.

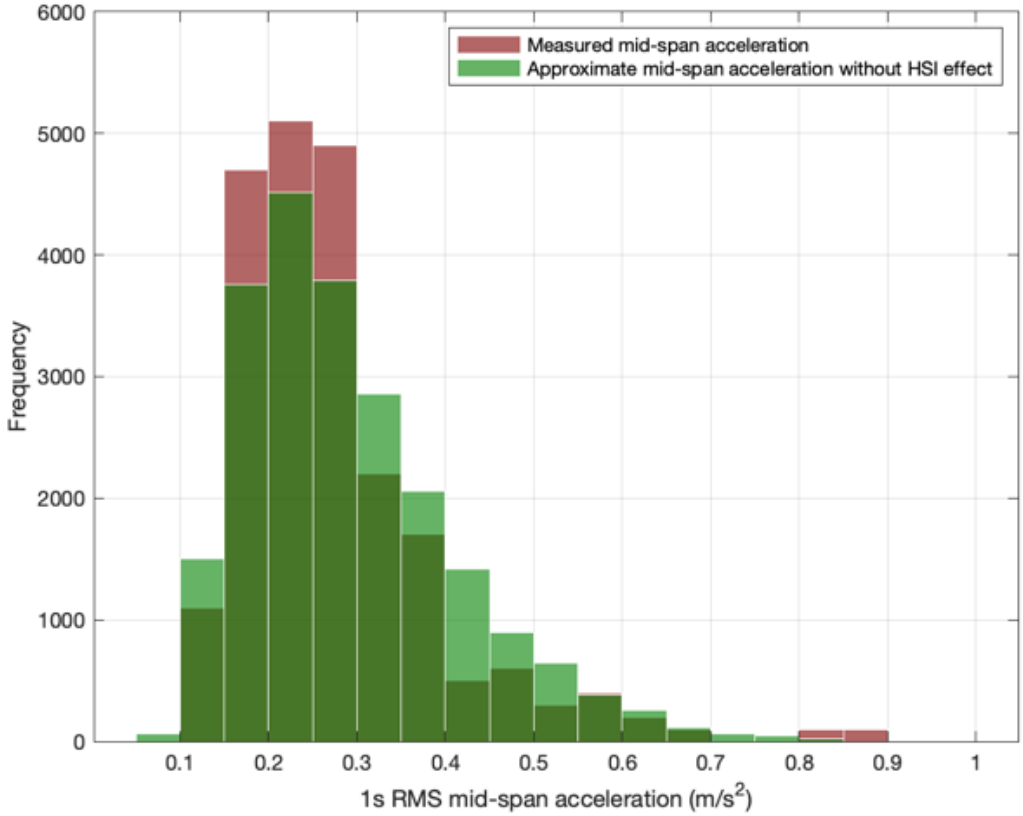

a) Histogram of the response at 1.5Hz walking frequency comparing measured acceleration vs SDOF approximation of structure

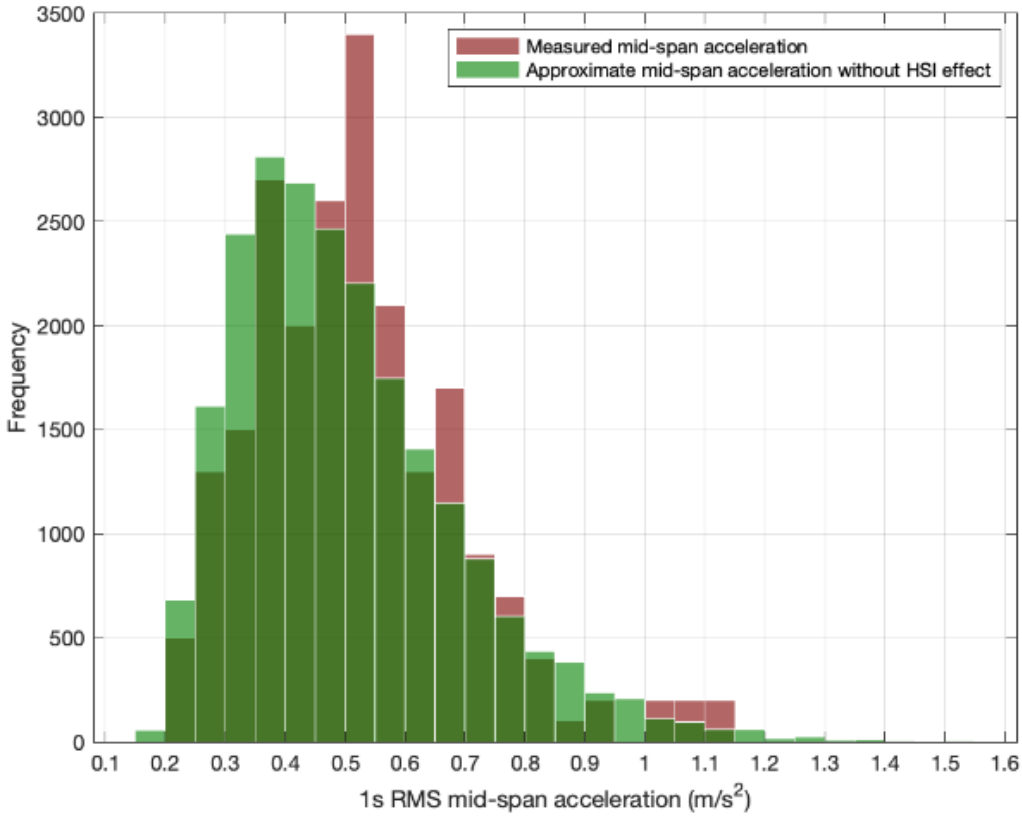

b) Histogram of the response at 1.9Hz walking frequency comparing measured acceleration vs SDOF approximation of structure

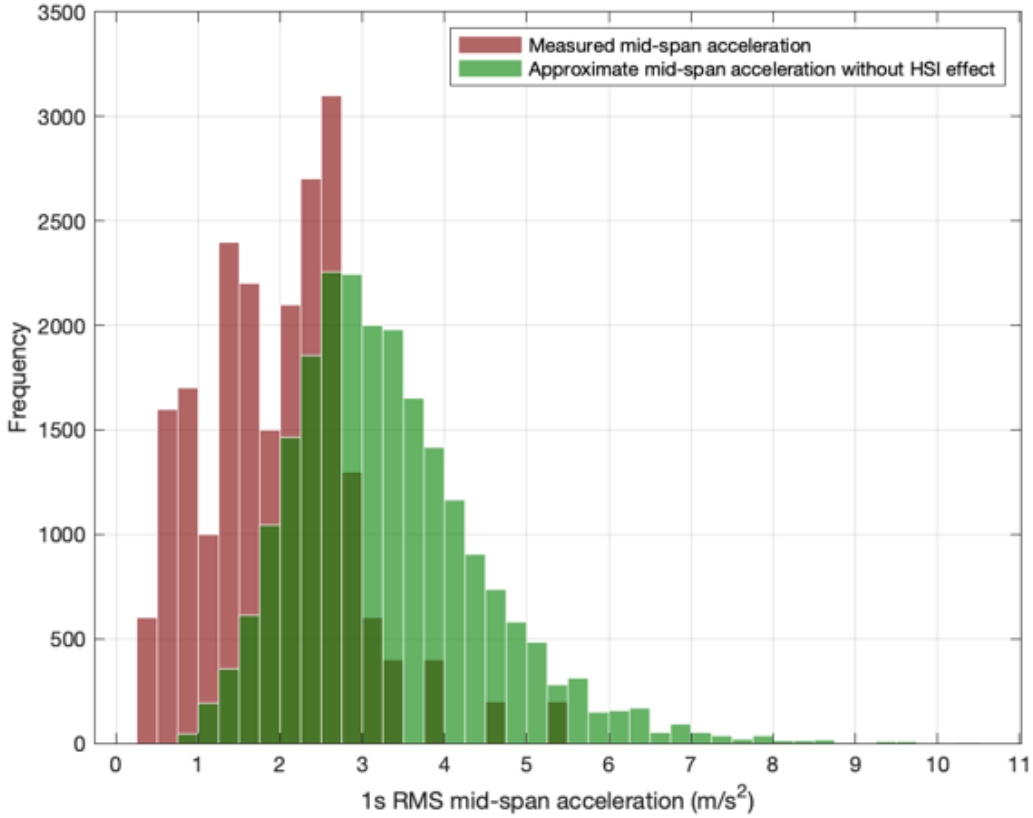

c) Histogram of the response at 2.3Hz walking frequency comparing measured acceleration vs SDOF approximation of structure

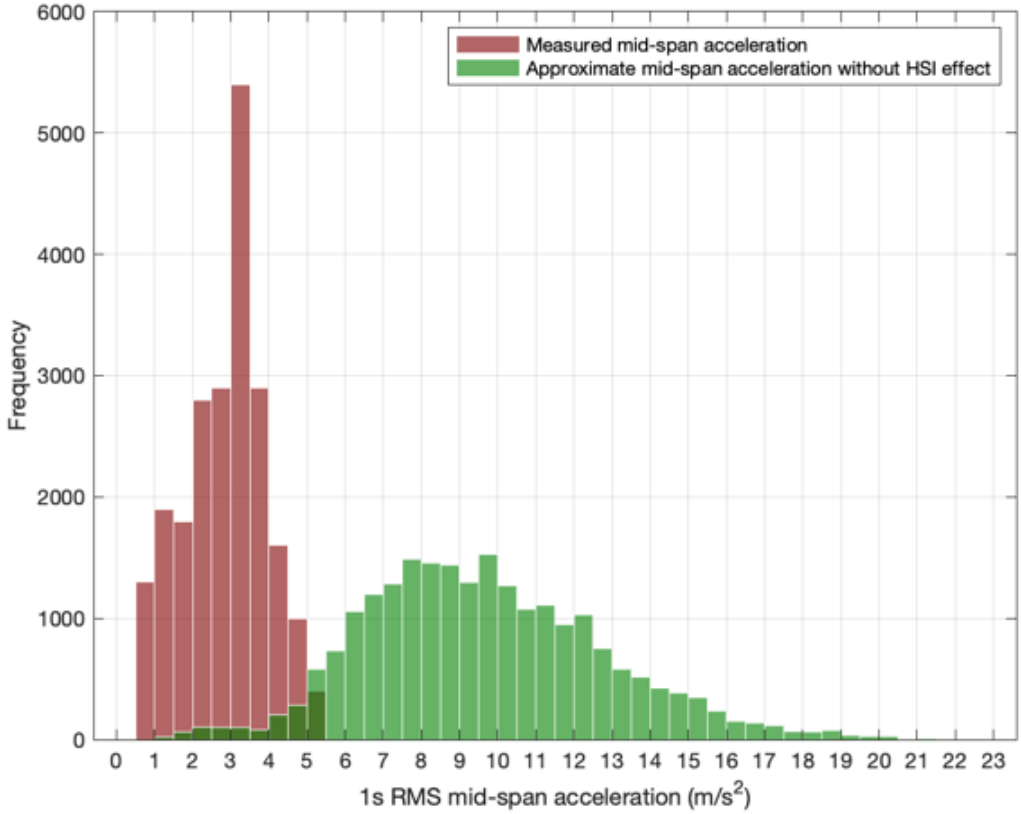

d) Histogram of the response at 2.5Hz walking frequency comparing measured acceleration vs SDOF approximation of structure

Figure 5.6: Histograms of filtered max 1s RMS acceleration for various walking frequencies comparing measured acceleration vs SDOF approximation of structure

Figure 5.6 a) and b), the magnitude of measured mid-span results provides a similar distribution to the numerical model that does not consider HSI effects. Both sets of figures demonstrate that at low ratios of walking to the structure's natural frequency, HSI effects are considered negligible. Performing the two sample KS test on the distributions for 1.5Hz and 1.9Hz at a significance level of 5%, both walking frequencies indicate that the distributions of acceleration response from the filtered measure response and SDOF numerical model come from the same distribution of response at their respective walking frequencies.

At values of walking frequency that are close to the structure's natural frequency, the prominence of HSI effects becomes evident. At 2.3Hz walking frequency, the measured and numerical distribution start to diverge, with the filtered measured results producing smaller accelerations than the numerical models with no HSI effects, therefore, the effects of the active HSI participant are seen to retard the acceleration response compared to the non-HSI effects model. At 2.5Hz walking frequency, the mean response of the measured accelerations is 3 times less than the numerical model, not considering HSI effects. As shown in the literature review (Chapter 2 Section 2.3), HSI has a prominent impact on resonant walking frequencies. Performing the KS test at a significance level of 5% for the 2.3Hz and 2.5Hz walking frequency, the test provides insufficient evidence to conclude that each set of HSI measurements and non-HSI model are from the same distribution of accelerations.

The distribution of filtered measured responses exhibits a reduction in variance compared to the non-HSI effects model when walking in a resonant mode. As ratios of walking frequency to the natural frequency of the structure converge to unity, the coupled system of the human and structure become synchronised, and the presence of the human reduces the acceleration response considerably. The effect is, however, counterintuitive in this scenario, as the largest reduction in acceleration response is seen when the structure undergoes resonance. Therefore, without the inclusion of modelling HSI effects, the maximum acceleration response of the structure will be overestimated.

The HSI parameters for the SDOF moving human model, namely the percentage of modal mass compared to actual mass, natural frequency, and modal damping ratio, are investigated in the proceeding section. Whilst the presented section suggests the need to model HSI, the accurate estimation of SDOF SMD parameters of the moving human is yet to be reviewed in the literature. Current moving human mechanical parameters are seldom reviewed compared to one other, with each researcher of the values in Chapter 2 Section 2.3.2.2 presenting their

results in isolation. No study has yet used the parameters found in research and validated the results on an independent structure.

5.4 Comparison of current moving HSI parameters

Of the 56 participants in Section 5.2.1, it is found that the mode of the participants' mass is 76kg, appearing five times, thus giving 10 total acceleration time histories of each walking frequency to compare (5 participants walking twice on the structure, measured at either side of the midspan averaged out to remove the torsional effect). Using the representation of the active human parameters (Table 5.2) and the sampled walking load of Racic and Brownjohn [52] at the appropriate walking frequency for the given mass of 76kg, an acceleration time history of the mid-span subject to the first vertical mode can be estimated. The baseline measurements undergo the same low pass filter of Section 5.2.1 to ensure only the structure's first vertical mode is represented. The numerical approximation for each walking frequency uses the numerical method laid out in Chapter 4 Section 4.1.2, considering the formulation of the MDOF system presented in Eq 86 and the non-linear representation of the structure's natural frequency and modal damping ratio in Section 5.1.2.

Table 5.2: SDOF SMD average moving HSI parameters of human participants

Author	Natural Frequency (Hz)	Modal Damping Ratio (%)	Percentage of modal mass compared to actual mass (%)
Shahabpoor et al. mode 1 [215]	2.85	29.5	100
Matsumoto et al. [41]	K = 279 N/mkg	Inferred through damping constant	83.3

Matsumoto et al. [202]	Inferred through stiffness constant and modal mass	Inferred through damping constant	89.8
Foschi [216]	3.3	33	100
Jimenez-Alonso [189]	2.76	47.2	84.0
Gomez et al.[217]	2.51 2.29 2.52	12 18 12	100
Zhang et al. [186]	1.85	30	100
Wang et al. [205]	$0.3049f_p$ +1.367	$(-0.2116f_p$ + 0.8737)*100	100
Ahmadi et al. [145]	Resonant Walking pace	(0.38ln(m)-1.42)*100	100
Van Nimmen et al. [218]	3.06	35	100

Figure 5.7-Figure 5.10 present the 1s RMS mid-span acceleration for all walking frequencies, comparing each model in Table 5.2 to the 10 filtered measurements at all for walking frequencies [1.5Hz, 1.9Hz, 2.3Hz and 2.5Hz]. For each walking frequency, the 12 models are compared to the filtered measurements, with a model that considers the moving load but not the HSI effects. The moving load model represents current guidance [16,19,20]. Toso et al. [54] model is not used, as it does not provide a realistic coverage of the parameters. At high or low walking frequency, the estimate of the modal parameters produces negative values. Such values are not feasible and represent the lack of data and where the data is overfitted.

The measure of fit is deduced visually. It is deemed a good fit or accurate if the numerical model's acceleration time history is within the bounds of the 10 reference time histories. Whilst this is not exclusively true or an objective measure, the 10 samples represent a subset of the anticipated results. Therefore, the middle range of the reference accelerations is approximated as the mean structural response for a 76kg person.

Figure 5.7 and Figure 5.8 present the filtered measurements and approximations of 1.5Hz and 1.9Hz walking. Both walking frequencies are invariant to HSI effects, with negligible differences between the moving force and modelled HSI parameters. Such an observation is anticipated considering the results of Section 5.3. This observation is expected due to the deviation of walking frequency away from the structure's natural frequency. As demonstrated in Figure 5.9 and Figure 5.10, at walking frequencies close to the structure's natural frequency, the HSI's effects become more prominent. 1.5Hz and 1.9Hz represent 60% and 76% of the natural frequency compared to 2.3Hz at 92% of the natural frequency. From Figure 5.7 and Figure 5.8 all representations of the HSI provide an accurate estimation.

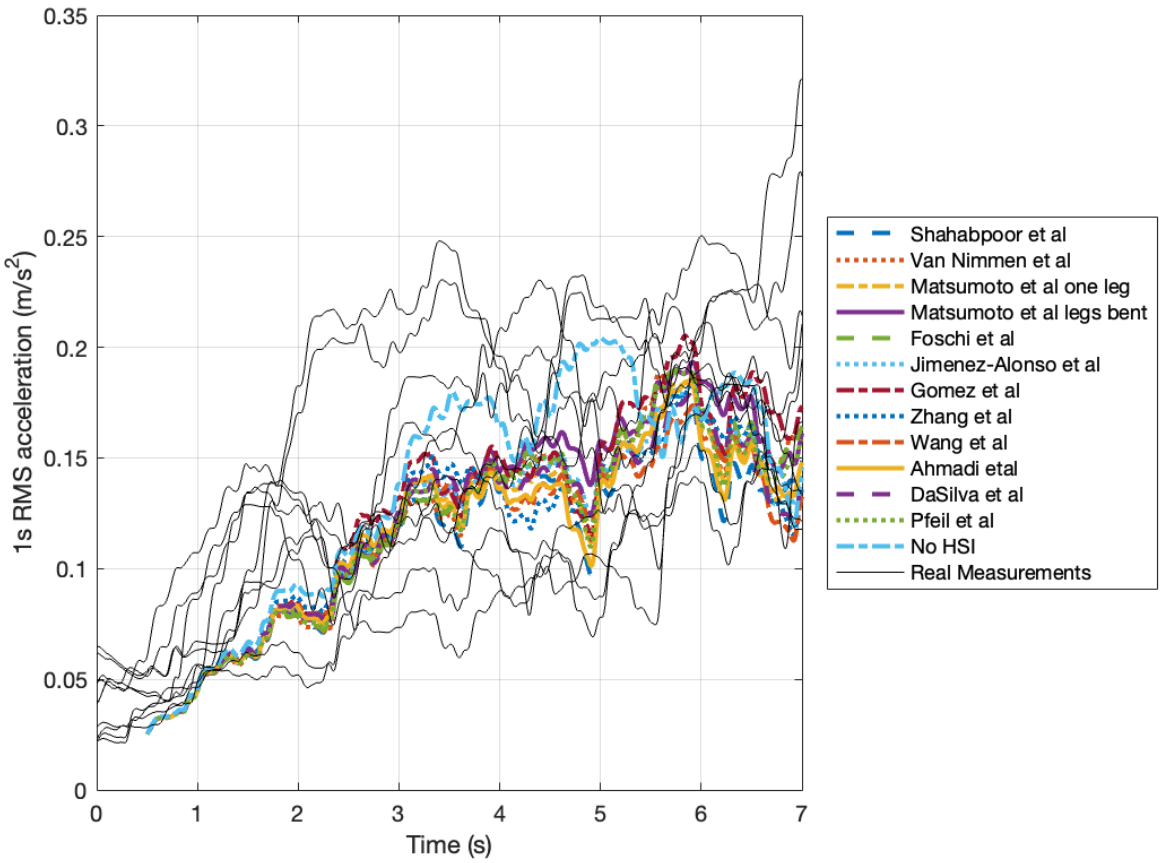

Figure 5.7: 1s RMS mid-span acceleration with participants walking at 1.5Hz using various authors' HSI SDOF SMD models of the active participant

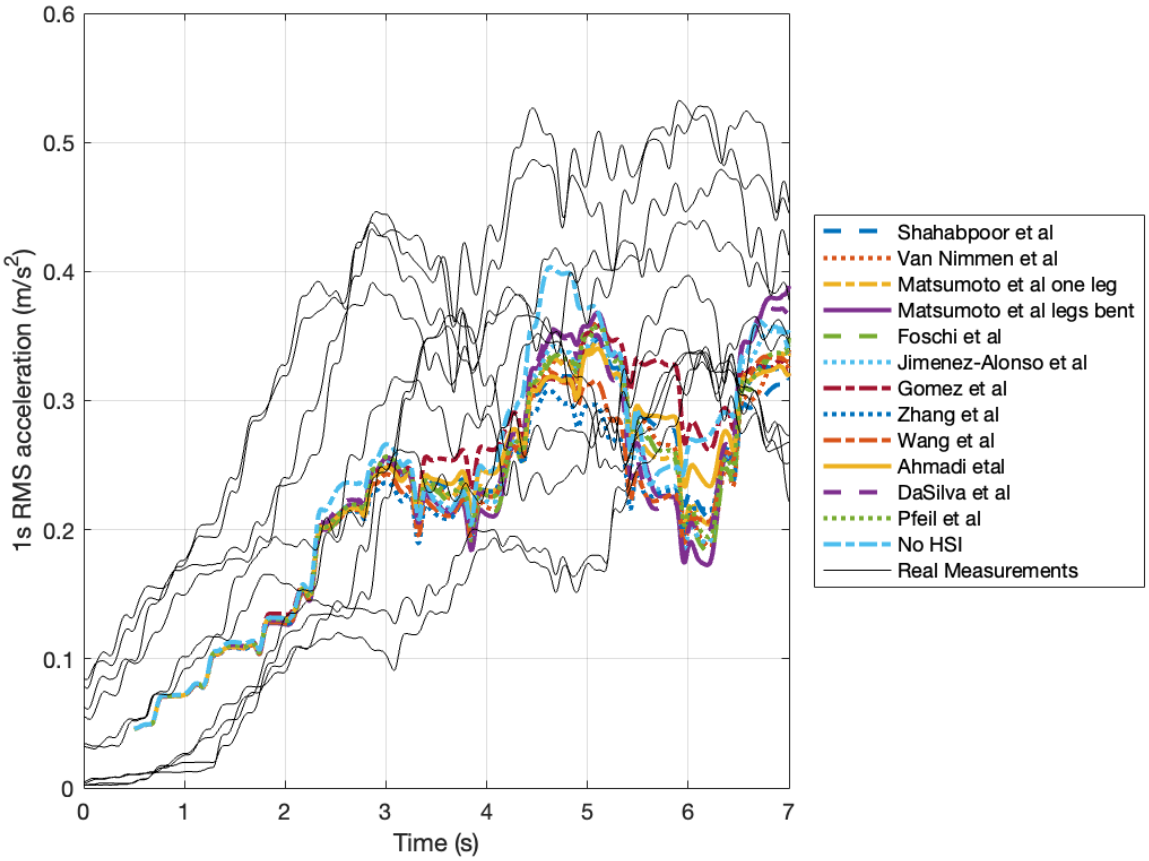

Figure 5.8: 1s RMS mid-span acceleration with participants walking at 1.9Hz using various authors' HSI SDOF SMD models of the active participant

Figure 5.9 presents the 1s RMS mid-span acceleration for 2.3Hz walking. In all cases, the models exist within the bounds of the average measured acceleration data. Without the effects of the HSI interaction, the approximated acceleration response is less than four of the ten monitored accelerations. The acceleration response of the non-HSI model is 40% and 80% less than the recorded acceleration time histories in some instances.

Two distinct bands of models are seen in Figure 5.9. The lower bound comprises Gomez et al. [217], Zhang et al. [186], Wang et al.[205] and Ahmadi et al[145]. Gomez et al. [217],

Zhang et al [186] , Wang et al.[205] and Ahmadi et al. [145] models present themselves with the lowest natural frequency of the human body from Chapter 2 Section 2.3.2.2 (2.51Hz, 1.85Hz, 2.15Hz and 2.5Hz, respectively). However, the modal damping ratio range from 12%, 30%, 39% and 23%, respectively, exhibiting no consistency in results. All four models present the percentage of modal mass compared to actual mass as 100%. As such, the natural frequency is viewed as the primary driver concerning the difference within the group.

The second and higher band of results present with natural frequencies of: 2.85Hz, 3.25Hz, 2.66Hz, 3.59Hz, 3.3Hz, 2.76Hz, 3.31Hz and 2.93Hz. The upper bound results all produce estimates above the structure's natural frequency. Even when the estimates are just above the natural frequency (e.g., in the case of Matsumoto et al. [202] with a value of 2.66Hz), a $0.5m/s^2$ difference in acceleration response is exhibited compared to the highest of the lower bound group with a natural frequency of 2.51Hz. The increase in the natural frequency of the modal estimate also corresponds to the increase in the acceleration response estimate. The recorded acceleration responses are consistent concerning each individual, with the average estimation of the first and second traverse providing almost identical acceleration time histories. Therefore, each individual provides a consistent walking force, or the participants have varying SDOF SMD HSI parameters.

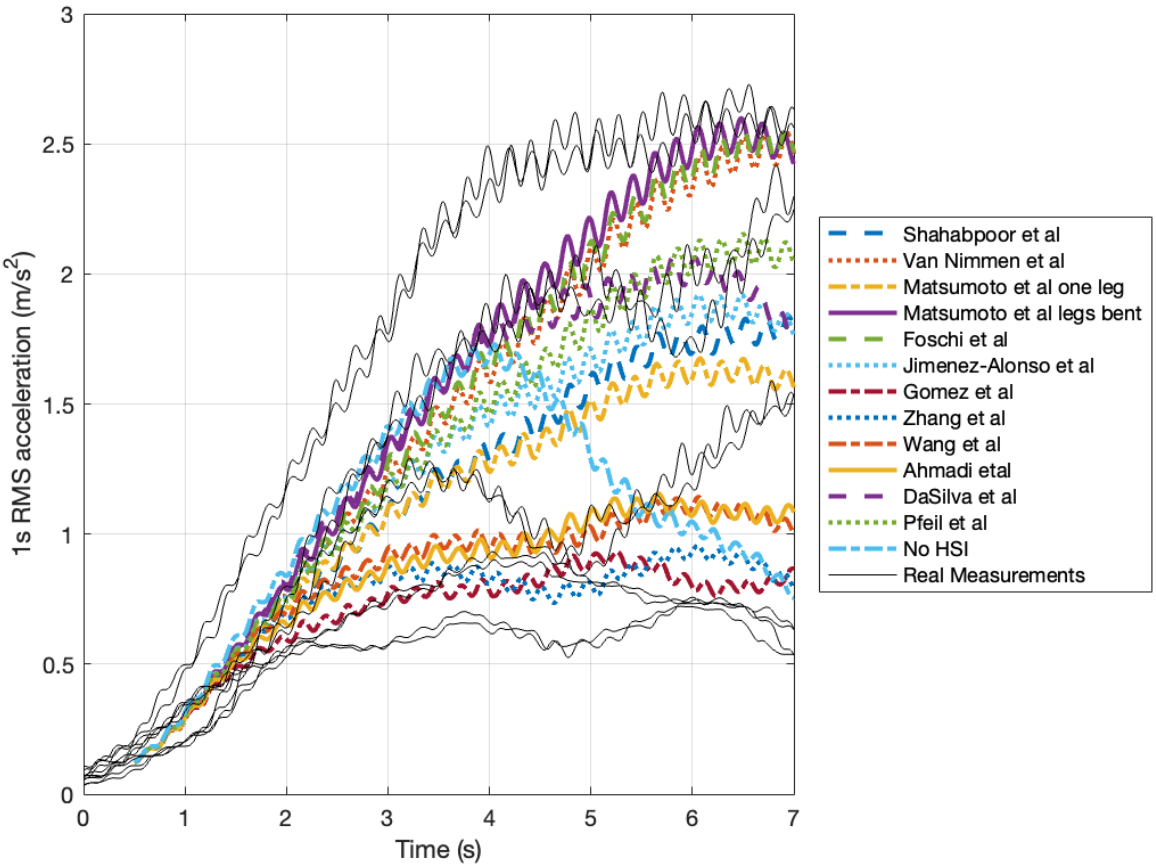

Figure 5.9: 1s RMS mid-span acceleration with participants walking at 2.3Hz using various authors' HSI SDOF SMD models of the active participant

In the case of 2.5Hz walking frequency (Figure 5.10) the acceleration magnitude of the non-HSI model provides an overestimation of the filtered measured responses. The inclusion of HSI effects both from the physical measurement and the mathematical representation provides a 300% reduction in the acceleration response compared to no HSI effects modelled. Therefore, HSI effects play a pivotal role in reducing the magnitude of the acceleration response at resonance. DaSilva et al. [106] HSI parameters result in an overestimate. This likely arises due to the lower percentage of modal mass compared to actual mass at 32%. If

the percentage of modal mass compared to actual mass of DaSilva et al. [106] is artificially changed to 100%, the resultant acceleration remains within the bounds of the measured results. The remaining models all represent one or several measured responses similarly. All models aside from DaSilva et al. [106] have modal damping ratio within 12% – 52% and natural frequencies of the human body within the range of 1.85Hz – 3.59Hz. The percentage of modal mass compared to actual mass is given in the range of 75% - 100%.

Analysis of the natural frequencies of various modal parameters in Figure 5.10 shows that many of the natural frequencies correspond to the resonant, or close to the resonant, frequency of the structure from which they are derived. Therefore, the validity of the natural frequency is questioned. It is hypothesised that the values of the natural frequency of the human body appear or become prominent as it is forcibly accelerated at the structure's natural frequency. Therefore, large amounts of energy are transferred into the human body due to the forced vibration, giving a falsehood of the values.

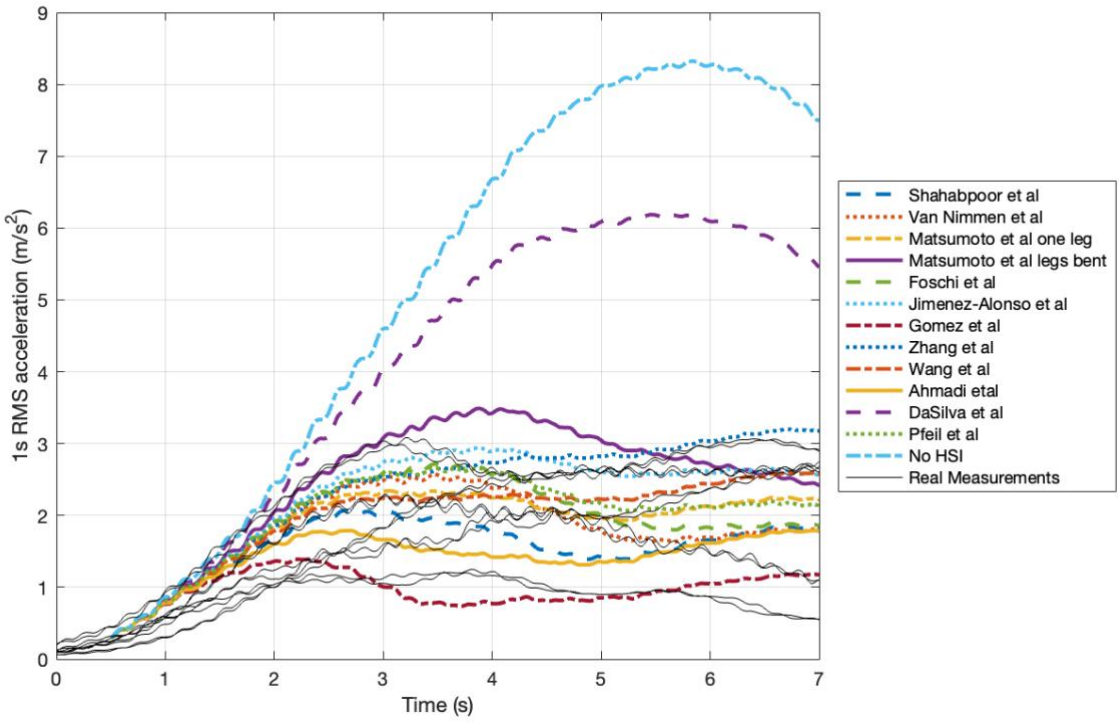

Figure 5.10: 1s RMS mid-span acceleration with participants walking at 2.5Hz using various authors' HSI SDOF SMD models of the active participant

It is seen that SDOF SMD moving HSI parameters and their effects play a pivotal role in the correct estimation of acceleration responses of flexible structures. Without this, the acceleration response at a resonant mode can be overestimated by more than 3 times. In all four cases of the walking frequencies, all parameter estimations produced an acceleration response within the range of the measured results, bearing that of DaSilva et al. [106] at 2.5Hz walking. The natural frequency and modal damping ratio of the moving human participant estimations vary, with no one estimate providing a conclusive best estimate, with respect to minimising the difference between predicted and actual acceleration of the GFRP bridge. The natural frequency of the human varies between 1.85Hz and 3.59Hz, and modal

damping ratio is from 12% up to 52%. The range of results suggests that multiple feasible estimations of the parameters occur.

5.5 Moving HSI parameter estimation through the acceleration response of the GFRP bridge

All 448 acceleration time histories (56 participants walking at 4 walking frequencies, performed twice and either flank estimations averaged) are used to estimate the moving human participant's approximate modal properties and their associated ranges. Section 5.5.1 presents the formulation of the inverse optimisation problem used to identify the associated range of SDOF SMD moving HSI parameters. Section 5.5.2 provides the resultant ranges and any co-dependent relationships of the modal properties through a comparison of the mean values at each walking frequency.

5.5.1 Methodology of the inverse problem

The mathematical optimisation problem has the usual form:

$$\min_{x} f(x) \quad \text{Eq 92}$$

$$Subject\ to\ g(x) = 0 \quad \text{Eq 93}$$

$$h(x) \leq 0 \quad \text{Eq 94}$$

$$x^{lower} \leq x \leq x^{upper} \quad \text{Eq 95}$$

Where x is the vector of design variables, $f(x)$ is the objective function, $g(x)$ is the vector of equality constraints, $h(x)$ is the vector of inequality constraints and x^{lower} and x^{upper} are the lower and upper limits of the design vectors, respectively. The optimisation is formulated to minimise the objective function, given that all the equality and inequality constraints are

satisfied. Within the context of the thesis, the optimised variables (x) are defined as the average modal properties of the human walking systems (Eq 96).

$$x = [f_h, m_h, \zeta_h] \quad \text{Eq 96}$$

Where f_h is the natural frequency of the moving human, m_h is the percentage of modal mass compared to actual mass and ζ_h is the modal damping ratio. All modal properties of the walking participant are taken from the first mode of the human. Previous research [198,203] has noted the presence of higher-order modes of the human system, however, they are not considered in this chapter. The average properties of the parameters are used in place of any time-dependent behaviour to reduce the order of complexity of the optimisation process.

The objective function within Section 5.5 is taken as the L_2 norm of the predicted and measured maximum mid-span 1s RMS acceleration. The maximum mid-span 1s RMS acceleration is used due to its frequent use in modern VSA [16,19,28]. Furthermore, the 1s RMS smooths out any unusual singular acceleration peaks and provides a more representative view of the acceleration time history.

No equality or inequality constraints are required for the optimisation, however, physical limits are needed to bound the design variables. Such a decision improves the speed of convergence of the optimisation due to the restricted parameter space. The upper and lower constraints of the design variables are appointed considering the previously published results of moving human parameters in Chapter 2 Section 2.3.2.2.

$$0.5Hz \leq f_h \leq 4Hz \quad \text{Eq 97}$$

$$50\% \leq m_h \leq 100\% \quad \text{Eq 98}$$

$$10\% \leq \zeta_h \leq 100\% \quad \text{Eq 99}$$

As the exact vertical walking forces are not known or recorded, the results of Chapter 4 Section 4.5 will be used as a surrogate. Racic et al. [52] vertical walking force model is therefore used. The vertical walking model is sampled 10 times per acceleration time history resulting in 10 different estimates of the design variables. The maximum 1s RMS acceleration prediction is found using the numerical estimation of the state space formulation (Chapter 4 Section 4.3.1). The only difference is the MDOF representation formulated in Eq 86.

Six different optimisation procedures are explored and compared in their ability to provide an optimal solution. The accuracy of the objective function dictates the criterion for best performance and the number of evaluations of the objective functions it took to achieve an optimal value. The six optimisation procedures are Interior point methods and Interior point methods with multiple start locations [256,257], Pattern search [258], Genetic Algorithm [259], Particle swarm [260], and Bayesian Optimisation [230,231]. For a full review of each algorithm, the reader is guided to the relevant references.

The acceleration time history is randomly selected from the 2.5Hz walking cases to provide a sample analysis. The results of 2.5Hz walking are chosen due to the effects the HSI plays at a resonant natural and walking frequency compared to other walking frequencies (Section 5.4). The participant's mass is taken randomly from the dataset, with the given mass selected as 65kg. Of the 2 averaged-out 1s RMS acceleration recorded for the 65kg individual, the associated target mid-span acceleration is 3.47 m/s^2. Table 5.3 provides the resultant modal properties of each optimisation algorithm based on 65kg participants walking at 2.5Hz and their walking force resulting in a 3.47 m/s^2 1s mid-span RMS acceleration. Each algorithm is

run three times independently at random start locations. As the optimisation problem is non-linear, there is no guarantee of reaching the optimal set of design parameters. Therefore, each algorithm's start position can dictate the optimisation procedure's result [257].

Table 5.3: Evaluation of optimisation methods to obtain average moving SDOF SMD estimation of a 65kg subject walking at 2.5Hz

	Solution				
Algorithm	f_h (Hz)	m_h (%)	ζ_h(%)	Objective function score	Number of evaluations
Genetic Algorithm	3.47	95.6	80.3	2.40e-9	26807
	1.96	75.0	58.9	1.80e-7	28703
	1.83	79.8	32.3	1.46e-7	22541
Particle Swarm	2.93	90.1	86.6	1.78e-8	62000
	3.20	100	100	9.47e-14	62000
	3.29	78.4	54.3	5.66e-10	62000
Pattern Search	4.00	100	67.9	1.71e-7	201
	3.00	55.0	32.9	2.93e-8	214
	1.70	92.5	36.5	4.92e-8	191
Bayesian Optimisation	2.84	84.8	79.2	1.55e-5	200
	2.71	85.7	83.9	1.07e-5	200
	3.10	87.1	76.0	1.51e-4	200

Interior Point method	2.57	75.2	69.1	4.47e-10	170
	1.96	72.3	50.6	5.63e-11	152
	1.91	77.2	21.2	4.34e-8	207
Multi-start interior point method	2.72	93.7	100	2.15e-14	16068
	3.10	98.4	99.2	2.00e-12	21564
	3.96	88.7	19.8	2.24e-12	14543

Compared to the target mid-span 1s RMS acceleration, the values of the objective functions for all optimisation methods provide differences. Thus, each estimate of the design variables in Table 5.3 provides a maximum mid-span acceleration within 1.51e-04 m/s^2 of the measured response. The acceleration time histories are measured to 0.000001 m/s^2 due to the sensitivity of the equipment. However, such levels of accuracy are not met. Electrical and other physical noises will cause low-level acceleration disturbances. Therefore, the stated level of accuracy will not be achieved in the physical system.

The various range of values for the design variables, combined with the similar objective function values, suggest that multiple local minima of the objective function must be present. This is seen through varying modal properties achieved by each algorithm and within repeat efforts of the same algorithm. The interior point method will be used with multiple starts to satisfy the accuracy requirements, although, a reduced number will be used than in Table 5.3. Table 5.3 used 150 different start positions. For the analysis of the data, only 5 will be used.

A brute force method using a grid search is utilised to compare results. The method searches systematically through all combinations of the design variables. Each design variable is discretised by 0.01Hz or 1% and searched within the upper and lower limits of the variables given in Eq 97. The minima are found at m_h =82%, f_h =1.91Hz, ζ_h =46% with an objective function value of 1.67e-06. Whilst the objective function is comparably low compared to the results of Table 5.3, the procedure requires 4,090,601 evaluations of the objective function

and, therefore, the grid search is more time intensive than any optimisation algorithm. The values of the grid search and Table 5.3 present comparable values to those in Chapter 2 Section 2.3.2.2 and Table 5.2 in isolation. The grid search results allow the objective function's topology to be visualised. Observing the percentage of modal mass compared to actual mass at 70%, 80%, 90% and 100%, the objective function surface concerning the natural frequency and modal damping ratio can be viewed (Figure 5.11).

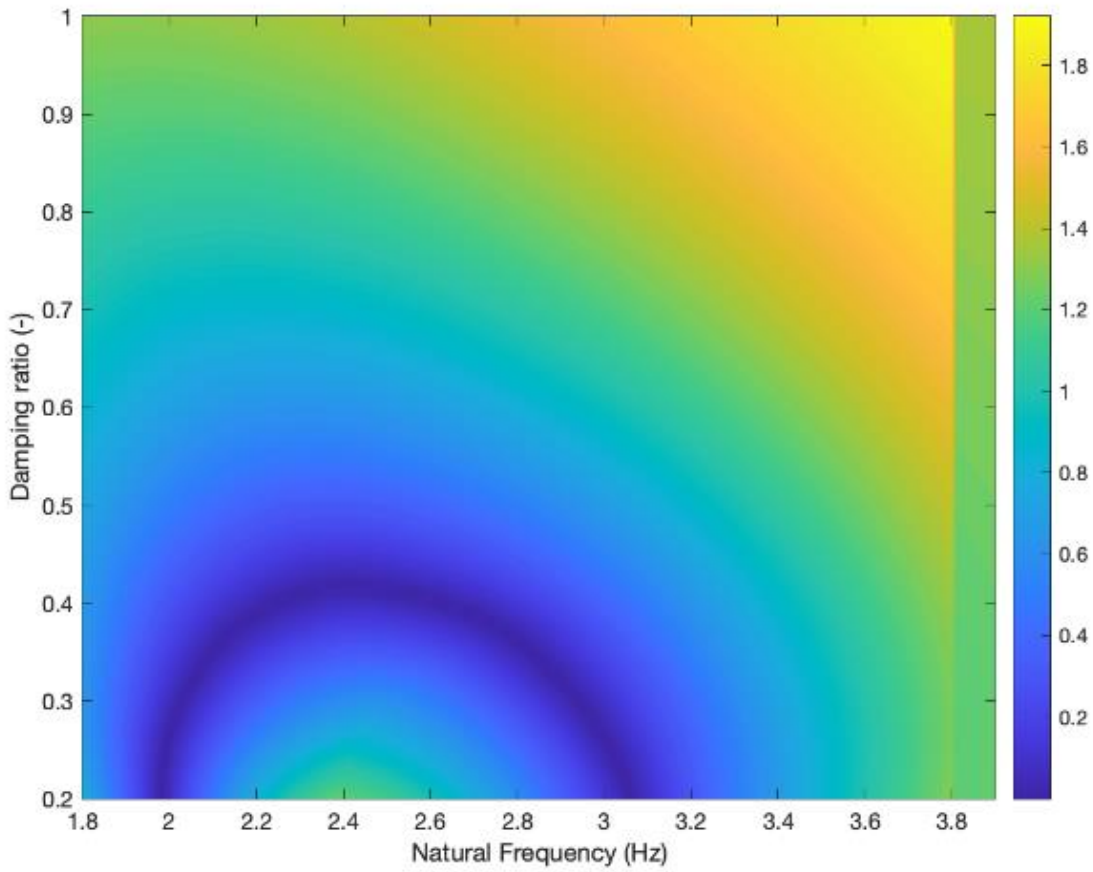

a) Objective function surface when percentage of modal mass compared to actual mass held at 70%, colours indicate Euclidean distance of mid-span acceleration comparing measured to numerical estimation

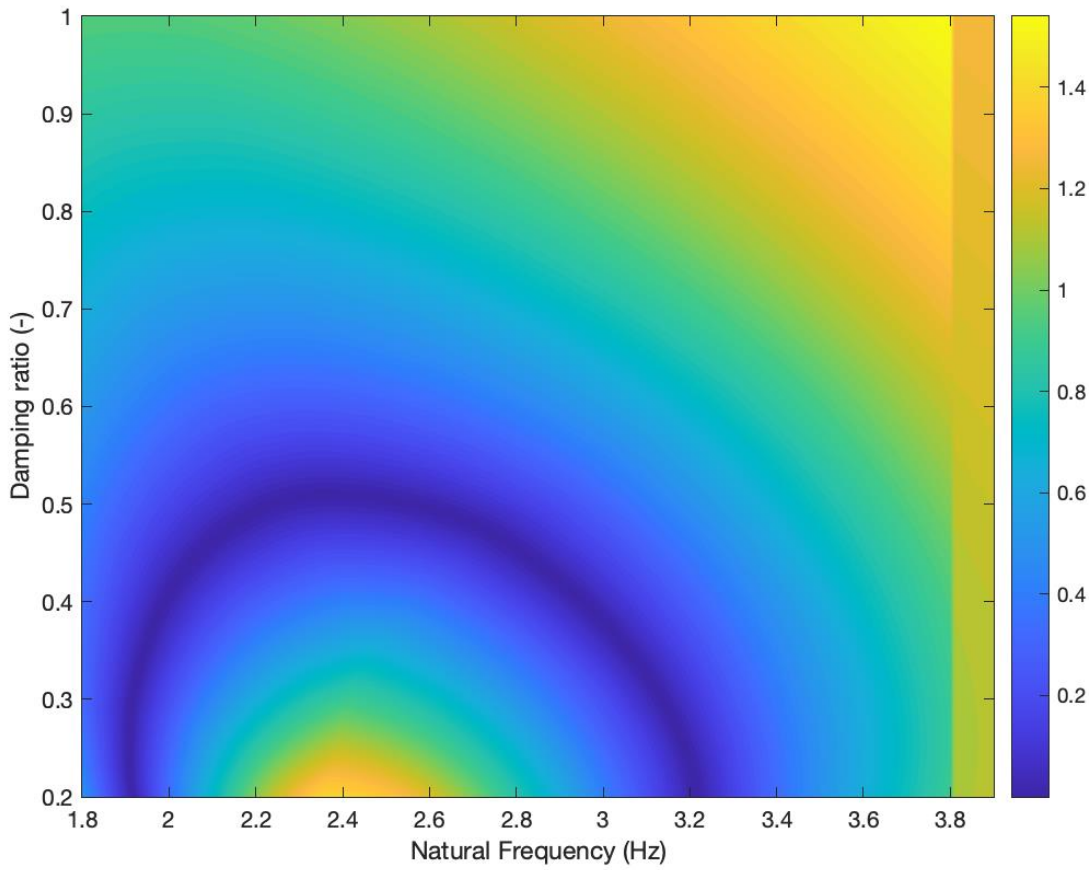

b) Objective function surface when percentage of modal mass compared to actual mass held at 80%, colours indicate Euclidean distance of mid-span acceleration comparing measured to numerical estimation

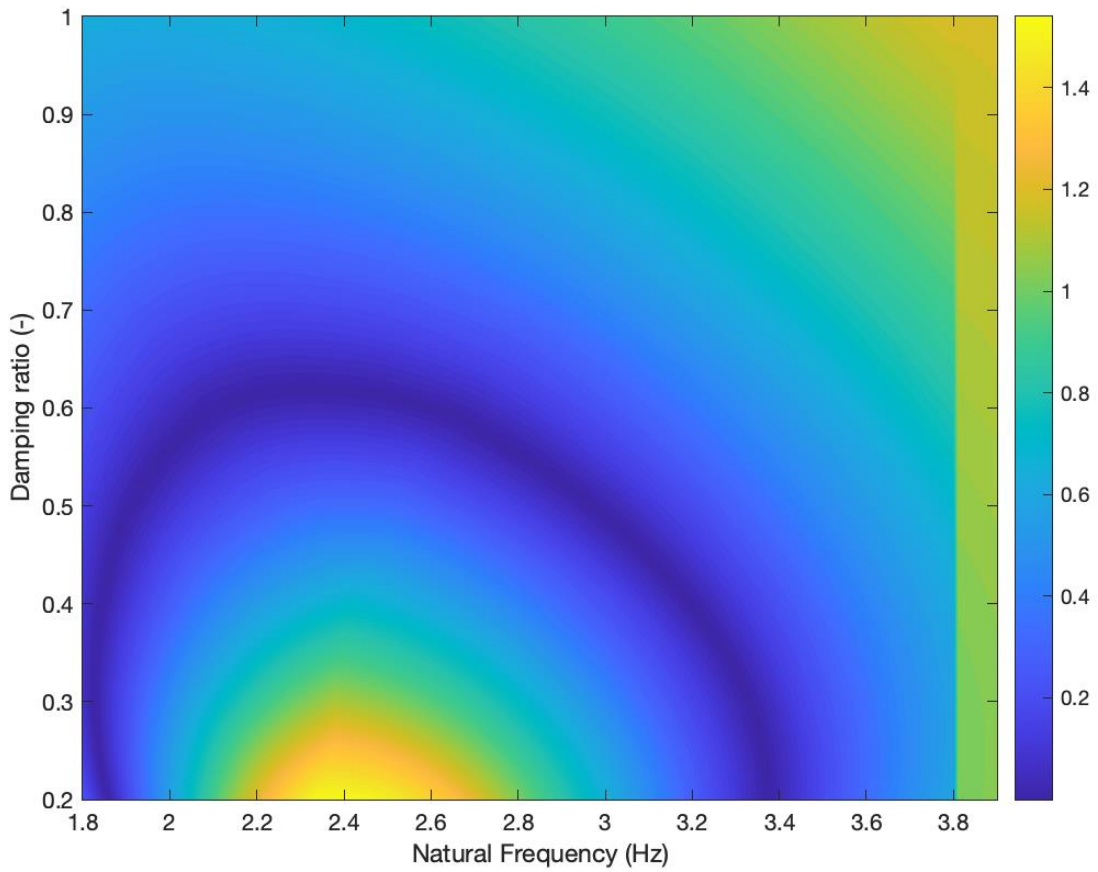

c) Objective function surface when percentage of modal mass compared to actual mass held at 90%, colours indicate Euclidean distance of mid-span acceleration comparing measured to numerical estimation

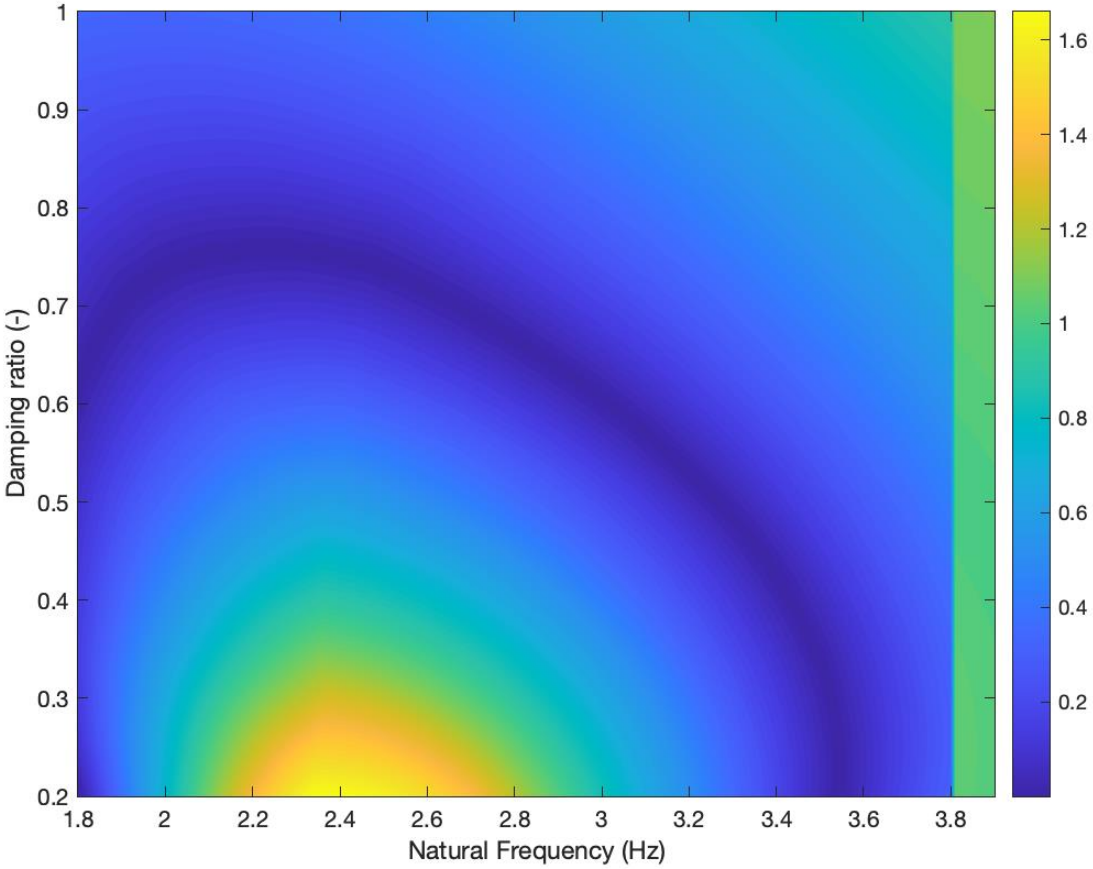

D) Objective function surface when percentage of modal mass compared to actual mass held at 100%, colours indicate Euclidean distance of mid-span acceleration comparing measured to numerical estimation

Figure 5.11: Visualisation of objective function topology for percentage of modal mass compared to actual mass at 70%, 80%, 90% and 100%, colours indicate Euclidean distance of mid-span acceleration comparing measured to numerical estimation

The colour of the figures represents the score of the objective function, with the global minimum location achieved at a zero score of the objective function. Figure 5.11 illustrates a ring of feasible solutions (low value of the objective function) that creates a valley through the variables. The darkest portions of the ring represent values within 0.04 m/s^2 of the

measured acceleration. There is no guarantee of convergence to the global minima for any of the used optimisation methods and it is evident that each algorithm finds locations of multiple local minima along the ring of possible results. Figure 5.11demonstrates that at increased percentage of modal mass compared to actual mass, the ring of feasible solutions grows in radius. The results of Figure 5.11 do not coincide well with the results seen in Table 5.2 for high percentage of modal mass compared to actual mass. From Figure 5.11 it is anticipated that the damping of the human participant should be almost double that of the recorded data. Only when lower percentage of modal mass compared to actual mass are assumed (70% and 80%) do the natural frequency and modal damping ratio converge with the published results in Table 5.2.

When a different vertical walking force is sampled from Racic et al.[52] at the same walking frequency, the optimisation results are different (Figure 5.11, Figure 5.12). The feasible range of modal damping ratio and natural frequency of the moving human appear upwards of 70% and above 3Hz, respectively. With increased percentage of modal mass compared to actual mass, the optimal set of design values increases to the upper bounds of the design variables. Therefore, the magnitude of the walking force model plays a significant role in determining the true optimal parameters. The walking force time histories are not recorded for each participant, so the walking force can only be inferred. Differences in the location of the optimal parameters occur due to the specific walking force sampled.

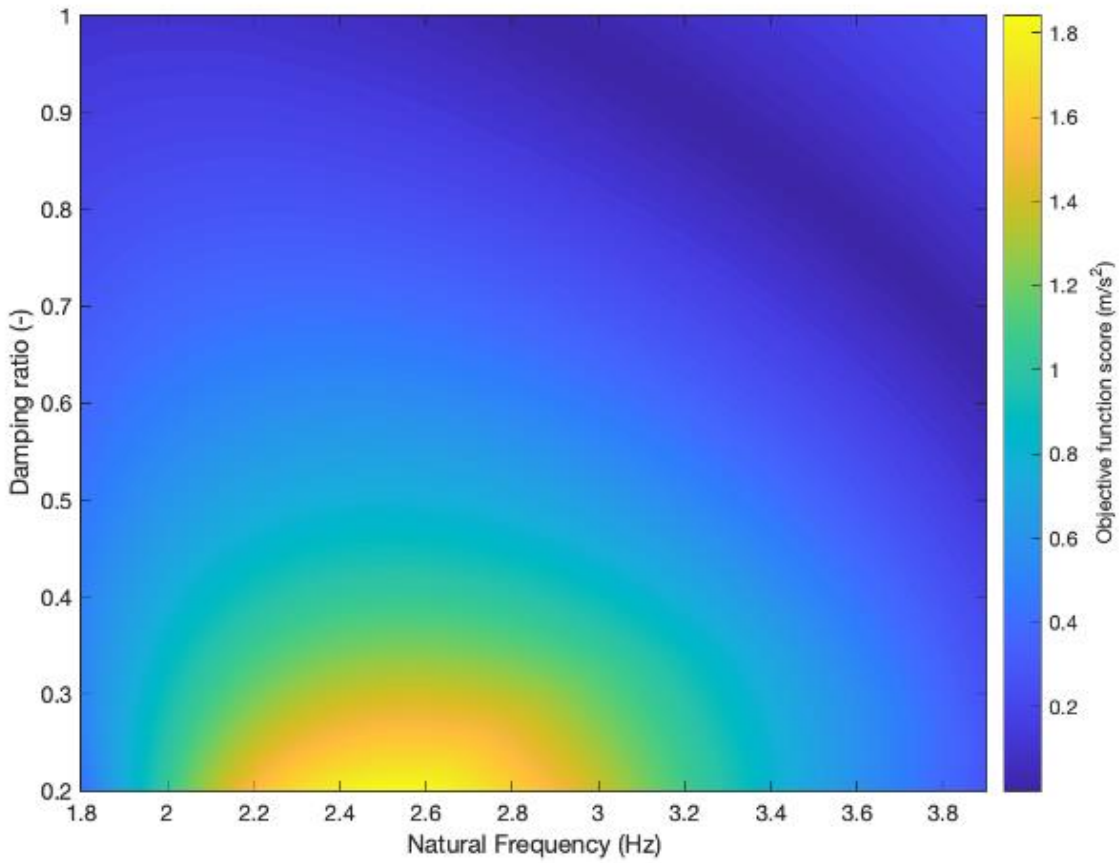

a) Objective function surface when percentage of modal mass compared to actual mass held at 70%, sample two, colours indicate Euclidean distance of mid-span acceleration comparing measured to numerical estimation

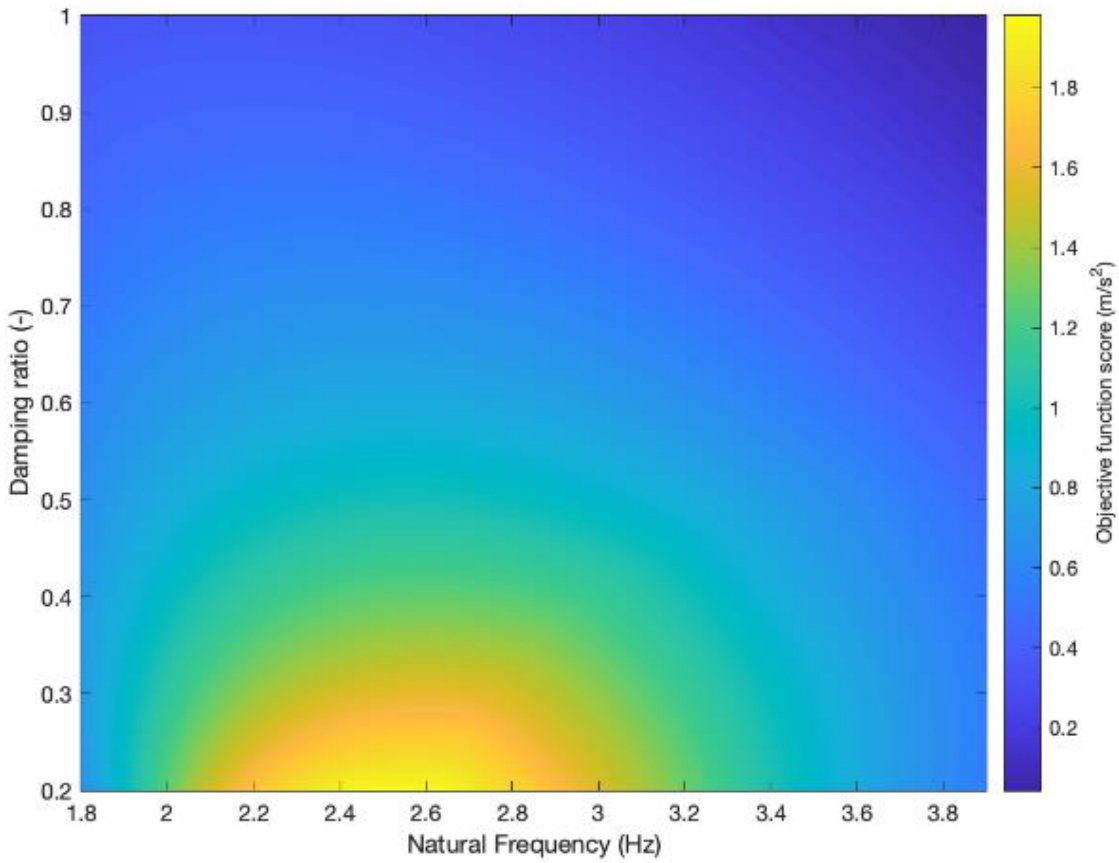

b) Objective function surface when percentage of modal mass compared to actual mass held at 80%, sample two, colours indicate Euclidean distance of mid-span acceleration comparing measured to numerical estimation

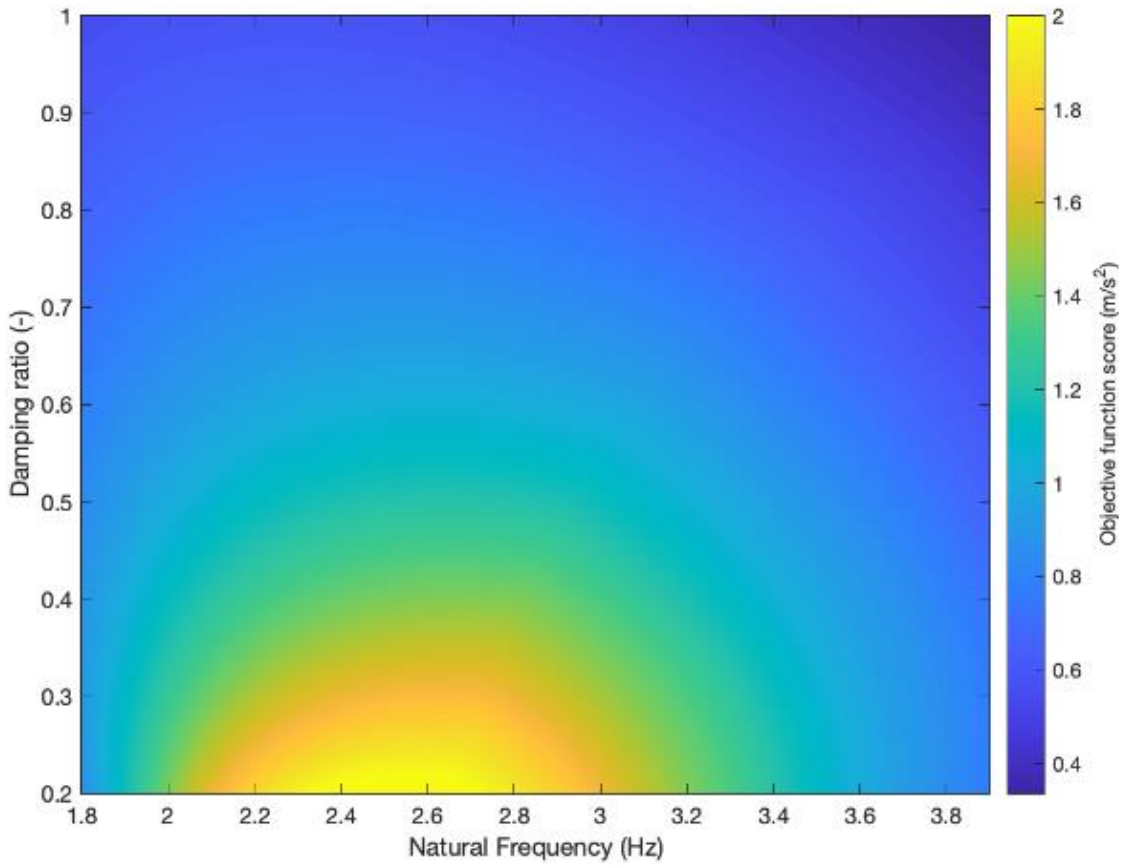

c) Objective function surface when percentage of modal mass compared to actual mass held at 90%, sample two, colours indicate Euclidean distance of mid-span acceleration comparing measured to numerical estimation

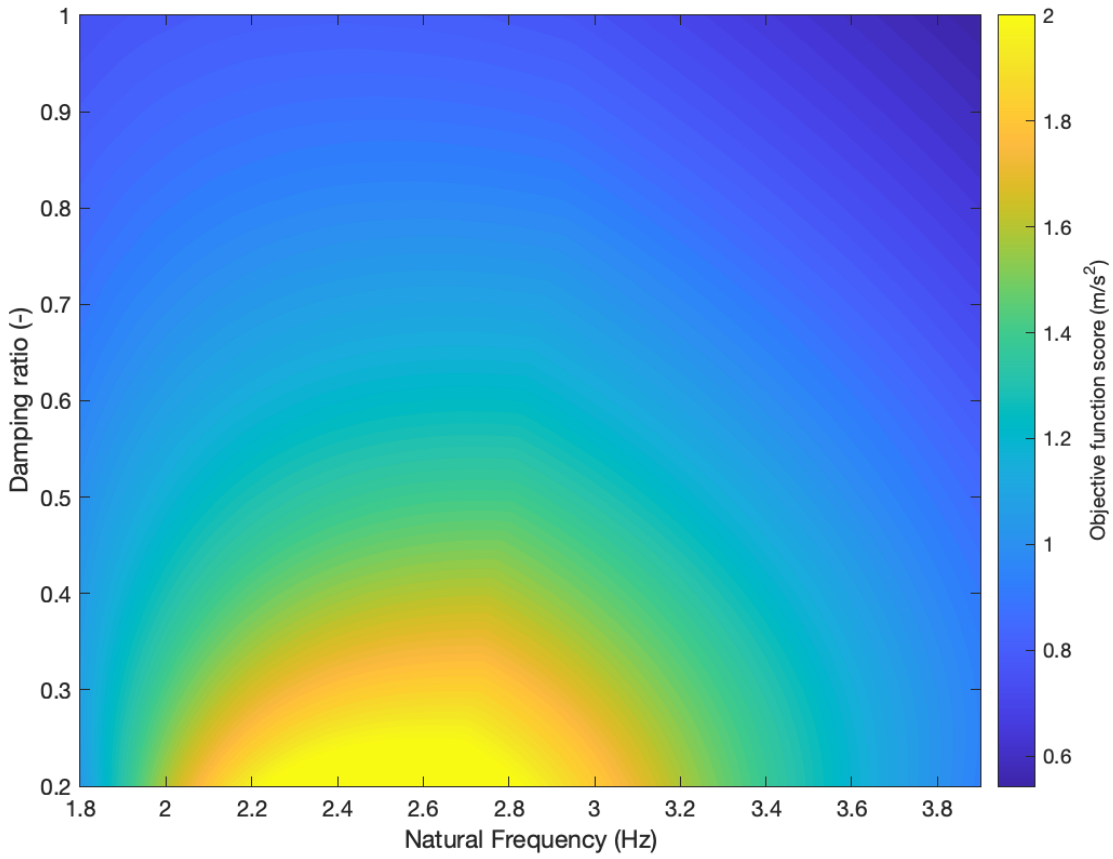

D) Objective function surface when percentage of modal mass compared to actual mass held at 100%, sample two, colours indicate Euclidean distance of mid-span acceleration comparing measured to numerical estimation

Figure 5.12: Visualisation of objective function topology for percentage of modal mass compared to actual mass at 70%, 80%, 90% and 100%, second sample walking force, colours indicate Euclidean distance of mid-span acceleration comparing measured to numerical estimation

To examine the full extent the walking force time history has on the design variables, the analysis of the 65kg participant walking at 2.5Hz, given a mid-span acceleration of 3.47 m/s^2, is compared when 100 different samples of vertical walking forces are optimised. The multi-start interior point method [256] is utilised for the analysis. Figure 5.13 illustrates the

variation of design variables due to the 100 samples. The results of each optimal design variable provide varying results, with the natural frequency varying from 1.5-4Hz. The optimisation problem is ill-poised and presents difficulty in estimating the true design parameters. The mean value of the parameters from the 100 samples is: $f_h = 2.50$Hz, $m_h = 80.64\%$, $\zeta_h = 70.67\%$. Whilst the natural frequency and percentage of modal mass compared to actual mass are within the ranges published in Chapter 2 Section 2.3.2.2, the modal damping ratio is double that of typical values seen in Chapter 2 Section 2.3.2.2. The distinct variability of each design variable, along with the associated combination, does not achieve the mean values.

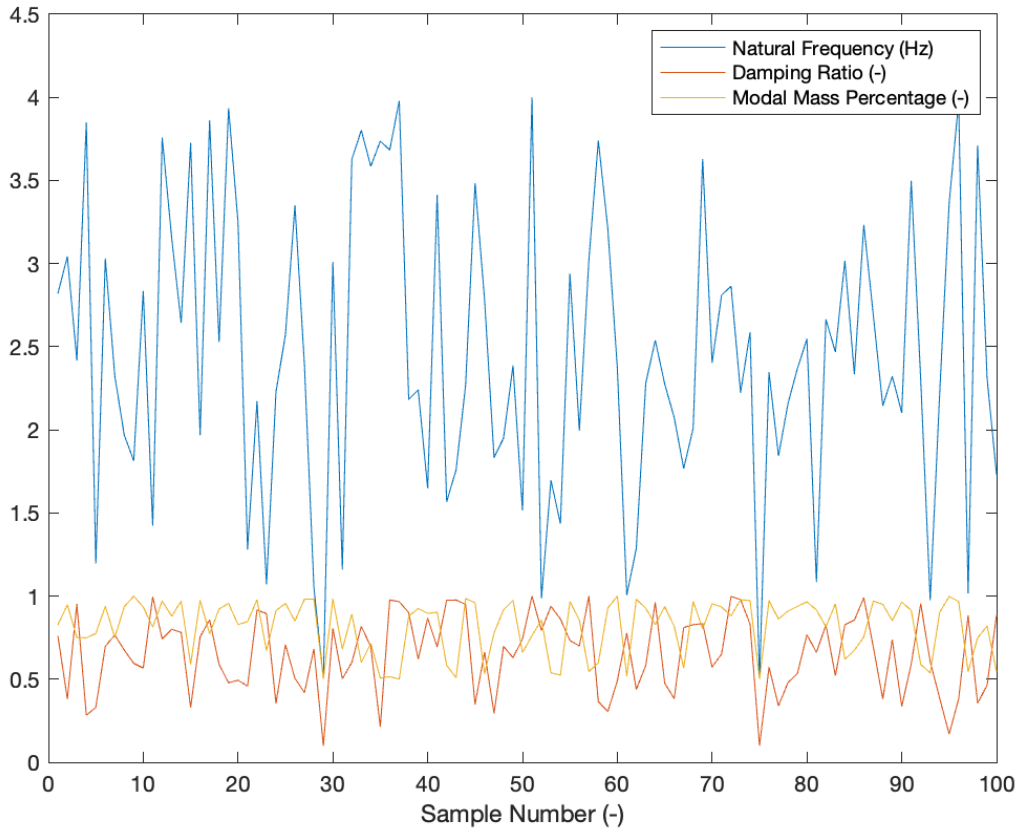

Figure 5.13: Parameter estimates of moving SDOF SMD HSI representation for 100 samples of walking force time history for a 65kg participant walking at 2.5Hz using Racic et al. [52] walking force model

To assess the validity of using the average values of the moving SDOF SMD HSI parameters, the 1s RMS acceleration is calculated for 100 sampled loads at 2.5Hz using a 65kg person, using the average SDOF SMD moving HSI parameters calculated previously. The results of this are seen Figure 5.14 compared to the measured acceleration response. Figure 5.14 demonstrates that the walking force is imperative in accurately estimating the parameters. The resultant 1s RMS acceleration will be over or under-predicted using only the average or singular values of the SDOF SMD moving HSI parameters. In the extreme case, this can be close to plus or minus 2m/s^2, over 50% under or overestimation compared to the measured

result. Whilst the average of walking force time histories compares the acceleration time history, there is a variance in the results from using the average parameters.

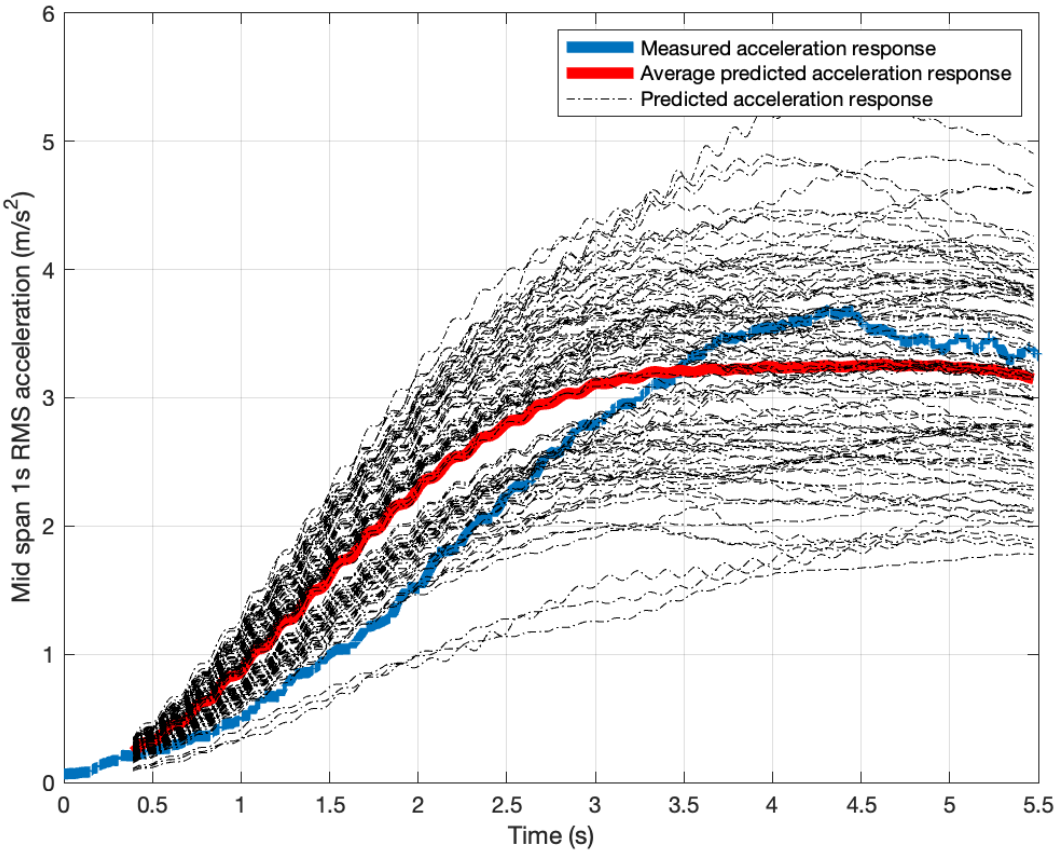

Figure 5.14: Measured acceleration response vs predicted acceleration response using average SDOF SMD moving HSI effect parameters and 100 samples of vertical walking forces of Racic et al. [52] at 2.5Hz and a 65kg mass

Combining Figure 5.13 and Figure 5.14, estimating the true design parameters is a complex issue without knowing the exact vertical walking force time histories. Without this, the predicted ranges of design parameters will likely be inherently inaccurate and provide a limitation to the thesis. The role of the walking force has seldom been explored in this

context, with previous researchers providing single deterministic values of the average SDOF SMD moving HSI parameters.

Figure 5.15 reassesses the analysis of Section 5.4 of the 76kg participants using 10 different samples of walking forces. Figure 5.15 further concluded that the vertical walking force is pivotal in the SDOF SMD moving HSI estimation. From Figure 5.15 many results provide a close estimate of the measured responses. DaSilva et al. [106] model provides a consistently poor estimation of acceleration, providing an overestimation (over double the mean value of the measured responses). The models of Ahmadi et al. [145], Shahabpoor et al. [203], Zhang et al. [204] and Matsumoto et al.[198] provide consistently close responses to the measured data across all walking force loads. All four models vary concerning each other. As such, the non-linear interaction of the modal damping ratio and natural frequency further demonstrates the non-linear topology of the objective function space. The results further conclude the importance of modelling HSI on flexible structures. When no HSI effects are modelled, the response can be over six times the measured response. The measured results are assumed to be representative of a broader sample population and it is difficult to determine if a model accurately describes the HSI effects or if the 10 measurements are statistically unlikely.

A potential limitation of the analysis is identified through the assumption of the 10 acceleration time histories being statistically representative of the global population. In the analysis of this section and others, it is assumed that the response of the recorded data is typical and representative. However, no metric or methodology exists for determining this statement unless multiple repeat experiments occur. Therefore, bias in the data may be present and skew the analysis.

At 1.5Hz and 1.9Hz walking frequencies in Figure 5.15, the variation of acceleration concerning each model is minimal at each new sample. As such, the actual value of the SDOF SMD moving HSI parameter is not essential, with all acceleration responses being within a narrow range for each new force sample. Therefore, the principal variation of

acceleration results from the different walking forces, not the SDOF SMD moving HSI parameters. There is minimal discrepancy between the non-HSI model and the other model. They are further providing evidence to suggest that at walking frequencies away from resonance, the actual accuracy of any HSI mathematical representation is more dependent on the walking force model used than the SDOF SMD moving HSI parameters. Assessing the SDOF SMD moving HSI parameters at low ratios of walking frequency to the structure's natural frequency will likely arise in multiple viable options for the SDOF SMD moving HSI parameters. Therefore, previous estimations that monitor the HSI may present errors due to the wide range of acceptable SDOF SMD moving HSI parameters for low ratios of walking to the natural frequency.

In the 1.5Hz scenario, all reference models, including the no HSI model, underestimate the acceleration response. Therefore, it is anticipated that the vertical walking force model must represent an underestimate in this scenario. Other plausible rationales are the exclusion or unknown interactive force term. The interactive force term may have increased force magnitude, resulting in an increased acceleration response.

At 2.3Hz walking frequency, the acceleration response is different concerning each modal parameters model for each walking force sample. The variation of acceleration concerning each modal parameter estimation is seen to vary significantly ($3m/s^2$, larger than any other walking frequency case). The spread of acceleration response appears to be dependent on the natural frequency of the human body. The lowest natural frequency models of Gomez et al. [217], Zhang et al. [186], Wang et al.[205] and Ahmadi et al. [145] are the only models that give an appropriate estimation of the acceleration response compared to the 76kg estimates. In a limited number of scenarios, choosing the wrong parameters can result in overestimating the acceleration response. The variation in the walking force can provide a difference in the acceleration approximation. Hence previous estimation variation may result from the variation in walking forces.

For 2.5Hz walking, including the SDOF SMD moving HSI parameter estimations is beneficial in all cases. Even when less reliable estimations such as DaSilva et al. [106] are used, the acceleration response is reduced. The parameters of all models, not including DaSilva et al. [106], provide a large variation with respect to each other. The natural frequency varies from 1.85Hz to 3.59Hz, and modal damping ratio from 12% to 52%. It is hypothesised that the diverse range may be attributed to the resonant response of the structure. As the structure undergoes resonant response, the SMD system of the human is mobilised. Therefore, force is induced in the SMD representation. This ingress of the resonant frequency causes a forcing frequency on the SMD system. The resonant walking assumption of the human SMD system's natural frequency may only result from the forcing frequency induced into the system and not a resonant mode of the human body.

Furthermore, the variation in SMD parameters at resonance may principally be the result of variations in walking force amplitude each human exerts and not the variation of the human parameters. As demonstrated in Section 5.5.1, multiple combinations of parameters satisfy the problem at a given walking force. Therefore, the assessment of the parameters may have been historically misrepresented as the variation in vertical forces. A meaningful estimation of the SDOF SMD moving HSI parameters can be achieved only by knowing the exact walking force time history. Otherwise, the estimation of the SDOF SMD moving HSI parameter may represent the effect of the perturbation of the walking force, which at a resonant response can be produce a variety of over and underestimations.

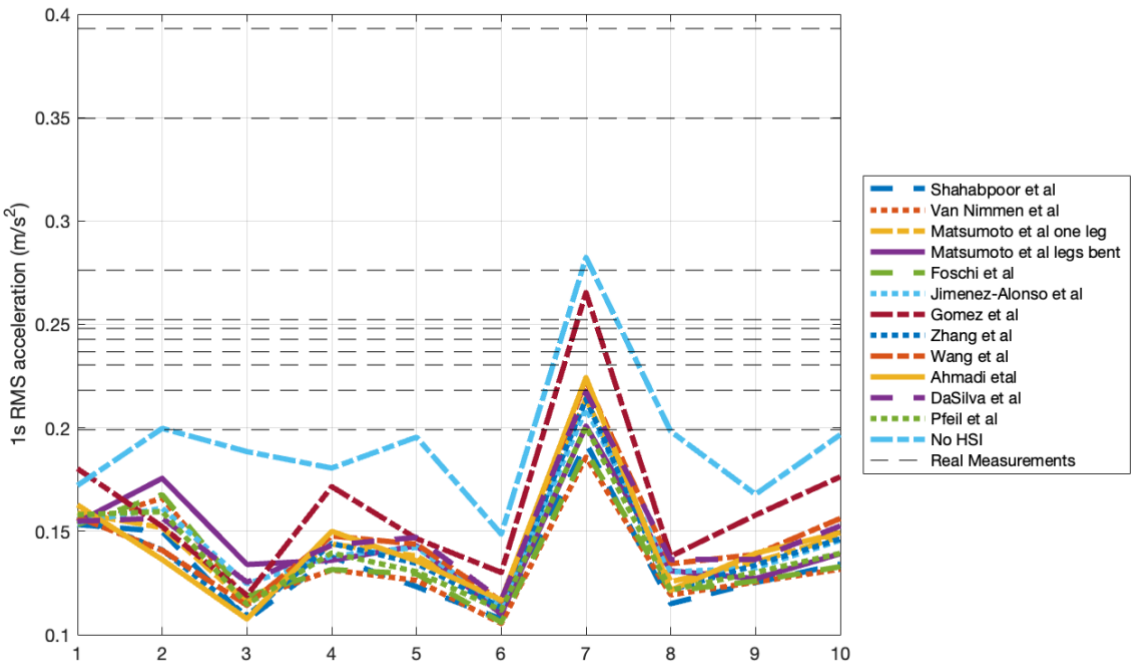

a) Max 1s RMS mid-span acceleration of 76Kg participants walking at 1.5Hz using various SDOF SMD moving HSI parameters and sampled walking force time histories compared to measured results

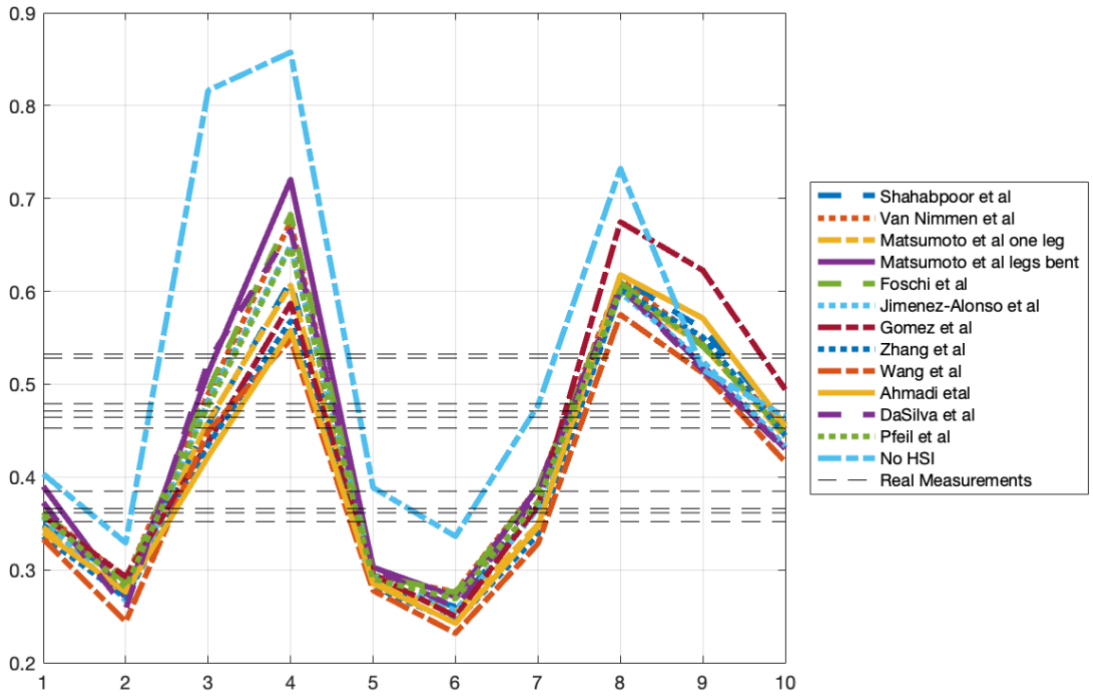

b) Max 1s RMS acceleration of 76Kg participants walking at 1.9Hz using various SDOF SMD moving HSI parameters and sampled walking force time histories compared to measured results

b)

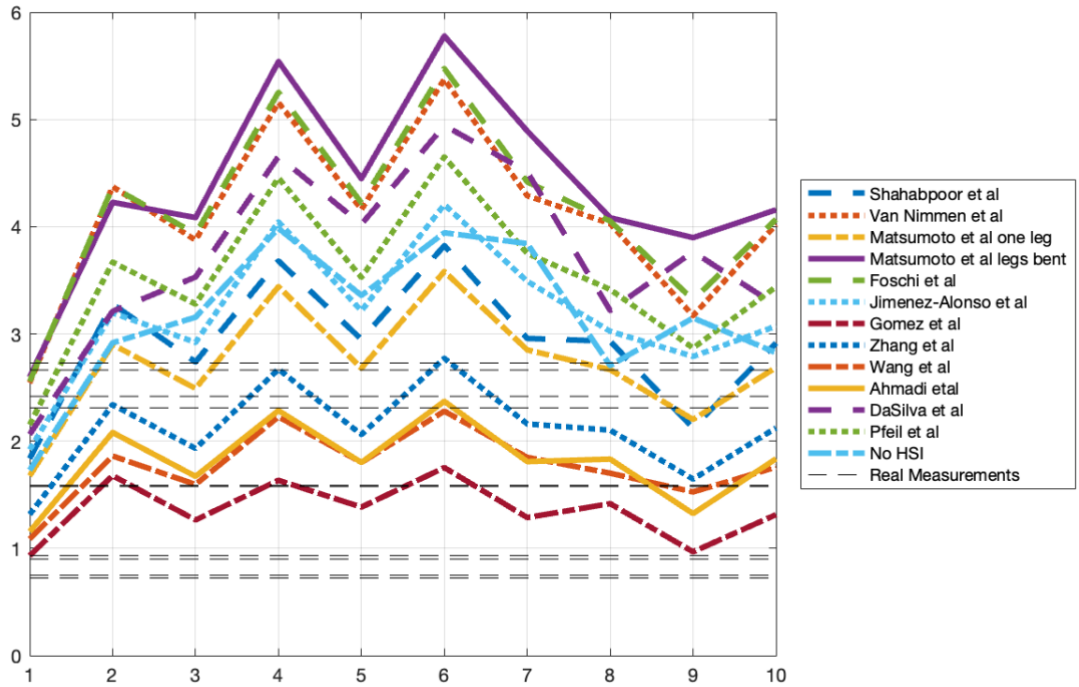

c) Max 1s RMS acceleration of 76Kg participants walking at 2.3Hz using various SDOF SMD moving HSI parameters and sampled walking force time histories compared to measured results

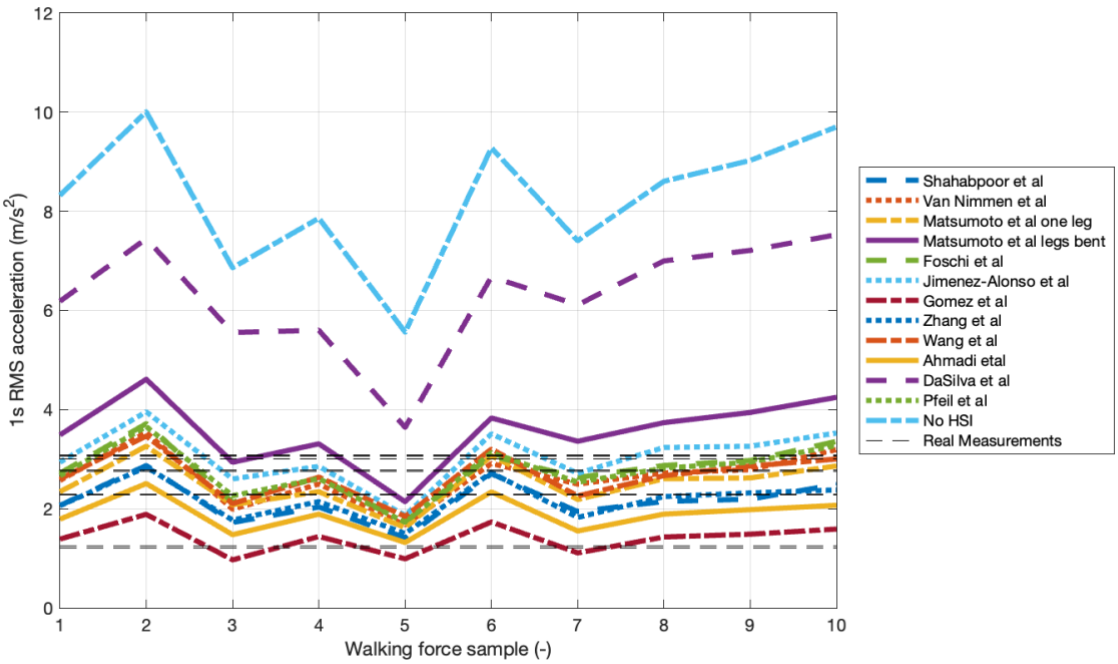

d) Max 1s RMS acceleration of 76Kg participants walking at 2.5Hz using various SDOF SMD moving HSI parameters and sampled walking force time histories compared to measured results

Figure 5.15: Max 1s RMS acceleration of 76Kg participants walking at 1.5Hz, 1.9Hz, 2.3Hz and 2.5Hz using various SDOF SMD moving HSI parameters and sampled walking force time histories

From Section 5.5.1 the best optimisation method, with respect to minimising the difference between predicted and actual acceleration of the GFRP bridge, is a trade-off of the interior point method and its multi-start variation. A compromise of 5 multi-start positions will be used in the proceeding section to allow for sufficient accuracy of the objective function, whilst also not taking more abundant computational time. Through the analysis of the optimisation methods, it is evident that many possible combinations and local minima of the objective function exist, therefore, consistent convergence to a common value is unlikely to occur. The precise estimate of each parameter is further complicated by not knowing the exact vertical walking force. The present section demonstrates that the predicted optimal

SDOF SMD moving HSI variables can vary for different samples of the same walking frequency, leading to an ill-poised optimisation problem. The unknown walking force time history also showed variations in the objective function topology.

Due to the lightweight nature of the structure, coupled with the close match in the first vertical bending mode and higher pacing walking frequencies. The acceleration response due to a resonant matching of the walking frequency and the natural frequency of the first vertical bending mode can be large in magnitude, in some instances reaching 50% of gravity. Therefore, any variation in the DLF value or other spatiotemporal parameters of walking can change the acceleration response of the structure. Furthermore, as seen in this subsection, the acceleration responses are contingent on the DLF of the first harmonic of walking. A 4m/s^2 variation in RMS acceleration response is seen purely based on the variation of DLF one at the resonant mode and walking frequency. This therefore may provide an obstacle in determining the precise SDOF SMD moving HSI parameters of the SDOF SMD representation of the moving human. Due to the precise walking force not being known for each of the crossings, the estimation of the SDOF SMD moving HSI parameters maybe inaccurate. Therefore, assuming 100 different samples of the vertical walking force for each crossing may provide a misguided estimate of the real SDOF SMD moving HSI parameters when the exact walking force is unknown. The results of this chapter could therefore be improved upon via determining the precise vertical walking force inclusive of the interactive walking term. This could be achieved through an insole measurement of the vertical walking force, however this is not performed in the PhD and serves as a limitation of the study.

5.5.2 Results of SDOF SMD moving HSI parameters estimated through inverse analysis of flexible GFRP bridge

Using the inverse method outlined in Section 5.5.1, the predicted design variables are assessed for all 448 acceleration time histories. For each of the 448 acceleration time

histories, the walking force is sampled 10 times from the model of Racic et al. [52]. The distribution of the results as a whole and for each crossing are compared to estimate if any dependent relationships occur. The results are separated into each design variable. Section 5.5.2.1 considers the average natural frequency of the moving human, whilst Section **Error! Reference source not found.** and Section 5.5.2.3 consider the average percentage of modal mass compared to actual mass and average modal damping ratio, respectively.

5.5.2.1 Average Natural Frequency

Table 5.4 provides the mean value of the average natural frequency at each walking frequency for all sampled walking forces. The results do not offer a unique consensus of the average natural frequency. Unlike Wang et al. [205], no walking frequency-dependent behaviour is exhibited. However, dependency or non-dependence is challenging, with only four distinct walking frequencies.

Table 5.4: Mean value of average natural frequency of moving participant

	Walking frequency			
	1.5Hz	1.9Hz	2.3Hz	2.5Hz
Mean (Hz)	2.455	1.727	1.997	2.506

Figure 5.16 provides the histogram of all values of the average natural frequency of the moving participants considering all samples. At 2.5Hz walking frequency, a clear peak in the result is seen at 2.5Hz. The result appears to form a symmetric distribution on either side of the peak. 1.5Hz walking produces a similar distribution to 2.5Hz walking. However, a cluster of results can be seen at the upper and lower limit of the design variable at 1.5Hz walking frequency. Such a distribution is not the actual prediction of the optimisation but the limits of the possible range of the parameters. Therefore, the mean of results for 1.5Hz walking frequency will be skewed due to the unnatural results predicted at the variable boundary. The

distribution of results for 1.9Hz walking in Figure 5.16b provides no meaningful insight, with a proportion of the development skewed to the lower limit of 0.5Hz. The remaining distribution of the result of 1.9Hz walking is erratic and does not provide a clear preferred value.

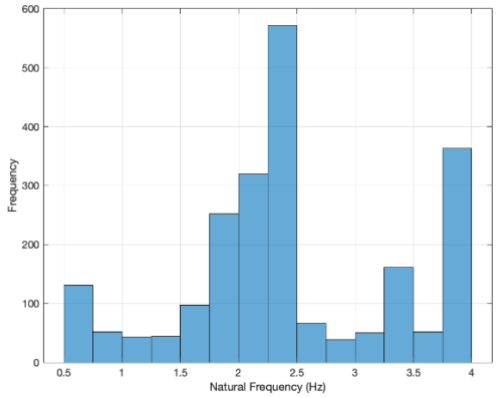

a) The average natural frequency of all moving participants at 1.5Hz walking frequency

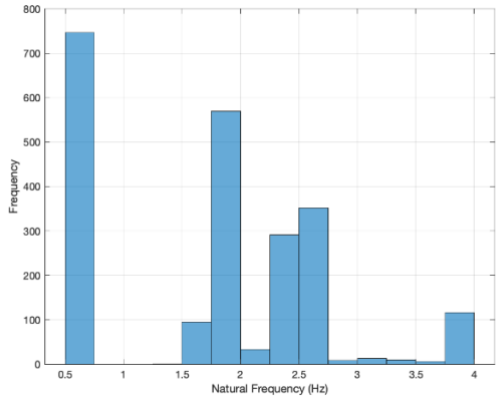

b) The average natural frequency of all moving participants at 1.9Hz walking frequency

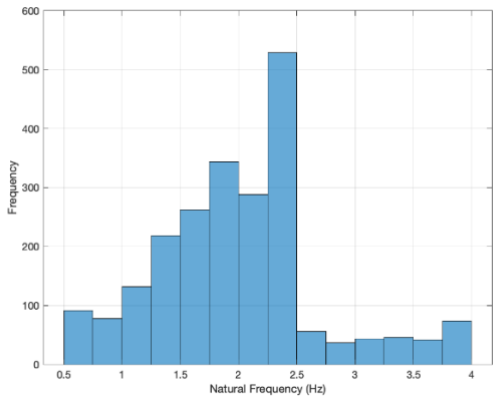

c) The average natural frequency of all moving participants at 2.3Hz walking frequency

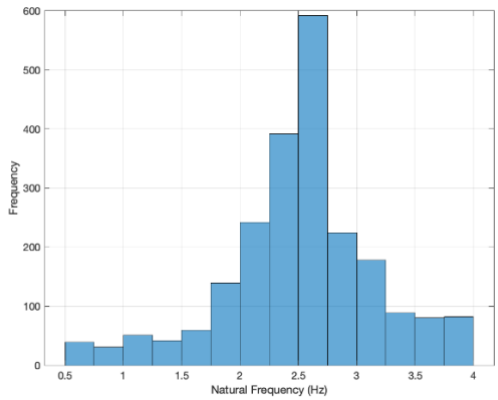

d) The average natural frequency of all moving participants at 2.5Hz walking frequency

Figure 5.16: Histogram of average natural frequency of moving participants at 1.5Hz, 1.9Hz, 2.3Hz, 2.5Hz walking frequencies, bin widths are set to 0.25Hz increments, all samples

When the mean value of the natural frequency is taken over all 10 samples for each walking occurrence, the successive distributions of each natural frequency become more established. Figure 5.17 exhibits a smaller variance of results compared to its Figure 5.16 counterparts. Furthermore, the cluster of results at either end of the natural frequency limits is absent in the average responses. The variation in walking force used for each sample provides a variation in mean natural frequency compared to the average response.

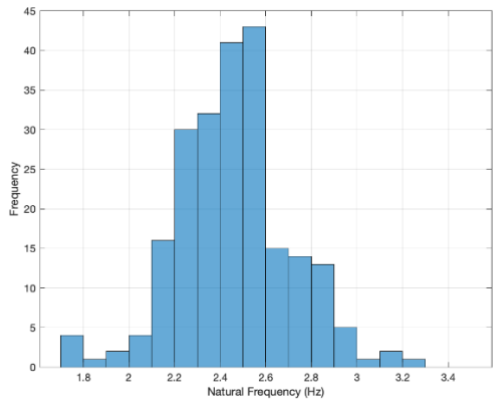

a) The mean result of the average natural frequency of moving participants at 1.5Hz walking frequency

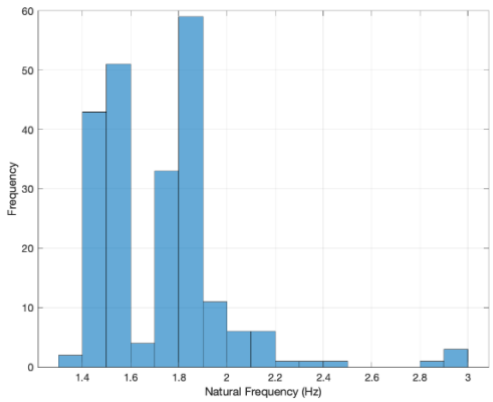

b) The mean result of the average natural frequency of moving participants at 1.9Hz walking frequency

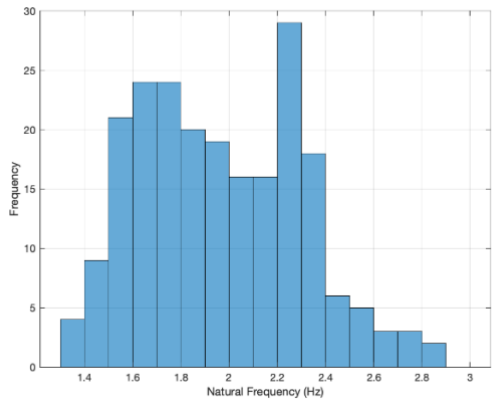

c) The mean result of the average natural frequency of moving participants at 2.3Hz walking frequency

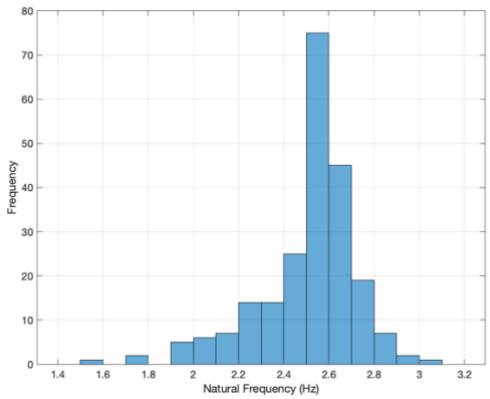

d) Mean result of the average natural frequency of moving participant at 2.5Hz walking frequency

Figure 5.17: Histogram of mean average natural frequency of moving participants at 1.5Hz, 1.9Hz, 2.3Hz, 2.5Hz walking frequencies, bin widths are set to 0.1Hz increments, mean of samples

Two major limitations of the natural frequency results are the lack of known walking force and the use of only 4 different walking frequencies. Whilst authors such as Ahmadi et al. [145] hypothesise the natural frequency of the moving human to be the resonant walking frequency, this chapter's results provide split observations. Whilst 1.5Hz and 2.5Hz walking frequencies produce the natural resonant frequency, the other walking frequencies do not. The magnitude of the mean values (Table 5.4) is comparable to those in Chapter 2 Section 2.3.2.2and Table 5.2. Whilst the unknown walking force provided a barrier to accurate results, the optimal values found are in close consensus with previously reported values.

5.5.2.2 Percentage of modal mass compared to actual mass

Table 5.5 presents the mean value of the average percentage of modal mass compared to actual mass for each walking frequency. The 1.5Hz, 2.3Hz, and 2.5Hz provide a consistent range of results, with 1.9Hz walking providing an outlier.

Table 5.5: Mean value of average percentage of modal mass compared to actual mass of moving participant

	Walking frequency			
	1.5Hz	1.9Hz	2.3Hz	2.5Hz
Mean (%)	86.1	59.3	85.0	87.7

Figure 5.18 further illustrates the consistent results of 1.5Hz, 2.3Hz and 2.5Hz walking frequencies. As anticipated from Chapter 2 Section 2.3.2.2, the results will be skewed towards 100% percentage of modal mass compared to actual mass in keeping with the previous results found in the literature. Whilst some researchers have published lower values of percentage of modal mass compared to actual mass (Chapter 2 Section 2.3.2.2), few provide a distribution of values. The results of 1.5Hz walking are likely skewed by a number of results at the lower boundary of 50%. 1.9Hz walking provides no consensus on the parameter, with a bimodal distribution of results peaked at either boundary limit. A variety of rationale can be attributed to the distribution, such as finding multiple local minima or participants not walking at the prescribed pace. In all cases but 1.9Hz walking pace, the results indicate that the mode of the results is 100% of percentage of modal mass compared to actual mass.

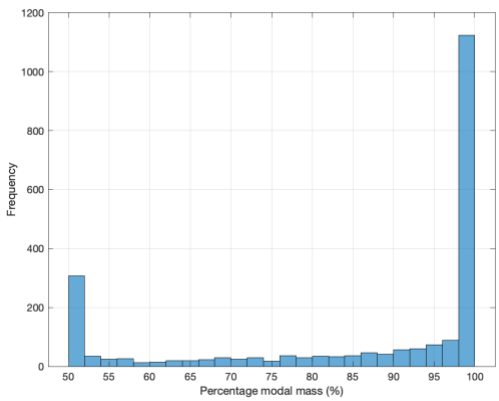

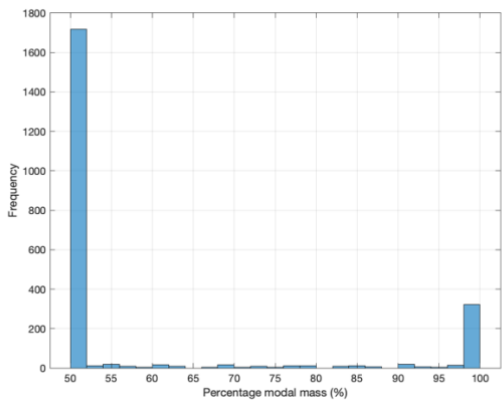

a) Average percentage of modal mass compared to actual mass of moving participant at 1.5Hz walking frequency

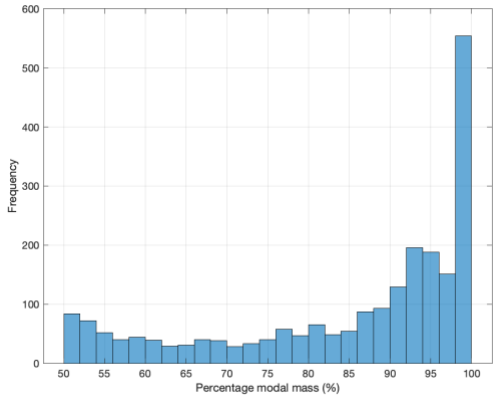

b) Average percentage of modal mass compared to actual mass of moving participant at 1.9Hz walking frequency

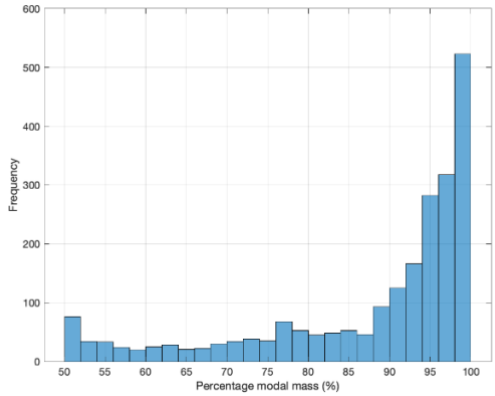

c) Average percentage of modal mass compared to actual mass of moving participant at 2.3Hz walking frequency

d) Average percentage of modal mass compared to actual mass of moving participant at 2.5Hz walking frequency

Figure 5.18: Histogram of average percentage of modal mass compared to actual mass of moving participants at 1.5Hz, 1.9Hz, 2.3Hz, and 2.5Hz walking frequencies. Bin widths are set to 2% increments, all samples

The mean results for each participant over the 10 samples (Figure 5.19) provide a differing picture in all walking frequency cases compared to the all-sample distribution (Figure 5.18). The distribution of the mean of each sample observes fewer extreme data points and is more closely distributed around the respective mean of all the results seen in Table 5.5. The results of Figure 5.19 indicate that the exact value of percentage of modal mass compared to actual mass is a continuum and not one distinct value. Figure 5.19c) illustrates a uniform distribution of results from 64%-98%. The values of Figure 5.19 are comparable to previously published results in Chapter 2 Section 2.3.2.2 and Table 5.2. Matsumoto [184,202] and Jimenez-Alonso et al.[189] both provide similar mean results consistent with 1.5Hz, 2.3Hz and 2.5Hz, however, not all researchers considered percentage of modal mass compared to actual mass in their respective optimisation procedures. The like-for-like

comparison is complex, with most researchers favouring 100% or a specific mass [158]. 1.9Hz walking produces different results from the other three walking frequencies.

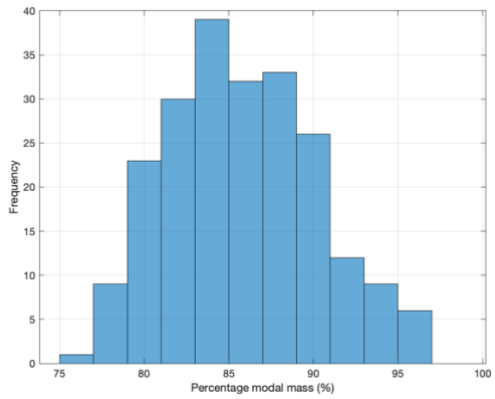

a) Average percentage of modal mass compared to actual mass of moving participant at 1.5Hz walking frequency

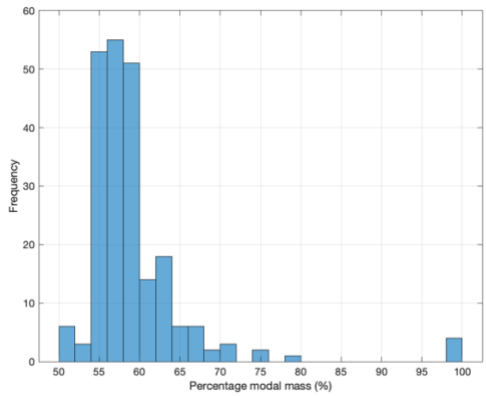

b) Average percentage of modal mass compared to actual mass of moving participant at 1.9Hz walking frequency

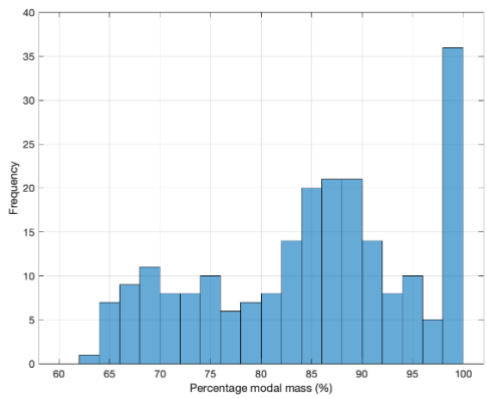

c) Average percentage of modal mass compared to actual mass of moving participant at 2.3Hz walking frequency

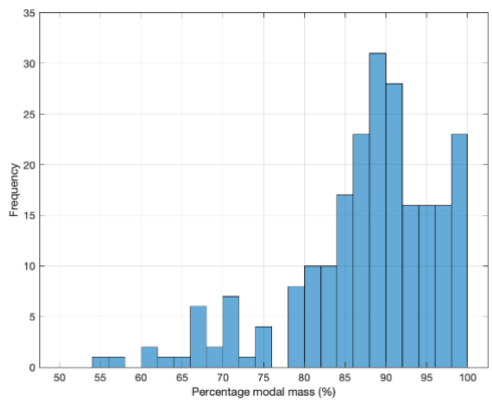

d) Average percentage of modal mass compared to actual mass of moving participant at 2.5Hz walking frequency

Figure 5.19: Histogram of average percentage of modal mass compared to actual mass of moving participants at 1.5Hz, 1.9Hz, 2.3Hz, 2.5Hz walking frequencies, bin widths are set to 2% increments, mean of samples

The mean percentage of modal mass compared to actual mass values seen in Table 5.5 for 1.5Hz, 2.3Hz and 2.5Hz provide consistent results with previous research, however, the three distributions of results of the mean sample values provide inconsistent distributions concerning each other. The results range from 60% to 100% percentage of modal mass compared to actual mass. Representing the data through the first-moment statistics or modal value can provide a biased view of the data. There appears to be no visual interpretation of a walking frequency-based dependency on the parameters. It is worth noting that the lack of diversity of the walking frequencies inhibits any meaningful data analysis of this dependent relationship.

5.5.2.3 Modal Damping Ratio

Table 5.6 presents the mean value of the average modal damping ratio for each walking frequency. The 1.5Hz, 2.3Hz and 2.5Hz provide a consistent range of results, with 1.9Hz walking providing a consistent outlier for all three design variables.

Table 5.6: Mean value of the average modal damping ratio of moving participant

	Walking frequency			
	1.5Hz	1.9Hz	2.3Hz	2.5Hz
Mean (%)	29.1	12.3	39.9	44.4

The results of Figure 5.20 provide inconclusive results. All the distributions of results, including all samples, offer a peak of results at the lower limit of the modal damping ratio. Thus, this value is obtained as it is the system boundary for this design variable and is not a true value. The consequence of the modal value of the data being 10% modal damping ratio results in a bias in the modal damping ratio seen in Table 5.6. The distribution of the results

remains approximately uniform, away from the upper and lower limits of the design variable. However, such a result is inconsistent with previously published results (Chapter 2 Section 2.3.2.2 and Table 5.2).

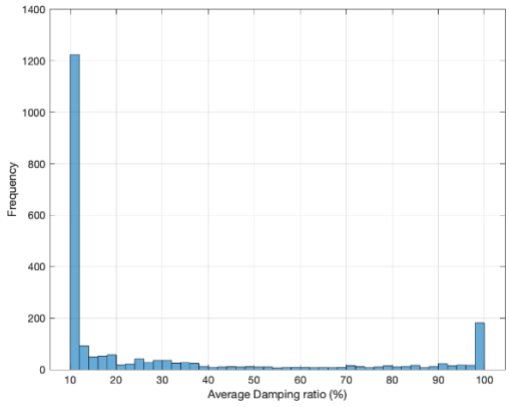

a) The average modal damping ratio of moving participants at 1.5Hz walking frequency

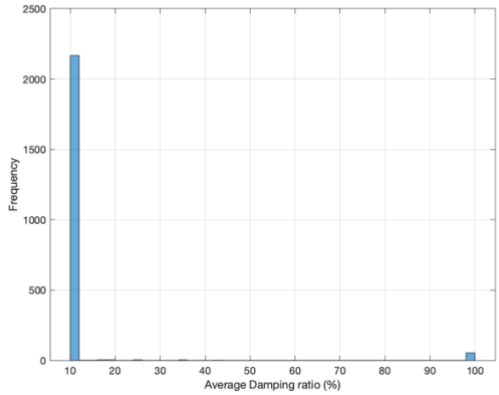

b) The average modal damping ratio of moving participants at 1.9Hz walking frequency

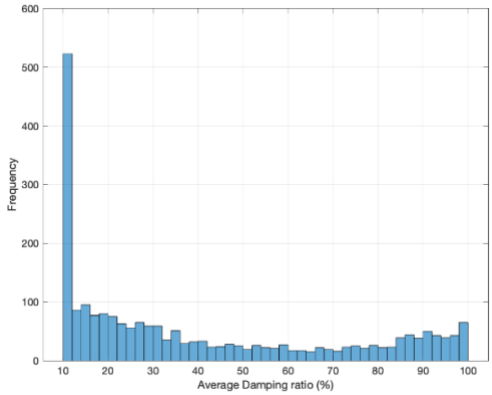

c) The average modal damping ratio of moving participants at 2.3Hz walking frequency

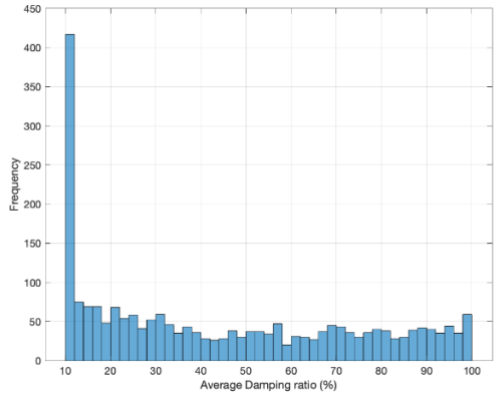

d) The average modal damping ratio of moving participants at 2.5Hz walking frequency

Figure 5.20: Histogram of the average modal damping ratio of moving participants at 1.5Hz, 1.9Hz, 2.3Hz, and 2.5Hz walking frequencies. Bin widths are set to 2% increments and all samples

Figure 5.21 provides the distributions of the mean values of the modal damping ratio over each walking case. Again, the values for 1.9Hz provide a peculiar distribution of results with a prominent peak at the system boundary. Therefore, using the mean of the results offers misinformed parameter statistics.

Figure 5.21 c) and d) provide a consistent response concerning each other, although, the results do not form any known distribution of results. Whilst the mean values are 39.88% and 44.38%, respectively, both exhibit a modal value of 10%, aligning with the system boundary, both values of the mean are skewed by the system limits. Previous researchers favour a normal distribution of results [174,203]. The mean results of Table 5.6 provide higher values for of the modal damping ratio for 2.3Hz walking and 2.5Hz than any results in Chapter 2 Section 2.3.2.2or Table 5.2. The mean results of 1.5Hz and 1.9Hz, whilst both provide a close estimation of previously published results, are skew by the system boundary result. The modal damping ratio results provide a broad range, unlike any seen in research thus far.

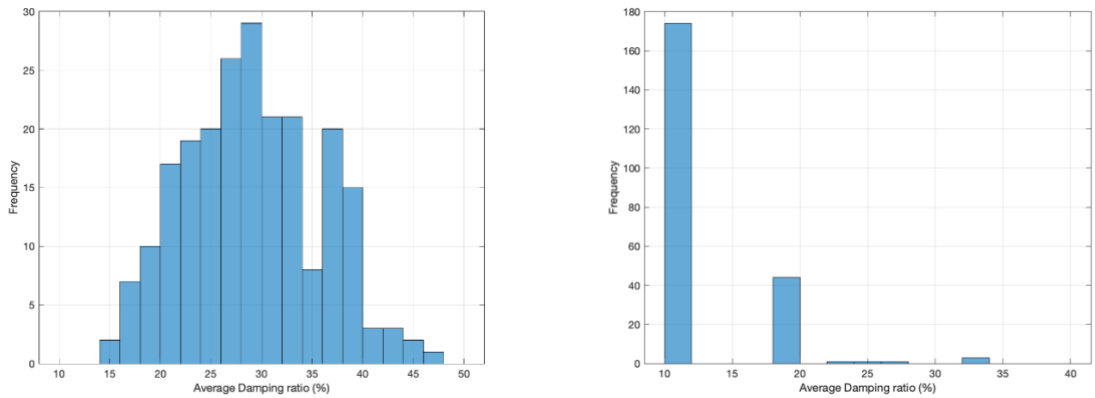

a) The average modal damping ratio of moving participants at 1.5Hz walking frequency

b) The average modal damping ratio of moving participants at 1.9Hz walking frequency

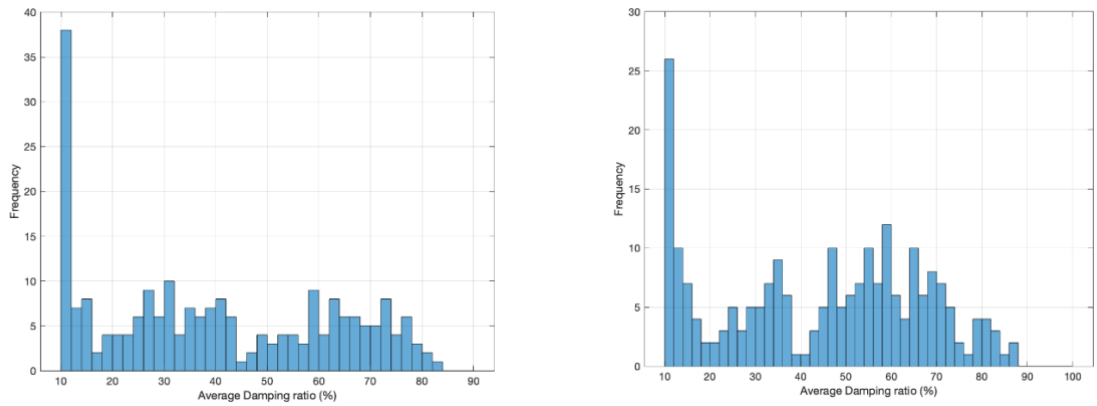

c) The average modal damping ratio of moving participants at 2.3Hz walking frequency

d) The average modal damping ratio of moving participants at 2.5Hz walking frequency

Figure 5.21: Histogram of the average modal damping ratio of moving participants at 1.5Hz, 1.9Hz, 2.3Hz, and 2.5Hz walking frequencies. Bin widths are set to 2% increments, mean of samples

Toso et al.[54], Pfeil et al. [214] and DaSilva et al. [106] all propose relationships of mass to modal damping ratio, however, Figure 5.22 provides little evidence to support any relationship. The data methodology of collection or optimisation have produced different results. Toso et al. [54] proposes a correlation coefficient of 0.4 for the mass-to-damping value, thus indicating a positive linear relationship of the mass to damping, however, Figure 5.22 provides a correlation value of 0.05, exhibiting no linear dependent behaviour. Like the present study, Pfeil et al. [214] obtained a mass-to- modal damping ratio correlation value of 0.02. DaSilva et al. [106] conversely establishes a correlation value of mass to damping value of 0.11 and a percentage of modal mass compared to actual mass to damping value of 0.9.

The aforementioned authors used the same methodology to establish the human and mechanical parameters, yet all provided seemingly different correlation values.

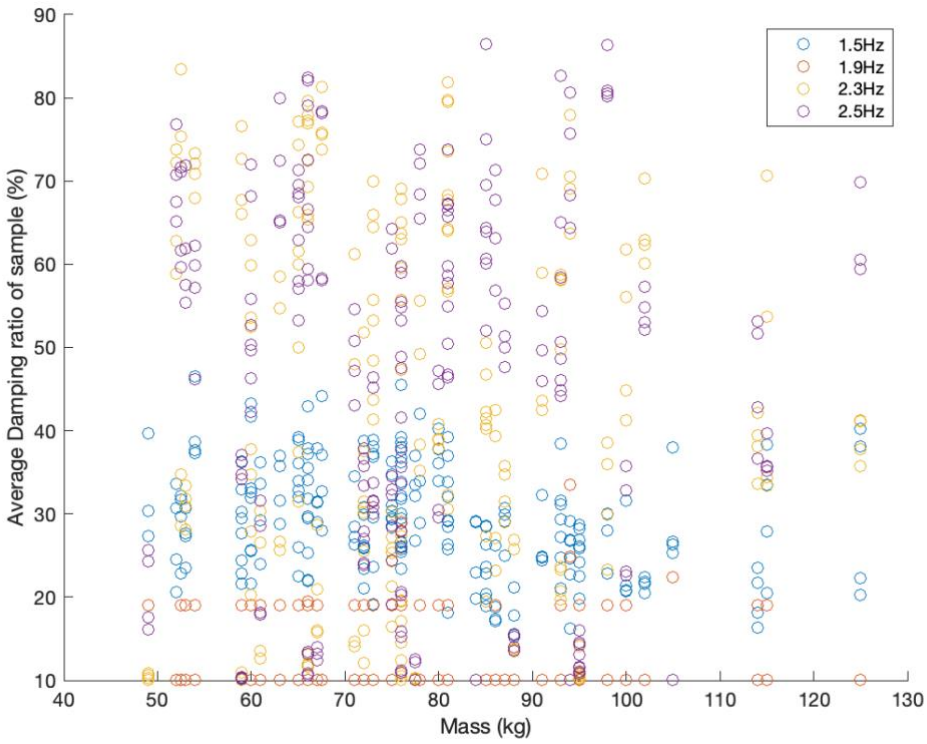

Figure 5.22: Mass of participants versus predicted modal damping ratio for all walking frequencies

5.5.2.4 Comparison of estimated SDOF SMD moving HSI parameters to measured data

The proceeding subsection provides a similar analysis to Section 5.4, although, only considering the parameter estimates of Section 5.5.2. The same assumptions regarding mass and walking frequency are used in Section 5.4. The mean values of each parameter are used based on the results found in Table 5.4, Table 5.5 and Table 5.6. Figure 5.23 visually represents the 1s RMS acceleration for each walking frequency.

For 1.5Hz walking, the average values of parameters result in an underestimation of the 1s RMS acceleration, however, the actual magnitude of the measured acceleration compared to predicted is significantly small that the effects of HSI can be ignored. This is evidenced Figure 5.7 when all values of the HSI produce a response likened to the non-HSI effects model. The acceleration responses for the average parameters are similar to that of Figure 5.7. To say one model is better than another at such low interactions of HSI effects (Section 5.3) is difficult to conclude.

The acceleration responses of 1.9Hz average walking parameters vary with each new walking force sample. The mean responses of each sample produce both an over and underestimate of the acceleration response. As described in Section 5.5.2, 1.9Hz provides difficulty in the optimisation procedure, resulting in unreliable estimates of the SDOF SMD moving HSI parameters.

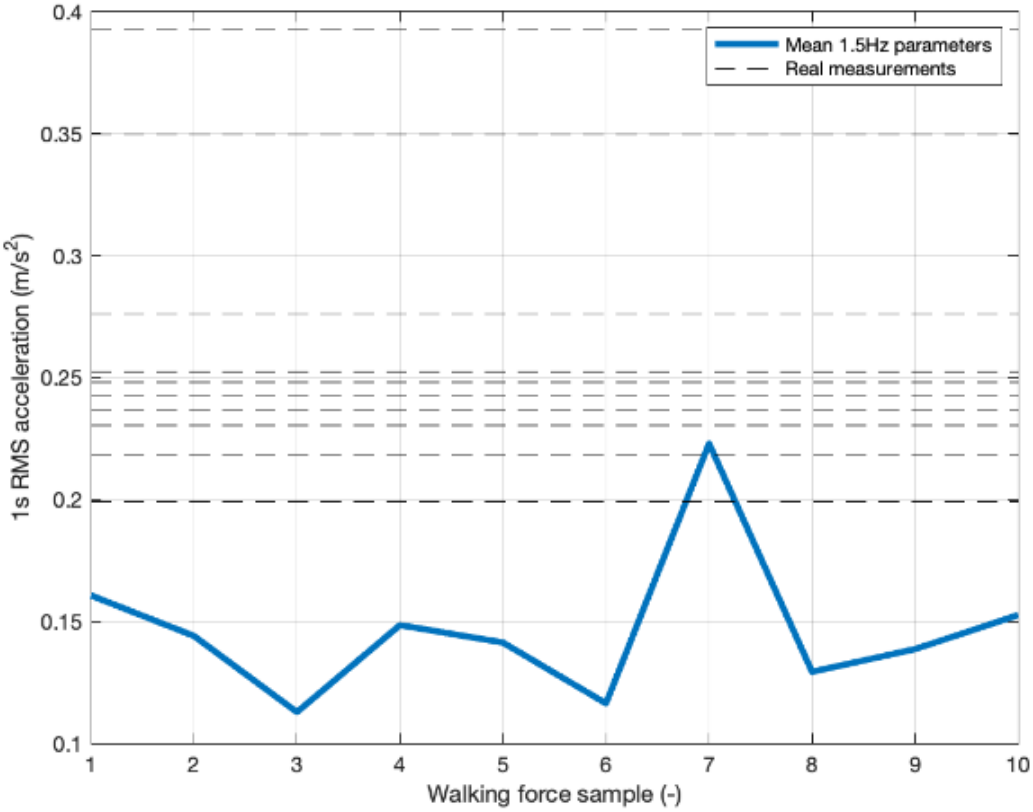

a) Acceleration response from10 sampled walking forces from Racic et al. [52] for 1.5Hz walking frequency using average SDOF SMD moving HSI parameters from Section 5.5.2.1-5.5.2.3.

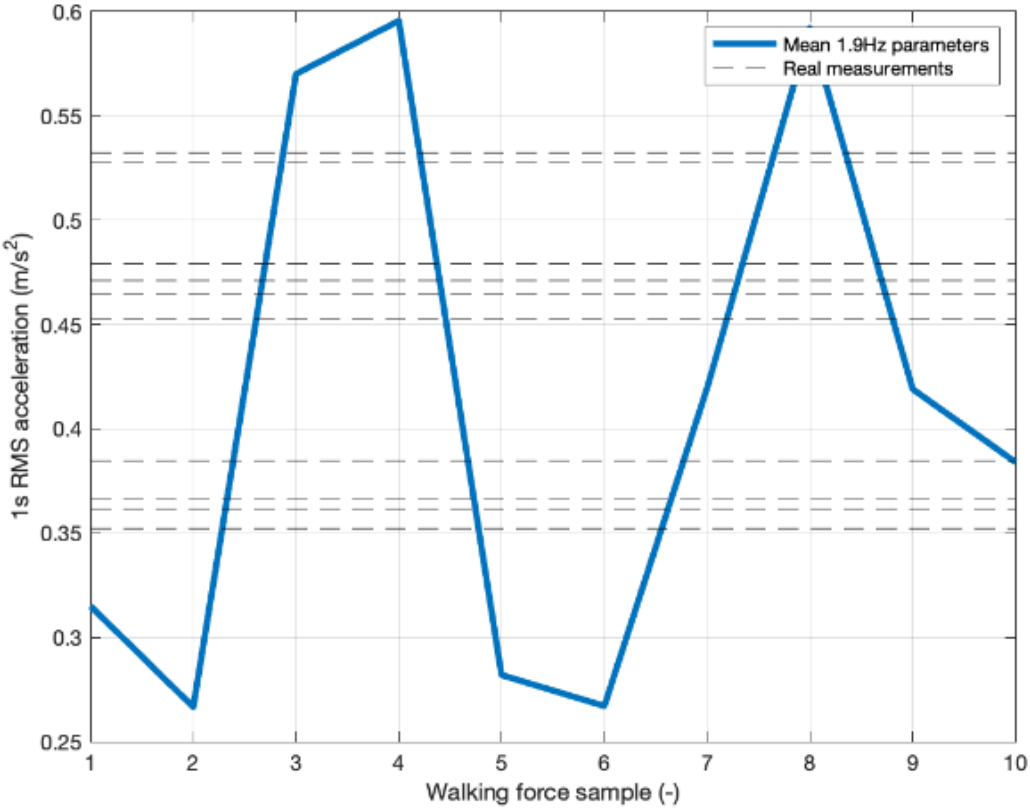

b) Acceleration response from10 sampled walking forces from Racic et al. [52] for 1.9Hz walking frequency using average SDOF SMD moving HSI parameters from Section 5.5.2.1-5.5.2.3.

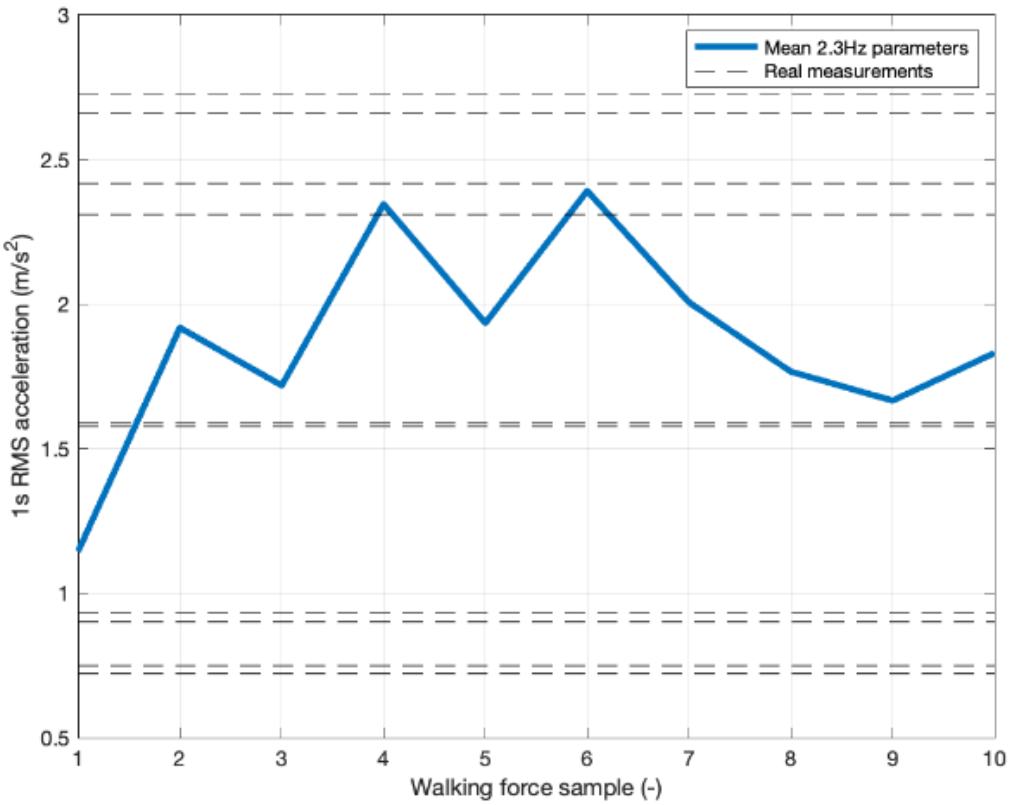

c) Acceleration response from10 sampled walking forces from Racic et al. [52] for 2.3Hz walking frequency using average SDOF SMD moving HSI parameters from Section 5.5.2.1-5.5.2.3.

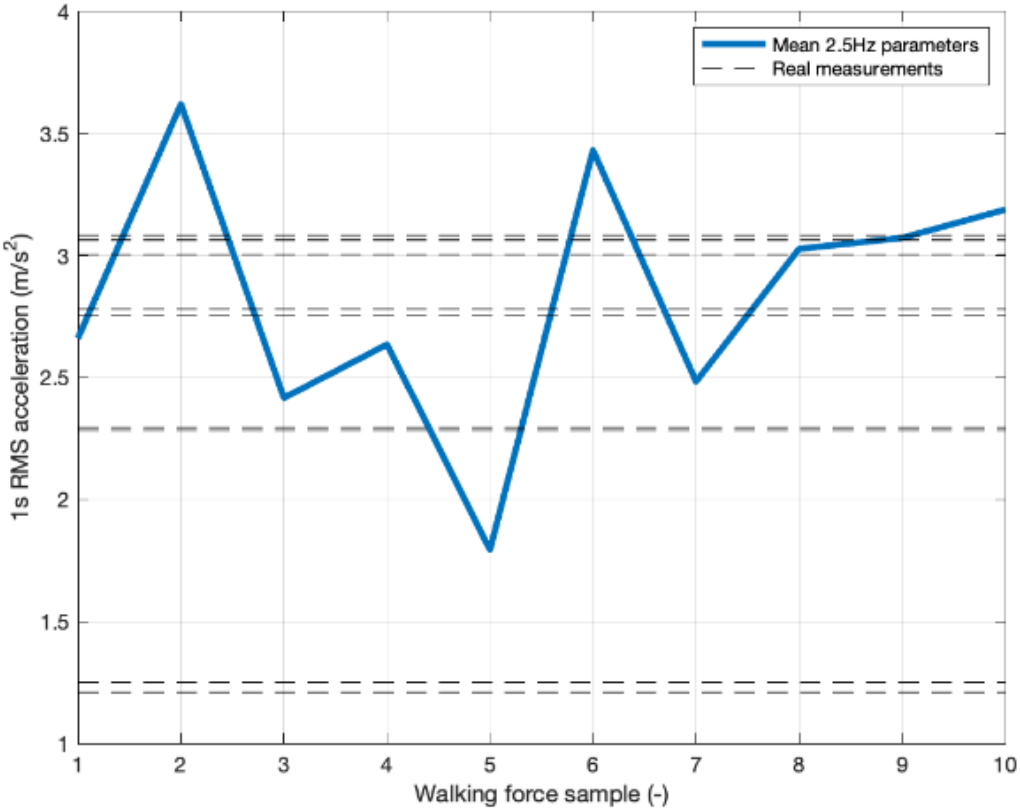

d) Acceleration response from10 sampled walking forces from Racic et al. [52] for 2.5Hz walking frequency using average SDOF SMD moving HSI parameters from Section 5.5.2.1-5.5.2.3.

Figure 5.23: Acceleration response from10 sampled walking forces from Racic et al. [52] for various walking frequencies using average SDOF SMD moving HSI parameters from Section 5.5.2.1-5.5.2.3.

The acceleration responses of 2.3Hz walking provides a reliable estimation compared to the measured results, consistently aligning within the centroid of all the measured results. The 2.3Hz walking frequency (Figure 5.9) exhibits a limitation for several models as a number overestimates the acceleration response [106,174,184,214,216] (Figure 5.9).

The acceleration results of 2.5Hz walking SDOF SMD moving HSI parameters provide a reliable estimate compared to the measured results. The acceleration results tend towards the

higher end of the measured cases, with three out of the ten responses providing a overestimate compared to the 10 measured results. Figure 5.15 presents more reliable estimates compared to the 10 measured cases, namely: Zhang et al. [204], Ahmadi et al. [145] and Shahabpoor et al. [203]. The three models [145,203,204] consistently provide acceleration responses within the measured results' limits. The percentage of modal mass compared to actual mass and modal damping ratio are not within the plausible range of previous research [145,203,204]. The modal damping ratio of 2.5Hz walking are estimated to be 1.5 times that of the three models and have a percentage of modal mass compared to actual mass of 15% less. Further investigation into the co-dependent combinations of the SDOF SMD moving HSI parameters is required.

Whilst the measured results are the baseline measurement in the four walking frequencies, it is not easy to ascertain whether the measured results are typical or extreme acceleration measurements. With significant amounts of further testing, the statement can be proven, and therefore it is only assumed that the 10 acceleration responses are representative. Only within the 2.3Hz walking pace do the mean SDOF SMD moving HSI parameters provide a more reliable estimate than any other model. The predicted parameters provide a close consensus on an individual estimate level for each sample force, with predicted errors in acceleration response less than 10^{-6} m/s^2.

5.6 Conclusions

The topic of HSI is nascent, marked by only a limited number of published data and baseline experiments available. This Chapter exclusively investigates the interaction of the moving human on the structure in the vertical direction.

Historically the effects of HSI are seen to retard the acceleration response of a structure and provide a closer estimate of the actual acceleration response. Section 5.3 demonstrates that

excluding the HSI effects of a walking participant can result in a 300% overestimation of the structure's acceleration response. Such overestimations can affect the design decisions regarding the structure's form and stiffness. At walking frequencies away from the resonant mode, the effects of the HSI become less prominent and, at very low ratios of walking frequency to the natural frequency, the effects of the HSI become irrelevant. Thus, not all structures are subjected to significant HSI effects. Currently, no HSI methodology is seen within guidance. This, however, may be attributed to the need for more consensus on results for the moving participant and other parameters, as seen in Chapter 2 Section 2.3.2.2, Table 5.2 and Section 5.5.2.

Section 5.4 compares the current estimation of the moving participant's natural frequency, percentage of modal mass compared to actual mass and modal damping ratio. All current estimations, bearing that of DaSilva et al. [106] at 2.5Hz walking, provide acceleration time histories within the range of measured acceleration. The current estimation of the SDOF SMD moving HSI parameters in literature provides a close prediction in acceleration responses. The walking force provides the most variation in acceleration response compared to the SDOF SMD moving HSI parameters. Hence, previous parameter estimations may provide erroneous acceleration results due to the limited assumptions of the vertical walking forces. The estimation of the parameters varies significantly, with the natural frequency ranging from 1.85Hz to 3.51Hz and the modal damping ratio from 12%-51%.

Section 5.5 demonstrates that estimating the moving human parameters derived from the structure's acceleration time history may provide an ill-poised optimisation problem. It was shown that many local minima occurred in the optimisation process, resulting in differing parameter estimates. Furthermore, not knowing the exact walking force signal can result in a myriad of different parameter estimates. Section 5.5 further demonstrates the structure is sensitive to the DLF value at a resonant walking frequency. Therefore, the variation of the approximations of the SDOF SMD moving HSI parameters may be attributed to the

sensitivity of the structure combined with the lightweight nature over the natural variation of the human body.

The results exhibited larger variation than that proposed by previous researchers. Some estimations may be biased due to several parameter estimations at the boundary of the optimisation process. No co-dependent modal parameter behaviour is seen concerning the percentage of modal mass compared to actual mass or walking frequency. Further investigation is required that allows the vertical walking force of the participant to be simultaneously measured. Whilst all values of the established parameters provide objective function measurements within 10^{-6} m/s^2 of the measured midspan 1s RMS acceleration, the parameters can vary within the entire range of the system boundaries.

From the experimental and numerical results of the chapter, it is the opinion of the author that current approximations of the moving SMD SDOF model's provide an accurate representation of the true values of the parameters. This statement is correct for all models tested, baring Da Silva et al. [106], inclusive of the results of the analysis in section 5.5. If a practicing engineering required an estimate of the parameter values of the SMD SDOF moving human, currently, choosing a point estimate from Table 5.2 will provide the best representation, with respect to minimising the difference between predicted and actual acceleration. However, further experiments are required across a broad range of natural frequencies and walking paces, with known vertical walking forces, before a truly accurate and all-encompassing estimate can be given for each parameter. The current single point estimation is reductive and requires refinement as the SMD SDOF moving human parameters will naturally vary depending on the various physiology of each human. Therefore, future estimations should provide a distribution of plausible parameter estimations.

Chapter 6 Conclusions and future work

For the design of lightweight and slender structures, the vibration serviceability assessment is often the governing criterion of the structural assessment. The evaluation of the dynamic response of a structure to walking forces is contingent on a several of force and modal assumptions. Whilst the modal properties of a structure and its construction materials are known to have a high level of accuracy, the vertical walking force represents the main uncertainty in any design scenario. Including HSI effects creates further uncertainty with various representations of the moving pedestrian.

In this thesis, a review of the current literature is conducted to identify the progress of historical and current vertical walking load models, and the improvement that HSI research has had on the accurate predictions of the acceleration response of numerical models verses their physical counterparts. Next, a new proposed walking load model is curated and evaluated against current high and low-frequency load models. Finally, the results of previous SMD SDOF moving HSI parameters are assessed on an independent, flexible structure to determine the accuracy of the acceleration response of the numerical approximation to physical system. In this final chapter, the main conclusions of the research are summarised and accompanied by recommendations for future research.

6.1 Main conclusions of the research

The proceeding subsections provide the executive conclusions of Chapter 2 – Chapter 5.

6.1.1 Literature Review

Historically the vertical force model for low-frequency structures is presented through a Fourier series approximation at each integer harmonic of the walking frequency. There is little consensus through the deterministic values or probabilistic ranges of the Fourier series parameters, with the largest variation evident in the representation of the DLF values. Current industrial guidance is parametrised using artificially upscaled datasets to produce the inter-subject variation. The resultant vertical walking loads need to be more consistent with real walking.

The vertical load model's frequency domain representation is often presented in a more complex manner. The procedure is laborious compared to the partner time domain models. Whilst some models claim to provide accurate acceleration results compared to real walking, this is not conclusively proven within literature or experimentally.

The topic of HSI is still in its early stages of research and is ongoing. Several critical knowledge gaps must be filled before an all-encompassing model and review can be conducted. The modal properties of the stationary SMD SDOF participant are known to have high levels of accuracy, with numerous results coinciding with a narrow range. However, the moving human creates more complications due to the time-varying properties. As such, there needs to be more consensus on the correct methodology or parameterisation of the moving human participant. Whilst the beneficial gain from modelling the HSI effects is demonstrated throughout research, the consistency of the parameterisation needs to be evident from study to study.

6.1.2 Fourier series approximation of vertical walking forces

A new Fourier series vertical load model accounts for the intra- and inter-subject variation of the walking frequency and DLF values. It is first shown that peaks in the frequency domain can be seen upwards of the 8th integer harmonic of walking. The walking force model

provides DLF information up to the 8th harmonic through a linear regression presented through a frequentist and Bayesian perspective. The values of the DLF are approximated using a novel method that accounts for DLF information surrounding the integer harmonics of walking frequency.

The intra-subject variation of the walking frequency and DLF values are experimentally shown to be formed from an independent normal distribution. The CoV of both parameters describing the intra-subject variation is best expressed through independent gamma distributions. The values of the CoV are comparable to that of previous researchers. The intra-subject variation is also proven to be sampled from a non-autoregressive process, and therefore the values of each new footstep sample are drawn from independent identical distributions.

Finally, the variation in the load model is investigated concerning the sex of the participant. Females are seen to walk at higher walking frequencies on average and lower DLF values concerning the same walking frequency as males. Females also walk at higher walking frequencies concerning walking velocity compared to males. Comparing the DLFs concerning walking velocities, the models of males and females perfectly align. Thus, such a conclusion provides evidence that walking velocity is the social driving force. If a male and female walked side by side at the same velocity, the male would walk at a slower pacing rate compared to the female on average. However, both would have identical DLF values.

6.1.3 Comparison of vertical loads

Comparing each vertical walking load model across diverse structural conditions provides a survey of results. This study's main finding reveals that the current industry load models produce inconsistent results. In the low-frequency models, all current industry models are outperformed by research models concerning the minimisation of acceleration output of real versus synthetic walking forces. Several industry load models overestimated the structural response by nearly double the acceleration compared to real vertical walking measurements.

Current industry guidance models provide the largest over and underestimation concerning the acceleration. The perpetual variation of the structure acceleration through industrial guidance models has likely resulted in several existing structures needing miss designed due to the overestimation of the load models.

The typical assumption of separate high and low-frequency walking load models is questioned, and evidence is supported to stop the use of this methodology. Fundamentally, the walking force characteristic does not change based on the structure's natural frequency, negating any HSI effects. The division of high and low-frequency models is only present due to the inability of historic load models not containing information in higher-order integer values of walking. The industry representation of high-frequency load models is shown to have a flawed assumption of non-resonant responses. Clear resonant responses in the acceleration spectra are seen in high-order harmonic integers of walking frequencies. With such peaks seen beyond the typical limit of the 4th harmonic currently used in industry low frequency models.

It is demonstrated that the current best representation of the vertical load force with respect to its acceleration output, compared to real walking measurements in both the high and low-frequency range are that of Racic et al. [52] and the new intra-subject proposed load model in Chapter 3 Section 3.4.1. They provide the consistent narrowest range of over and under-estimation of the acceleration response compared to the acceleration of the real walking loads. Therefore, it is recommended that the use of either, Racic et al. [52] or the new intra-subject proposed load model in Chapter 3, be used in place of any other load model given in guidance.

6.1.4 Moving human structure interaction effects

Chapter 5 advocates for the inclusion of HSI effects in the current VSA. The hypothesis of HSI becoming more prominent at resonant frequencies is supported and shown experimentally and numerically. When the HSI effects are not accounted for in numerical

simulations, the acceleration response at resonant walking paces is overestimated by 300% compared to the measured responses. At low ratios of walking frequency to the natural frequency of a structure (away from unity), the beneficial effects of the HSI are not evident. When pedestrians walk at frequencies away from non-resonant walking frequencies, there is no distinguishing difference between approximations of the acceleration when HSI effects are not explicitly modelled.

The acceleration response due to the average SDOF SMD moving HSI parameters of the human, represented as an SDOF SMD, is compared to several measured acceleration responses of real participants. All SDOF SMD representations of the moving human produce acceleration time histories within the range of measured acceleration results, barring that of Da Silva et al.[106], at a resonant walking pace. It is concluded that a range of natural frequency (1.85Hz to 3.51Hz), percentage of modal mass compared to actual mass (72%-100%), and modal damping ratio (12%-51%) of the moving human exist. Current estimates of the parameters view the values as deterministic; however, the latter section of Chapter 5 suggests that a wide range of approximate parameters exist in various combinations.

If a practicing engineering required an estimate of the parameter values of the SMD SDOF moving human, currently, choosing a point estimate from Table 5.2 will provide the best representation, with respect to minimising the difference between predicted and actual acceleration of the structure. However, further experiments are required across a broad range of natural frequencies and walking paces, with known vertical walking forces, before an all-encompassing estimate can be given for each parameter of the SMD SDOF moving human.

An inverse analysis of the vertical acceleration of a flexible GFRP bridge is used to approximate the SDOF SMD moving HSI parameters from 56 participants. It is demonstrated that due to each participant's unknown walking force, variation in the estimated parameters is likely. Previous estimates of the moving SMD parameters all base their estimations on the assumption of a deterministic representation of walking. The inherent variability of the walking force results in different estimates of the human modal parameters. Whilst the mean

values of the estimated parameters provide some consensus, the values within the ranges of all results far exceed that of any other published results. Furthermore, the specific combination of results is rarely presented as the mean value, with the results showing conditionally considerable variation.

The structure used in Chapter 5 was flexible, resulting in a significant acceleration response at resonant walking paces compared to the acceleration due to gravity. Hence, any perturbation in the DLF at the resonant walking pace resulted in a substantial variation in acceleration response. This effect, combined with the unknown vertical force function has resulted in an ill poised optimisation problem that is sensitive to the inputs. Thus, providing inconsistent results in the analysis of section 5.5.

6.2 Recommendations for future research

Based on the conclusions stated in Section 6.1, recommendations for future research can be made and are listed below concerning vertical load models and the HSI effects.

6.2.1 Vertical walking loads

The vertical load models of Racic et al.[52] and Chapter 3 are attributed with the most reliable of all models. The author notes that the results are only verified analytically and on the same dataset from which the models are derived. Results should be compared with a new set of treadmill data or more precise measurement methods, such as a pressure insole monitor, thus, providing a control set of results that are not used to model any data and defuse bias.

Ahmadi et al. [91] provides a study comparing the GFR through force plates and pressure soles. A larger scale test should be conducted, than that of the thesis, that considers all modern measurement techniques. The study will provide evidence to conclude if all

methodologies offer consistent results. Current ‘best’ estimations of vertical walking are taken from treadmill data..

The experimental validation of high-frequency load models needs further investigation because there does not exist a sizeable experimental campaign of verification. Therefore, the acceleration response of a structure with an adjustable first vertical mode of vibration should be compared to numerical simulations considering only the first vertical mode. The result should be compared for various walking paces to demonstrate the application of resonance at high-order harmonics and the accuracy of high-frequency models in non-resonant cases. A benefit of testing relatively high-frequency structures is that the HSI's effects become negligible. As such, acceleration measurements of the structure are nearly only attributed to the walking force. The experiment can be conducted in a similar vein to Chapter 4, although in comparison to real acceleration measurements of people walking at frequencies above 10Hz natural frequency, and not real walking forces simulated on a structure.

As this research aims to replicate vertical walking forces, it is challenging to comprehend when the end goal is reached. Therefore, it may become more beneficial for a continuously updating dataset of treadmill walking loads to be curated. For example, the dataset of Racic et al. [52], with several orders of magnitude in size, along with more representation from different nations, sex, ages, and weight. The dataset can be used directly instead of any synthetic vertical walking loads. The measurements will be actual vertical walking loads and not synthetic, thus removing many modelling errors.

6.2.2 Human Structure interaction

The major limitation of Chapter 5 is the unknown walking forces used to obtain each acceleration measurement. If the experiment was conducted again with each participant wearing pressure insoles, the exact vertical walking force of the participant could be used to provide precise estimations through the optimisation procedure outlined in Chapter 5.

The structure used in Chapter 5 has a natural frequency of approximately 2.5Hz, as does the approximated natural frequency of the human body. As a result, it is not easy to separate if the resonance of the structure or the human body or both exacerbates HSI effects. The procedure laid out in Chapter 5, utilising pressure insoles, should be run on a structure that can vary its natural frequency. The experiment will then be run with multiple persons over multiple walking frequencies for each structure's natural frequency. If pressure insoles are utilised, participants do not need to be prompted to walk at various walking frequencies, as the natural variation of walking frequencies throughout the population can be harnessed and resonant and non-resonate walking paces can be prompted for each structure's natural frequency. The result will provide a conclusive dataset of measurements that can be used to form new estimates of the SDOF SMD moving HSI parameters represented through an SMD system or otherwise. Such a structure is presently observed in Universidad de Oviedo [261].

New and emerging methodologies, such as physics informed neural networks have provided promising result to model various ODE and PDE. This methodology could be used to inform, and improve the predictions of Chapter 5. Physics informed neural networks have been shown to provide accurate inverse and forward analysis problems on several ODE and PDE problems [262].

References

[1] M. Gonçalves, A. Pavic, Environmental Impact of Structural Modifications in Office Floors To Satisfy Vibration Serviceability, EURODYN 2020 XI International Conference on Structural Dynamics. (2020) 1924–1931. https://doi.org/10.47964/1120.9156.19504.

[2] V. Racic, J. Morin, Data-driven modelling of vertical dynamic excitation of bridges induced by people running, Mech Syst Signal Process. 43 (2014) 153–170. https://doi.org/10.1016/j.ymssp.2013.10.006.

[3] V. Racic, J. Chen, A. Pavic, Advanced fourier-based model of bouncing loads, Conference Proceedings of the Society for Experimental Mechanics Series. (2019) 367–376. https://doi.org/10.1007/978-3-319-74421-6_49.

[4] J. Chen, G. Ding, S. Živanović, Stochastic Single Footfall Trace Model for Pedestrian Walking Load, International Journal of Structural Stability and Dynamics. 19 (2019). https://doi.org/10.1142/S0219455419500299.

[5] M. Gonçalves, A. Pavic, R. Pimentel, Vibration serviceability assessment of office floors for realistic walking and floor layout scenarios: Literature review, Advances in Structural Engineering. 23 (2020) 1238–1255. https://doi.org/10.1177/1369433219888753.

[6] T. Fitzpatrick, P. Dallard, S. le Bourva, A. Low, R. Smith, M. Willford, Linking London: the millennium bridge, Royal Academy of Engineering, 2001.

[7] S. Strogatz, D. Abrams, A. McRobie, B. Eckhardt, B. Ott, Crowd synchrony on the Millennium bridge, Nature. 438 (2005) 43–44.

[8] D.E. Newland, Vibration of the London Millennium Bridge: cause and cure, International Journal of Acoustics and Vibration. 8 (2003) 9–14.

[9] A. Pavic, Results of IStructE 2015 survey of practitioners on vibration serviceability IStructE Survey questionnaire, in: SECED, 2019: pp. 1–8.

[10] J. Orr, M. Drewniok, I. Walker, T. Ibell, A. Copping, S. Emmitt, Minimising energy in construction: Practitioners' views on material efficiency, Resour Conserv Recycl. 140 (2019) 125–136. https://doi.org/10.1016/j.resconrec.2018.09.015.

[11] C. Dunant, M. Drewniok, S. Eleftheriadis, J. Cullen, J. Allwood, Regularity and optimisation practice in steel structural frames in real design cases, Resour Conserv Recycl. 134 (2018) 294–302. https://doi.org/10.1016/j.resconrec.2018.01.009.

[12] C. Kennedy, Innovative Thinker | Why lean design creates floor vibration challenge, New Civil Engineer. (2021). https://www.newcivilengineer.com/innovative-thinking/innovative-thinker-alex-pavic-on-why-lean-design-creates-floor-vibration-challenge-02-07-2021/ (accessed August 9, 2021).

[13] W. Ferdous, Y. Bai, T.D. Ngo, A. Manalo, P. Mendis, New advancements, challenges and opportunities of multi-storey modular buildings – A state-of-the-art review, Eng Struct. 183 (2019) 883–893. https://doi.org/10.1016/j.engstruct.2019.01.061.

[14] L. Hanagan, Active Control of Floor Vibrations, Polytechnic Institute and State University, Virginia, 1994.

[15] J.M.W. Brownjohn, C.J. Middleton, Procedures for vibration serviceability assessment of high-frequency floors, Eng Struct. 30 (2008) 1548–1559. https://doi.org/10.1016/j.engstruct.2007.10.006.

[16] T.M. Murray, D.E. Allen, E.E. Ungar, Floor vibrations due to human activity AISC DG 11, AISC American Institute of Steel Construction, 2016.

[17] A.S. Mohammed, A. Pavic, V. Racic, Improved model for human induced vibrations of high-frequency floors, Eng Struct. 168 (2018) 950–966. https://doi.org/10.1016/j.engstruct.2018.04.093.

[18] C.J. Middleton, Dynamic performance of high frequency floors, University of Sheffield, 2009.

[19] A.L. Smith, S.J. Hicks, P.J. Devine, Design of Floors for Vibration : A New Approach, 2007.

[20] M.R. Willford, P. Young, A Design Guide for Footfall Induced Vibration of Structures, The Concrete Society, 2006.

[21] ISO, ISO 10137 Bases for design of structures-serviceability of buildings and walkways against vibrations, 2007.

[22] BSI, BS 6472-1:2008 - Guide to evaluation of human exposure to vibration in buildings, British Standard. (2008).

[23] Z. Muhammad, P. Reynolds, O. Avci, M. Hussein, Review of Pedestrian Load Models for Vibration Serviceability Assessment of Floor Structures, Vibration. 2 (2018) 1–24. https://doi.org/10.3390/vibration2010001.

[24] Z. Muhammad, P. Reynolds, Vibration Serviceability of Building Floors: Performance Evaluation of Contemporary Design Guidelines, Journal of

Performance of Constructed Facilities. 33 (2019) 1–17. https://doi.org/10.1061/(ASCE)CF.1943-5509.0001280.

[25] J. Wang, J. Chen, A comparative study on different walking load models, Structural Engineering and Mechanics. 63 (2017) 847–856. https://doi.org/10.12989/sem.2017.63.6.847.

[26] E. Ahmadi, C. Caprani, S. Živanović, N. Evans, A. Heidarpour, A framework for quantification of human-structure interaction in vertical direction, J Sound Vib. 432 (2018) 351–372. https://doi.org/10.1016/j.jsv.2018.06.054.

[27] Z. Muhammad, P. Reynolds, J. Hudson, Evaluation of Contemporary Guidelines for Floor Vibration Serviceability Assessment, in: Dynamics of Civil Structures, Volume 2 Proceedings of the 35th IMAC, A Conference and Exposition on Structural Dynamics 2017, 2017: pp. 339–346.

[28] A. Pavic, M. Willford, Technical Report 43 Post-tensioned floors Design Handbook- Appendix G, 2nd ed., Concrete Society, 2008.

[29] J. Brownjohn, A. Pavic, P. Omenzetter, A spectral density approach for modelling continuous vertical forces on pedestrian structures due to walking, Canadian Journal of Civil Engineering. 31 (2004) 65–77. https://doi.org/10.1139/l03-072.

[30] K. Van Nimmen, P. Van den Broeck, G. Lombaert, F. Tubino, Pedestrian-Induced Vibrations of Footbridges: An Extended Spectral Approach, Journal of Bridge Engineering. 25 (2020) 04020058. https://doi.org/10.1061/(asce)be.1943-5592.0001582.

[31] V. Racic, A. Pavic, J. Brownjohn, Experimental identification and analytical modelling of human walking forces: Literature review, J Sound Vib. 326 (2009) 1–49. https://doi.org/10.1016/j.jsv.2009.04.020.

[32] C.F. Dunant, M.P. Drewniok, J.J. Orr, J.M. Allwood, Good early stage design decisions can halve embodied CO2 and lower structural frames' cost, Structures. 33 (2021) 343–354. https://doi.org/10.1016/j.istruc.2021.04.033.

[33] J. Orr, M. Cooke, T. Ibell, C. Smith, N. Watson, Design for Zero, Institution of Structural Engineers, 2021. https://doi.org/10.1259/0007-1285-8-87-183-b.

[34] S. Živanović, A. Pavić, Probabilistic modeling of walking excitation for building floors, Journal of Performance of Constructed Facilities. 23 (2009) 132–143. https://doi.org/10.1061/(ASCE)CF.1943-5509.0000005.

[35] A. Mohammed, A. Pavic, Human-structure dynamic interaction between building floors and walking occupants in vertical direction, Mech Syst Signal Process. 147 (2021) 107036. https://doi.org/10.1016/j.ymssp.2020.107036.

[36] C. Caprani, E. Ahmadi, Formulation of human–structure interaction system models for vertical vibration, J Sound Vib. 377 (2016) 346–367. https://doi.org/10.1016/j.jsv.2016.05.015.

[37] J. Chen, R. Xu, M. Zhang, Acceleration response spectrum for predicting floor vibration due to occupant walking, J Sound Vib. 333 (2014) 3564–3579. https://doi.org/10.1016/j.jsv.2014.03.023.

[38] J. Brownjohn, V. Racic, J. Chen, Universal response spectrum procedure for predicting walking-induced floor vibration, Mech Syst Signal Process. 70–71 (2016) 741–755. https://doi.org/10.1016/j.ymssp.2015.09.010.

[39] S. Krenk, Dynamic response to pedestrian loads with statistical frequency distribution, J Eng Mech. 138 (2012) 1275–1281. https://doi.org/10.1061/(ASCE)EM.1943-7889.0000425.

[40] F. Tubino, Probabilistic assessment of the dynamic interaction between multiple pedestrians and vertical vibrations of footbridges, J Sound Vib. 417 (2018) 80–96. https://doi.org/10.1016/j.jsv.2017.11.057.

[41] G. Piccardo, F. Tubino, Equivalent spectral model and maximum dynamic response for the serviceability analysis of footbridges, Eng Struct. 40 (2012) 445–456. https://doi.org/10.1016/j.engstruct.2012.03.005.

[42] C. Caprani, Application of the pseudo-excitation method to assessment of walking variability on footbridge vibration, Comput Struct. 132 (2014) 43–54. https://doi.org/10.1016/j.compstruc.2013.11.001.

[43] S. Živanović, Probability-Based Estimation of Vibration for Pedestrian Structures due to Walking, University of Sheffield, 2006.

[44] M. Willford, C. Field, Predicting footfall-induced vibration : Part 1, Structures and Buildings. 160 (2007) 65–72.

[45] S.C. Kerr, Human induced loading on staircases, University College London, 1998. http://discovery.ucl.ac.uk/1318004/.

[46] H.A.U. Nguyen, Walking Induced Floor Vibration Design and Control, (2013) 340.

[47] F.W. Galbraith, M. V. Barton, Ground Loading from Footsteps, J Acoust Soc Am. 48 (1970) 1288–1292. https://doi.org/10.1121/1.1912271.

[48] M.P. Murray, G.B. Spurr, S.B. Sepic, G.M. Gardner, L.A. Mollinger, Treadmill vs. floor walking: Kinematics, electromyogram, and heart rate, J Appl Physiol. 59 (1985) 87–91. https://doi.org/10.1152/jappl.1985.59.1.87.

[49] R. Kram, T.M. Griffin, J.M. Donelan, Y.H.U.I. Chang, T.M. Griffin, J. Maxwell, Force treadmill for measuring vertical and horizontal ground reaction forces, J Appl Physiol. 85 (1998) 764–769.

[50] E.C. Jansen, D. Vittas, S. Hellberg, J. Hansen, Normal gait of Young and old men and women: Ground reaction force measurement on a treadmill, Acta Orthop. 53 (1982) 193–196. https://doi.org/10.3109/17453678208992200.

[51] Z. Muhammad, P. Reynolds, Probabilistic Multiple Pedestrian Walking Force Model including Pedestrian Inter- and Intrasubject Variabilities, Advances in Civil Engineering. 2020 (2020) 1–14. https://doi.org/10.1155/2020/9093037.

[52] V. Racic, J. Brownjohn, Stochastic model of near-periodic vertical loads due to humans walking, Advanced Engineering Informatics. 25 (2011) 259–275. https://doi.org/10.1016/j.aei.2010.07.004.

[53] Z. Zhang, B. Zhang, J. Wei, P. Luo, C. Cui, A Stochastic Study on the Distribution Parameters of Random Individual Walking Excitations, in: AEI 2017: Resilience of the Integrated Building, 2017: pp. 495–505.

[54] M.A. Toso, H.M. Gomes, F.T. da Silva, R.L. Pimentel, Experimentally fitted biodynamic models for pedestrian-structure interaction in walking situations, Mech Syst Signal Process. 72–73 (2016) 590–606. https://doi.org/10.1016/j.ymssp.2015.10.029.

[55] SETRA, Footbridges - Assessment of vibrational behaviour of footbridges under pedestrian loading, 2006.

[56] T. Murray, D. Allen, E. Ungar, Floor vibrations due to human activity - DG-11 (10M797), 2001.

[57] B.R. Ellis, T. Ji, J.D. Littler, The response of grandstands to dynamic crowd loads, Proceedings of the Institution of Civil Engineers: Structures and Buildings. 140 (2000) 355–365. https://doi.org/10.1680/stbu.2000.140.4.355.

[58] P. Reynolds, A. Pavic, Effects of False Floors on Vibration Serviceability of Building Floors. II: Response to Pedestrian Excitation, Journal of Performance of Constructed Facilities. 17 (2003) 87–96. https://doi.org/10.1061/(asce)0887-3828(2003)17:2(87).

[59] M. García-Diéguez, J.L. Zapico-Valle, Statistical Modeling of the Relationships between Spatiotemporal Parameters of Human Walking and Their Variability, Journal of Structural Engineering. 143 (2017) 04017164. https://doi.org/10.1061/(asce)st.1943-541x.0001899.

[60] S.V. Ohlsson, Ten years of floor vibration research—a review of aspects and some results, in: Proceedings of the Symposium/Workshop on Serviceability of Buildings (Movements, Deformations, Vibrations), NRCC Institute for Research in Construction, New Orleans, USA, 1988: pp. 419–434.

[61] T.A. Wyatt, A.F. Dier, Building in steel, the way ahead, 1989.

[62] S. Živanović, A. Pavić, P. Reynolds, Probability-based prediction of multi-mode vibration response to walking excitation, Eng Struct. 29 (2007) 942–954. https://doi.org/10.1016/j.engstruct.2006.07.004.

[63] M. García-Diéguez, V. Racic, J.L. Zapico-Valle, Complete statistical approach to modelling variable pedestrian forces induced on rigid surfaces, Mech Syst Signal Process. 159 (2021). https://doi.org/10.1016/j.ymssp.2021.107800.

[64] W.D. Varela, M.S. Pfeil, N. de P.A. da Costa, Experimental Investigation on Human Walking Loading Parameters and Biodynamic Model, Journal of

Vibration Engineering and Technologies. 8 (2020) 883–892. https://doi.org/10.1007/s42417-020-00197-3.

[65] J. Blanchard, B. Davies, W. Smith, Design criteria and analysis for dynamic loading of footbridges, in: Proceeding of a Symposium on Dynamic Behaviour of Bridges at the Transport and Road Research Laboratory, London, 1977: pp. 90–106.

[66] H. Bachmann, W. Ammann, Vibrations in structures: induced by man and machines, 1987.

[67] J.H. Rainer, G. Pernica, D.E. Allen, Dynamic loading and response of footbridges, Canadian Journal of Civil Engineering. 15 (1988) 66–71.

[68] D.E. Allen, T.M. Murray, Design Criterion for Vibrations Due to Walking, Engineering Journal (AISC). 30 (1993) 117–129.

[69] M. Willford, C. Field, Predicting footfall-induced vibration : Part 2, (2007) 73–79.

[70] Y. Matsumoto, T. Nishioka, H. Shiojiri, K. Matsuzaki, Dynamic Design of Footbridges, Proceedings of the International Association for Bridge and Structural Engineering. 2 (1978) 1–15. https://doi.org/10.5169/seals-33221.

[71] A. Pachi, T. Ji, Frequency and velocity of people walking, Structural Engineer. 83 (2005) 36–40.

[72] W.D. Varela, R.C. Battista, Control of vibrations induced by people walking on large span composite floor decks, Eng Struct. 33 (2011) 2485–2494. https://doi.org/10.1016/j.engstruct.2011.04.021.

[73] H. Schulze, Dynamic effects of the live load on footbridges, Signal Und Schiene. 24 (1980) 91–93.

[74] H. Kramer, H.W. Kebe, Man-induced structural vibrations, Der Bauingenieur. 54 (1980) 195–199.

[75] A. Mohammed, A. Pavic, Effect of Walking people on Dynamic Properties of Floors, Procedia Eng. 199 (2017) 2856–2863. https://doi.org/10.1016/j.proeng.2017.09.561.

[76] K. Van Nimmen, P. Van den Broeck, P. Verbeke, C. Schauvliege, M. Mallié, L. Ney, G. De Roeck, Numerical and experimental analysis of the vibration serviceability of the Bears' Cage footbridge, Structure and Infrastructure Engineering. 13 (2017) 390–400. https://doi.org/10.1080/15732479.2016.1160133.

[77] A. McRobie, G. Morgenthal, J. Lasenby, M. Ringer, Section model tests on human – structure lock-in, Proceedings of the Institution of Civil Engineers - Bridge Engineering. 156 (2003) 71–79. https://doi.org/10.1680/bren.2003.156.2.71.

[78] S.C. Kerr, N.W.M. Bishop, Human induced loading on flexible staircases, Eng Struct. 23 (2001) 37–45. https://doi.org/10.1016/S0141-0296(00)00020-1.

[79] M. Whittle, Gait Analysis An Introduction, 4th ed., Elsevier, 2007.

[80] E. Bassoli, K. van Nimmen, L. Vincenzi, P. van den Broeck, A spectral load model for pedestrian excitation including vertical human-structure interaction, Eng Struct. 156 (2018) 537–547. https://doi.org/10.1016/j.engstruct.2017.11.050.

[81] H. Dang, S. Živanović, Influence of Low-Frequency Vertical Vibration on Walking Locomotion, Journal of Structural Engineering. 142 (2016) 04016120. https://doi.org/10.1061/(asce)st.1943-541x.0001599.

[82] C. Butz, M. Feldmann, C. Heinemeyer, G. Sedlacek, B. Chabrolin, A. Lamaire, M. Lukić, P.-O. Martin, E. Caetano, Á. Cunha, A. Goldack, A. Keil, M. Schlaich, Advanced load models for synchronous pedestrian excitation and optimised design guidelines for steel footbridges, 2008.

[83] F. Ricciardelli, C. Briatico, E.T. Ingólfsson, C.T. Georgakis, Experimental validation and calibration of pedestrian loading models for footbridges, in: Proceedings of International Conference on Experimental Vibration Analysis for Civil Engineering Structures, 2007.

[84] F. Venuti, L. Bruno, An interpretative model of the pedestrian fundamental relation, Comptes Rendus - Mecanique. 335 (2007) 194–200. https://doi.org/10.1016/j.crme.2007.03.008.

[85] World Health Organization, The SuRF Report 2, (2005).

[86] S.C. Walpole, D. Prieto-Merino, P. Edwards, J. Cleland, G. Stevens, I. Roberts, The weight of nations: An estimation of adult human biomass, BMC Public Health. 12 (2012) 1. https://doi.org/10.1186/1471-2458-12-439.

[87] L. Pedersen, C. Frier, Sensitivity of footbridge vibrations to stochastic walking parameters, J Sound Vib. 329 (2010) 2683–2701. https://doi.org/10.1016/j.jsv.2009.12.022.

[88] K. Portier, J. Keith-Tolson, S. Roberts, Body weight distributions for risk assessment, Risk Analysis. 27 (2007) 11–26. https://doi.org/10.1111/j.1539-6924.2006.00856.x.

[89] C. Caprani, J. Qu, S. Zivanovic, N. Evans, E. Ahmadi, Quantification of human-structure interaction, in: MATEC Web of Conferences, 2015.

[90] E. Ahmadi, C. Caprani, S. Živanović, A. Heidarpour, Vertical ground reaction forces on rigid and vibrating surfaces for vibration serviceability assessment of

structures, Eng Struct. 172 (2018) 723–738. https://doi.org/10.1016/j.engstruct.2018.06.059.

[91] E. Ahmadi, C. Caprani, S. Zivanovic, A. Heidarpour, Assessment of human-structure interaction on a lively lightweight GFRP footbridge, Eng Struct. 199 (2019).

[92] O. Celik, C. Dong, F. Catbas, Measurement of Human Loads Using Computer Vision, in: Dynamics of Civil Structures, Volume 2 Proceedings of the 36th IMAC, A Conference and Exposition on Structural Dynamics 2018, 2018: pp. 191–195.

[93] Y. Wang, J. Brownjohn, K. Dai, M. Patel, An Estimation of Pedestrian Action on Footbridges Using Computer Vision Approaches, Front Built Environ. 5 (2019) 1–11. https://doi.org/10.3389/fbuil.2019.00133.

[94] K. Van Nimmen, G. Lombaert, I. Jonkers, G. De Roeck, P. Van Den Broeck, Characterisation of walking loads by 3D inertial motion tracking, J Sound Vib. 333 (2014) 5212–5226. https://doi.org/10.1016/j.jsv.2014.05.022.

[95] V. Racic, A. Pavic, J. Brownjohn, Modern facilities for experimental measurement of dynamic loads induced by humans: A literature review, Shock and Vibration. 20 (2013) 53–67. https://doi.org/10.3233/SAV-2012-0727.

[96] J. Brownjohn, M. Bocian, D. Hester, Forced vibration testing of footbridges using calibrated human shaker and wireless sensors, Procedia Eng. 199 (2017) 417–422. https://doi.org/10.1016/j.proeng.2017.09.134.

[97] E. Shahabpoor, A. Pavic, Estimation of tri-axial walking ground reaction forces of left and right foot from total forces in real-life environments, Sensors (Switzerland). 18 (2018). https://doi.org/10.3390/s18061966.

[98] C. Petersen, H. Werkle, Dynamik der Baukonstruktionen (Dynamics of building constructions), Springer, 2017.

[99] BSI, BS 5400: Steel, concrete and composite bridges—part 2: Specification for loads; appendix c: Vibration serviceability requirements for foot and cycle track bridges, 1978.

[100] B. Ellis, On the response of long-span floors to walking loads generated by individuals and crowds, Structural Engineer. 78 (2000) 17–25.

[101] Architectural Institute of Japan, AIJ Recommendations for Loads on Buildings (2004), Japan, 2004.

[102] M. Willford, An investigation into crowd-induced vertical dynamic loads using available measurements, Structural Engineer. 79 (2001) 21–25.

[103] H. Bachmann, Case studies o f structures with man-induced vibrations, Journal of Structural Engineering. 118 (1992) 631–647.

[104] M. García-Diéguez, V. Racic, J.L. Zapico-Valle, Complete statistical approach to modelling variable pedestrian forces induced on rigid surfaces, Mech Syst Signal Process. 159 (2021). https://doi.org/10.1016/j.ymssp.2021.107800.

[105] F. da Silva, R. Pimentel, Biodynamic walking model for vibration serviceability of footbridges in vertical direction, Proceedings of the 8th International Conference on Structural Dynamics, EURODYN 2011. (2011) 1090–1096.

[106] F. DaSilva, H. Brito, R. Pimentel, Modeling of crowd load in vertical direction using biodynamic model for pedestrians crossing footbridges, Canadian Journal of Civil Engineering. 40 (2013) 1196–1204. https://doi.org/10.1139/cjce-2011-0587.

[107] J. Wheeler, Prediction and Control of Pedestrian-Induced Vibration in Footbridges, Journal of the Structural Division. 108 (1982).

[108] S.V. Ohlsson, Floor Vibrations and Human Discomfort, Chalmers University of Technology, 1982.

[109] K.P. Murphey, Machine learning: a probabilistic perspective, MIT press, 2012. https://doi.org/10.1007/978-94-011-3532-0_2.

[110] C. Bishop, Pattern Recognition and Machine Learning, Springer, Cambridge, 2006.

[111] A. Mohammed, A. Pavic, Simulation of people's movements on floors using social force model, Conference Proceedings of the Society for Experimental Mechanics Series. (2019) 39–46. https://doi.org/10.1007/978-3-319-74421-6_6.

[112] T.P. Andriacchi, J.A. Ogle, J.O. Galante, Walking speed as a basis for normal and abnormal gait measurements, J Biomech. 10 (1977) 261–268.

[113] F.C. Harper, W.J. Warlow, B.L. Clarke, The forces applied to the floor by the foot in walking, London, 1961.

[114] S. Gomez, J. Marulanda, P. Thomson, J.J. Garcia, D. Gomez, A.R. Ortiz, S. Dyke, J. Caicedo, S. Rietdyk, Benchmark Problem for Assessing Effects of Human-Structure Interaction in Footbridges, in: Dynamics of Civil Structures, Volume 2 Proceedings of the 35th IMAC, A Conference and Exposition on Structural Dynamics 2017, 2017: pp. 213–222.

[115] S. Živanović, Benchmark footbridge for vibration serviceability assessment under the vertical component of pedestrian load, Journal of Structural Engineering (United States). 138 (2012) 1193–1202. https://doi.org/10.1061/(ASCE)ST.1943-541X.0000571.

[116] J.E.A. Bertram, A. Ruina, Multiple walking speed-frequency relations are predicted by constrained optimization, J Theor Biol. 209 (2001) 445–453. https://doi.org/10.1006/jtbi.2001.2279.

[117] C. Sahnaci, M. Kasperski, Simulation of random pedestrian flow, Proceedings of the 8th International Conference on Structural Dynamics, EURODYN 2011. (2011) 1040–1047.

[118] C. Sahnaci, M. Kasperski, Random loads induced by walking, in: Proceedings of the Sixth European Conference on Structural Dynamics, 2005: pp. 441–446.

[119] S. Buchmueller, U. Weidmann, Parameters of pedestrians, pedestrian traffic and walking facilities, Zurich, 2007.

[120] U. Weidmann, Transport technology for pedestrians: transport-technical properties of pedestrian traffic, evaluation of literature (in German), 1993.

[121] J. Fruin, Pedestrian planning and design, 1971.

[122] B.D. Hankin, R.A. Wright, Passenger Flow in Subways, in: Operational Research Society's Open Conferenc, 1958: p. 81. https://doi.org/10.2307/3006732.

[123] P. Koushki, Walking characteristics in Central Riyadh, Saudi Arabia, 114 (1988) 735–744.

[124] W.H.K. Lam, J.F. Morrall, H. Ho, Pedestrian flow characteristics in Hong Kong, Transp Res Rec. (1995) 56–62.

[125] J. Pauls, Calculating evacuation times for tall buildings, Fire Saf J. 12 (1987) 213–236. https://doi.org/10.1016/0379-7112(87)90007-5.

[126] F. Ricciardelli, C. Briatico, E.T. Ingólfsson, C.T. Georgakis, Experimental validation and calibration of pedestrian loading models for footbridges, in:

Experimental Vibration Analysis for Civil Engineering Structures, Porto, Portugal, 2006: pp. 189–199.

[127] C. Butz, A Probabilistic Engineering Load Model for Pedestrian Streams, in: Proceedings of the Third International Conference Footbridge, Porto, Portugal, 2008.

[128] M.R. Virkler, S. Elayadath, Pedestrian speed-flow-density relationships, Transp Res Rec. (1994) 51–58.

[129] W. Daamen, Modelling Passenger Flows in Public Transport Facilities, 2004.

[130] L. Pedersen, C. Frier, Footbridge Vibrations Predicted by Stochastic Load Model, in: Dynamics of Civil Structures, Volume 2 Proceedings of the 36th IMAC, A Conference and Exposition on Structural Dynamics 2018, 2018: pp. 51–57.

[131] T. Keller, A. Weisberger, J. Ray, S. Hasan, R. Shiavi, D. Spengler, Relationship between vertical ground reaction force and speed during walking, slow jogging, and running, Clinical Biomechanics. 11 (1996) 253–259.

[132] K. Masani, M. Kouzaki, T. Fukunaga, Variability of ground reaction forces during treadmill walking, J Appl Physiol. 92 (2002) 1885–1890. https://doi.org/10.1152/japplphysiol.00969.2000.

[133] M. Feldmann, C. Heinemeyer, C. Butz, E. Caetano, A. Cunha, F. Galanti, A. Goldack, O. Hechler, S. Hicks, A. Keil, M. Lukic, R. Obiala, M. Schlaich, G. Sedlacek, A. Smith, P. Waarts, Design of floor structures for human induced vibrations Prepared under the JRC-ECCS cooperation agreement for the evolution of Eurocode 3 (programme of CEN / TC 250) Design of floor structures for human induced vibrations, 2009.

[134] BSI, BS EN 1990:2002+A1:2005 - Eurocode. Basis of structural design, 2002.

[135] A. Pavic, P. Reynolds, S. Prichard, M. Lovell, Evaluation of mathematical models for predicting walking-induced vibrations of high-freqeuncy floors, International Journal of Structural Stability and Dynamics. (2003).

[136] D.E. Newland, An Introduction to Random Vibrations, spectral and wavelet analysis, (1993).

[137] I. Elishakoff, Probabilistic Methods in the Theory of Structures: Strength of Materials, Random Vibrations, and Random Buckling., 2017.

[138] A.G. DAVENPORT, Note on the Distribution of the Largest Value of a Random Function With Application To Gust Loading., Proceedings of the Institution of Civil Engineers. 28 (1964) 187–196. https://doi.org/10.1680/iicep.1964.10112.

[139] J. Chen, J. Wang, J. Brownjohn, Power Spectral-Density Model for Pedestrian Walking Load, Journal of Structural Engineering (United States). 145 (2019). https://doi.org/10.1061/(ASCE)ST.1943-541X.0002248.

[140] L. Pedersen, C. Frier, Predictions of Footbridge Vibrations and Influencing Load Model Decisions, in: Dynamics of Civil Structures, Volume 2: Proceedings of the 38th IMAC, A Conference and Exposition on Structural Dynamics 2020, 2020: pp. 151–157.

[141] H. Sadeghi, P. Allard, F. Prince, H. Labelle, Symmetry and limb dominance in able-bodied gait: A review, Gait Posture. 12 (2000) 34–45. https://doi.org/10.1016/S0966-6362(00)00070-9.

[142] G. Piccardo, F. Tubino, Equivalent spectral model and maximum dynamic response for the serviceability analysis of footbridges, Eng Struct. 40 (2012) 445–456. https://doi.org/10.1016/j.engstruct.2012.03.005.

[143] F. Tubino, G. Piccardo, Serviceability assessment of footbridges in unrestricted pedestrian traffic conditions, Structure and Infrastructure Engineering. 12 (2016) 1650–1660. https://doi.org/10.1080/15732479.2016.1157610.

[144] A. Ferrarotti, F. Tubino, Equivalent spectral model for pedestrian-induced forces on Footbridges: A generalized formulation, COMPDYN 2015 - 5th ECCOMAS Thematic Conference on Computational Methods in Structural Dynamics and Earthquake Engineering. (2015) 2469–2483. https://doi.org/10.7712/120115.3551.800.

[145] E. Ahmadi, C. Caprani, S. Živanović, A. Heidarpour, Experimental validation of moving spring-mass-damper model for human-structure interaction in the presence of vertical vibration, Structures. 29 (2021) 1274–1285. https://doi.org/10.1016/j.istruc.2020.12.007.

[146] K. van Nimmen, G. Lombaert, G. de Roeck, P. van den Broeck, The impact of vertical human-structure interaction on the response of footbridges to pedestrian excitation, J Sound Vib. 402 (2017) 104–121. https://doi.org/10.1016/j.jsv.2017.05.017.

[147] C. Gallegos-Calderón, J. Naranjo-Pérez, I.M. Díaz, J.M. Goicolea, Identification of a human-structure interaction model on an ultra-lightweight FRP footbridge, Applied Sciences (Switzerland). 11 (2021) 1–22. https://doi.org/10.3390/app11146654.

[148] I.M. Díaz, C.A. Gallegos, J. Ramírez Senent, C.M.C. Renedo, Interaction Phenomena to Be Accounted for Human-Induced Vibration Control of Lightweight Structures, Front Built Environ. 7 (2021) 1–16. https://doi.org/10.3389/fbuil.2021.658529.

[149] E. Zall, Footbridge Dynamics Human-Structure Interaction, KTH Royal Institute of technology , 2018.

[150] P. Archbold, J. Keogh, C. Caprani, P. Fanning, A Parametric Study of Pedestrian Vertical Force Models for Dynamic Analysis of Footbridges, EVACES – Experimental Vibration Analysis for Civil Engineering Structures. (2011) 35–44.

[151] P.J. Fanning, P. Archbold, A. Pavic, A novel interactive pedestrian load model for flexible footbridges, Proceedings of the 2005 SEM Annual Conference and Exposition on Experimental and Applied Mechanics. (2005) 573–580.

[152] C. Lee, C. Farley, Determinats of the center of mass trajectory in human walking and runnig, J Exp Biol. (1998) 2935–2944.

[153] H. Geyer, A. Seyfarth, R. Blickhan, Compliant leg behaviour explains basic dynamics of walking and running, Proceedings of the Royal Society B: Biological Sciences. 273 (2006) 2861–2867. https://doi.org/10.1098/rspb.2006.3637.

[154] S. Rapoport, J. Mizrahi, E. Kimmel, O. Verbitsky, E. Isakov, Constant and variable stiffness and damping of the leg joints in human hopping, J Biomech Eng. 125 (2003) 507–514. https://doi.org/10.1115/1.1590358.

[155] A. Arampatzis, G.-P. Bruk, V. Metzler, The effect of speed on leg stiffness and joint kinetics in human running, J Biomech. 32 (1999) 1349–1353.

[156] E. Shahabpoor, A. Pavic, V. Racic, Structural vibration serviceability: New design framework featuring human-structure interaction, Eng Struct. 136 (2017) 295–311. https://doi.org/10.1016/j.engstruct.2017.01.030.

[157] E. Agu, M. Kasperski, Influence of the random dynamic parameters of the human body on the dynamic characteristics of the coupled system of structurecrowd, J Sound Vib. 330 (2011) 431–444. https://doi.org/10.1016/j.jsv.2010.06.029.

[158] K. van Nimmen, A. Pavic, P. van den Broeck, A simplified method to account for vertical human-structure interaction, Structures. 32 (2021) 2004–2019. https://doi.org/10.1016/j.istruc.2021.03.090.

[159] H. v. Dang, S. Živanović, Modelling pedestrian interaction with perceptibly vibrating footbridges, FME Transactions. 41 (2013) 271–278.

[160] M. Bocian, J.H.G. Macdonald, J.F. Burn, Biomechanically Inspired Modeling of Pedestrian-Induced Vertical Self-Excited Forces, Journal of Bridge Engineering. 18 (2013) 1336–1346. https://doi.org/10.1061/(ASCE)BE.1943-5592.0000490.

[161] J.H.G. Macdonald, Pedestrian-induced vibrations of the Clifton Suspension Bridge, UK, Proceedings of the Institution of Civil Engineers: Bridge Engineering. 161 (2008) 69–77. https://doi.org/10.1680/bren.2008.161.2.69.

[162] J. Brownjohn, Energy dissipation from vibrating floor slabs due to human-structure interaction, Shock and Vibration. 8 (2001) 315–323. https://doi.org/10.1155/2001/454139.

[163] F. Ricciardelli, A. Pizzimenti, Lateral Walking-Induced Forces on Footbridges, Journal of Bridge Engineering. 12 (2007) 677–688. https://doi.org/10.1061/(asce)1084-0702(2007)12:6(677).

[164] J. Milton, J.A. Nessler, S. Heredia, J. Be, Walking on a Vertically Oscillating Treadmill : Phase Synchronization and Gait Kinematics, PLoS One. (2017) 1–15. https://doi.org/10.6084/m9.figshare.3774048.

[165] F. Venuti, L. Bruno, Crowd-structure interaction in lively footbridges under synchronous lateral excitation: A literature review, Phys Life Rev. 6 (2009) 176–206. https://doi.org/10.1016/j.plrev.2009.07.001.

[166] A. McRobie, G. Morgenthal, D. Abrams, J. Prendergast, Parallels between wind and crowd loading of bridges, Philosophical Transactions of the Royal Society

A: Mathematical, Physical and Engineering Sciences. 371 (2013). https://doi.org/10.1098/rsta.2012.0430.

[167] M.J. Griffin, J. Erdreich, Handbook of human vibration, London, 1990.

[168] E. Shahabpoor, A. Pavic, V. Racic, Interaction between Walking Humans and Structures in Vertical Direction: A Literature Review, Shock and Vibration. 2016 (2016). https://doi.org/10.1155/2016/3430285.

[169] C.A. Jones, P. Reynolds, A. Pavic, Vibration serviceability of stadia structures subjected to dynamic crowd loads: A literature review, J Sound Vib. 330 (2011) 1531–1566. https://doi.org/10.1016/j.jsv.2010.10.032.

[170] J.W. Dougill, J.R. Wright, J.G. Parkhouse, R.E. Harisson, Human structure interaction during rhythmic bobbing, The Structural Engineer. 21 (2006) 32–39.

[171] P. Archbold, B. Mullarney, Interaction Between Pedestrian Loading and Vibration Response of a Laboratory-Scale FRP Composite Footbridge, in: New York City Bridge Conference 2017, 2017.

[172] P. Archbold, B. Mullarney, M. Carrig, Variations in vertical loading from walking due to surface vibrations, in: Footbridge 2014: 5th International Conference, Footbridges: Past, Present & Future, 2014.

[173] P. Archbold, J. Keogh, C. Caprani, P. Fanning, A Parametric Study of Pedestrian Vertical Force Models for Dynamic Analysis of Footbridges, EVACES – Experimental Vibration Analysis for Civil Engineering Structures. (2011) 35–44.

[174] K. van Nimmen, P. van den Broeck, G. Lombaert, Inverse identification of the pedestrian characteristics governing human-structure interaction, Procedia Eng. 199 (2017) 2889–2894. https://doi.org/10.1016/j.proeng.2017.09.583.

[175] F. Walley, St James Park bridge, Proceedings of the Institution of Civil Engineers. 12 (1959) 217–222.

[176] D.E. Allen, J.H. Rainer, Vibration criteria for long-span floors, Canadian Journal of Civil Engineering. 3 (1976) 165–173.

[177] A. Ebrahimpour, R.L. Sack, P.D. Van Kleek, Computing crowd loads using a nonlinear equation of motion, Comput Struct. 41 (1991) 1313–1319. https://doi.org/10.1016/0045-7949(91)90268-Q.

[178] S. Živanović, J. Russell, M. Pavlović, X. Wei, J. Mottram, Effects of pedestrian excitation on two short-span FRP footbridges in Delft, Conference Proceedings of the Society for Experimental Mechanics Series. (2019) 143–150. https://doi.org/10.1007/978-3-319-74421-6_19.

[179] J.M. Russell, X. Wei, S. Živanović, C. Kruger, Vibration serviceability of a GFRP railway crossing due to pedestrians and train excitation, Eng Struct. 219 (2020) 0–13. https://doi.org/10.1016/j.engstruct.2020.110756.

[180] K. Lenzen, Vibration of steel joist–concrete slab floors., Engineering Journal (AISC). 3 (1966) 165–173.

[181] J.M.W. Brownjohn, Energy dissipation in one-way slabs with human participation, Asia Pacific Vibration Conference. (1999) 155–160. http://www.tech.plym.ac.uk/soe/james/my_papers/SHAKEN2.pdf.

[182] S. Zhang, L. Xu, J. Qin, Vibration of lightweight steel floor systems with occupants: Modelling, formulation and dynamic properties, Eng Struct. 147 (2017) 652–665. https://doi.org/10.1016/j.engstruct.2017.06.008.

[183] E. Shahabpoor, A. Pavic, V. Racic, S. Zivanovic, Effect of group walking traffic on dynamic properties of pedestrian structures, J Sound Vib. 387 (2017) 207–225. https://doi.org/10.1016/j.jsv.2016.10.017.

[184] Y. Matsumoto, M. Griffin, Dynamic Response of the Standing Human Body Exposed To Vertical Vibration: Influence of Posture and Vibration Magnitude, J Sound Vib. 212 (1998) 85–107.

[185] S. Rapoport, J. Mizrahi, E. Kimmel, O. Verbitsky, E. Isakov, Constant and variable stiffness and damping of the leg joints in human hopping, J Biomech Eng. 125 (2003) 507–514. https://doi.org/10.1115/1.1590358.

[186] M. Zhang, C.T. Georgakis, J. Chen, SMD Model Parameters of Pedestrians for Vertical Human-Structure Interaction, in: Conference Proceedings of the Society for Experimental Mechanics Series, 2015: pp. 311–317. https://doi.org/10.1007/978-3-319-15248-6.

[187] J. Lou, M. Zhang, J. Chen, Identification of Stiffness, Damping and Biological Force of SMD Model for Human Walking, in: Dynamics of Civil Structures, Volume 2: Proceedings of the 33rd IMAC, 2015: pp. 331–337.

[188] J. Máca, M. Valášek, Interaction of human gait and footbridges, Proceedings of the 8th International Conference on Structural Dynamics, EURODYN 2011. (2011) 1083–1089.

[189] J.F. Jiménez-Alonso, A. Sáez, A direct pedestrian-structure interaction model to characterize the human induced vibrations on slender footbridges, Informes de La Construccion. 66 (2014) 1–9. https://doi.org/10.3989/ic.13.110.

[190] B.R. Ellis, T. Ji, Human-structure interaction in vertical vibrations, Proceedings of the Institution of Civil Engineers: Structures and Buildings. 122 (1997) 1–9. https://doi.org/10.1680/istbu.1997.29162.

[191] L. Wei, M.J. Griffin, Mathematical models for the apparent mass of the seated human body exposed to vertical vibration, J Sound Vib. 212 (1998) 855–874. https://doi.org/10.1006/jsvi.1997.1473.

[192] R. Sachse, A. Pavic, P. Reynolds, Parametric study of modal properties of damped two-degree-of-freedom crowd-structure dynamic systems, J Sound Vib. 274 (2004) 461–480. https://doi.org/10.1016/j.jsv.2003.08.052.

[193] R. Coermann, The mechanical impedance of the human body in sitting and standing position at low frequencies, Hum Factors. 4 (1962) 227–253.

[194] X. Zheng, J. Brownjohn, Modeling and simulation of human-floor system under vertical vibration, Proceedings of SPIE, Smart Structures and Materials. 4327 (2001) 513–520.

[195] J. Sim, A. Blakeborough, M. Williams, Modelling effects of passive crosds on grandstand vibration, Proceedings of the Institution of Civil Engineers: Structures and Buildings. 159 (2006) 261–272. https://doi.org/10.1680/stbu.2006.159.5.261.

[196] IStructE, Dynamic performance requirements for permanent grandstands subject to crowd action: recommendations for management, design and assessment, Institution of Structural Engineers, London, 2008.

[197] R. Hashim, T. Ji, P. Mandal, Q. Zhang, D. Zhou, Human-structure interaction experiments to determine the dynamic properties of the standing human body in vertical vibration, Structures. 26 (2020) 934–946. https://doi.org/10.1016/j.istruc.2020.04.040.

[198] G.H.M.J. Subashi, Y. Matsumoto, M.J. Griffin, Apparent mass and cross-axis apparent mass of standing subjects during exposure to vertical whole-body vibration, J Sound Vib. 293 (2006) 78–95. https://doi.org/10.1016/j.jsv.2005.09.007.

[199] ISO, BS ISO 5982. Mechanical vibration and shock. Range of idealized values to characterize human biodynamic response under whole-body vibration, 2019.

[200] C.W. Suggs, C.F. Abrams, L.F. Stikeleather, Application of a Damped Spring-Mass Human Vibration Simulator in Vibration Testing of Vehicle Seats, Ergonomics. 12 (1969) 79–90. https://doi.org/10.1080/00140136908931030.

[201] P. Boileau, X. Wu, S. Rakheja, Definition of A range of idealized values to characterize seated body biodynamic response under vertical vibration, J Sound Vib. 215 (1998) 841–862.

[202] Y. Matsumoto, M.J. Griffin, Mathematical models for the apparent masses of standing subjects exposed to vertical whole-body vibration, J Sound Vib. 260 (2003) 431–451. https://doi.org/10.1016/S0022-460X(02)00941-0.

[203] E. Shahabpoor, A. Pavic, V. Racic, Identification of mass-spring-damper model of walking humans, Structures. 5 (2016) 233–246. https://doi.org/10.1016/j.istruc.2015.12.001.

[204] M. Zhang, C.T. Georgakis, J. Chen, Biomechanically Excited SMD Model of a Walking Pedestrian, ASCE Journal of Bridge Engineering . 21 (2016). https://doi.org/10.1061/(ASCE)BE.1943.

[205] H. Wang, J. Chen, J.M.W. Brownjohn, Parameter identification of pedestrian's spring-mass-damper model by ground reaction force records through a particle filter approach, J Sound Vib. 411 (2017) 409–421. https://doi.org/10.1016/j.jsv.2017.09.020.

[206] A. Mohammed, A. Pavic, Evaluation of Mass-Spring-Damper Models for Dynamic Interaction Between Walking Humans and Civil Structures, in: Proceedings of the 35th IMAC, A Conference and Exposition on Structural Dynamics 2017, 2017: pp. 169–177.

[207] B. Whittington, D. Thelen, A Simple Mass-Spring Model with Roller Feet can induce the Ground Reactions Observed in Human Walking, J Biomech Eng. 131 (2009) 1–7.

[208] S. Živanović, B. Lin, H.V. Dang, S. Zhang, M. Ćosić, C. Caprani, Q. Zhang, Evaluation of Inverted-Pendulum-with-Rigid-Legs Walking Locomotion Models for Civil Engineering Applications, Buildings. 12 (2022) 1216. https://doi.org/10.3390/buildings12081216.

[209] B. Lin, Q. Zhang, F. Fan, S. Shen, A damped bipedal inverted pendulum for human–structure interaction analysis, Appl Math Model. 87 (2020) 606–624. https://doi.org/10.1016/j.apm.2020.06.027.

[210] J.W. Qin, S.S. Law, Q.S. Yang, N. Yang, Pedestrian-bridge dynamic interaction, including human participation, J Sound Vib. 332 (2013) 1107–1124. https://doi.org/10.1016/j.jsv.2012.09.021.

[211] H. Liang, W. Xie, P. Wei, D. Ai, Z. Zhang, Identification of dynamic parameters of pedestrian walking model based on a coupled pedestrian–structure system, Applied Sciences (Switzerland). 11 (2021). https://doi.org/10.3390/app11146407.

[212] G.A. Bertos, D.S. Childress, S.A. Gard, The vertical mechanical impedance of the locomotor system during human walking with applications in rehabilitation, Proceedings of the 2005 IEEE 9th International Conference on Rehabilitation Robotics. 2005 (2005) 380–383. https://doi.org/10.1109/ICORR.2005.1501124.

[213] S. Kim, S. Park, Leg stiffness increases with speed to modulate gait frequency and propulsion energy, J Biomech. 44 (2011) 1253–1258. https://doi.org/10.1016/j.jbiomech.2011.02.072.

[214] M. Schubert Pfeil, W. Diniz Varela, N. de Paula Amador da Costa, Experimental calibration of a one degree of freedom biodynamic model to simulate human walking-structure interaction, Eng Struct. 262 (2022). https://doi.org/10.1016/j.engstruct.2022.114330.

[215] E. Shahabpoor, A. Pavic, V. Racic, Identification of walking human model using agent-based modelling, Mech Syst Signal Process. 103 (2018) 352–367. https://doi.org/10.1016/j.ymssp.2017.10.028.

[216] R.O. Foschi, G.A. Neumann, F. Yao, B. Folz, Floor vibration due to occupants and reliability-based design guidelines, Canadian Journal of Civil Engineering. 22 (1995) 471–479.

[217] D. Gomez, S.J. Dyke, S. Rietdyk, Experimental Verification of a Substructure-Based Model to Describe Pedestrian–Bridge Interaction, Journal of Bridge Engineering. 23 (2018). https://doi.org/10.1061/(asce)be.1943-5592.0001204.

[218] K. van Nimmen, K. Maes, S. Živanović, G. Lombaert, G. de Roeck, P. van den Broeck, Identification and Modelling of Vertical Human- Structure Interaction, in: Dynamics of Civil Structures, Volume 2 : Proceedings of the 33rd IMAC, A Conference and Exposition on Structural Dynamics, 2015., 2015: pp. 319–330.

[219] H. Geyer, A. Seyfarth, R. Blickhan, Compliant leg behaviour explains basic dynamics of walking and running, Proceedings of the Royal Society B: Biological Sciences. 273 (2006) 2861–2867. https://doi.org/10.1098/rspb.2006.3637.

[220] J.H.G. Macdonald, Lateral excitation of bridges by balancing pedestrians, Proceedings of the Royal Society A: Mathematical, Physical and Engineering Sciences. 465 (2009) 1055–1073. https://doi.org/10.1098/rspa.2008.0367.

[221] Hiep. V Dang, Experimental and numerical modelling of walking locomotion on vertically vibrating low-frequency structures, Univeristy of Warwick, 2014.

[222] D.V. Ruiz, C. Magluta, N. Roitman, Experimental verification of biomechanical model of bipedal walking to simulate vertical loads induced by humans, Mech Syst Signal Process. 167 (2022) 108513. https://doi.org/10.1016/j.ymssp.2021.108513.

[223] F.E. Zajac, R.R. Neptune, S.A. Kautz, Biomechanics and muscle coordination of human walking: Part II: Lessons from dynamical simulations and clinical implications, Gait Posture. 17 (2003) 1–17. https://doi.org/10.1016/S0966-6362(02)00069-3.

[224] V. Racic, Personal Communication, (2020).

[225] F. Massey, The Kolmogorov-Smirnov Test for Goodness of Fit, J Am Stat Assoc. 46 (1951) 68–78.

[226] R. van de Schoot, S. Depaoli, R. King, B. Kramer, K. Märtens, M.G. Tadesse, M. Vannucci, A. Gelman, D. Veen, J. Willemsen, C. Yau, Bayesian statistics and modelling, Nature Reviews Methods Primers. 1 (2021). https://doi.org/10.1038/s43586-020-00001-2.

[227] M.J. Bayarri, J.O. Berger, The interplay of Bayesian and frequentist analysis, Statistical Science. 19 (2004) 58–80. https://doi.org/10.1214/088342304000000116.

[228] C.Edward. Rasmussen, C.K.I. Williams, Gaussian processes for machine learning, MIT Press, 2006.

[229] I.B.Y.C.A. Goodfellow, Deep Learning, 1st ed., MIT Press, 2016.

[230] P.I. Frazier, A Tutorial on Bayesian Optimization, ArXiv:1807.02811 [Stat.ML]. (2018). http://arxiv.org/abs/1807.02811.

[231] J. Snoek, H. Larochelle, R.P. Adams, Practical Bayesian optimization of machine learning algorithms, Adv Neural Inf Process Syst. 4 (2012) 2951–2959.

[232] D. Nguyen, S. Gupta, S. Rana, A. Shilton, S. Venkatesh, Bayesian Optimization for Categorical and Category-Specific Continuous Inputs, ArXiv:1911.12473 [Cs.LG]. (2019). http://arxiv.org/abs/1911.12473.

[233] M. Cowles, C. Davis, On the Origins of the .05 Level of Statistical Significance, American Psychologist . 37 (1982) 553–558.

[234] R. Nuzzo, Scientific method: Statistical errors, Nature. 506 (2014) 150–152. https://doi.org/https://doi.org/10.1038/506150a.

[235] U. Simonsohn, L. Nelson, J. Simmons, P-Curve: A Key to the File-Drawer, J Exp Psychol Gen. 143 (2014) 534–547. https://doi.org/10.1037/a0033242.supp.

[236] T. Strutz, Data fitting and uncertainty. A practical introduction to weighted least squares and beyond., Springer, 2016.

[237] R. Engle, Autoregressive Conditional Heteroscedasticity with Estimates of the Variance of United Kingdom Inflation, Econometrica. 50 (1982) 987–1007.

[238] Mathworks, Least squares fitting, (2021). https://uk.mathworks.com/help/curvefit/least-squares-fitting.html (accessed November 5, 2021).

[239] T. Bayes, An essay towards solving a problem in the doctrine of chances, Philosophical Transactions of the Royal Society A: Mathematical, Physical and Engineering Sciences. 53 (1763) 370–418.

[240] W.K. Hastings, Monte Carlo Sampling Methods Using Markov Chains and Their Applications, 1970. https://about.jstor.org/terms.

[241] N. Metropolis, A.W. Rosenbluth, M.N. Rosenbluth, A.H. Teller, E. Teller, Equation of state calculations by fast computing machines, J Chem Phys. 21 (1953) 1087–1092. https://doi.org/10.1063/1.1699114.

[242] S. Duane, A.D. Kennedy, B.J. Pendleton, D. Roweth, HYBRID MONTE CARLO, 1987.

[243] S. Geman, D. Geman, Stochastic Relaxation, Gibbs Distributions, and the Bayesian Restoration of Images, IEEE Trans Pattern Anal Mach Intell. PAMI-6 (1984) 721–741. https://doi.org/10.1109/TPAMI.1984.4767596.

[244] A. Gelman, J.B. Carlin, H.S. Stern, D.B. Dunson, A. Vehtari, D.B. Rubin, J. Carlin, H. Stern, D. Rubin, D. Dunson, Bayesian Data Analysis Third edition, 1995.

[245] H.V. Dang, S. Živanović, Experimental characterisation of walking locomotion on rigid level surfaces using motion capture system, Eng Struct. 91 (2015) 141–154. https://doi.org/10.1016/j.engstruct.2015.03.003.

[246] S. Zivanovic, A. Pavic, Probabilistic approach to subjective assessment of footbridge vibration, (2007).

[247] Office for national statistics, What is the difference between sex and gender? Exploring the difference between sex and gender, looking at concepts that are important to the Sustainable Development Goals., (2019). https://www.ons.gov.uk/economy/environmentalaccounts/articles/whatisthedifferencebetweensexandgender/2019-02-21 (accessed October 31, 2022).

[248] S. Živanović, A. Pavic, P. Reynolds, Vibration serviceability of footbridges under human-induced excitation: A literature review, 2005. https://doi.org/10.1016/j.jsv.2004.01.019.

[249] M.B. Semaan, L. Wallard, V. Ruiz, C. Gillet, S. Leteneur, E. Simoneau-Buessinger, Is treadmill walking biomechanically comparable to overground walking? A systematic review, Gait Posture. 92 (2022) 249–257. https://doi.org/10.1016/j.gaitpost.2021.11.009.

[250] W.D. Varela, R.C. Battista, Control of vibrations induced by people walking on large span composite floor decks, Eng Struct. 33 (2011) 2485–2494. https://doi.org/10.1016/j.engstruct.2011.04.021.

[251] K. Atkinson, W. Han, D. Stewart, Numerical Solutions of Ordinary differential equations, 1st ed., John Wiley & Sons, 2009. www.copyright.com.

[252] J.M. Russell, J.T. Mottram, S. Zivanovic, X. Wei, Design and Performance of a Bespoke Lively All-FRP Footbridge, 2019.

[253] S. Zivanovic, Personal Communication, (2022).

[254] R.W. Clough, J. Penzien, Dynamics of Structures, McGraw-Hill, New York, NY, 1994.

[255] A. Chopra, Dynamics of structures., Pearson Education India, 2007.

[256] R.H. Byrd, · Jean, C. Gilbert, J. Nocedal, A trust region method based on interior point techniques for nonlinear programming, Math. Program., Ser. A. 89 (2000) 149–185. https://doi.org/10.1007/s101070000189.

[257] J.-G. Liu, An interior trust region algorithm for nonlinear minimization with linear constraints, Source: Journal of Computational Mathematics. 20 (2002) 225–244. https://www.jstor.org/stable/43693757.

[258] C. Audet, J.E. Dennis, S.J. Optim, Analysis of generalized pattern searches, Society for Industrial and Applied Mathematics. 13 (2003) 889–903. http://www.caam.rice.edu/.

[259] D. Goldberg, Genetic Algorithms in search, optimization & machine learning, 1st ed., Addison Wesley, 1989.

[260] J. Kennedy, R. Eberhart, Particle swarm optimization, in: Proceedings of ICNN'95 - International Conference on Neural Networks, IEEE, n.d.: pp. 1942–1948. https://doi.org/10.1109/ICNN.1995.488968.

[261] M.L.Z.-V. j García-Diéguez, The Uniovi footbridge, Youtube, Spain, 2021. https://www.youtube.com/watch?v=kkeh251xkNA (accessed February 7, 2023).

[262] A. Sholokhov, Y. Liu, H. Mansour, S. Nabi, Physics-informed neural ODE (PINODE): embedding physics into models using collocation points, Sci Rep. 13 (2023). https://doi.org/10.1038/s41598-023-36799-6.

Appendix A Maximum error and percentage error of acceleration response for low frequency content of vertical walking signals

Table 6.1: Maximum Error and percentage error for low-frequency content for 0.5% modal damping ratio

		Maximum relative error				Maximum percentage error			
Model number	Load model	Maximum overestimation RMS [m/s^2, (%)]	Location (Natural frequency, Walking pace) [Hz, Hz]	Maximum underestimation RMS [m/s^2, (%)]	Location (Natural frequency, Walking pace) [Hz,Hz]	Maximum overestimation percentage [m/s^2, (%)]	Location (Natural frequency, Walking pace) [Hz,Hz]	Maximum underestimate percentage [m/s^2, (%)]	Location (Natural frequency, Walking pace) [Hz,Hz]
1	AISC Design Guide 11 [16]	-0.90, (-119)	2, 2	0.058, (44)	8.25, 2.1	-0.70, (-442)	4, 2	0.029, (60)	7.75, 2.2

2	ISO 10137 [21]	-0.47, (-62)	2, 2	0.14, (30)	2.5, 2.4	-0.35, (-325)	3, 1.5	0.049, (75)	5.75, 2.3
3	Technical report 43 appendix G [28]	-0.63, (-54)	2.5, 2.5	0.15, (80)	9.75, 2.4	-0.50, (-200)	1.5, 1.5	0.11, (99)	10, 2
4	CCIP Mean value [20]	-0.62, (-53)	2.5, 2.5	0.13, (27)	2.5, 2.4	-0.48, (-193)	1.5, 1.5	0.075, (93)	10.5, 2.1
5	CCIP design value [20]	-0.82, (-70)	2.5, 2.5	0.11, (94)	10.5, 2.1	-0.28, (-265)	3, 1.5	0.11, (94)	10.5, 2.1
6	SCI P354 [19]	-0.76, (-100)	2, 2	0.062, (49)	5.25, 1.7	-0.23, (-170)	6, 2	0.045, (65)	3, 2
7	SETRA [55]	-57, (-75)	2, 2	0.16, (32)	2.5, 2.4	-0.33, (-245)	6, 2	0.051, (69)	3.5, 2.3

8a	Chapter 3 Section 3.4.1 inter-subject	-0.36, (-31)	2.5, 2.5	0.18, (38)	2.5, 2.4	-0.04, (-69)	8, 1.6	0.06, (80)	6.25, 2.5
8b	Chapter 3 Section 3.4.2 inter-subject plus walking frequency and DLF intra-subject	-0.22, (-19)	2.5, 2.5	0.2, (29)	2.25, 2.2	-0.05, (-51)	6.75, 1.7	0.013, (59)	10, 1.5
9	Zivanovic et al. [62]	-0.27, (-108)	1.5, 1.5	0.2, (95)	10, 2.5	-0.27, (-108)	1.5, 1.5	0.2, (95)	10, 2.5
10	García-Diéguez et al. [63]	-0.13, (-17)	2, 2	0.08, (90)	12.75, 2.1	-0.05, (-94)	9, 2.5	0.08, (89)	12.75, 2.1
11	Racic et al. [52]	-0.31, (-27)	2.5, 2.5	0.15, (19)	2.25, 2.3	-0.11, (-40)	5, 2.5	0.13, (35)	1.75, 1.7

12	Muhammad et al.[51]	-0.18, (-25)	2.5, 2.5	0.17, (62)	5, 2.5	-0.02, (-132)	0.75, 1.5	0.03, (78)	9.5, 1.6
13	Varela et al. [64]	-0.56, (-48)	2.5, 2.5	0.18, (50)	1.75, 1.7	-0.19, (-176)	3, 1.5	0.13, (99)	7.25, 1.8

Table 6.2: Maximum Error and percentage error for low-frequency content for 1% modal damping ratio

		Maximum relative error				Maximum percentage error			
Model number	Load model	Maximum overestimation RMS [m/s^2, (%)]	Location (Natural frequency, Walking pace) [Hz, Hz]	Maximum underestimation RMS [m/s^2, (%)]	Location (Natural frequency, Walking pace) [Hz,Hz]	Maximum overestimation percentage [m/s^2, (%)]	Location (Natural frequency, Walking pace) [Hz,Hz]	Maximum underestimate percentage [m/s^2, (%)]	Location (Natural frequency, Walking pace) [Hz,Hz]
1	AISC Design Guide 11 [16]	-0.53, (-99)	2, 2	0.024, (40)	3.25, 2.2	-0.38, (-346)	4, 2	0.017, (46)	7.75, 2.2
2	ISO 10137 [21]	-0.25, (-47)	2, 2	0.10, (94)	2.5, 2.4	-0.18, (-234)	3, 1.5	0.033, (66)	6, 2.4
3	Technical report 43	-0.36, (-42)	2.5, 2.5	0.093, (80)	9.75, 2.5	-0.28, (-155)	1.5, 1.5	0.069, (96)	10, 2

	appendix G [28]								
4	CCIP Mean value [20]	-0.35, (-41)	2.5, 2.5	0.082, (20)	2.5, 2.4	-0.28, (-155)	1.5, 1.5	0.075, (93)	10.5, 2.1
5	CCIP design value [20]	-0.48, (-57)	2.5, 2.5	0.074, (91)	10.5, 2.1	-0.14, (-186)	3, 1.5	0.074, (91)	10.5, 2.1
6	SCI P354 [19]	-0.44, (-82)	2, 2	0.03, (49)	3.25, 2.2	-0.13, (-118)	4, 2	0.030, (55)	3, 2
7	SETRA [55]	-0.32, (-59)	2, 2	0.10, (25)	2.5, 2.4	-0.16, (-175)	6, 2	0.037, (61)	3.5, 2.3
8a	Chapter 3 Section 3.4.1 inter-subject	-0.19, (-23)	2.5, 2.5	0.13, (33)	2.5, 2.4	-0.013, (-29)	8, 1.6	0.041, (74)	6.25, 2.5
8b	Chapter 3 Section 3.4.2 inter-subject plus walking	-0.11, (-13)	2.5, 2.5	0.11, (21)	2.25, 2.2	-0.03, (-30)	4.75, 1.6	0.009, (55)	10, 1.5

	frequency and DLF intra-subject								
9	Zivanovic et al. [62]	-0.18, (-98)	1.5, 1.5	0.12, (93)	10, 2.5	-0.18, (-98)	1.5, 1.5	0.12, (93)	10, 2.5
10	García-Diéguez et al. [63]	-0.1, (-61)	2.75, 2.5	0.06, (86)	12.75, 2.1	-0.03, (-77)	9, 2.5	0.05, (86)	12.75, 2.1
11	Racic et al. [52]	-0.16, (-20)	2.5, 2.5	0.06, (12)	2.25, 2.3	-0.05, (-30)	5, 2.5	0.064, (24)	1.7, 1.75
12	Muhammad et al.[51]	-0.11, (-13)	2.5, 2.5	0.11, (60)	5, 2.5	-0.019, (-125)	0.75, 1.5	0.02, (75)	9.5, 1.6
13	Varela et al. [64]	-0.31, (-37)	2.5, 2.5	0.11, (95)	2.4, 2.5	-0.21, (-118)	5, 2.5	0.088, (98)	7.25, 1.8

Table 6.3: Maximum Error and percentage error for low-frequency content for 2% modal damping ratio

Maximum relative error	Maximum percentage error

Model number	Load model	Maximum overestimation RMS [m/s^2, (%)]	Location (Natural frequency, Walking pace) [Hz, Hz]	Maximum underestimation RMS [m/s^2, (%)]	Location (Natural frequency, Walking pace) [Hz,Hz]	Maximum overestimation percentage [m/s^2, (%)]	Location (Natural frequency, Walking pace) [Hz,Hz]	Maximum underestimate percentage [m/s^2, (%)]	Location (Natural frequency, Walking pace) [Hz,Hz]
1	AISC Design Guide 11 [16]	-0.27, (-80)	2, 2	0.012, (30)	8, 2.1	-0.19, (-268)	4, 2	0.012, (30)	8, 2.1
2	ISO 10137 [21]	-0.12, (-100)	1.5, 1.5	0.03, (9)	2.5, 2.4	-0.082, (-165)	3, 1.5	0.02, (54)	6, 2.4
3	Technical report 43 appendix G [28]	-0.145, (-27)	2.5, 2.5	0.054, (72)	9.75, 2.5	-0.15, (-123)	1.5, 1.5	0.041, (94)	10, 2
4	CCIP Mean value [20]	-0.161, (-30)	2.5, 2.5	0.045, (89)	10.5, 2.1	-0.141, (-119)	1.5, 1.5	0.045, (89)	10.5, 2.1

5	CCIP design value [20]	-0.24, (-44)	2.5, 2.5	0.043, (86)	10.5, 2.1	-0.169, (-144)	1.5, 1.5	0.043, (86)	10.5, 2.1
6	SCI P354 [19]	-0.22, (-64)	2, 2	0.015, (39)	3, 2	-0.046, (-81)	6.25, 2.1	0.015, (39)	3, 2
7	SETRA [55]	-0.16, (-85)	1.75, 1.8	0.04, (12)	2.5, 2.4	-0.11, (-164)	1.5, 1.6	0.023, (50)	3.5, 2.3
8a	Chapter 3 Section 3.4.1 inter-subject	-0.07, (-13)	2.5, 2.5	0.064, (19)	2.5, 2.4	-0.07, (-13)	2.5, 2.5	0.026, (64)	6.25, 2.5
8b	Chapter 3 Section 3.4.2 inter-subject plus walking frequency and DLF intra-subject	-0.04, (-8)	2.5, 2.5	0.06, (19)	2.5, 2.4	-0.014, (-23)	3.75, 1.9	0.006, (53)	9.75, 1.5

9	Zivanovic et al. [62]	-0.1, (-87)	1.5, 1.5	0.07, (89)	10, 2.5	-0.1, (-87)	1.5, 1.5	0.073, (89)	10, 2.5
10	García-Diéguez et al. [63]	-0.07, (-47)	2.75, 2.5	0.049, (77)	13, 2.5	-0.02, (-59)	7, 2.5	0.029, (89)	19.5, 2.4
11	Racic et al. [52]	-0.06, (-12)	2.5, 2.5	0.024, (10)	2, 2.1	-0.02, (-20)	5, 2.5	0.011, (20)	7.25, 2.5
12	Muhammad et al.[51]	-0.06, (-12)	2.5, 2.5	0.068, (63)	4.75, 2.4	-0.013, (-99)	0.75, 1.5	0.0121, (71)	9.5, 1.6
13	Varela et al. [64]	-0.14, (-26)	2.5, 2.5	0.06, (95)	4.75, 1.5	-0.1, (-88)	5, 2.5	0.054, (97)	7.25, 1.8

Table 6.4: Maximum Error and percentage error for low-frequency content for 5% modal damping ratio

		Maximum relative error				Maximum percentage error			
Model number	Load model	Maximum overestimation RMS [m/s^2, (%)]	Location (Natural frequency, Walking pace) [Hz, Hz]	Maximum underestimation RMS [m/s^2, (%)]	Location (Natural frequency, Walking pace) [Hz,Hz]	Maximum overestimation percentage [m/s^2, (%)]	Location (Natural frequency, Walking pace) [Hz,Hz]	Maximum underestimate percentage [m/s^2, (%)]	Location (Natural frequency, Walking pace) [Hz,Hz]
1	AISC Design	-0.15, (-145)	1.75, 1.8	0.004, (15)	8, 2.1	-0.068, (-227)	3.5, 1.8	0.004, (15)	8, 2.1

	Guide 11 [16]								
2	ISO 10137 [21]	-0.0455, (-45)	1.75, 1.8	0.011, (27)	3.5, 2.4	-0.028, (-104)	3, 1.5	0.0086, (37)	6, 2.4
3	Technical report 43 appendix G [28]	-0.0569, (-56)	1.75,1.5	0.029, (69)	10,2.5	-0.05, (-95)	1.5,1.5	0.01, (88)	10,1.7
4	CCIP Mean value [20]	-0.0544, (-54)	1.75, 1.8	0.02, (79)	10.5, 2.1	-0.05, (-90)	1.5, 1.5	0.006, (80)	10.5,1.5
5	CCIP design value [20]	-0.08, (-31)	2.5, 2.5	0.018, (73)	10.5, 2.1	-0.63, (-111)	1.5, 1.5	0.005, (76)	10.5,1.5
6	SCI P354 [19]	-0.08, (-81)	1.75, 1.8	0.0027, (9)	3.25, 2.1	-0.08, (-81)	1.75, 1.8	0.0027, (10)	3, 2
7	SETRA [55]	-0.1, (-110)	1.75, 1.7	0.02, (16)	2.5, 2.3	-0.10, (-201)	1.5, 1.6	0.01, (30)	3.5, 2.3

8a	Chapter 3 Section 3.4.1 inter-subject	-0.006, (-2)	2.5, 2.5	0.018, (19)	2.25, 2.1	-0.004, (-4)	1.75, 1.8	0.0081, (49)	2.25, 1.5
8b	Chapter 3 Section 3.4.2 inter-subject plus walking frequency and DLF intra-subject	-0.009, (-10)	1.75, 1.8	0.017, (14)	2.25, 2.1	-0.0057, (-17)	3.75, 1.9	0.0037, (48)	10, 1.5
9	Zivanovic et al. [62]	-0.05, (-49)	1.75, 1.8	0.034, (13)	2.5, 2.5	-0.03, (-80)	1.5, 1.6	0.0323, (78)	10, 2.5
10	García-Diéguez et al. [63]	-0.032, (-26)	2.75, 2.5	0.012, (64)	10.75, 2.1	-0.01, (-42)	6.75, 2.3	0.003, (69)	13, 1.5
11	Racic et al. [52]	-0.013, (-5)	2.5, 2.5	0.009, (6)	2, 2.1	-0.007, (-12)	5, 2.5	0.0051, (15)	7.25, 2.4

12	Muhammad et al.[51]	-0.025, (-10)	2.5, 2.5	0.0324, (56)	4.75, 2.4	-0.01, (-66)	2.25, 1.5	0.006, (63)	9.5, 1.6
13	Varela et al. [64]	-0.0374, (-15)	2.5, 2.5	0.029, (90)	4.75, 1.6	-0.032, (-56)	5, 2.5	0.013, (95)	7.5, 1.5

Appendix B Maximum error and percentage error of acceleration response for high frequency content of vertical walking signals

Table 6.5: Maximum error and percentage error for high-frequency content for 0.5% modal damping ratio

		Maximum relative error				Maximum percentage error			
Model Number	Load Model	Maximum overestimation RMS [m/s^2, (%)]	Location (Natural frequency, Walking pace) [Hz, Hz]	Maximum underestimation RMS [m/s^2, (%)]	Location (Natural frequency, Walking pace) [Hz,Hz]	Maximum overestimation percentage [m/s^2, (%)]	Location (Natural frequency, Walking pace) [Hz,Hz]	Maximum underestimate percentage [m/s^2, (%)]	Location (Natural frequency, Walking pace) [Hz,Hz]
1	AISC Design Guide 11 [16]	-0.008, (-43)	20, 1.9	0.15, (76)	10, 2.5	-0.0077, (-67)	20, 1.5	0.15, (76)	10, 2.5

4	CCIP Mean value [20]	-0.0068, (-60)	20, 1.5	0.15, (76)	10, 2.5	-0.0068, (-60)	20, 1.5	0.15, (76)	10, 2.5
5	CCIP design value [20]	-0.016, (-81)	18.25, 1.9	0.14, (69)	10, 2.5	-0.013, (-115)	20, 1.5	N/a	N/a
6	SCI P354 [19]	-0.04, (-202)	10.25, 2.3	N/a	N/a	-0.026, (-767)	20, 1.5	0.14, (70)	12.5, 2.5
8a	Chapter 3 inter-subject Section 3.4.1	-0.09, (-64)	11.5, 2.3	0.11, (62)	12.25, 2.5	-0.09, (-64)	11.5, 2.3	0.012, (96)	19.75, 1.5
8b	Chapter 3 inter-subject plus walking frequency and DLF intra-subject	-0.02, (-15)	11.5, 2.3	0.05, (36)	12.25, 2.4	-0.01, (-32)	13.25, 1.9	0.01, (84)	18.75, 1.5

	Section 3.4.2								
11	Racic et al.[52]	-0.0185, (-17)	10, 2	0.047, (26)	12.25, 2.5	-0.0055, (-23)	11, 1.7	0.023, (34)	19.75, 2.4
12	Muhammad et al. [51]	-0.0015, (-12)	18.75, 1.5	0.1, (53)	12.5, 2.5	-0.0015, (-12)	18.75, 1.5	0.0292, (72)	10, 1.7

Table 6.6: Maximum error and percentage error for high-frequency content for 1% modal damping ratio

		Maximum relative error				Maximum percentage error			
Model Number	Load Model	Maximum overestimation RMS [m/s^2, (%)]	Location (Natural frequency, Walking pace) [Hz, Hz]	Maximum underestimation RMS [m/s^2, (%)]	Location (Natural frequency, Walking pace) [Hz,Hz]	Maximum overestimation percentage [m/s^2, (%)]	Location (Natural frequency, Walking pace) [Hz,Hz]	Maximum underestimate percentage [m/s^2, (%)]	Location (Natural frequency, Walking pace) [Hz,Hz]
1	AISC Design Guide 11 [16]	-0.014, (-97)	18.25, 1.9	0.08, (63)	10, 2.5	-0.012, (-140)	20, 1.5	0.082, (64)	12.5, 2.5
4	CCIP Mean value [20]	-0.012, (-88)	18.25, 1.9	0.085, (65)	10.5, 2.5	-0.01, (-123)	20, 1.5	0.085, (65)	10.5, 2.5
5	CCIP design value [20]	-0.022, (-154)	18.25, 1.9	0.067, (52)	10.5, 2.5	-0.017, (-208)	20, 1.5	0.067, (52)	10.5, 2.5
6	SCI P354 [19]	-0.029, (-129)	19, 2.2	0.06, (45)	12.5, 2.5	-0.021, (-265)	20, 1.5	0.06, (45)	12.5, 2.5

8a	Chapter 3 inter-subject Section 3.4.1	-0.022, (-26)	11, 2.2	0.059, (48)	12.25, 2.5	-0.022, (-26)	11, 2.2	0.0078, (94)	19.75, 1.5
8b	Chapter 3 inter-subject plus walking frequency and DLF intra-subject Section 3.4.2	-0.013, (-21)	10.75, 2.2	0.029, (44)	19.75, 2.5	-0.0086, (-23)	11.25, 1.9	0.0067, (83)	20, 1.5
11	Racic et al.[52]	-0.006, (-17)	10, 2.2	0.026, (22)	12.25, 2.5	-0.0033, (-18)	11, 1.7	0.013, (30)	19.75, 2.4
12	Muhammad et al. [51]	-0.0004, (-6)	18.5, 1.5	0.067, (52)	12.5, 2.5	-0.0004, (-6)	18.5, 1.5	0.02, (70)	10, 1.7

Table 6.7: Maximum error and percentage error for high-frequency content for 2% modal damping ratio

		Maximum relative error				Maximum percentage error			
Model Number	Load Model	Maximum overestimation RMS [m/s^2, (%)]	Location (Natural frequency, Walking pace) [Hz, Hz]	Maximum underestimation RMS [m/s^2, (%)]	Location (Natural frequency, Walking pace) [Hz,Hz]	Maximum overestimation percentage [m/s^2, (%)]	Location (Natural frequency, Walking pace) [Hz,Hz]	Maximum underestimate percentage [m/s^2, (%)]	Location (Natural frequency, Walking pace) [Hz,Hz]
1	AISC Design Guide 11 [16]	-0.018, (-154)	19, 2	0.033, (41)	10, 2.5	-0.014, (-252)	20, 1.5	0.032, (42)	12.5, 2.5

4	CCIP Mean value [20]	-0.017, (-168)	18.25, 1.9	0.035, (43)	10, 2.5	-0.013, (-235)	20, 1.5	0.035, (43)	10, 2.5
5	CCIP design value [20]	-0.03, (-167)	19, 2.2	0.02, (25)	12.5, 2.5	-0.02, (-352)	20, 1.5	0.02, (26)	12.5, 2.5
6	SCI P354 [19]	-0.04, (-116)	10, 2.3	0.01, (11)	12.5, 2.5	-0.024, (-436)	20, 1.5	0.01, (11)	12.5, 2.5
8a	Chapter 3 inter-subject Section 3.4.1	-0.004, (-8)	11, 2.2	0.026, (33)	12.25, 2.5	-0.002, (-12)	13.25, 1.9	0.005, (92)	19.5, 1.5
8b	Chapter 3 inter-subject plus walking frequency and DLF intra-subject Section 3.4.2	-0.008, 19	10.75, 2.2	0.018, 45	20, 2.5	-0.008, 19	10.75, 2.2	0.0045, 81	20, 1.5

11	Racic et al.[52]	-0.003, (-12)	10, 2.2	0.012, (16)	12.25, 2.5	-0.003, (-12)	10, 2.2	0.0075, (26)	19.75, 2.4
12	Muhammad et al. [51]	N/a	N/a	0.041, (52)	12.5, 2.5	N/a	N/a	0.01, (66)	10, 1.6

Table 6.8: Maximum error and percentage error for high-frequency content for 5% modal damping ratio

Maximum relative error	Maximum percentage error

Model Number	Load Model	Maximum overestimation RMS [m/s^2, (%)]	Location (Natural frequency, Walking pace) [Hz, Hz]	Maximum underestimation RMS [m/s^2, (%)]	Location (Natural frequency, Walking pace) [Hz,Hz]	Maximum overestimation percentage [m/s^2, (%)]	Location (Natural frequency, Walking pace) [Hz,Hz]	Maximum underestimate percentage [m/s^2, (%)]	Location (Natural frequency, Walking pace) [Hz,Hz]
1	AISC Design Guide 11 [16]	-0.02, (-183)	20, 2.3	N/a	N/a	-0.016, (-469)	20, 1.5	N/a	N/a
4	CCIP Mean value [20]	-0.021, (-170)	20, 2.3	N/a	N/a	-0.015, (-442)	20, 1.5	N/a	N/a
5	CCIP design value [20]	-0.034, (-154)	10.25, 2.3	N/a	N/a	-0.02, (-632)	20, 1.5	N/a	N/a
6	SCI P354 [19]	-0.04, (-202)	10.25, 2.3	N/a	N/a	-0.026, (-767)	20, 1.5	0.007, (66)	8.75, 1.5
8a	Chapter 3 inter-subject	N/a	N/a	0.011, (33)	13.25, 2.5	N/a	N/a	0.0029, (87)	20,1.5

	Section 3.4.1								
8b	Chapter 3 inter-subject plus walking frequency and DLF intra-subject Section 3.4.2	-0.002, (-7)	11.25, 2.3	0.01, (47)	20, 2.5	-0.002, (-7)	11.25, 2.3	0.0027, (78)	20, 1.5
11	Racic et al.[52]	-0.0005, (-2)	10, 2.2	0.0057, (20)	14.75, 2.4	-0.0003, (-4)	15, 2.5	0.005, (22)	17.25, 2.4
12	Muhammad et al. [51]	N/a	N/a	0.02, (51)	12.5, 2.5	N/a	N/a	0.006, (63)	9.5, 1.6

Appendix C Maximum error and percentage error for the variance of acceleration of vertical walking signals

Table 6.9: Error of variance of acceleration at 0.5, 1, 2, 5% modal damping ratio

		Maximum relative error				Maximum percentage error			
Model Number	Load Model	Maximum overestimation RMS [m/s^2, (%)]	Location (Natural frequency, Walking pace) [Hz, Hz]	Maximum underestimation RMS [m/s^2, (%)]	Location (Natural frequency, Walking pace) [Hz,Hz]	Maximum overestimation percentage [m/s^2, (%)]	Location (Natural frequency, Walking pace) [Hz,Hz]	Maximum underestimate percentage [m/s^2, (%)]	Location (Natural frequency, Walking pace) [Hz,Hz]
5% Modal damping ratio									

3	Technical report 43 appendix G [28]	-0.0004, (-35)	1.5, 1.5	0.0031, (56)	2.5, 2.5	-0.0004, (-35)	3, 1.5	0.00001, (99)	10,1.7
8a	Chapter 3 inter-subject Section 3.4.1	-0.0008, (-333)	1.5, 1.5	0.004, (78)	2.5, 2.5	-0.0008, (-333)	1.5, 1.5	10^-6, (99)	20,1.5
8b	Chapter 3 inter-subject plus walking frequency and DLF intra-subject Section 3.4.2	-10^{-5}, (-56)	5.25, 2.2	0.0055, (97)	2.5, 2.5	-10^{-6}, (-82)	4.75, 1.9	10^{-6}, (99)	19.25, 1.7

9	Zivanovic et al. [62]	-0.003, (-160)	2.25, 2.3	0.0014, (24)	2.5, 2.5	-0.0003, (-376)	3, 1.5	0.0002, (99)	12.25, 2.5
10	García-Diéguez et al. [63],	-0.0018, (-109)	2.75, 2.5	0.024, (43)	2.5, 2.5	-0.0006, (-843)	3.5, 2.5	10^-5, (96)	13, 1.8
11	Racic et al. [52]	-0.0004, (-21)	2.25, 2.3	0.002, (33)	2.5, 2.5	-10^-5, (-96)	7, 2.5	10^-5, (79)	6.25, 2.4
12	Muhammad et al.[51]	-0.0002, (-170)	3.75, 1.8	0.005, (97)	2.5, 2.5	-10^-5, (-289)	0.75, 1.6	0.0001, (100)	19.25, 2.5
2% Modal damping ratio									
3	Technical report 43 appendix G [28]	-0.0006, (-49)	1.5, 1.5	0.0162, (88)	2.5, 2.5	-0.0004, (-103)	3, 1.5	0.0002, (99)	9.75, 1.9

8a	Chapter 3 inter-subject Section 3.4.1	-0.0027, (-205)	1.5, 1.5	0.019, (75)	2.5, 2.5	-10^-5, (-283)	10.5, 1.5	10^-6, (97)	19.5, 1.6
8b	Chapter 3 inter-subject plus walking frequency and DLF intra-subject Section 3.4.2	-10^-5, (96)	4, 2.3	0.028, (97)	2.5, 2.5	-10^{-5}, (-126)	5.75, 2.5	10^{-6} , (99)	19.5, 1.6
9	Zivanovic et al. [62]	-0.0084, (-88)	2, 2	0.012, (64)	2.5, 2.4	-0.0015, (-357)	3, 1.5	0.0006, (100)	10.25, 2.5
10	García-Diéguez et al. [63],	-0.009, (-396)	2.75, 2.5	0.013, (52)	2.5, 2.5	-0.0006, (-1395)	5.75, 2.5	10^-5, (96)	12.75, 1.8

11	Racic et al. [52]	-0.0008, (-72)	4.75, 2.4	0.011, (61)	2.5, 2.4	-10^-5, (-162)	7, 2.5	0.0002, (85)	6.25, 2.4
12	Muhammad et al.[51]	-0.0007, (-53)	4, 2	0.02, (87)	2.5, 2.5	-0.0004, (-1126)	1, 2	10^-5, (100)	8.25, 1.5
1% Modal damping ratio									
3	Technical report 43 appendix G [28]	-0.0019, (-42)	1.5, 1.5	0.059, (88)	2.25, 2.2	-0.0017, (-129)	3, 1.5	0.0002, (99)	9.75, 1.6
8a	Chapter 3 inter-subject Section 3.4.1	-0.012, (-271)	1.5, 1.5	0.059, (87)	2.25, 2.2	-0.0002, (-530)	10.5, 1.5	10^-5, (99)	19.25, 1.7
8b	Chapter 3 inter-subject plus walking frequency and	-0.0003, (-436)	5.75, 2.5	0.087, (95)	2.5, 2.5	-0.0003, (-436)	5.75, 2.5	-10^{-5}, (100)	19.25, 1.7

	DLF intra-subject Section 3.4.2								
9	Zivanovic et al. [62]	-0.0034, (-165)	3, 1.5	0.079, (73)	2.25, 2.2	-0.0009, (-302)	3.5, 1.9	0.0037, (99)	9.75, 2.4
10	García-Diéguez et al. [63],	-0.019, (-730)	2.75, 2.5	0.050, (60)	2.5, 2.5	-0.0015, (-2845)	5.75, 2.5	0.0002, (99)	12.75, 1.8
11	Racic et al. [52]	-0.0038, (-108)	5, 2.5	0.085, (81)	2.25, 2.3	-0.0015, (-198)	7, 1.9	0.028, (91)	1.75, 1.7
12	Muhammad et al.[51]	-0.0016, (-62)	3.75, 1.9	0.061, (59)	2.25, 2.3	-0.0002, (-724)	1, 1.9	0.0001, (100)	9.5, 1.5
0.5% Modal damping ratio									

3	Technical report 43 appendix G [28]	-0.0065, (-181)	3, 1.5	0.21, (95)	2.25, 2.2	-0.0052, (-115)	3, 1.5	0.0008, (99)	9.75, 1.6
8a	Chapter 3 inter-subject Section 3.4.1	-0.03, (-138)	1.5, 1.5	0.2, (94)	2.25, 2.2	-0.0008, (-381)	10.5, 1.5	10^-5, (100)	20, 1.7
8b	Chapter 3 inter-subject plus walking frequency and DLF intra-subject Section 3.4.2	-0.001, (-373)	5.5, 2.5	0.21, (95)	2.5, 2.5	-10^{-5}, (-665)	5.75, 2.5	0.0001, (100)	17.5, 1.7

9	Zivanovic et al. [62]	-0.041, (-49)	2, 2	0.13, (74)	2.25, 2.2	-0.001, (-406)	2.75, 1.5	0.008, (100)	9.75, 2.4
10	García-Diéguez et al. [63],	-0.028, (-1030)	2.75, 2.5	0.1265, (65)	2.25, 2.3	-0.015, (-1677)	3, 2.5	0.0007, (100)	12.75, 1.8
11	Racic et al. [52]	-0.012, (-147)	5, 2.5	0.17, (80)	2.25, 2.3	-0.0004, (-312)	7, 1.9	0.066, (94)	1.75, 1.7
12	Muhammad et al.[51]	-0.027, (-20)	2.5, 2.5	0.092, (64)	2, 2	-0.0016, (-1063)	1, 2	0.0005, (100)	19.5, 1.5